# A CONCEPTUAL LEVEL FRAMEWORK FOR WING BOX STRUCTURAL DESIGN AND ANALYSIS USING A PHYSICS-BASED APPROACH

A Dissertation
Presented to
The Academic Faculty

by

Charles L. Potter

In Partial Fulfillment
of the Requirements for the Degree
Doctor of Philosophy in the
School of Aerospace Engineering

Georgia Institute of Technology
May 2016

# A CONCEPTUAL LEVEL FRAMEWORK FOR WING BOX STRUCTURAL DESIGN AND ANALYSIS USING A PHYSICS-BASED APPROACH

Approved by:


Professor Dimitri N. Mavris, Advisor
School of Aerospace Engineering
*Georgia Institute of Technology*

Professor Graeme J. Kennedy
School of Aerospace Engineering
*Georgia Institute of Technology*

Professor Daniel P. Schrage
School of Aerospace Engineering
*Georgia Institute of Technology*

Dr. Neil R. Weston
School of Aerospace Engineering
*Georgia Institute of Technology*

Dr. Steven G. Russell
Triumph Aerostructures
*Vought Aircraft Division*



Date Approved: 24 November 2015

*For my grandfather,*

*Norman L. Miller*

# ACKNOWLEDGEMENTS

Finishing my PhD is the greatest accomplishment of my career as a student. I could not have accomplished this without the support of several people from both my professional and personal life. These people deserve my thanks and gratitude.

First I'd like to thank my family for their love and support. The process to obtain a PhD is long and stressful. My family both instilled in me character that allowed me to accomplish this feat, as well as provided support to survive the last two years.

Second I'd like to thank my friends both professional and personal. My professional colleagues helped me develop the ideas and skills that shaped this document. My personal friends provided distraction and reminded me that there is more to life than research.

I'd like to thank the people who contributed to the research this dissertation covers: Vadim Kim and Zhimin Liu at ASDL as well as Steven Russell at Triumph Aerostructures.

Finally, I'd like to thank my adviser Dr. Dimitri Mavris for providing guidance both academically and professionally, and for giving me the opportunity to study and work at ASDL. ASDL has been a major influence on me both professionally and personally.

# TABLE OF CONTENTS

# LIST OF TABLES

# LIST OF FIGURES

# SUMMARY

There are many challenges facing the aerospace industry that can be addressed with new concepts, technologies, and materials. However, current design methods make it difficult to include these new ideas early in the design of aircraft. This is especially true in the structures discipline, which often uses weight-based methods based upon statistical regressions of historical data. For new concepts, technologies, and materials these historical regressions either do not exist or could yield inaccurate results making them unfit for use. Without the use of historical regressions there will be a knowledge gap in early design stages when decisions have a large effect on the cost committed and where much of the design freedom is locked-in. A way to address this knowledge gap is to use physics based structural analysis and design to create more detailed structural data and incorporate life cycle cost analysis earlier in the design process. Thus, the research objective is to develop a physics-based structural design and analysis framework to incorporate new methods, concepts, technologies, and materials into the conceptual design phase.

During the conceptual design phase a large number of alternatives exist. Thus, the conceptual design phase is typically characterized by design space exploration to investigate as many alternatives as possible. However, current physics-based structural analysis and design methods typically use high fidelity modeling and analysis tools that are computationally expensive. A long run time limits the ability to thoroughly explore the large number of design alternatives during the conceptual design phase. To incorporate physics-based structural analysis and design into the conceptual design phase a balance must be struck between fidelity and exploration. To understand these trades the design space is characterized via a literature survey and simple experiments.

The design space characterization yields research observations that are used as guidance for creating a physics-based structural analysis modeling & simulation framework that uses classical structural analysis to be implemented in design space exploration. The modeling & simulation framework utilizes these concepts to increase designer knowledge while reducing design cycle time: classical structural analysis routines, a parametric geometry model, a multi-level optimization strategy, and activity based cost analysis.

A proof of concept is carried out through experimentation. The first set of experiments tests the general observations used to create the modeling & simulation framework. A two dimensional design space exploration is performed on the physics-based wing box substructure design problem to create surrogate models for the wing box weight and cost. Using the surrogate models the local minima and the global minimum are found for the multi-objective optimization problem. Then, several optimization algorithms are executed in search of the global optimum. By mapping the success rate of the algorithm against the number of function calls required to converge the experiment showed that a large number of evaluations are needed to locate the global minimum due to the complex and discontinuous nature of the design space.

The second set of experiments compared the proposed framework against two 'best practice' methods. The first comparison was against another framework that uses finite element analysis. By comparing the two models it was shown that the proposed framework had a large difference in the predicted weight; however, the resulting optimized substructure configuration matched that of the higher fidelity analysis. Thus, the use of classical structural analysis for physics-based structural design can be considered as a viable option. The second comparison illustrated the effect of introducing physics-based structural design and analysis on the weight and cost Pareto Frontier. This comparison illustrated that more variability is captured

by introducing the physical substructure into the design problem. The increased information also yielded more accurate results and better design alternatives.

The primary contributions of this thesis are to the field of conceptual aircraft structural design. Contributions are made to the implementation of physics-based structural design in the form of research observations, an example physics-based framework, and validation of concept through experimentation. Additionally, the use of parametric geometry modeling and implementation of substructure sizing using multi-level optimization and classical structural analysis will be unique contributions to existing literature. Finally, this thesis will serve as an example of increasing designer knowledge earlier in the design process and illustrate the benefits of doing so.

# CHAPTER I

# INTRODUCTION

Airplanes play a vital role in modern day society. They are used to transport goods across the world, allow people to traverse the globe in hours rather than days, and are among the most strategic assets in modern warfare. Since the invention of powered flight the airplane has evolved to meet challenges demanded by society. As the airplane evolves so too must the aircraft industry. The challenges described through the remainder of this section represent some of the demands that will continue to force the evolution of aircraft and the aircraft industry.

**Rising demand for air travel:** Global demand for air travel and cargo is on the rise. From 2000 to 2015 air traffic has doubled and both Boeing and Airbus believe that this trend will continue over the next 15 years [2, 26]. Manufacturers will need to make more airplanes with greater revenue passenger mile capabilities to satisfy airlines and meet the growing demand. In addition, the increase in air traffic has raised concerns of the public, environmentalists, and governments about the emissions due to air traffic. If air traffic continues to grow so too will the green house gases and other harmful emissions that come with it [74, 203]. The rising demand for air travel will be one of the important challenges for airlines and aircraft manufacturers over the next few decades.

**International competition:** The arrival of new markets and rising demand for air travel worldwide has increased competition internationally amongst both airlines and manufacturers. In these new markets several airlines have arisen to increase competition with well established legacy airlines which results in lower ticket prices [76, 168].

Domestically, the deregulation of the airline industry as well as the rise of low-cost carriers like Southwest Airlines have increased competition resulting in reduced airfares [33]. The small number of manufacturers means there is less competition to provide the airlines with airplanes, resulting in higher acquisition costs and therefore greater expenses. In addition gas prices continue to increase raising expenses even further. These three factors: reduced income from increased competition, high expenses due to few aircraft manufacturers, and rising gas prices have had a negative impact on airline profits [31, 179] and will continue to be an issue for airlines.

Competition between manufacturers is different from competition between airlines. Airlines have a large consumer base while manufacturers can only sell a limited number of products to either the airlines or government agencies such as NASA or the U.S. Military. This suffocating market means there are few manufacturers. However, the aircraft manufacturing environment remains highly competitive as scheduling concerns are nearly as important as monetary concerns. The reason is that airplane design takes so long and is exceedingly expensive. Design manufacturers need to secure purchasing commitments before manufacturing can begin due to the high cost and long design time. These commitments are often given to the manufacturer that has better projected what future markets will demand [132]. However, significant delays in product delivery or problems during early years of the product's service life not only hurts the reputation of the manufacturer but also gives an advantage to the few remaining manufacturers. Thus, even though there are fewer aircraft manufacturers, competition to secure purchase orders remains high and will shape the aircraft industry for years to come.

**Emphasis on life cycle cost:** An important concept in today's aerospace industry is design for affordability [135, 176]. This idea has shifted the focus of design from designing based solely on performance to designing based on how to produce the best

product at the lowest life cycle cost. Life cycle cost is the total cost of the aircraft from the inception of the concept through the aircraft's retirement. It can be broken down into the acquisition cost and the operating cost. The acquisition cost can be viewed in two ways: for the customer it is the price that the aircraft is purchased for, while for the manufacturer it is the research, development, testing, and evaluation (RDT&E) cost, the cost of production, and profit. The operating cost is broken down into direct operating cost (DOC) and indirect operating cost (IOC). Direct operating costs are the costs associated with flying the plane such as fuel cost, flight crew salaries, and maintenance. Indirect operating costs are the additional costs that come with managing the aircraft such as insurance, training, and facility costs. Affordability can be improved by increasing the performance or lowering life cycle cost. Hence meeting the challenges associated with managing life cycle cost are equally as important as meeting the challenges associated with achieving performance requirements [130].

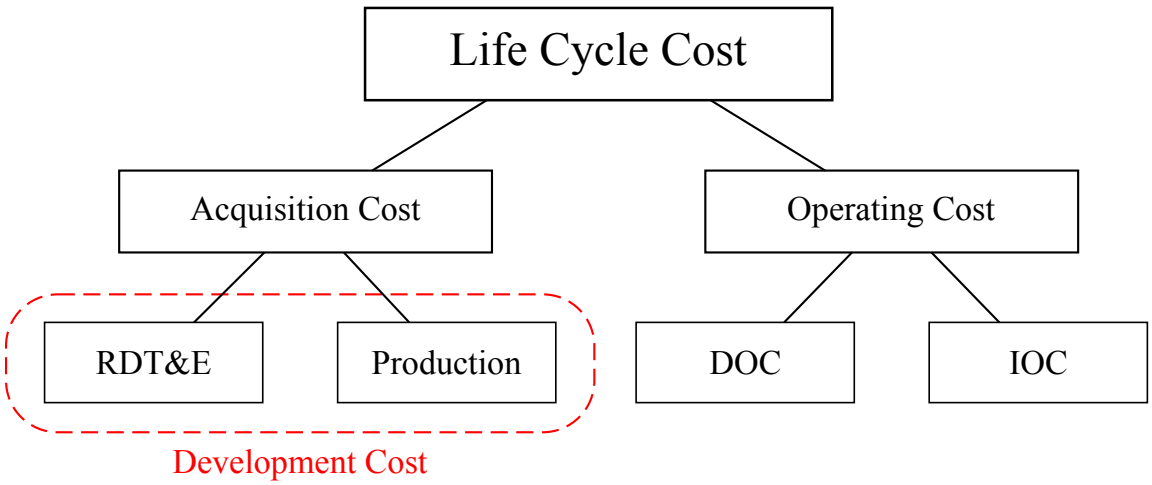


Figure 1: Breakdown of Life Cycle Cost [174]

**Government regulation on emissions:** Several international and government aviation organizations have set goals to reduce overall aircraft emissions in response to worldwide increase in air travel. In October 2010 the International Civil Aviation Organization (ICAO) addressed climate change issues in resolution A37-19 [98] with

the following goals:

> "achieve a global annual average fuel efficiency improvement of 2 percent until 2020 and an aspirational global fuel efficiency improvement rate of 2 percent per annum from 2021 to 2050, calculated on the basis of volume of fuel used per revenue tonne kilometer performed"

and

> "achieve a collective medium term global aspirational goal of keeping the global net carbon emissions from international aviation from 2020 at the same level"

In the United States, the Federal Aviation Administration (FAA) is setting goals similar to the international community [75]. For FY2013 the FAA set a performance target to:

> "improve aviation fuel efficiency by at least 2 percent per year, through FY2025, as measured by the calendar year 2012 fuel burned per miles flown, relative to the calendar year 2000 baseline"

Both the ICAO and FAA mention reducing $CO_2$ emissions which they hope to achieve with increased fuel efficiency. Emissions like $CO_2$ and $NO_x$ are the result of the combustion of the fuel and thus can be measured and modeled in stoichiometric proportions to the fuel burned [100, 116]. This implies that meeting goals to improve fuel efficiency will also reduce aircraft emissions. Although these regulations will have to be addressed directly by airlines, the entire aerospace industry must respond to them by creating more efficient aircraft as well as operating them more efficiently.

**Global supply chains:** Globalization has been one of the key drivers of the economy in the 21st century and has already affected the aircraft industry. For example, to

reduce development time and cost and distribute risk amongst more companies, Boeing outsourced approximately 70% of the manufacturing and development for the 787 Dreamliner to both domestic and global suppliers [200]. While it is simple to outsource to domestic partners, outsourcing to international partners presents a large list of difficulties such as: currency exchange fluctuations, increased shipping time, tariffs/duties, and availability of skilled labor [141]. Despite these challenges aerospace companies continue to invest in global supply chains to gain an advantage over their competition in overseas markets [62, 68]. This is true even in the defense sector of the aerospace industry, in large part due to procurement budgets shrinking since the end of the Cold War, with the limitation that only allied countries are involved [125]. In order to decrease the risks and increase the benefits of a global supply chain manufacturers are using management frameworks that allow for incorporating design decisions across the supply chain and takes into account manufacturing and scheduling considerations during the design process [169]. Controlling global supply chains will directly impact design decisions as well as costs, thus impacting the aircraft industry as a whole.

The above challenges can be summarized as follows: manufacturers need to improve aircraft **performance** to deal with new regulations and remain competitive; airlines must become leaner by managing **life cycle cost** from acquisition to retirement, and manufacturers must produce designs that better enable this; the entire industry must address both current and projected **environmental** concerns as the number of aircraft grows to meet rising demand; and manufacturers must identify and address **manufacturing** challenges early in order to avoid costly redesigns, maintain competitive schedules, manage global supply chains, and produce better products while controlling costs.

## *1.1 Problem Motivation*

The motivating interest for this thesis is to address the four challenges identified previously: performance, life cycle cost, environmental, and manufacturing. A literature search shows that these challenges can be addressed by improving aircraft structures and structural design methods, and that these improvements can be accomplished with two approaches. First, aircraft structures can be improved by using new concepts, technologies, and materials to reduce airframe weight. Second, using new design methods will increase designer knowledge early in the design process and enable cost and manufacturing considerations to be incorporated into early trade studies. These two concepts will now be discussed further.

### 1.1.1 New Concepts, Technologies, and Materials to Reduce Weight

In the past, concepts, technologies, and materials that were state of the art for their time were used to reduce airframe weight [48, 162]. This trend will continue in future aircraft. Reduction of airframe weight will address three of the previously mentioned challenges facing the aircraft industry today: improved **performance**, reduced fuel burn which will alleviate **environmental** concerns, and reduced **life cycle cost** through decreased fuel costs.

#### *1.1.1.1 Improved Performance*

First principle understanding of how improved performance is achieved through reduction of structural weight is illustrated by the Breguet Range Equation. The

Breguet Range Equation for jet aircraft is shown below in Equation 1 .

$$R = \frac{V}{c_t}\frac{L}{D}\ln\frac{W_i}{W_f} \tag{1}$$

Where:

$R =$ Aircraft Range

$V =$ Velocity of Aircraft

$c_t =$ Thrust Specific Fuel Consumption

$L =$ Lift Produced by Aircraft

$D =$ Drag Produced by Aircraft

$W_i =$ Initial Weight of Aircraft

$W_f =$ Final Weight of Aircraft

The final term in Equation 1 contains the weight ratio $W_i/W_f$. This term expresses the effect of the structural efficiency on the performance of the aircraft. A breakdown of the initial weight $W_i$ and the final weight $W_f$ into their components are given in Equations 2 and 3.

$$W_i = W_{MEW} + W_{PL} + W_{Fuel} \tag{2}$$

$$W_f = W_{MEW} + W_{PL} \tag{3}$$

In Equation 2 and Equation 3 the weights are broken down into: the Payload Weight $W_{PL}$, the Fuel Weight $W_{Fuel}$, and the Manufacturer's Empty Weight (MEW) $W_{MEW}$. For a given aircraft with a given mission it is assumed that the Payload Weight is fixed. If we ignore the trivial solution of increasing range by increasing the amount of fuel, the only way to improve the weight ratio is to lower the MEW. Using real values for several different types of aircraft [1] it can be calculated that a 5% reduction in MEW will result in a theoretical increase in range between 3% and 4%. As the majority of this weight is the aircraft structures, it stands to reason that by reducing structural weight the range of the aircraft increases [48, 90, 117].

#### *1.1.1.2 Alleviate environmental concerns*

In response to environmental concerns, NASA formed the Environmentally Responsible Aviation (ERA) program. The purpose of this program is to "explore and assess new vehicle concepts and enabling technologies through system-level experimentation to simultaneously reduce fuel burn, noise, and emissions" [208]. A reduction in the gross weight of an empty aircraft, which can be achieved through reduction of structural weight, can lead to a reduction of fuel burn [13, 162]. Therefore, many of the technologies identified and investigated within the ERA program involve reducing the overall structural weight of the aircraft [20, 184]. Emissions like $CO_2$ and NOx are the result of the combustion of the fuel and thus can be measured and modeled in stoichiometric proportions to the fuel burn [100, 116]. Thus, reducing airframe weight will reduce fuel burn, and reducing fuel burn will reduce the amount of emissions that an aircraft releases into the atmosphere.

| TECHNOLOGY BENEFITS* | TECHNOLOGY GENERATIONS (Technology Readiness Level = 4-6) | | |
|---|---|---|---|
| | N+1 (2015) | N+2 (2020**) | N+3 (2025) |
| Noise (cum margin rel. to Stage 4) | -32 dB | -42 dB | -71 dB |
| LTO NOx Emissions (rel. to CAEP 6) | -60% | -75% | -80% |
| Cruise NOx Emissions (rel. to 2005 best in class) | -55% | -70% | -80% |
| Aircraft Fuel/Energy Consumption ‡ (rel. to 2005 best in class) | -33% | -50% | -60% |

* Projected benefits once technologies are matured and implemented by industry. Benefits vary by vehicle size and mission. N+1 and N+3 values are referenced to a 737-800 with CFM56-7B engines, N+2 values are referenced to a 777-200 with GE90 engines
** ERA's time-phased approach includes advancing 'long-pole' technologies to TRL 6 by 2015
‡ $CO_2$ emission benefits dependent on life-cycle $CO_2$ per MJ for fuel and/or energy source used

Figure 2: NASA's Subsonic Transport System Level Metrics [20]

In addition to reducing the structural weight through new technologies, the ERA program also seeks to alleviate environmental concerns with new configurations. The ERA program uses NASA's Subsonic Transport System Level Metrics, listed in Figure 2. In order to achieve these goals, several studies have been launched to identify which

technologies will be needed in order to meet these goals. NASA believes that the N+1 goals can be achieved by re-winging traditional tube-and-wing (T&W) designs with more efficient engines. However, satisfying N+2 and N+3 goals is more difficult and will require new technologies and configurations. One such configuration is the Hybrid Wing Body (HWB). Studies have shown it to be a viable solution to achieving N+2 metrics [185] by reducing fuel burn through improved aerodynamics and structural efficiency. However, HWB configurations present many challenges to standard design methods [122].

#### *1.1.1.3 Reduce life cycle cost*

In addition to the environmental benefits, reduction of fuel burn through reduced structural weight will decrease life cycle cost. The basic premise can easily be explained through the DOC and the acquisition cost. The relationship between weight and DOC has long been established [22]. There are many different factors that define this relationship, one of which is fuel efficiency. A significant portion of the DOC, between 10 percent to 25 percent depending upon the aircraft [13, 51], is the fuel cost as illustrated in Figure 3. If a decrease in structural weight causes a decrease in fuel burn it will also decreases the fuel cost and the overall life cycle cost.

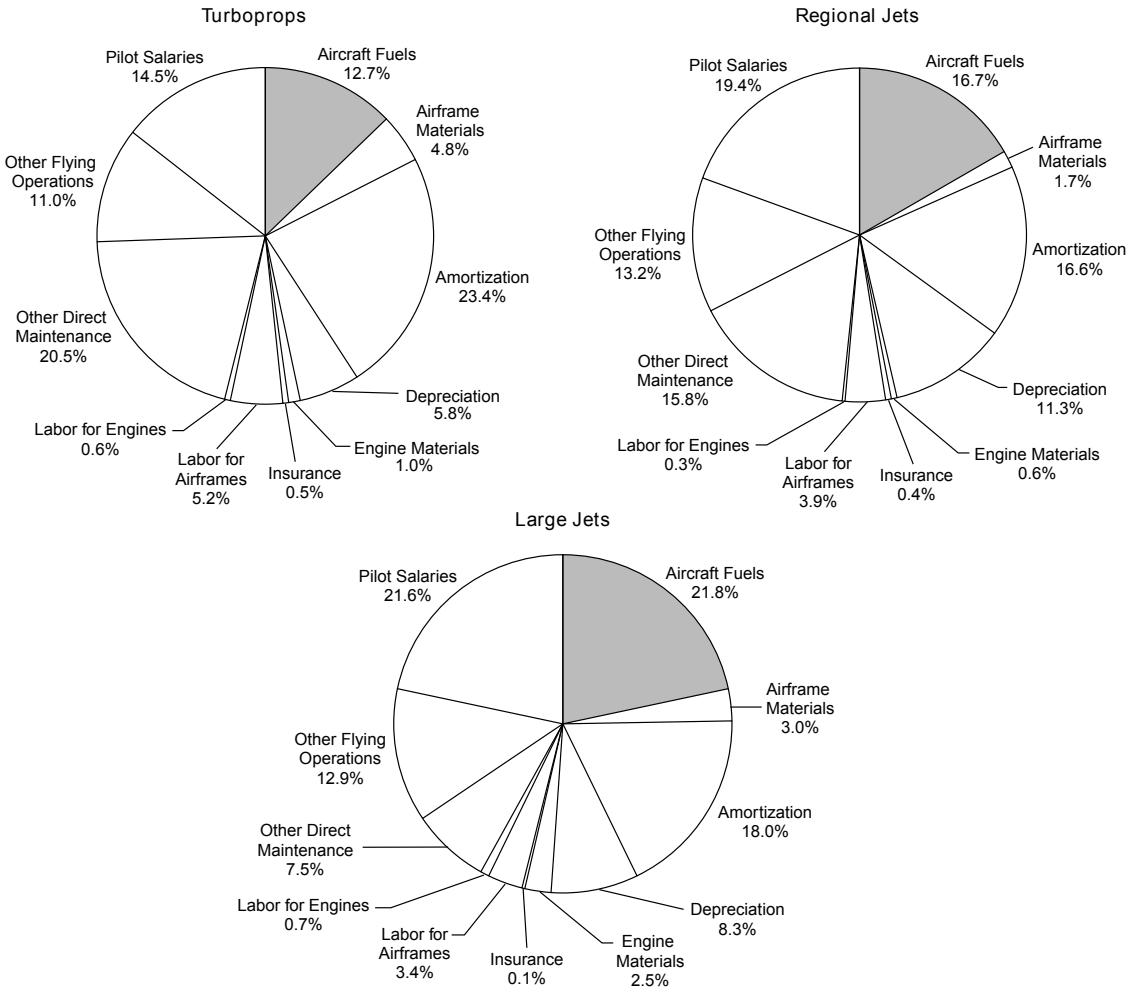


Figure 3: DOC + Insurance breakdown for different aircraft types in 1999 [13]

### 1.1.2 New Design Methods

In 1996 the National Science Foundations's Strategic Planning Workshop predicted a paradigm shift in Aerospace Engineering [186]. The goal of the paradigm shift was to increase designer knowledge while limiting the cost committed and keeping design freedom high early in the design process, as illustrated by Figure 4. The importance of increasing design knowledge is based upon the fact that so much is decided during the initial phases of design [171]. By increasing design knowledge earlier in the design process major drivers of cost and performance can be included in important trade studies [51,134,182]. The new information can then be used to attend to the challenges

the aerospace industry faces today.

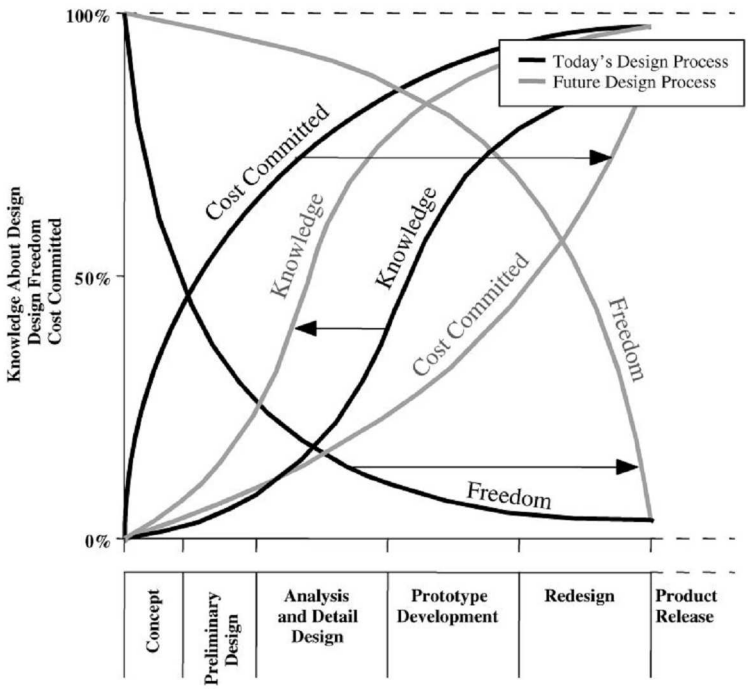


Figure 4: Intended Effects of Paradigm Shift [134]

Implementing new design methods with emphasis on structures will create several relevant benefits. The increased designer knowledge early in the design process obtained with new design methods can be used to improve early trade studies resulting in an aircraft with improved **performance**. In addition, the increased designer knowledge can be used to enable more detailed cost analyses to assess **life cycle cost** more accurately. Finally, the increased design knowledge will enable design for **manufacturing** and assembly methods. These statements will be elaborated on below.

#### *1.1.2.1 Improved Early Trade Studies*

Previous efforts have shown that using increased designer knowledge can: enable more sophisticated analysis to better represent the design space [45], capture important interactions between disciplines [40], and incorporate cost and manufacturing earlier

in the design process [170]. Some examples of increased designer knowledge provided by these methods include but are not limited to: more detailed geometric information pertaining to the substructure [14, 88] and what the major drivers of the aircraft weight and performance are [65]. The increased designer knowledge in early design phases means that more information is available for trade studies resulting in improved performance [183].

#### *1.1.2.2 Cost Analysis*

As competition among airplane manufacturers rises it becomes more important that accurate cost modeling is used to predict life cycle cost and what drives it. There are many different methods for cost modeling that rely on a mix of expertise, vehicle parameters, and hard methodical accounting. Three traditional methods used in aerospace engineering are: Analogous, Parametric, and Bottom-up [50, 52]. During conceptual design analogous costing methods are most prevalent [50] because companies typically have access to a large database of previous aircraft and manufacturing processes to base their assumptions off of [174,178]. One problem with performing cost analysis this way is when incorporating new concepts, technologies, or materials. An example is the use of advanced composite materials in aerospace parts. Conventional cost accounting and cost estimating procedures, which are typically analogous, may produce systematically biased estimates for composite parts due to application of *rules of thumb* derived from experience with aluminum manufacturing [85]. These biases not only produce inaccuracies but also convolude what drives the cost. To use composites effectively a clear understanding of the cost and its drivers is needed. Therefore the typical weight based methods used with analogous costing methods may not be enough. More sophisticated bottom-up and parametric cost modeling can be used to get a more accurate assessment of labor costs, but these methods will require more than just the weight of an aircraft and its parts [12]. The substructure geometry

and materials must be considered as well as the manufacturing processes associated with them. This knowledge typically does not exist in early stages of design with current methods.

#### *1.1.2.3 Design for Manufacturing and Assembly*

Increasing designer knowledge in the early design stages can help by enabling Design For Manufacturing and Assembly (DFMA) methods [30] which seek to use the increased design knowledge to make products that are more cost effective to manufacture. DFMA has been applied both as a method to simplify the manufacture of parts through design [81] and as a way to achieve more efficient product definitions at the conceptual design stage [112]. The drawback of DFMA is that it requires more detail than is typically generated during the conceptual design phase. In order to implement DFMA new methods that increase design knowledge need to be used.

## *1.2 Structures Throughout Aircraft Design*

Having established a motivation for research into structural design, a brief description of current practices will be used to illustrate a shortcoming of these methods. This shortcoming makes it difficult for current methods to adapt to the problems that the aerospace industry faces today. A description of the aircraft design process will be provided to clarify why current structural design methods are used in each phase. Then a simple explanation of structural design methods used in each phase of aircraft design will be presented. This information will lead to the problem definition.

### 1.2.1 Aircraft Design Phases

The aircraft design process is a lengthy, expensive, and difficult endeavor. The process can last for years, and must incorporate several different disciplines: aerodynamics, structures, controls, propulsion, and others. These disciplines all have several interdependencies which makes the problem difficult to solve. To mitigate these difficulties,

the process is divided into phases where the problem is scoped to appropriate levels of detail. At the end of each of these phases design decisions are made and some aspect of the final product is either estimated or *locked-in* so that work can move forward. The aircraft design process is broken into three design phases: conceptual, preliminary, and detailed. Raymer provides a description of each of the design phases [174]. For convenience they are summarized below:

**Conceptual Design Phase:** The first design phase is the conceptual design phase. This is the phase where initial sizing, weight, cost, and performance metrics are assessed to see if a technically feasible and economically viable aircraft exists that meets the requirements presented. During the conceptual design phase a large number of design alternatives are assessed and trade studies are performed. The design layout is fluid, constantly changing due to failure to meet requirements or seeking improvement in the design metrics. Conceptual design typically relies on first principle equations or heuristic data to rapidly assess different alternatives. At the end of the conceptual design phase an initial concept and shape is selected but with very limited detail.

**Preliminary Design Phase:** After the conceptual design phase concludes, work begins on the preliminary design phase. The primary objective of the preliminary design phase is to mature the conceptual design far enough to decide whether to build the aircraft or not. During this phase each of the discipline specialists begins work on their specific area of expertise resulting in less collaboration between the disciplines than during the conceptual design phase. Enough of the design is defined that initial testing on aerodynamics, structures, and propulsion can begin. Tools in the preliminary design phase should still be able to rapidly assess different alternatives, but at a higher fidelity than conceptual design tools.

**Detailed Design Phase:** The final design phase is referred to as the detailed design phase. By the end of the detailed design phase the concept must have enough definition that it can be used for manufacturing. Furthermore, many of the small parts that are not considered during the preliminary design phase must be designed to fit in with the larger elements. Every element of the structures, electronics, interior, and other systems of the aircraft must be finalized. Since the final aircraft design must be documented at the end of this phase, the tools used usually involve sophisticated Computer Aided Design (CAD) tools. These tools can model parts with sufficient detail as well as link the highest fidelity analyses possible, such as Finite Element Method (FEM) or Computational Fluid Dynamics (CFD). The detailed design phase ends when manufacturing of the first aircraft begins.

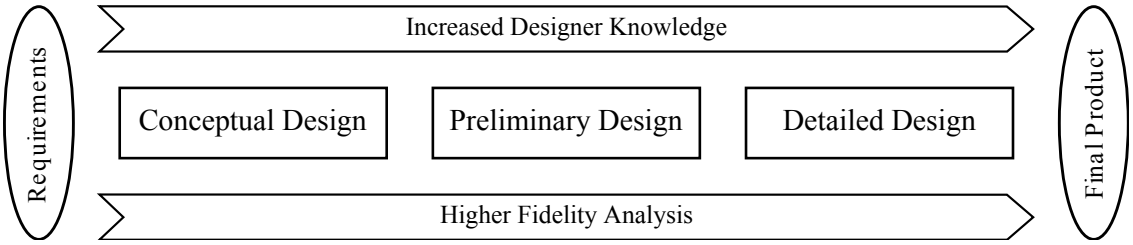


Figure 5: Aircraft Design Process

The key takeaway from the discussion on aircraft design is that as the design progresses through each design phase, there is an increase in two aspects of design: knowledge of the aircraft being designed and analysis fidelity. This is shown in Figure 5. These two concepts are highly intertwined. As design decisions are made, more information about the design is gained; in turn, there is more detailed information to use for analysis which enables higher fidelity tools. For instance, finite element analysis (FEA) requires a geometric representation of the substructure which is not available early in the design process. Another contributor to the correlation between increased design knowledge and higher fidelity analysis is the relationship between analysis fidelity and run time. Higher fidelity analysis routines typically have longer

run times which means that fewer cases can be run. At the beginning of the aircraft design process little is known about the final product and many trades have to be made. Therefore, analysis routines with faster run times are used so that more cases can be run. Likewise at the end of the design process there is a greater amount of design knowledge and fewer trades are expected to be performed. This means that higher fidelity routines with slower run times can be used. The correlation between knowledge of the aircraft being designed and analysis fidelity ends up being one of the biggest factors in the choices made in structural analysis methods used in each design phase.

### 1.2.2 Structures Methods Used at Each Design Phases

Increasing designer knowledge, higher fidelity analyses, and their correlations are important in understanding why certain structural design methods are used at each design phase. Descriptions of such structural design methods are provided below. They are presented chronologically backwards as structural analysis in the detailed design phase is the easiest to understand.

#### *1.2.2.1 Detailed Structural Design Methods*

The main objective of structural design and analysis in the detailed design phase is certification of the aircraft and preparing the design for fabrication [7, 174]. During the detailed design phase the majority of the design trades have been completed so there is no longer any need to rapidly test multiple design configurations. Instead, the design must now be modeled in enough detail so that it can be fabricated. The only addition to the design are some of the finer details not included in preliminary design, such as doors, structural clips, and brackets [7, 174]. The design is modeled using the most detailed CAD tools because a significant amount of detail is demanded during this phase. Only one design configuration will be studied and only one model is needed because the design is essentially frozen [45]. Additionally, the highest fidelity

analysis will be used to ensure that the aircraft will be certified. This typically means that computationally intensive 3D FEA suites are used, such as CATIA [41] or NASTRAN [146, 151], as they provide the means to represent and analyze detailed models as well as provide the ability to organize this data for manufacturing.

#### *1.2.2.2 Preliminary Structural Design Methods*

The preliminary design phase is when the concept is first considered in enough detail for the discipline specialists to contribute [174]. From an airplane configuration standpoint very little will change during the preliminary design phase because most of the decisions about the configuration are made during the conceptual design phase [7]. Instead the preliminary design phase investigates important details about the selected concept. From a structures perspective, preliminary design is where detailed information about the substructures is first considered.

There are two important characteristics of preliminary design that shape the modeling and analysis tools used. The first is the large number of trades left to be performed. Even though the configuration does not change substantialy during preliminary design, there are still numerous trades to be performed on the substructure and its layout [102]. Thus, it is reasonable to assume that modeling and analysis tools used in the preliminary design phase will have shorter run times so that more alternatives can be explored in the time available. The second is the multi-disciplinary aspect of the preliminary design phase. At this point each of the disciplines begins to contribute to the design. Yet, considering each discipline one at a time is not sufficient as the interactions between them can be what defines the design [157, 192]. In order to capture these interactions it is necessary to use modeling and analysis tools that are higher fidelity.

The previous paragraph illustrates conflicting needs between faster run times and higher fidelity analysis. Thus, structures in the preliminary design phase is

characterized by a balance between fidelity and run time. At the beginning, when designer knowledge is at its lowest, structures are simplified to their basic functions. Lower fidelity analysis tools, when compared to the detailed design phase, are used to assess whether or not the structure will fail [6, 45]. A good example is simplifying substructures to planes and then using 2D FEA for analysis [6, 103]. Throughout the preliminary design phase knowledge about the design increases allowing tools with higher fidelity to be used.

#### *1.2.2.3 Conceptual Structural Design Methods*

The conceptual design phase is the most perplexing design phase for structural analysis. The phase is characterized by a lack of design knowledge and a large amount of design uncertainty associated with the problem itself [90]. Higher fidelity analysis routines used in the preliminary and detailed design phases are impractical for the conceptual design phase because: there is not enough knowledge to make a model with enough detail, and they are incapable of handling the design uncertainties [183]. Without these tools it is unclear how to proceed with structural analysis. This is why during conceptual design structural analysis typically is not performed. A quote from Raymer explains:

> "the conceptual designer may never do any structural analysis. The conceptual designer relies upon an experienced eye to ensure that sufficient space is provided for the structural members. The only direct impact of structures during the initial stages of conceptual design is in the weights estimation" [174]

Instead of structural analysis, traditional structural sizing methods use weight estimation to represent the structures. A review of traditional structural sizing will illustrate this point. First constraint analysis and mission analysis of weight fractions are used to size the aircraft and give an estimate of starting Gross Takeoff Weight

($W_{TO}$) [7, 174, 178]. Next the empty weight ($W_E$) of the aircraft is based on statistical regressions based on historical aircraft data such as Equation 4 and depicted in Figure 6. In Equation 4, $A$ and $B$ are the regression coefficients based off of historical data. Once the empty weight is selected, the weights of different components are estimated as a fraction of the empty weight. Essentially, during the conceptual design phase the structure is simplified into a weight and the general shape of the aircraft is calculated through heuristic methods.

$$W_E = \exp\left[(\log W_{TO} - A)/B\right] \tag{4}$$

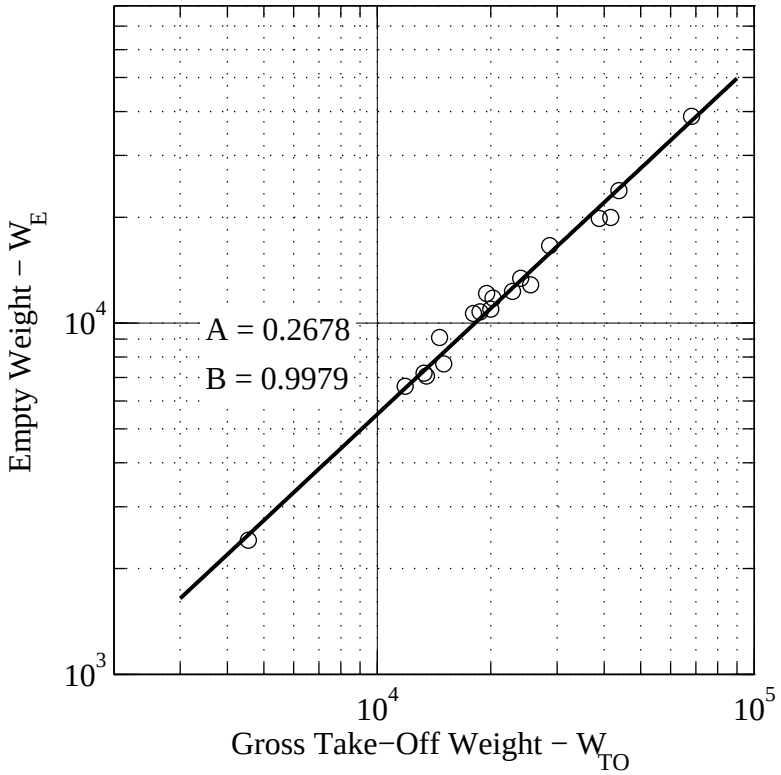


Figure 6: Weight Trends for Business Jets [178]

These historical regressions are very useful in the conceptual design phase because they are based on fully formed aircraft. For fully formed aircraft all the necessary trades

have already been carried out which means for those designs no design uncertainty exists. In addition all the design knowledge for those aircraft is available in detailed weight and cost breakdowns. Furthermore, they are computationally inexpensive. The combination of no design uncertainty, large amounts of design knowledge, and inexpensive analysis are what make historical regressions so useful in the conceptual design phase. However, there exist major flaws in using historical regressions which will be discussed in the next section.

## *1.3 Problem Definition*

Historical regressions are useful during the conceptual design phase. However, they are reliant upon information from previous aircraft. As mentioned in the beginning of this chapter, new concepts, technologies, and materials will be needed in order to solve the challenges the aircraft industry currently faces. By the definition of new concepts, technologies, and materials, it is impossible to account for them directly in historical regressions. The current solution to this problem is to use so called *calibration factors* to alter the values in the regressions. Some examples are shown in Table 1.

Table 1: Weight estimation *fudge factors* [174]

| Category | Weight group | Fudge factor (multiplier) |
|---|---|---|
| Advanced composites | Wing | 0.85-0.90 |
| | Tails | 0.83-0.88 |
| | Fuselage\nacelle | 0.90-0.95 |
| | Landing gear | 0.95-1.00 |
| | Air induction system | 0.83-0.88 |
| Braced wing | Wing | 0.82 |
| Braced biplane | Wing | 0.6 |
| Wood fuselage | Fuselage | 1.60 |
| Steel tube fuselage | Fuselage | 1.80 |
| Flying hull boat | Fuselage | 1.25 |
| Carrier based aircraft | Fuselage and landing gear | 1.2-1.3 |

This method has several shortcomings such as uncertainty in the values used and scalability issues. It also assumes that historical information exists when there may have been no previous use of the concept or technology. Below are examples of how historical regressions have failed in the past or may fail in the future:

**Hybrid Wing Body:** As previously mentioned the Hybrid Wing Body (HWB) concept can be used to address environmental issues in the future [185]. HWB aircraft is a new concept; therefore no historical data exists. For HWB, traditional methods based on historical regressions cannot be used without significant alterations. Attempts have been made to adapt empirical data from Tube-and-Wing aircraft because they have similar substructure layouts, as shown in Figure 7. The data or equation is then input into the traditional sizing methods to generate a conceptual design [32, 122]. However, recent studies have suggested that the accuracy of the weight results is less than ideal because of the unique configuration and that these calculations must be made using physics-based models [91, 114]. Regardless, it is clear that traditional

design methods are not ideal for designing revolutionary concepts.

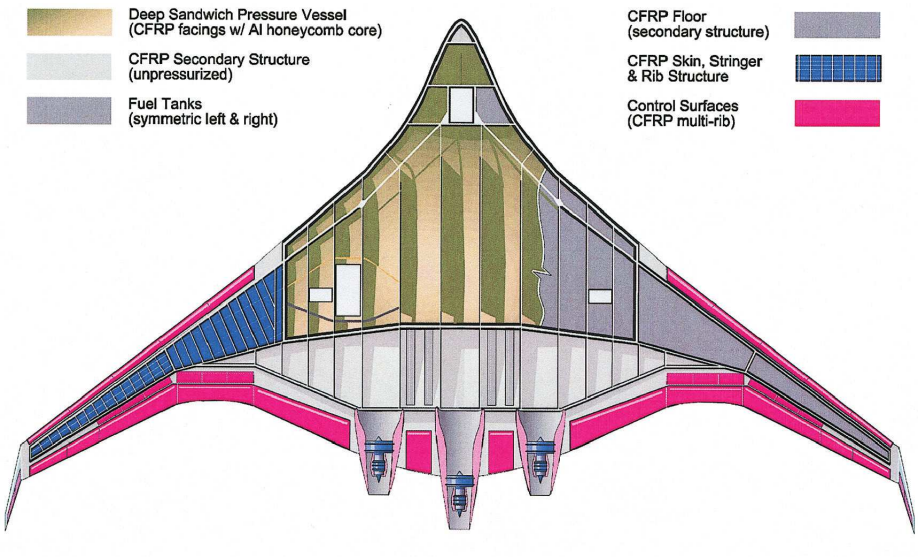


Figure 7: Structural layout of second-generation BWB [122]

**Composite Materials:** Significant time and effort has been spent adapting traditional design methods based on historical regressions for composite materials [195]. However, the success of using these methods is predicated upon two actions: gathering enough data to adapt regressions to composite materials and making assumptions to simplify the composites. As the use of composites becomes more common, more data is gathered which increases accuracy in these methods. However, the simplifying assumptions that leave the composites in a state commonly referred to as *black aluminum*, leave questions about the practicality of adapting historical regressions to composites. From a weight standpoint the simplifications ignore some of the benefits that the directionality of composite materials present for saving weight [198]. In addition cost regressions, which are typically based on weight, have trouble accurately predicting the cost and identify the drivers of cost because the majority of the cost of composites is due to the labor costs not the material costs [85]. Adopting new methods to incorporate composites will be beneficial in tackling the challenges that face the aerospace industry.

**Joint Strike Fighter:** The F-35 Joint Strike Fighter (JSF) is a tactical aviation fighter developed by Lockheed Martin [82]. The purpose of the JSF program was to curtail the enormous costs typically associated with tactical aviation programs by building a common airplane to serve three branches of the US military: Air Force, Navy, and Marine Corps. Additionally this program sought foreign investment from NATO allies. With so many differing organizations and objectives, it was decided to make three variations: conventional take-off and landing (CTOL), carrier-based (CV), and short take-off and vertical landing (STOVL). The STOVL variation presents the most technical challenges [27]. In 2004 Lockheed Martin realized that the STOVL variation was overweight. The culprit for the error was the traditional empirical mass estimating methods based off of historical regressions [66]. Although the airframe had been modeled and analyzed using CAD and FEM, the mass was estimated using parametric models based upon statistical analysis of previous aircraft data [44]. These methods proved to be inadequate [44]. As the design progressed, more and more structural weight was needed in order to account for the STOVL capabilities making the original mass estimates increasingly worse.

At this point a summary of what has been discussed will illustrate the problem this thesis dissertation seeks to address. In the absence of structural analysis, parametric weight estimates based upon historical regressions are used to fill in the necessary structural information during the conceptual design phase. This method is valid because the historical regressions are based off of fully formed designs of similar aircraft with all the weight, manufacturing, and cost data. However, in response to the challenges that the aerospace industry faces today new concepts, technologies, and materials are needed. Under these circumstances empirical methods based on historical regressions may not be adequate. In the absence of historical data there is a knowledge gap formed between the early portions of the conceptual design phase

and the early preliminary design phase where the substructure is first considered and physics-based analysis is used.

A consequence of this knowledge gap is that early design decisions have a large impact on the other phases [186]. In addition most of the development costs and resources are committed early in the design process. Industry estimates that around 70% to 80% of Life Cycle Cost is committed at the end conceptual design phase [171]. These cost critical decisions are made with incomplete data due to the knowledge gap. If mistakes are made early, either due to the knowledge gap or attempting to adapt historical regressions, and redesigns are necessary they are going to be expensive. The *rule of ten* says that later design changes can cost as much as ten times more than those in the early stages [39]. Therefore increasing designer knowledge early in the design process, including addressing the knowledge gap, is important.

## *1.4 Research Objective*

The knowledge gap due to the lack of historical data has been a problem studied widely within the aerospace industry. A proposed solution that addresses this problem, as well as many others in the aerospace industry, is to use methods driven by physics-based analysis [199]. Physics-based analysis refers to using disciplinary analysis tools that model the governing equations derived from the physics of the problem as well as multi-disciplinary methods to capture the interactions between the disciplines [135]; this is opposed to traditional handbook methods that rely on historical data [7,174,178]. Physics-based analysis solves the current problem by: increasing designer knowledge earlier in the design process which enables the use of new concepts, technologies, and materials; and allowing for incorporation of additional disciplines that are usually left out of handbook methods, like cost and manufacturing. This leads to the overall research objective:

**Overall Research Objective**

Develop a physics-based structural design method to incorporate new concepts, technologies, and materials into the conceptual design phase.

The use of physics-based analysis is not a new idea in aerospace engineering, especially in the modeling of structures. However, there has been one major problem with their use in aircraft design. The use of physics-based models requires long run times [120,155] which in turn limits the number of analysis runs that may be performed during the time available for conceptual design; a fact that conflicts with the desire to explore the large number of alternatives during the conceptual design phase [113]. Much of the current effort to incorporate physics-based modeling is focused on using high fidelity modeling and analysis routines such as CFD and FEA tools [**?**, 53, 148]. These methods tend to have high run times for each design cycle associated with them. Also, these high fidelity tools tend to use the majority of available computation power on modeling and analysis while ignoring the significant efforts that are needed for optimization [206], a problem best illustrated by the quote:

> "Yet, in 2004 structural practitioners hear the same refrain from structural analysts that was heard in 1971: a single structural analysis takes several hours or even several days to run on my computer; how can I even afford to think about optimization?" [206]

In order to implement a new physics-based structural analysis method for the conceptual design phase, a balance between modeling, analysis, and optimization with emphasis on exploring the available design space must be investigated.

The overall research objective will be accomplished by fulfilling the following research objective. First, the design space will be characterized through several

research observations by performing small experiments and literature surveys.

---

**Research Objective 1**

Characterize the wing substructure configuration design problem to identify major challenges of modeling & simulation for structural analysis and optimization using simple experiments and literature review.

---

Next, a literature survey of current structural design and optimization methods will define the methods available to accomplish the overall research objective.

---

**Research Objective 2**

Compare current structural design, analysis, and optimization methods based upon metrics that will identify which methods are most appropriate for the conceptual design phase.

---

Then, a framework to implement physics-based analysis will be proposed based upon the research observations made while fulfilling Research Objective 1 and the options identified while fulfilling Research Objective 2.

---

**Research Objective 3**

Develop a framework using the previously identified structural analysis and optimization methods based upon research observations made from characterizing the design problem.

---

Finally, the proposed method will be tested against previously used methods based on historical regressions.

---

**Research Objective 4**

Test the developed methodology against previously used methods that use historical regressions to draw conclusions on using physics-based analysis in the conceptual design phase.

---

# CHAPTER II

# DESIGN SPACE CHARACTERIZATION OF THE SUBSTRUCTURE CONFIGURATION PROBLEM

Chapter 1 established the overall problem to be addressed. An overall research objective was proposed and then decomposed into four research objectives. The first research objective focuses on characterizing the substructure configuration design space.

---

**Research Objective 1**

Characterize the wing substructure configuration design problem to identify major challenges of modeling & simulation for structural analysis and optimization using simple experiments and literature review.

---

In this chapter the physics-based substructure design problem was defined. Then, an example problem was used to characterize the substructure design space. The design of an entire aircraft is an immense problem that would require years of work by a team of experts. To complete the research in a reasonable time the work that will be addressed in both the example problem and the rest of the thesis is scoped down to a wing box substructure design problem. Thus, this chapter begins with a description of the wing box substructure. Additionally, previous work on the topic is introduced along with a tool that is used for the design space characterization. The rest of the chapter makes several research observations using the previous work and experimentation. These research observations are used in later chapters to aid in completing the overall research objective.

## *2.1 Physics-Based Structural Design*

The overall research objective is to develop a physics-based structural design method appropriate for the conceptual design phase. Structural design in the conceptual design phase typically does not include physics-based structural analysis. Including physics-based structural analysis will alter the design problem significantly, as will be shown in this chapter. The general practices of structural design, analysis, and optimization will be discussed in Chapter 3; however, to understand how physics-based structural analysis will alter the design problem it is necessary to understand some basic principles of physics-based structural design and analysis. These principles are discussed below.

Structural design is the process of defining a structure (configuration, materials, and dimensions) to withstand the design loads without failure [108, 153]. Each structural alternative is tested for failure using structural analysis, which is evaluating the deformations and stresses within a solid object due to the applied loads [4, 17]. Structural design cannot happen without structural analysis. The underlying principles of structural analysis are based on solid mechanics; for aerospace structures this typically is limited to linear elasticity [17, 34]. Therefore, an understanding of the principles of linear elasticity will illustrate how physics-based structural design and analysis will alter the conceptual design problem.

The governing equations of linear elasticity are derived from three sets of equations: the kinematic equation, constitutive equations, and equilibrium equation [17]. The *kinematic equations* (i.e. strain-displacement equations) are equations that define the strain on the structure in terms of the displacement. The set of 3D kinematic equations are depicted in Equations 5 and 6 where $\epsilon$ is the strain in the solid, $\gamma$ is the

angular strain (i.e. shear strain), and $u$ is the displacement in a given direction.

$$\epsilon_1 = \frac{\partial u_1}{\partial x_1} \qquad \epsilon_2 = \frac{\partial u_2}{\partial x_2} \qquad \epsilon_3 = \frac{\partial u_3}{\partial x_3} \tag{5}$$

$$\gamma_{23} = \frac{\partial u_2}{\partial x_3} + \frac{\partial u_3}{\partial x_2} \qquad \gamma_{23} = \frac{\partial u_2}{\partial x_3} + \frac{\partial u_3}{\partial x_2} \qquad \gamma_{23} = \frac{\partial u_2}{\partial x_3} + \frac{\partial u_3}{\partial x_2} \tag{6}$$

To form the governing equation the kinematic equation result in terms that must be integrated across the dimensions of the substructure. Therefore, it is necessary to represent the geometry in order to solve the kinematic terms in the linear elasticity governing equations.

The *constitutive equations* are derived from material science and define the mechanical behaviors of the material. For elastic materials this means applying Hooke's law which defines a linear relationship between the stresses ($\sigma$ and $\tau$) and strains ($\epsilon$ and $\gamma$) within a structure. A representation of Hooke's law in three dimensions for an isotropic material is shown in Equation 7.

$$\begin{Bmatrix} \epsilon_x \\ \epsilon_y \\ \epsilon_z \\ \gamma_{yz} \\ \gamma_{zx} \\ \gamma_{xy} \end{Bmatrix} = \begin{bmatrix} \frac{1}{E} & \frac{-\nu}{E} & \frac{-\nu}{E} & 0 & 0 & 0 \\ \frac{-\nu}{E} & \frac{1}{E} & \frac{-\nu}{E} & 0 & 0 & 0 \\ \frac{-\nu}{E} & \frac{-\nu}{E} & \frac{1}{E} & 0 & 0 & 0 \\ 0 & 0 & 0 & \frac{(1+\nu)}{E} & 0 & 0 \\ 0 & 0 & 0 & 0 & \frac{(1+\nu)}{E} & 0 \\ 0 & 0 & 0 & 0 & 0 & \frac{(1+\nu)}{E} \end{bmatrix} \begin{Bmatrix} \sigma_x \\ \sigma_y \\ \sigma_z \\ \tau_{yz} \\ \tau_{zx} \\ \tau_{xy} \end{Bmatrix} \tag{7}$$

The terms $E$ and $\nu$ are material properties that are unique to a given material. While it is mathematically possible to solve for material properties it is typically unreasonable to solve for these values during structural design. Instead, to solve the constitutive equations during structural design a set of materials is selected and compared. This will be discussed in further detail later in this chapter.

The *equilibrium equations* express the balance of the internal and external forces for an element of the solid. These equations are derived using either Newton's Laws

(i.e. Newtonian Mechanics) or the principle of virtual work or energy (i.e. analytical mechanics). These equations are often problem specific and will not be discussed further.

During the conceptual design phase the governing equations of linear elasticity are ignored by current methods and instead the structure is assumed to be a point mass weight. To include physics-based structural design and analysis in the conceptual design phase these equations must be addressed. As previously discussed, the kinematic equations require some representation of the geometry of the solid and the constitutive equations require that the material of the structure be known to solve the governing equation. Therefore, to introduce physics-based structural design into the conceptual design phase the materials and geometry of the structure need to be represented. This presents a series of new challenges which will be discussed throughout the remainder of the chapter.

## *2.2 Example Wing Box Design Problem*

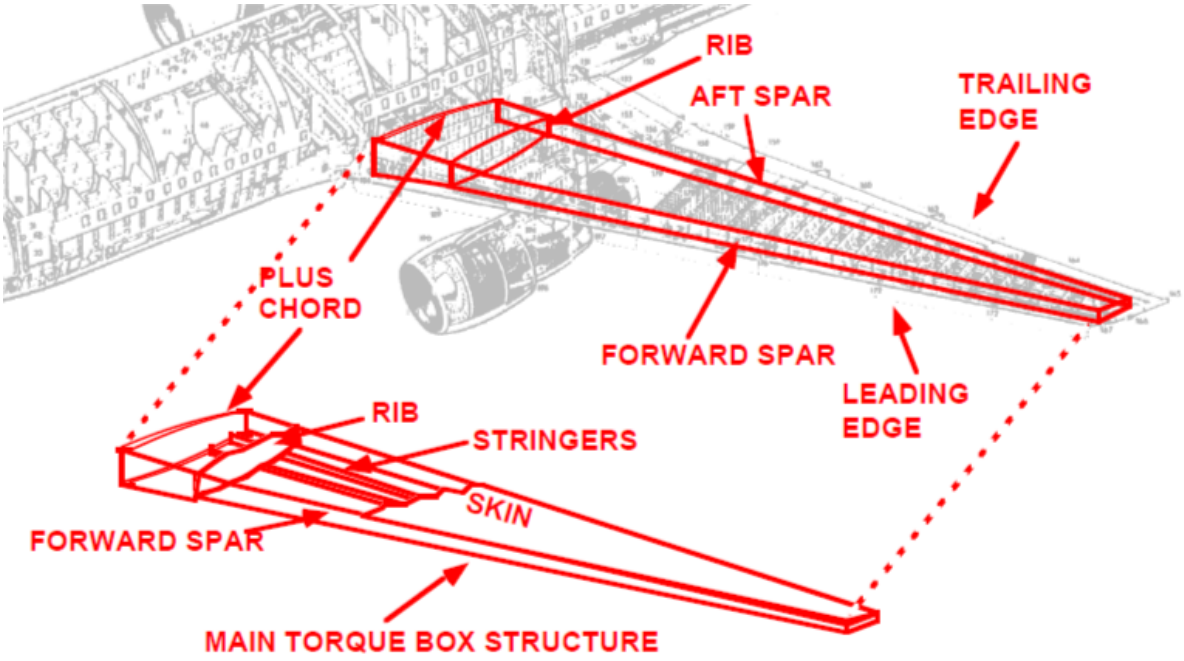


Figure 8: Wing box substructure [210]

An example is used to illustrate the difficulties of the substructure layout problem. This example focuses on the substructure of a wing box. The wing box is defined as the portion of the wing between the front spar and the rear spar along the entire span of the wing; a conventional wing box arrangement is depicted in Figure 8. The elements that make up a conventional wing box arrangement are the ribs, spars, and cover panels which consist of the skin and stringers. There are two types of ribs: the stub ribs and the main ribs. The stub ribs are the inboard ribs and are typically defined parallel to the free stream. The main ribs are the outboard ribs and are all parallel to a defined angle. The cover panels are typically stiffened skin panels with stringers that run parallel to one another along the entire span of the wing, or until it approaches the bounds of the wing box. Each of these elements contain a number of features. These included webs, caps, web stiffeners, panels, etc. Each of these features has geometric variables associated with them (areas, lengths, and thicknesses). Some of these values are determined by the substructure layout and wing geometry, such as the rib length and height. The rest are dimensions that have to be selected as part of the design process.

An example is used to illustrate the difficulties of the substructure layout problem. This example is the result of ongoing research that seeks to automate the previously manual and tedious efforts to design the substructure layout of an aircraft's wing box during the preliminary design phase [167, 180]. Structural analysis in preliminary design typically uses tools or routines suitable for evaluating structural elements or components rather than the entire structure. At the preliminary design stage, the structure can be broken down into a collection of components, each of which can often be idealized to capture the essential behavior of the structural concept without the complicating geometrical details. These components, such as the wing cover, spar and ribs, can be analyzed without reference to complicating features, such as joints, cutouts and fittings. These details must eventually be considered later in the design

process; however, during preliminary design there is usually only time and available information to approximate them.

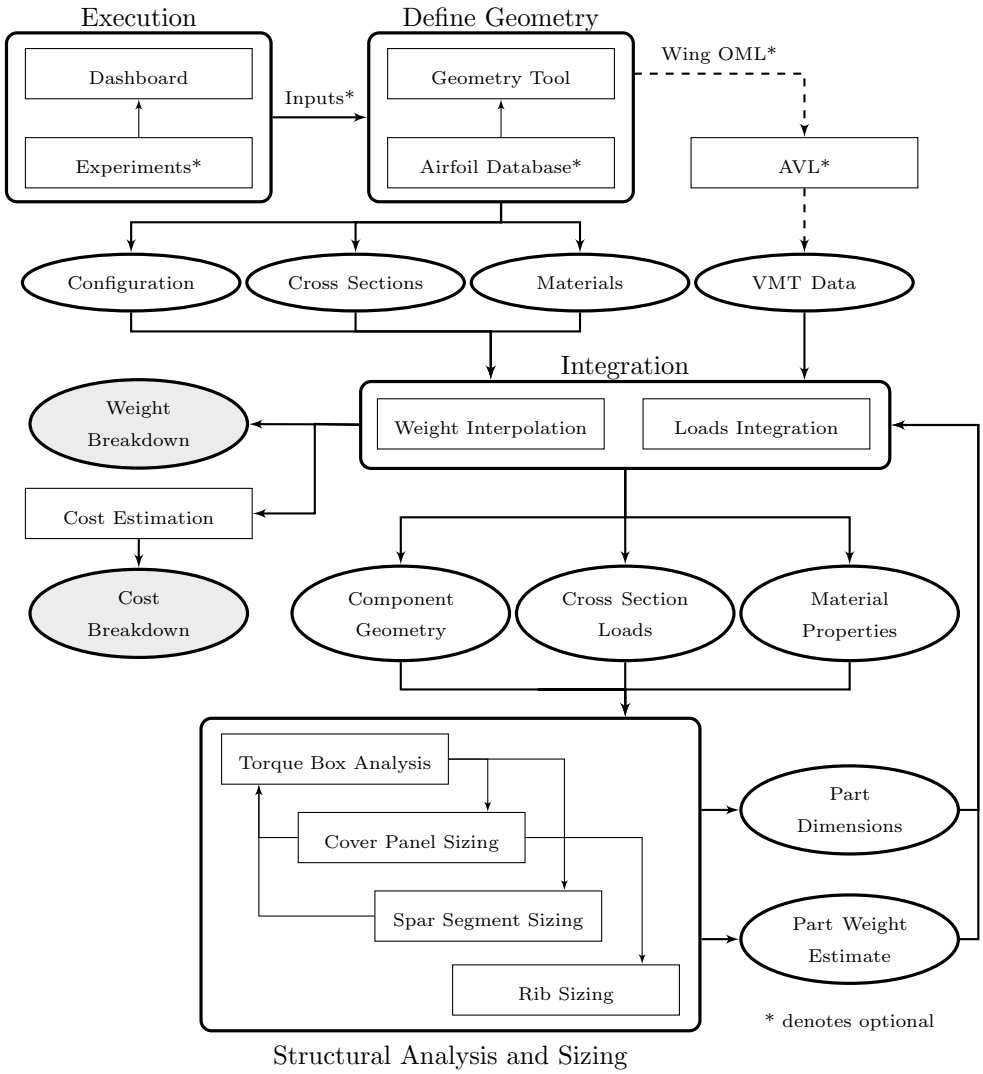


Figure 9: SPANDSET Flow Chart

To perform structural analysis and optimization a toolkit is used. With the goal of automating and parameterizing an already existing suite of substructure analysis tools to enable automated rapid preliminary design phase structural sizing for performing design space exploration, Triumph Aerostructures - Vought Aircraft Division (TAVAD) and Aerospace Systems Design Laboratory (ASDL) at the Georgia Institute of Technology are developing SPANDSET (Structure Preliminary ANalysis

and Design Space Evaluation Toolkit). This toolkit uses classical analysis methods instead of computationally intensive Finite Element Method (FEM) tools to carry out structural analysis and sizing. This trade in fidelity results in a large increase in execution speed and a reduction in design cycle time. The analysis method was developed by Triumph for use in preliminary wing box sizing. ASDL is developing a framework to integrate two important aspects: a multi-level optimization strategy using the Triumph developed tools and methods, and a parametric geometry tool. In SPANDSET, the weight of the entire wing box for a particular substructure layout is calculated by sizing each component using the analysis routines and then reassembled via the multi-level strategy illustrated in Figure 6. After the weight is sized, the cost for the given wing and the resulting substructure layout is calculated using weight, geometric, and manufacturing data.

To illustrate the potential of sacrificing fidelity for exploration, a design space exploration was performed using SPANDSET. The variables selected are shown in Table 2. The ranges selected are conservative because this experiment is merely a proof of concept. They are expressed in terms of a percentage of the change in the positive and negative direction normalized based upon baseline values. Unlike the conceptual problem that this dissertation is focused on, the initial size and shape of the wing has already been decided. Thus, all the variables selected pertain to the substructure positioning or orientation (except for load fraction which is applied to the external loads).

Once the design variables and their ranges were selected a design of experiments was run to create surrogate models that capture the design space. The creation of the surrogate models was necessary because the design cycle time, even though had been drastically reduced through automation, is still on the order of minutes. To perform trade studies the instantaneous results of surrogate models are preferred over the minutes that SPANDSET requires. The surrogate modeling technique used was used

| Name | Variable | Range (%) |
|---|---|---|
| Load Factor | n | 10 |
| Front Spar Root Chord Percent | FS_Chdpct1 | 40 |
| Front Spar Tip Chord Percent | FS_Chdpct2 | 33 |
| Rear Spar Tip Chord Percent | RS_Chdpct1 | 7 |
| Wing Box Ratio | WB_RATIO | 6 |
| Divide Span | MR_DIVIDE | 42 |
| Main Rib Spacing | MR_SPACING | 37 |
| Divide Rib Percent | MR_RIBPct | 77 |
| Stub Rib Spacing | SR_SPACING | 60 |
| Stringer Upper Spacing | ST_USPACING | 50 |
| Stringer Lower Spacing | ST_LSPACING | 38 |
| Percent Chord Orientation | REF_ChdPct | 22 |

Table 2: Design Variable and Ranges

on an Artificial Neural Net (ANNs). Formulating ANNs attempts to create a surrogate model by mimicking the pattern recognition skills of actual neural networks [211]. Using a combination of the ANNs and direct results from SPANDSET several research observations are made. These observations are discussed in the next section.

The data used in this example problem is of a proprietary nature so they have been normalized so that the responses are the percent changes with respect to the baseline values. The calculations are shown in Equation 8. The design variables have been normalized by expressing them as the percent of the range from the minimum. The result is a percentage of the range from the minimum value; 0 percent is the minimum value and 100 percent is the maximum value. The calculations to normalize the design variables are shown in Equation 9.

$$\% \text{ Change} = \frac{Y - Y_{base}}{Y_{base}} \tag{8}$$

$$\% \text{ Range} = \frac{x - x_{min}}{\text{Range}} \tag{9}$$

During the course of the example problem, several important observations were made regarding the substructure design problem. Although the example problem focuses on the wing box substructure design problem, these observations are applicable to other structures design problems. These observations will be discussed in the sections below.

## *2.3 Combinatorially Large Design Space*

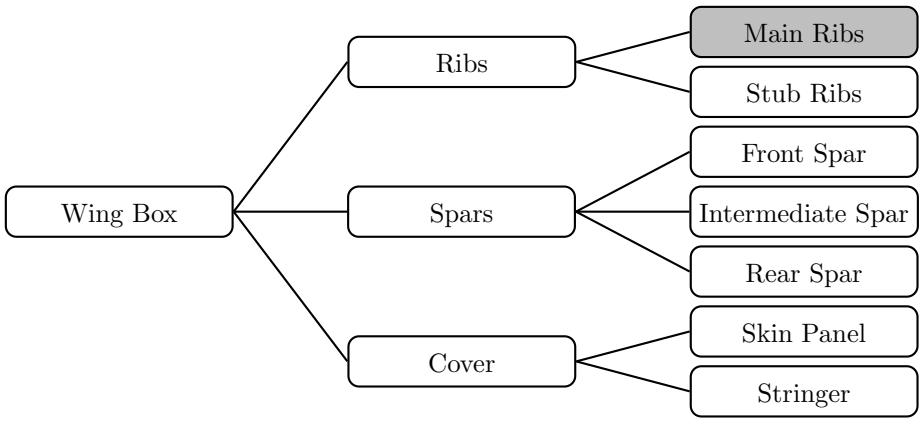


Figure 10: Decomposition of Wing Box Substructure

The best way to illustrate the combinatorially large design space of the wing box substructure design problem is through physical decomposition. The top level of the decomposition is shown in Figure 10. It breaks the wing box into its respective components. The size of the design space at this point is dependent on the number of each component. Additionally, each element requires several geometric details in order to be represented: height, length, location, orientation, etc. If each value is defined individually, then the number of design variables is already on the order of 100. Thus, even for a small number of elements the design space has already become quite large.

So far it has been shown that the problem is quite large due to the number of components. However, there are still several variables associated with sizing the components that must be included. To illustrate this, Figure 11 shows decomposition

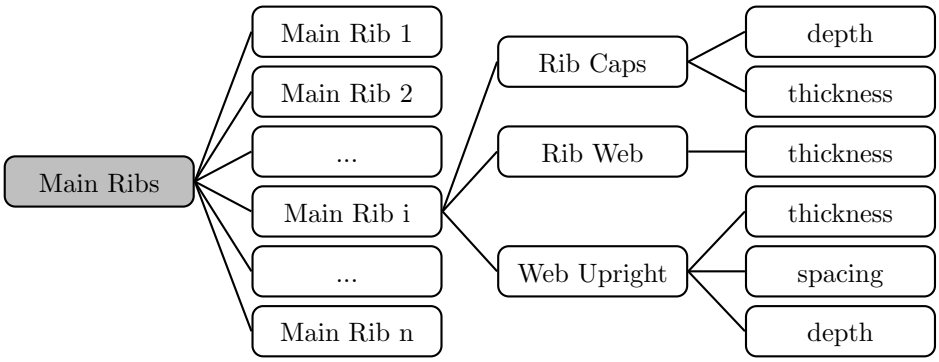


Figure 11: Decomposition of Main Rib element

of a main rib. This figure first decomposes the main ribs into each individual rib. There are $n$ ribs total. The total number of ribs varies between different wing configurations. If the wing is a horizontal stabilizer the number of ribs could be as low as 5. If the wing is for a jumbo jet the number could be as large as 30. Once they are broken down into each individual rib it is then broken down into its features. Each rib is assumed to have the same features, depicted in Figure 71. The number of features ($f$), as well as the number of variables associated with the features, is dependent upon the level of detail desired for the geometry tool. Regardless of how detailed the geometric model is, the component sizing introduces a new set of variables into an already burdensomely large problem.

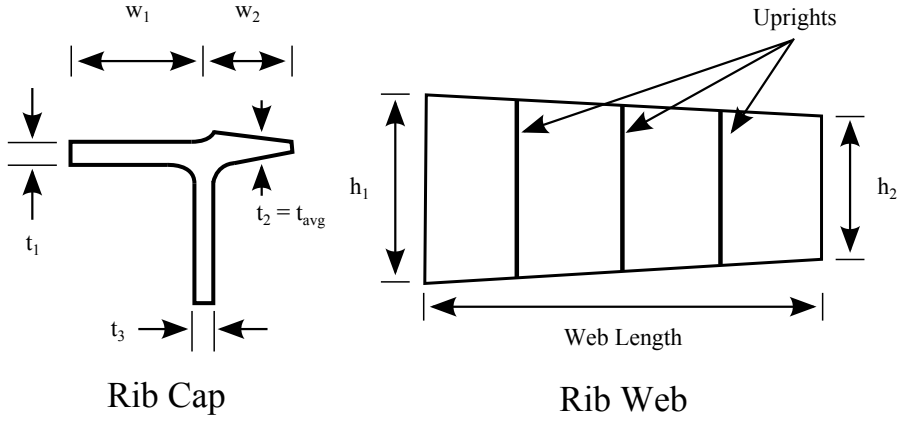


Figure 12: Detailed Drawing of Rib Features

To understand the combinatorial nature of the problem, consider how many design

variables are needed to size all the ribs. There are $n$ ribs with $f$ feature design variables. For the example problem the number of feature variables is 6 ($f = 6$) so that means $6n$ design variables must be selected in order to size the ribs. Each feature then introduces a new set of dimension variables into the problem. The large number of variables means the problem is susceptible to the curse of dimensionality. The curse of dimensionality is a blanket description of the various problems that arise in analyzing and organizing data with high-dimensionality that do not occur with similar low-dimensionality problems [18, 97]. In the example problem the range of values for $n$ is 10 to 17. That means that the number of design variables necessary could be as high as 102 just to size the ribs. This is a large number yet it does not include the other elements of the wing box: spars and covers.

Additionally, the problem runs into issues dealing with consistency. As mentioned before the value of $n$ takes on a range of values. This is because $n$ is dependent on another design variable. The rib spacing is the parallel distance between ribs and defines the number of ribs. As the values of the rib spacing increases the final rib moves further away from the planform root until it passes a point where it can no longer exist within the wing planform. At this point that rib and all the variables that are associated with it are deleted. The opposite occurs as the rib spacing decrease and a rib is added. The fact that the number of design variables changes limits some of the methods that can be used in optimization.

The decomposition leads to the first research observation:

---

**Research Observation 1**

The design space is combinatorially large to the point where the curse of dimensionality will make solving the problem burdensome. In addition the number of design variables is dependent on other design variables and so it changes with every new configuration.

---

## 2.4 Discrete Design Decisions

In addition to the combinatorially large design space there are a number of discrete design decisions that make the design problem more difficult depending upon the level of detail and selections made. The two most influential discrete design decisions in structural design are the configuration of the substructure and the materials used.

### 2.4.1 Configuration Selection

To understand how important configuration decisions are in the design process, examples of different configurations at different levels of the substructure layout are illustrated. First consider the different configurations for the stringer features illustrated in Figure 13. The Z-shape and the J-shape are the most commonly used. To define them, the thickness of the three portions would have to be defined as well as the lengths of the top and bottom caps and the height of the stringer itself. Since the two are so similar it is relatively easy to switch between the two because at most two variables would be added or removed. However, because the stringer can span the entire wing, it is unreasonable to assume that the thickness will be constant from root to tip; thus the thickness and height values may need to be defined at several points along the span of the wing. Additionally, there are a large number of stringers. The result is that these variables may need to be defined hundreds of times. A simple change in the configuration of the stringer features can have a huge impact on the difficulty of the problem. The Z-shape and the J-shape are very similar and so the number of variables needed to define each is similar, but if the configuration changes to a hat-shape even more variables will need to be incorporated. This will make the effect of changing the feature configuration even worse.

Next, consider the configuration decisions that go into each part. Figure 14 illustrates different spar configurations. The example problem uses the built-up web configuration for its spars. The design variables that are specific to this configuration

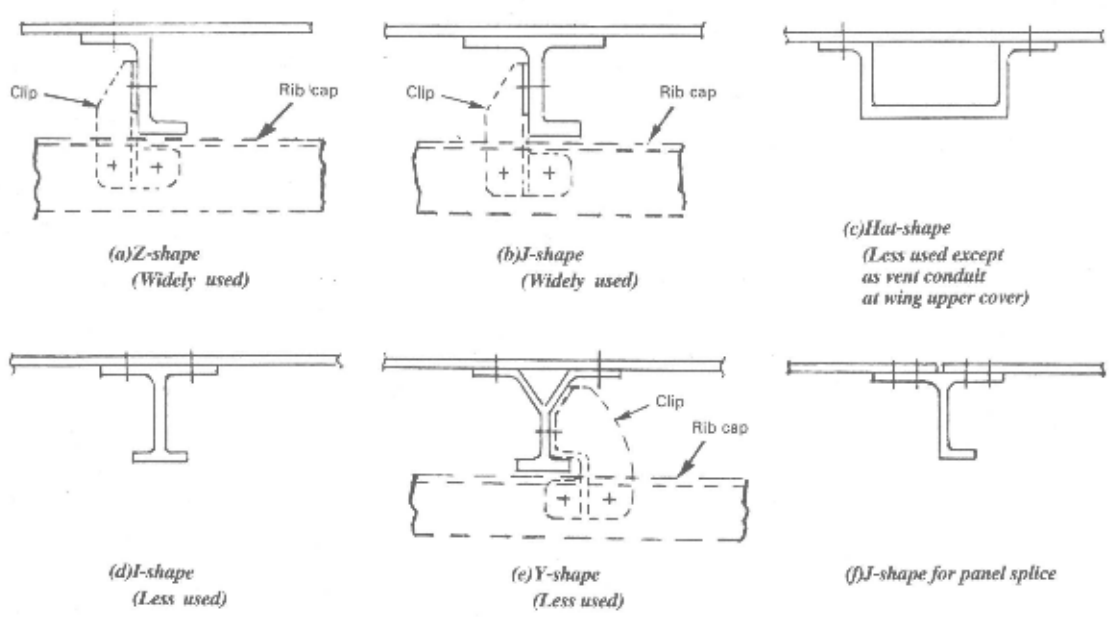


Figure 13: Typical Wing Skin-Stringer Panels [153]

are the spacings between the web uprights; the features of this configuration are the web, web stiffeners, and the spar caps. If the configuration were changed a whole new set of variables and features would be needed, which would change the design problem significantly. Changing the configuration will affect both the number of design variables and the features and their configurations (including the problems mentioned in the previous paragraph). If the built-up web configuration were changed to the built-up truss then the features used in the configuration (web, web stiffeners) would be different (trusses). This change in features then introduces a new set of sizing variables. This is another example of how configuration selections complicate the design problem.

### 2.4.2 Material Selection

A brief literature search on material selection and the methods to perform material selection is included in Section 3.1.2. Here, enough information will be discussed to show why material selection results in discrete design decisions. In every engineering design problem that deals with a physical product a material will need to be selected [69].

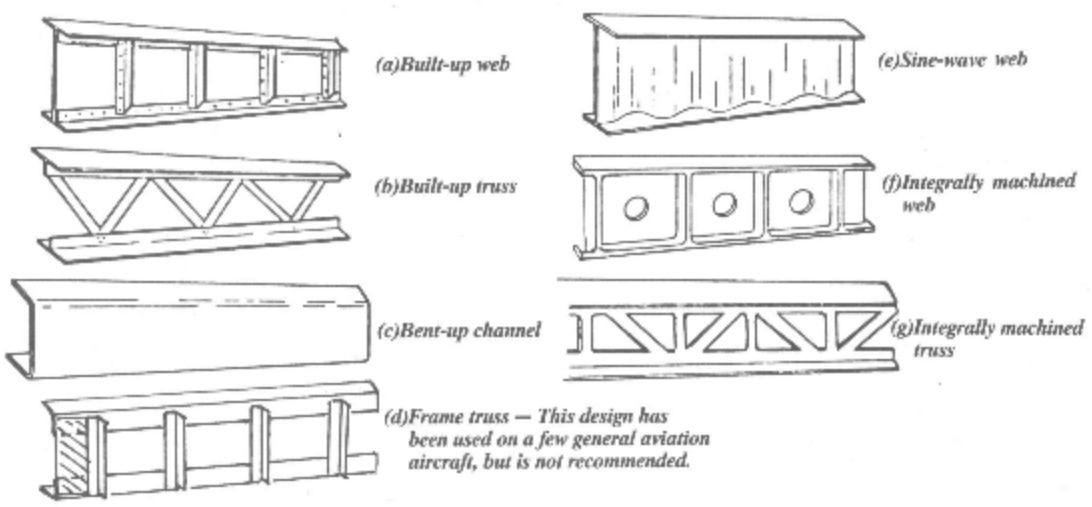


Figure 14: Typical Spar Configurations [153]

The material selection problem is typically a discrete problem in that the material is being selected from a permissible set of entities chosen based on several different design requirements [10, 71]. The reason for this will be discussed later. First a basic understanding of material science and engineering is needed

Material science and engineering is a field of science applying the properties of matter to various design and engineering problems to produce a material with a predetermined set of properties [37]. Materials are engineered by altering either the chemical composition of the material or the process through which the material is made. An example of this is an alloy. The alloy can be engineered by deciding the portions that each element is represented or by altering the various heat treatments or the age-hardening process [89, 165, 205]. It is through material science and engineering that many of the materials commonly used were first introduced into aerospace engineering. For instance most aluminum alloys were created to replace existing materials used throughout industry [205], and composite materials were introduced for their specific directional capabilities [177]. By altering these properties the material scientist can take a finite number of elements and turn them into a wide variety of engineering materials with a range of property values like those shown in Figure 12.

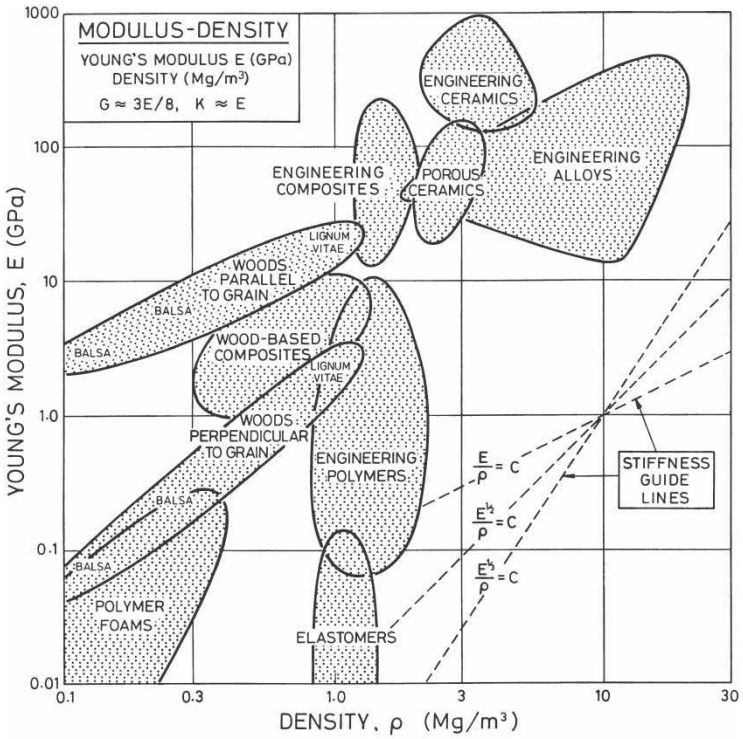


Figure 15: Material Property Chart [209]

Due to advances in manufacturing technologies and material concepts, an aerospace engineer has a wide variety of lightweight materials to choose from [38]. Yet, material selection ends up being a discrete design problem in that the materials are limited to a library of materials to choose from rather than designing or optimizing a material along with the product [11, 71]. The reasons for this are as much economical as practical. For practical purposes this is done because the coupling of the material selection and the configuration of the structure as a result of the constitutive behavior of materials [11, 17]. This coupling results in material selection and its methods evolving with the design [59, 71]. In the early stages of design simple comparisons of ideal material parameters are used to rank the materials [59, 173]; only towards the end of the design process is there enough detailed configuration data to tailor a material using material engineering as previously discussed [164].

The economic reasons for limiting the design to a discrete design problem are risk and business related. It is risky to make decisions based on introducing never before

used technologies, like new materials [164]. This motivates designers, especially in the aerospace industry, to opt for more conservative material selection; choosing from a list of previously used materials to eliminate the risk of costly redesigns [150]. Another reason for using a library is that aerospace engineers are not material engineers. To incorporate material engineering into an aerospace company would require additional man power and overhead. This is why these tasks are outsourced to other companies [87]. It is a more efficient business model to design materials based on the common needs of several similar design problems throughout industry and market them as a list of product they offer [16, 154].

Research into configuration and material selection lead to the following observation:

---

**Research Observation 2**

The structures design problem includes several discrete design decisions. These discrete design decisions are most prevalent in the configuration and material selections.

---

## *2.5 Highly Constrained Non-linear Structural Analysis*

SPANDSET uses analysis routines to size each component separately. These analysis routines apply failure and manufacturing constraints to a structural optimization problem for each feature of each component. Like most of structural analysis, the equations for the constraints are often highly non-linear because several non-linear equations are combined into one non-linear constraint. The reason for this is the general practice of using margins of safety [5, 43, 72, 73]. The term margin of safety is discussed in Section 3.3.2.1, but a brief description will be provided here for convenience. Margins of safety consists of a ratio of the stress or force at which point the structure fails (failure strength) and the loads that the structure is designed for (limit load).

The equation for margin of safety is shown below.

$$\textbf{Margin of Safety} = \frac{\text{Failure Strength}}{\text{Limit Load}} - 1 \tag{10}$$

A margin of safety can be thought of as a measure of the structure's ability to handle additional loads beyond what it was designed for. A value greater than zero means that when the structure is subjected to the design loads it will not fail. Margins of safety are used as a way to handle uncertainty during design by making sure that the structure is able to handle loads greater than the design loads should the need arise. This is done by making the margin of safety constraint some value greater than zero.

The equation for margin of safety is a non-linear equation. It will be characterized by a range of values from very large to very small. Additionally, the equations for $FailureStrength$ and $LimitLoad$ are also non-linear equations for most loading conditions. An example is the Euler buckling load from Chapter 3. It has been shown that the equation for the critical buckling load of a thin plate is a non-linear equation [17, 25] based upon the material properties and dimensions of the plate. In addition the limit load from Equation 10 is based on the external loads. To calculate the stress in the rib web due to the bending moment there will be a non-linear term $M/EI$ used. This combination of non-linear equations in an already non-linear equation will result in a highly non-linear set of equations.

When these highly non-linear margin of safety constraints are applied to the sizing problem, a large portion of the design space is eliminated. The likelihood of this happening increases as more constraints are added. There are multiple constraints for each analysis routine; thus, it is expected that a large portion of the sizing design space will be eliminated for each analysis routine. To further investigate this, an experiment is run in an attempt to quantify the degree to which the design space is constrained. A 20,000 design of experiments (10,000 Latin Hyper Cube, 10,000 Monte Carlo) is used to evaluate points using each of the analysis routines in SPANDSET. For each point the structure is analyzed but not sized so that each point is assessed

for feasibility. There are three such analysis routines: the cover analysis, the spar segment analysis, and the rib analysis. However, for brevity only the rib analysis routine will be shown.

Figure 16 shows a plot of 5,000 (the full amount is too many for graphing) randomly sampled points from the 20,000. The y-axis of the plots display the calculated value of of the margin of safety of the upright web column. The values ranged from $10^{-4}$ to $10^{4}$; thus, the y-axis is plotted on a log scale. The x-axis of each plot represents one of the 12 variables that effects the margin of safety of the upright web column. These variables include the loads that effect the margin of safety, several rib sizes required to calculate the margin of safety, and the dimensions that the margin of safety will size. In Figure 16 no constraints have been applied. Figure 17 shows the same set of points after the constraint on the margin of safety has been applied. Typically when enforcing this constraint a value greater than zero is used, but for this experiment the most conservative value of zero is used to assess feasibility in order to illustrate how constrained the design space is. At this point the number of points eliminated from the initial 20,000 can be counted. With just one constraint 17.33% of the design space has been eliminated. More points will be infeasible when the rest of the constraints are applied. There is only one additional constraint for the rib analysis. The second constraint (the margin of safety for the moment of inertia required) eliminates more points after the first constraint has already been applied. These points are represented as the gold points in Figure 17. When this constraint is applied by itself it is responsible for eliminating 34.99% of the design space, but many of these points overlap with the other constraint. When both constraints are applied simultaneously 47.56% of the design space is eliminated. Thus, the degree to which the rib sizing problem is constrained has been quantified.

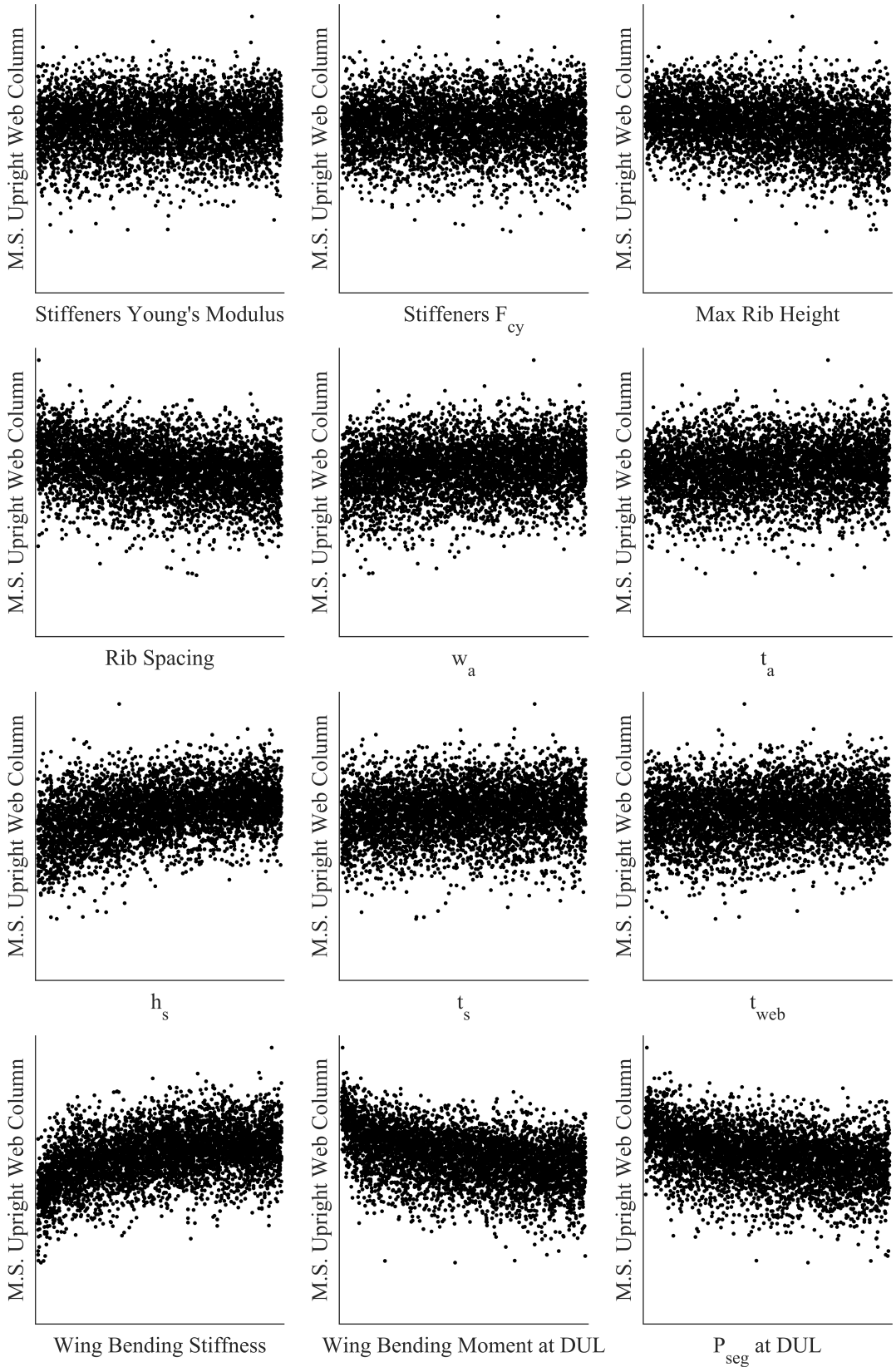


Figure 16: Margin of Safety of the Upright Web Column Design - Unconstrained

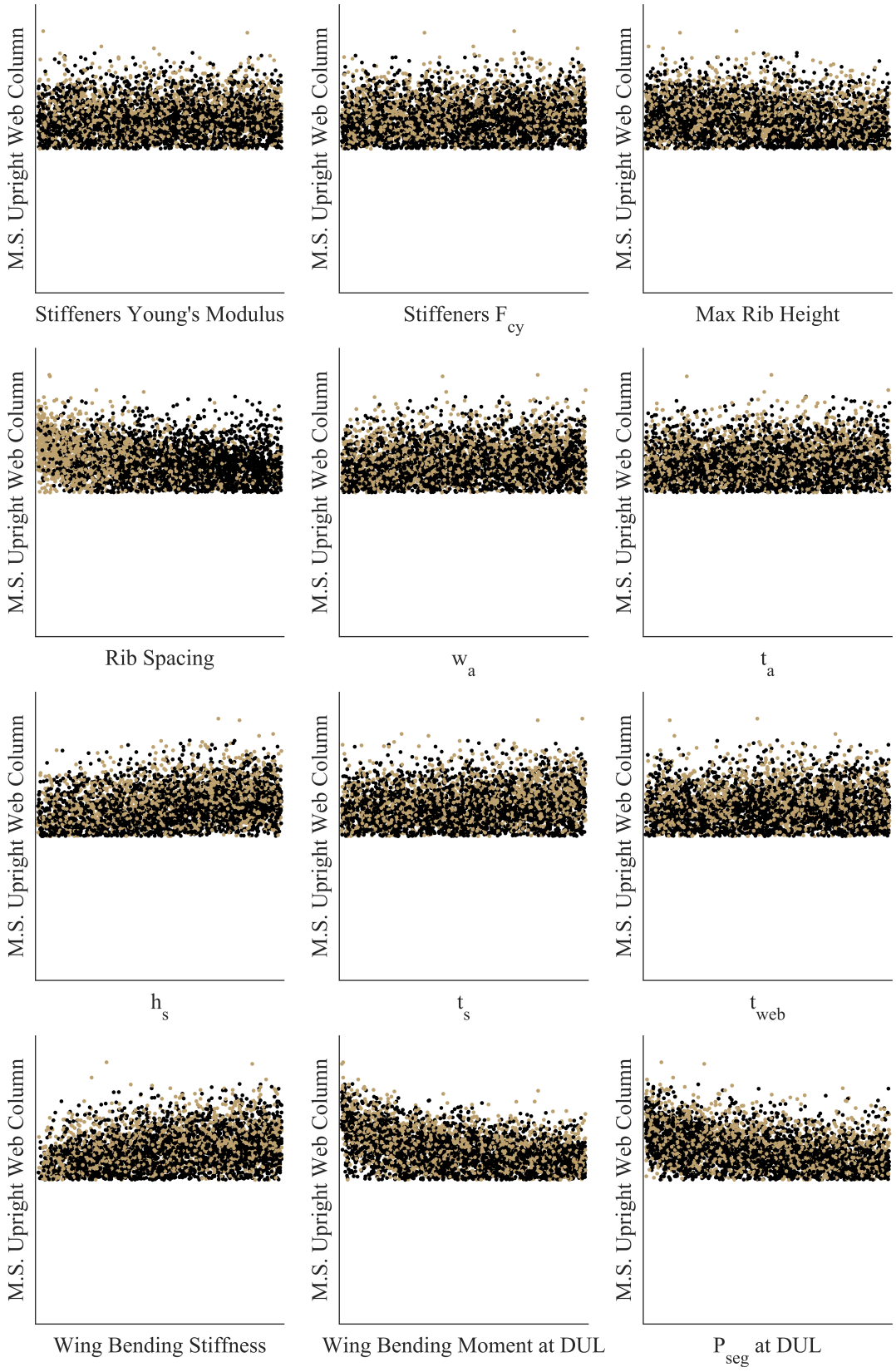


Figure 17: Margin of Safety of the Upright Web Column Design - Feasible Region

This experimental procedure is repeated for each of the analysis routines. The results are shown in Table 3, Table 4, and Table 5. The first column lists the percentage of variables that affect the margin of safety. The second column list the percent of point eliminated by each margin of safety individually. The final column shows the number of points eliminated by each margin as the margins are applied from top to bottom. Several of the values in these columns are zero or near zero. This does not mean the constraint has no affect on the feasibility of the problem. Instead, it is an outcome of the order in which the margins were applied. The final row represents the percentage of points eliminated by all the margins of safety for each analysis routine.

Table 3: Highly Constrained Results - Rib Analysis

| Constraint | # Variables | Failed (%) | Total Fails (%) |
|---|---|---|---|
| M.S. Moment of Inertia Required | 11 | 34.99 | 34.99 |
| M.S. Upright Web Column | 12 | 17.33 | 12.57 |
| Total | - | - | 47.56 |

Table 4: Highly Constrained Results - Cover Analysis

| Constraint | # Variables | Failed (%) | Total Fails (%) |
|---|---|---|---|
| M.S. Skin Buckling | 7 | 37.71 | 37.71 |
| M.S. EJ + Shear Interaction | 18 | 37.44 | 10.22 |
| M.S. Column Stability (Johnson-Euler) | 13 | 25.88 | 0.00 |
| M.S. Damage Tolerance | 10 | 13.03 | 1.52 |
| M.S. Section Crippling | 12 | 12.01 | 0.00 |
| Total | - | - | 49.44 |

Table 5: Highly Constrained Results - Spar Analysis

| Constraint | # Variables | Failed (%) | Total Fails (%) |
|---|---|---|---|
| M.S. Web Moment of Inertia Required | 9 | 67.67 | 67.67 |
| M.S. Lower Cap Column | 18 | 48.66 | 18.33 |
| M.S. Upper Cap Column | 18 | 48.23 | 6.31 |
| M.S. Upper Cap DDT | 7 | 34.14 | 1.94 |
| M.S. Lower Cap DDT | 7 | 33.52 | 1.36 |
| M.S. Web Shear Rupture | 16 | 29.00 | 2.08 |
| M.S. Lower Cap Max Compression | 17 | 28.14 | 0.01 |
| M.S. Upper Cap Max Compression | 17 | 27.93 | 0.01 |
| M.S. Lower Cap Crippling | 18 | 22.34 | 0.00 |
| M.S. Upper Cap Crippling | 18 | 22.22 | 0.01 |
| M.S. Web Force Crippling (Shear) | 21 | 20.36 | 0.07 |
| M.S. Web Upright Column | 21 | 16.81 | 0.01 |
| M.S. Web Crippling Cutoff | 21 | 10.00 | 0.00 |
| Total | - | - | 97.78 |

For each analysis routine at least 45% of the design space is infeasible. For the spar analysis less than 3% of the design space is feasible. This is due to the combination of the non-linear analysis and the numerous constraints. One thing that could cast doubt on the results is that the ranges for the design of experiments may have been set too large and many of the points are eliminated because the inputs make no sense. This is not the case. Figure 17 shows there are feasible results along the entire range for every variable. This emphasizes that the infeasible points are not a result of one variable but the combination of variables. Thus, the number of failed cases is independent of the range of the variables that affect the constraint. It should also be noted that these results do not necessarily mean that an optimized result cannot be obtained. These are merely initial points, and the numerical optimization problem for each analysis routine is relatively simple to solve. For the Spar Analysis, which has over 97% of its design space rendered infeasible by the constraint, the optimization problem almost

always converges to a result.

From these results the following research observation is made:

---

**Research Observation 3**

Due to the highly non-linear nature of structural analysis, a large portion of the design space for each analysis routine is rendered infeasible when the numerous constraints are applied.

---

## *2.6 Multimodal Design Space*

In this section a simple experiment is used to illustrate that the design space is multimodal. The experiment uses one hundred initial points to minimize the total wing box weight using the variables in Table 2 as the design variables. The initial points were selected using a 100 point Latin Hyper Cube which gives a better distribution across the design space than randomly selecting values [140]. A gradient-based optimizer was then used to minimize the total wing box weight that is represented by the ANN surrogate model created in previous research. The results are shown in Figure 18 and Table 6.

Figure 18 is a scatter plot of all the initial points, represented as circles, and the final optimized point, represented as a square. The squares and circles that are white represent the first possible outcome of optimization; the squares and circles that are black represent the second possible outcome of the optimization. Table 6 contains the final design variable values, the final outputs from the optimization, and a baseline value to compare it with. The data is normalized according as described in Section 2.2 and the variables are the same as those listed in Table 2.

The results show that two different optimum values were found; thus the design space is multimodal. However, there are several factors that may cast doubt upon this observation and its importance to the design problem. The first factor is that the

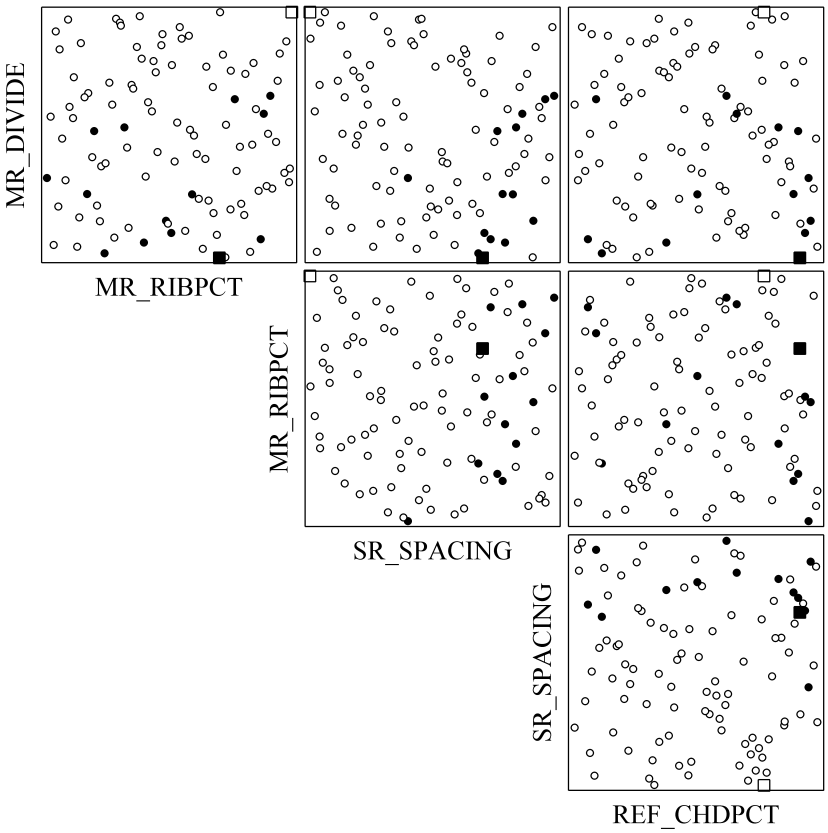


Figure 18: Multimodal Scatter Plot

second optimized value has much fewer initial values implying that the results could be due to noise or algorithm errors. The second factor is that there is no discernible relationship between the initial points and the optimized values. The black circles are distributed throughout the white circles and at times are further from the black square than the white square. These factors may cast doubt upon the validity of the optimization. To verify that the second optimized value is in fact a minimum of the objective function a screening test is run. The ANN surrogate model for weight will once again be used to calculate the objective function across the entire range of each design variable with different optimized value in Table 6. Each variable will be treated one at a time and the other design variables will be set to their optimized values. The results are plotted in Figure 19.

From the screening test we can see that both results from the optimization are in

Table 6: Multimodal Optimization Results

| Variables | Baseline | Opt. 1 (%) | Opt. 2 (%) |
|---|---|---|---|
| FS_CHDPCT1 | 25.40 | 100.00 | 100.00 |
| FS_CHDPCT2 | 51.24 | 100.00 | 100.00 |
| MR_DIVIDE | 50.42 | 100.00 | 0.00 |
| MR_RIBPCT | 15.25 | 100.00 | 70.45 |
| MR_SPACING | 32.50 | 0.00 | 0.00 |
| RS_CHDPCT1 | 80.90 | 0.00 | 0.00 |
| SR_SPACING | 28.89 | 0.00 | 70.39 |
| ST_LSPACING | 33.33 | 0.00 | 0.00 |
| ST_USPACING | 22.22 | 0.00 | 0.00 |
| WB_RATIO | 8.77 | 0.00 | 0.00 |
| REF_CHDPCT | 65.21 | 77.70 | 92.31 |
| Objective Function | - | -15.21 | -15.09 |

fact minima of the objective function. It also reveals a possible cause of the multiple optimization solutions. For two variables the slope and general shape of the screening test remains the same. The values change slightly as one end curves up or down by comparison. However, for the other two variables the slope is completely reversed and the values switch from maximum to minimum or minimum to almost maximum. This change in slope is due to correlations between the design variables. This is the cause of the multimodal nature of the design space.

Another factor that may cast doubt on the importance of the multimodal nature of the design space on the design problem is the final optimized responses. They are separated by about one tenth of a percent. In addition from Table 6 we can see that only four of the eleven design variables change. This may lead to the conclusion that the two outcomes are so similar that there is no need to differentiate between them. This conclusion is false. The reason is that the problem is a multi-objective problem, as will be discussed in the next section. Though there may be a small difference in

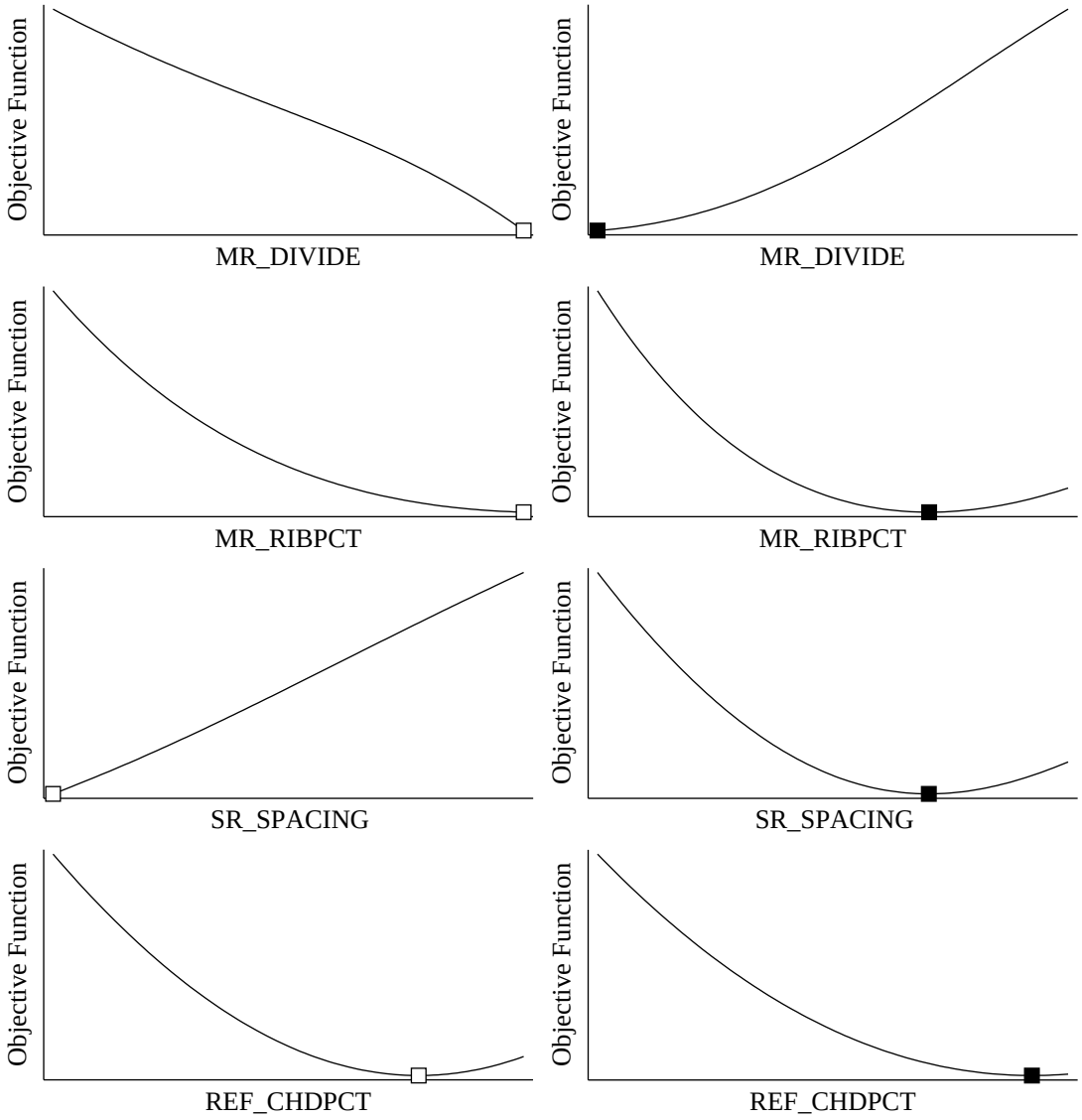


Figure 19: Multimodal Screening Test

weight the difference in cost could be large. As for the design variables, they may be similar values but they produce very different geometries. The geometries for the two optima are shown in Figure 20. The main difference between the two geometries is the division between the number of stub ribs (inboard ribs parallel to fuselage) and the number of main ribs (outboard ribs with user defined orientations). In the first optimum the divide rib is located closer to the wing root. This results in less stub ribs and more main ribs. The opposite is true for the second optimum. In addition, the

second optimum has more ribs than the first. So even though the resulting weights are different there is clearly a difference in the geometry which will propagate throughout the rest of the design.

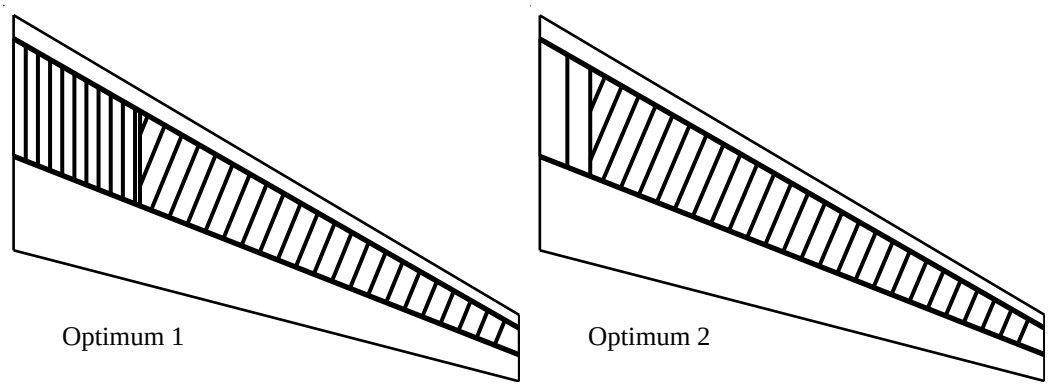


Figure 20: Multimodal Geometries

The results discussed in this section lead to the following research observations:

---

**Research Observation 4**

The multimodal nature of the design problem makes the design process more difficult. It cannot be assumed that numerical optimization will result in the same output for any initial point; thus, the design space will need to be explored thoroughly in order to identify all the local minima of the objective function.

---

## *2.7 Multi-Objective Design Problem*

One of the motivations of this thesis listed in Chapter 1 is to include life cycle cost in the early stages of design. This means that both the weight and the cost of the aircraft must be taken into account. The result is that the problem is a multi-objective problem. This observation is trivial if optimizing the two objectives results in the same outcome; if minimizing cost also minimizes weight then no additional considerations need be given to the problem. But for the wing box, and even structures in general, the trade between weight and cost is well documented [80, 104, 171]. This means that

multi-objective optimization (MOO) will need to be utilized.

Section 5.3.1 discusses the basic concepts of MOO. However, this section introduces enough information to understand the example. The example to be carried out illustrates how the problem is multi-objective and what effect this will have on the design methodology used. For the example the weighted sums method for MOO is used along with the ANN surrogate models mentioned earlier. The objective function is listed in Equation 11:

$$F(\bar{x}) = w_1 \cdot \text{Weight}(\bar{x}) + w_2 \cdot \text{Cost}(\bar{x}) \tag{11}$$

$$1 = w_1 + w_2 \tag{12}$$

In Equation 11 the design variables $\bar{x}$ are selected to minimize the the objective function and the $Weight$ and $Cost$ function are normalized so that the much larger cost value does not dominate the weight values. For this example the values $w_1$ and $w_2$ will be run with values between 0 and 1 such that Equation 12 is satisfied. The design variables are those variables shown in Table 2.

The results are shown in Figure 21. The weight and cost are graphed on the same scale for convenience but they do not have the same values. As expected the weight and cost are at their largest value when their respective weightings are at 0, meaning that response is not being considered in the optimization. Likewise they are at their lowest value when their weightings are at 1, meaning only that response is being considered in the optimization. The design variable values and their associated responses are shown in Table 7. The values are once again normalized because of the proprietary nature of the research. Both the results and design variables are normalized in the same manner as discussed in Section 2.2.

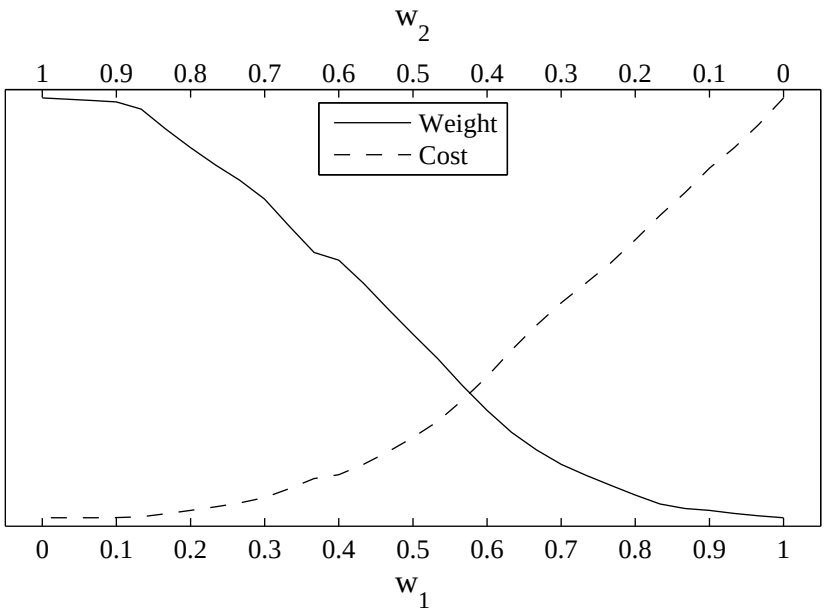


Figure 21: Multi-Objective Weight/Cost Trade-Off

The data shown in Table 7 illustrates what makes a multi-objective design problem difficult. It establishes a relationship between the weight and cost. For instance using data from Table 7 the maximum and minimum optimal values can be determined. Any value greater than the minimum value can be considered a penalty to that response. Following this logic it would be easy to associate the cost penalty of decreasing the overall weight. A similar analysis can be performed for decreasing the cost. This means there is no way to improve one response without worsening the other response. This behavior is common in MOO and is called Pareto optimal. Pareto optimal is when one response can not be improved without degrading any other responses. The set of all existing Pareto optimum points is called the Pareto Frontier.

Table 7: Multi-Objective Optimization Results

| $w_1$ | 1 | 11/15 | 1/2 | 4/15 | 0 |
|---|---|---|---|---|---|
| $w_2$ | 0 | 4/15 | 1/2 | 11/15 | 1 |
| FS_CHDPCT1 | 100.00 | 100.00 | 100.00 | 100.00 | 100.00 |
| FS_CHDPCT2 | 100.00 | 100.00 | 94.84 | 100.00 | 100.00 |
| MR_DIVIDE | 100.00 | 48.29 | 64.21 | 65.25 | 68.32 |
| MR_RIBPCT | 100.00 | 77.04 | 27.55 | 0.00 | 0.00 |
| MR_SPACING | 0.00 | 0.00 | 67.10 | 100.00 | 100.00 |
| RS_CHDPCT1 | 0.00 | 0.00 | 0.00 | 0.00 | 0.00 |
| SR_SPACING | 21.54 | 49.95 | 100.00 | 100.00 | 100.00 |
| ST_LSPACING | 0.00 | 13.88 | 39.09 | 74.73 | 100.00 |
| ST_USPACING | 0.00 | 36.82 | 67.74 | 100.00 | 100.00 |
| WB_RATIO | 0.00 | 0.00 | 0.00 | 0.00 | 0.00 |
| REF_CHDPCT | 97.16 | 100.00 | 100.00 | 100.00 | 100.00 |
| MR_ZPCT | 0.00 | 0.00 | 0.00 | 0.00 | 0.00 |
| ST_YPCT | 0.00 | 11.92 | 18.17 | 27.93 | 35.17 |
| Weight | -14.75 | -11.61 | -1.19 | 11.32 | 16.26 |
| Cost | -7.29 | -25.76 | -41.13 | -48.06 | -49.15 |

The responses are not the only values of interest in Table 7. The optimized design variable also reveals how the multi-objective design problem makes the design process more difficult. About half the variables assume the same value regardless of optimizing for cost, weight, or anywhere in between. The rest of the variables will change values based upon the weightings. Some of these variables are shown in the Pareto Frontier in Figure 22. These plots show that because of the continuous values of the weightings the design variables can take on multiple values. The design variable tends to start at either its maximum or minimum values and the majority of the optimal values will occur at these points. This is because the data is being pulled from a proof of concept experiment; thus, the ranges were kept relatively small. If the ranges were increased the general curve formed in the middle of the Pareto Frontiers would likely continue

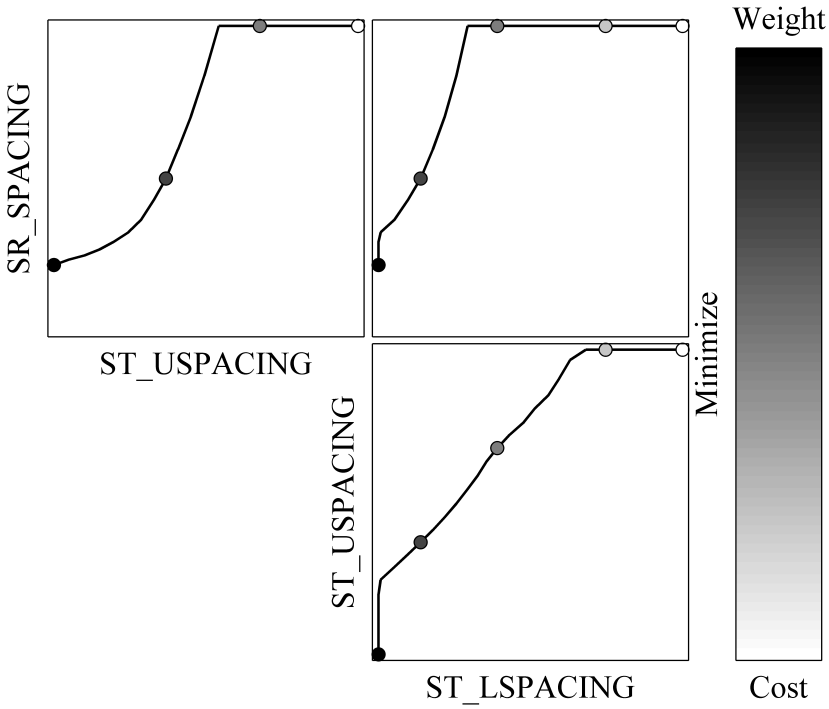


Figure 22: Multi-objective Pareto frontier

in this manner. Despite the small ranges it can still be deduced that because of the multi-objective problem the design variables can take on different values. If this were not the case selecting these design variables automatically would be a trivial matter, but instead there will likely need to be direct involvement in selecting the appropriate design. This leads to the research observation:

---

**Research Observation 5**

The multi-objective nature of the design problem is non-trivial. Significant effort will have to be taken to implement multi-objective design optimization as well as identify how much is willing to be sacrificed from the responses to improve the other response.

---

## 2.8 Discontinuous Design Space

The design space of a structural layout problem is inherently a discontinuous design space meaning that the responses as a function of the design variables have discontinuities. The discontinuities are due in part to the discrete design decision discussed in Section 2.4. If a new material is selected or a different configuration is chosen, a discontinuous jump in the responses would be expected. However, the majority of the discontinuities are due to continuous design variables applied to disjointed responses. Figure 23 is used to illustrate this point. In Figure 23 the design variable is the main rib spacing. This value is the perpendicular distance between each of the main ribs. As the value increases the distance between the ribs increases until the last rib is no longer able to fit on the wing box and is removed. The configuration on the left of Figure 23 has a smaller main rib spacing and a larger number of ribs. As the main rib spacing is increased in the center configuration in Figure 23, the final main rib moves closer to the tip. Finally, in the right configuration in Figure 23 the final rib cannot fit in the wing box as it has moved beyond the span. The rib is removed so there is one less rib that needs to be accounted for in the total weight and cost of the wing box.

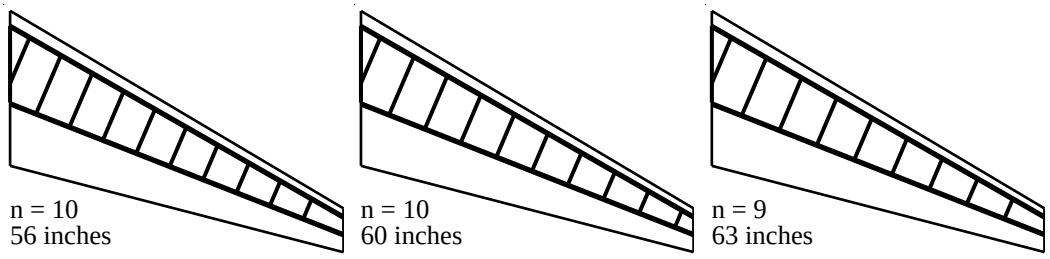


Figure 23: continuous variable applied to disjointed response

A small experiment is used to illustrate what the effects are of the continuous design variable on the responses. For the experiment a range of the upper stringer spacing was selected. Values along the range were identified where a stringer is either added or removed (two values, one on each side). Finally, points are evenly distributed between these values, including the values themselves. All of these values were then

input one at a time into a baseline configuration and used to run SPANDSET to calculate various weights and costs for the resulting wing box configuration.

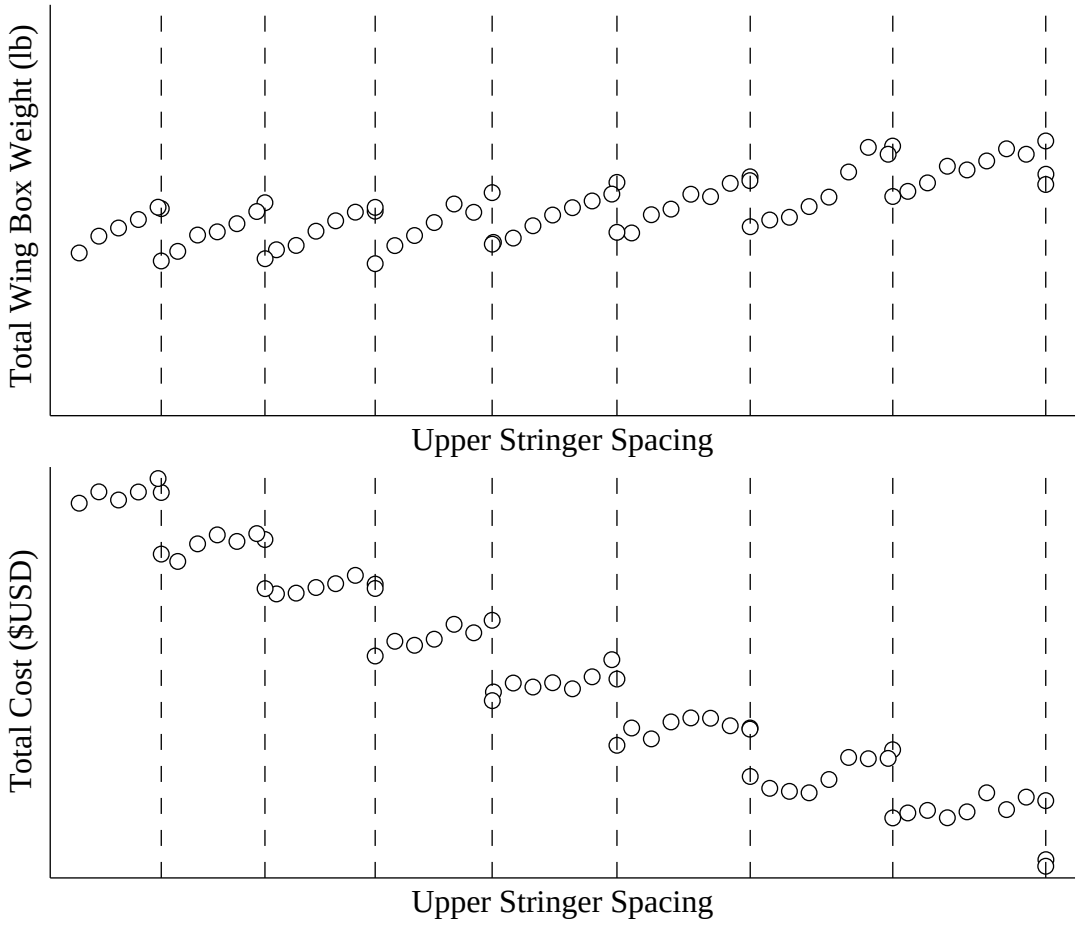


Figure 24: Wing Box Weight and Cost vs Upper Stringer Spacing

Figure 24 shows the resulting total cost and total weight of the wing box for the experiment. In Figure 24 the dotted lines represent the values of the upper stringer spacing at which point a stringer is either added or removed. In the figure it may appear that two points lay on this dotted line. Actually, these two points lay on either side of the dotted line with values separated by only one thousandth of an inch. Even though there is such a small difference between these two points there is a noticeable jump in the responses from one point to the next. This jump is made more noticeable by the fact that the points in between the dotted line have a linear trend. This discontinuous behavior can be seen throughout the design problem.

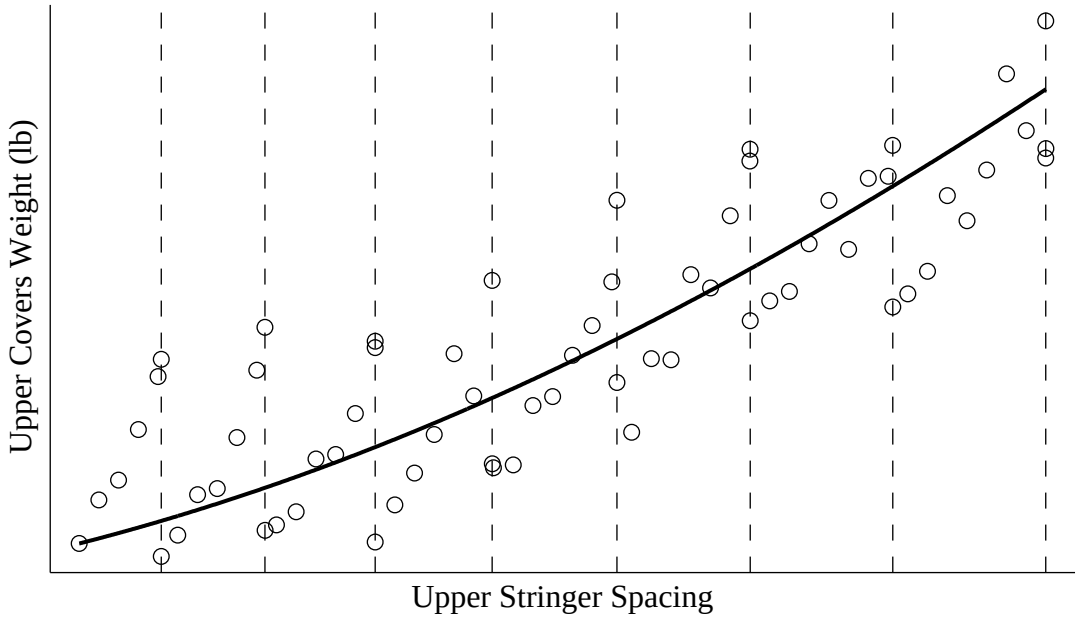


Figure 25: Wing Box Upper Cover Weight vs Upper Stringer Spacing

The fact that the design space is discontinuous has a large effect on the previous two observations. Numerical optimization is discussed in Chapter 3. This discussion states that a convex set is needed to find a unique optimum. If the set is not convex there can still be an optimum but there will likely be more than one and the local optima will have to be compared to find the global optimum. From Section 2.6 it has already been shown that the design space does have more than one local minimum. This observation was made based upon an ANN surrogate model created from a previous design of experiments run through SPANDSET. This model is represented by the line in Figure 25 which is adjusted for the error between the actual values and the surrogate model. This figure illustrates that the surrogate model does not capture the discontinuities. It instead creates a smooth response with fewer local minima than the actual response; thus, the previous two observations were made without these additional local minima. This means the multimodal nature of the design space will be exacerbated by the discontinuities. As it has already been shown that these discontinuities exist for both the weight and the cost, these same problems will also

make the multi-objective problem more difficult to solve.

The result of the experiment leads to the final research observation:

---

**Research Observation 6**

The discontinuous nature of the design space complicates the already multimodal and multi-objective design problem.

---

## *2.9 Summary*

In this chapter the following research observations were made:

- RO1: Combinatorially Large Design Space (Section 2.3)
- RO2: Discrete Design Decisions (Section 2.4)
- RO3: Highly Constrained Non-Linear Analysis (Section 2.5)
- RO4: Multimodal Design Space (Section 2.6)
- RO5: Multi-objective Design Problem (Section 2.7)
- RO6: Discontinuous Design Space (Section 2.8)

These observations have been discussed individually; however, a larger observation can be made bout the design problem when looking at several of them together. Previously, the multimodal nature of the design space was discussed (Research Observation 4). Multimodal design problems are difficult to solve using linear optimization because there is no guarantee that the minimum local minima has been found. To solve this different optimization solutions will need to be compared for several different initial values. The problem is further compounded by the fact that the design space is discontinuous (Research Observation 6). The discontinuities will increase the number of local minima; thus, more cases will need to be investigated. Furthermore, the multi-objective design problem (Research Observation 5) required that more cases be run to compare designs using different weightings for the objectives, and the discrete

design decisions (Research Observation 2) cannot be addressed mathematically but only through enumeration of the options. Each new observation made about the design problems leads to the conclusion that more analysis executions are required; however, the cumulative effect of each observation compounds the number of executions required substantially. This leads to the following proposition:

---

**Framework Proposition 1**

Due to the complex & discontinuous nature of the physics-based structural analysis design space, a strategy of exploration requiring a large number of analysis executions will be required.

---

# CHAPTER III

# STRUCTURAL DESIGN, ANALYSIS, & OPTIMIZATION

Chapter 1 established the overall problem to be addressed. An overall research objective was proposed and then decomposed into four research objectives. The first objective focuses on studying current structural analysis and optimization methods for use in the conceptual design phase.

---

**Research Objective 2**

Compare current structural design, analysis, and optimization methods based upon metrics that will identify which methods are most appropriate for the conceptual design phase.

---

In this chapter a literature survey of structural design, analysis, and optimization will identify different methods that will satisfy the overall research objective. The principles of structural design, structural analysis, and structural optimization and how they relate to each other will be discussed. Then, a further breakdown of each subject will identify several methods that could be used in addressing the overall research objective. Additionally, metrics to compare the methods will be introduced. These metrics will be used to assess the different methods and identify which ones will be appropriate for the conceptual design phase. Structural design, analysis, and optimization have many applications across all fields of engineering and design. For this literature search the scope is limited to methods that can be applied to an airplane wing.

## *3.1 Structural Design*

Structural design is a design problem found in many fields of engineering [24, 111, 143, 172] which combines the concepts of structural analysis [17], structural optimization [86, 108], and engineering design [60]. **Structural Design** is the process of defining a structure (configuration, materials, and dimensions) to withstand the design loads that it is subjected to without failure [108, 153]. Structural design typically incorporates aspects of multi-disciplinary analysis, modeling & simulation, material science, and optimal design. The combination of all these advanced concepts makes structural design a complex problem; therefore, a brief description of the basic elements of structural design will be provided below.

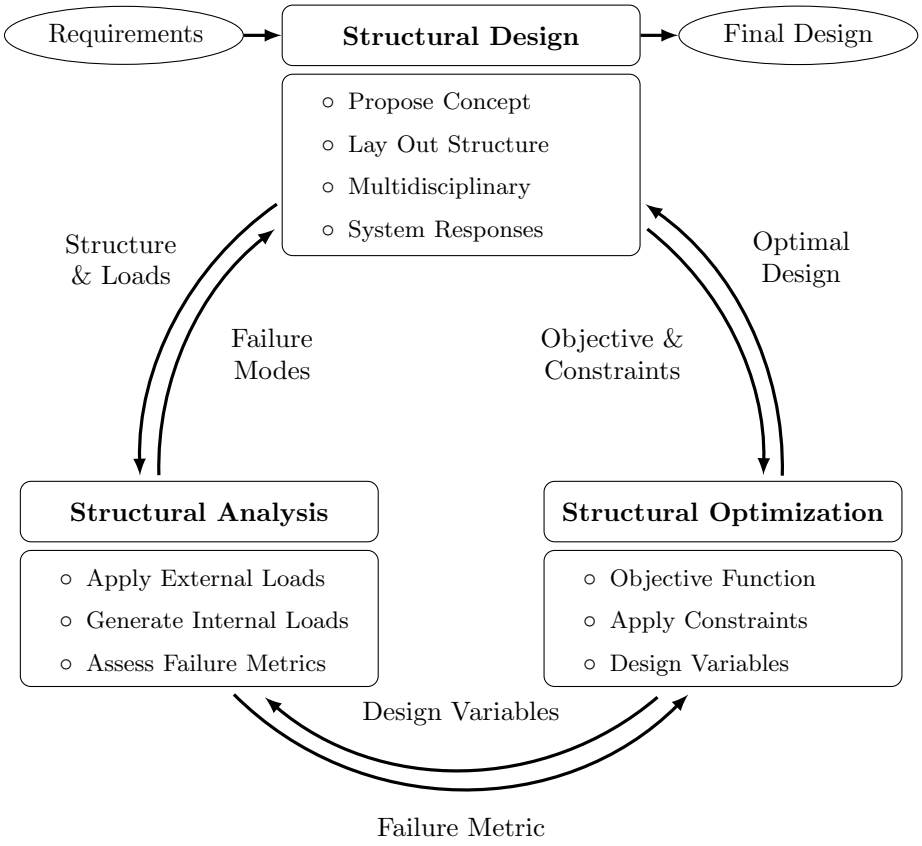


Figure 26: Structural Design Process

Figure 26 depicts the basic elements of structural design. The design process begins with a list of requirements. For aerospace structural design, these requirements

can be expressed as mission requirements (e.g. payload weight and dimensions), size constraints (e.g. wing span limited by airport), load conditions [174], and regulations [73]. The entire structural design process is highly dependent on the sub-problems structural analysis and structural optimization. Structural analysis calculates the internal loads of a structure subjected to external loads and assesses whether the structure is able to withstand the external loads without failing. Structural optimization uses the failure criterion to optimize several design variables automatically to reduce the dimensionality of the problem. The sub-problems will be discussed in greater detail later in this chapter. In this section the steps that are unique to the structural design problem will be discussed.

The first step in structural design is to propose a concept to be evaluated. For the majority of aerospace structural design there is an assumed form that has arisen from industry norms [153, 174, 178]; however, physics-based structural design allows for exploration of novel concepts as well [23, 114, 207]. Regardless of the proposed concept, the structure must be defined to evaluate the design as well as supply the necessary data to the structural analysis and structural optimization sub-problems. Defining the structure can vary based on the fidelity, but for all physics-based approaches, the geometry of the substructure must be represented with material properties assigned to each portion of the structure. Finally, the design must be evaluated. While proposing a concept is a vague open ended task, the other portions of structural design have well established methods to choose between.

### 3.1.1 Lay Out Structure

The following is a literature review is performed for geometry modeling in structural design problems. First, metrics are defined that can be used to assess the benefits and costs of using the design methods. Then methods that can be used in physics-based structural design during the conceptual design phase will be discussed.

There are many ways to quantify the complexity of a geometric model. The size of the object or the number of parts might be good metrics. These metrics portray the scale of the structure being analyzed or how many unique parts must be analyzed. However, these metrics are inconsistent. The complexity required to model a wing box [123] may be less than the complexity required to model a part of the wing box (i.e. a stiffened cover panel) [58]. An appropriate metric to represent the complexity of a geometric model is **degrees of freedom** (DOF). In structures problems degrees of freedom can vary from three DOF for point mass representation [174] to millions for high-fidelity finite element analysis (FEA) [106]. Each DOF represents a variable that needs to be solved in a system of equations. Increasing the DOF of a problem generally means an increase in the phenomena able to be captured resulting in increased accuracy. However, this increase in accuracy comes at a cost as the more DOF a model has the more variables need to be solved. A result of increasing DOF is that the run time increases. To achieve the research objective of incorporating physics-based analysis into the conceptual design phase a balance between run time and accuracy will need to be struck with an appropriate value for DOF.

The final metric considered for the geometry modeling is the **level of detail**. The level of detail is not a quantitative metric but qualitative. Below is listed some possible levels of details.

- *Equivalent*: The entire structure is being represented by an equivalent structural member such as a beam or a flat plate. The simplification reduces the level of detail significantly so that several details will need to be extrapolated from data to represent the geometry.
- *Simplified*: The components of the substructure layout are represented but no features are include. An example is simplifying a spar to a plane without any spar caps or connectors.
- *Preliminary*: At this level of detail the substructure is represented with some

features included. However, some of the finer details that would be needed for fabrication are left off to simplify the analysis.

- *Fabrication*: The structure is fully modeled in enough detail to fabricate the product.

As previously mentioned the level of detail inherently increases throughout the aircraft design process [174]. To replace historical regressions with physics-based analysis, a well-suited level of detail will need to be selected based upon the detail necessary to accurately represent both the aircraft weight and life cycle cost during the conceptual design phase.

### 3.1.2 Select Materials

In every engineering design problem that deals with a physical product, a material will need to be selected [69]. The material selection problem is typically a discrete problem in that the material is being selected from a permissible set of entities chosen based on several different design requirements [10,71]. Even by limiting the materials considered to a library of preexisting materials the selection process is still technically challenging. This is due to the combination of a wide variety of lightweight materials to choose from due to advances in manufacturing technologies and material concepts [38] and the fact that these materials are selected based upon a large number of criteria [69, 191]. The result is that material selection is open-ended and usually leads to several possible solutions [71]. Because of this a systematic approach to consider all the competing criteria, include as many materials as possible, and assess the benefits of each material selection beyond its material properties is needed [11].

The material selection problem consists of two major steps: screening / rejection and ranking [10, 71]. Material selection is unique compared to the other portions of the structural design problem because it deals with selecting from a list of available materials. As such, at the beginning of material selection all of the permissible

materials must be considered as viable choices. During the screening / rejection phase the permissible set of materials is reduced to a reasonable number through the use or combination of various techniques. These techniques include [71]:

- *Rigid Materials and Process Requirements*: Eliminate materials based upon technical feasibility requirements
- *Cost per unit property material method*: Calculate the cost divided by some property (e.g. length or stiffness) and rank them.
- *Ashby's Method*: Use material property plots to visually eliminate less suitable materials based upon the requirements.
- *Dargie's Method*: Using an existing library of material classifications codes rank materials using the combination of suitability matrices and a compatibility matrix.

The screening  rejection phase of material selection is an important phase. All these methods rely solely upon the material properties and do not require the use of physics-based structural analysis. Additionally, many of them require direct designer interaction which eliminates the possibility of automation. These two characteristics imply that the screening / rejection phase of material selection is beyond the scope of the current research. Therefore, all future experiments involving material selection will assume this step has already been performed and a limited number of candidate materials will be assumed based upon common aerospace materials.

The ranking stage of the material selection process involves ranking alternatives based upon quantifiable metrics. These metrics can either be calculated based on the material properties of the material alone or the performance of the material in the system [10, 59]. In Chapter 1 the motivation included increasing designer knowledge through implementation of physics-based structural optimization. Additionally, when considering physics-based structural design methods the importance of the coupling of the material with the configuration must be considered. Therefore, only the later

methods will be considered. Material ranking techniques seek to combine several different material properties and performances into one quantifiable metric. Common techniques used to create a metric for ranking include [71]:

- *Weighted properties*: Apply weightings to either property or performance values and sum all the criteria into one metric.
- *Digital logic*: Methodically compares criteria two at a time to determine weighting for weighted property method.
- *Performance index*: To sum metrics for each criterion, compare materials based upon a criterion and the highest material is assigned a value of 100 while all the other values are scaled proportionately.

The ranking step of material selection is applicable to physics-based structural analysis. Therefore, implementation of material ranking will need to be considered when formulating a physics-based approach to conceptual design phase aircraft design.

### 3.1.3 Evaluate Design

There are many different metrics across several different disciplines to evaluate a structural design in aerospace engineering. To scope the research and future design problem only the two most common design metrics, weight and cost, will be considered in this dissertation.

#### *3.1.3.1 Weight Estimation*

The first step of weight estimation will be identifying which components need to be included in the overall weight estimation. Figure 27 illustrates a breakdown most of the components that contribute to the overall weight of the wing substructure. However, not all the components need to be included in the weight estimation. It is up to the engineer to decide which components are necessary for the weight estimation. For instance, in the conceptual design phase it may be impractical to include all the

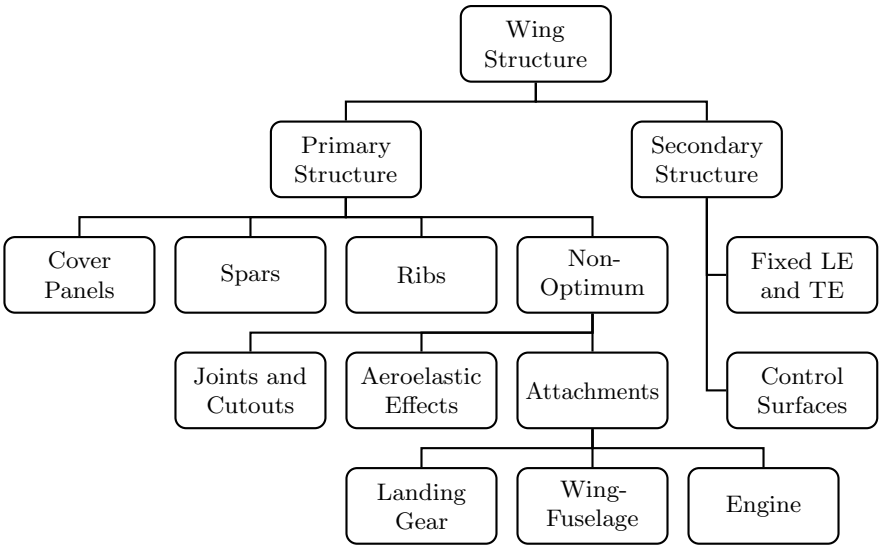


Figure 27: Wing Structure Weight Breakdown [202]

joints and cutouts. Also, in some cases the concept chosen may not include elements of the weight breakdown. If the engine and landing gear are not attached to the wing then those attachment weights need not be included. A list of contributing weight components will be needed to perform weight estimation.

After the contributing weight components are selected, the weights must be calculated by some method. A literature search reveals that the existing methods fall into one of the following categories.

**Weight Penalty or Weight Margin:** A weight penalty or a weight margin is used when there is not enough information to assess the weight or when collecting the information required to assess the weight is too difficult. For these reasons weight penalties and weight margins are commonly used in early design phases. Examples include: adding a weight margin to a spar because accounting for each rivet needed for assembly is difficult in early design stages, or when designer experience can be utilized to assess the weight (e.g. mounting the landing gear).

**Parametric Weight Estimate:** Parametric weight estimation is the most common weight estimation method in preliminary design stages [153, 174, 178, 202]. Parametric weight estimation uses either historic data or analysis to establish parametric relations between the dimension of the part and weight of the part.

**Partial Weight Computation:** It is preferable to estimate the weight based upon the full layout of the structure, the dimensions and thicknesses of each part, and the material properties. However, this requires a large amount of effort. A simpler method is to estimate the weight of portions of the structure and then integrate or interpolate to extract the entire weight of the structure. For example, a few skin panel weights can be used to estimate the weight of all the skin panels using interpolation rather than calculating the weight of each skin panel.

**Full Weight Computation** : The most accurate form of weight estimation is to calculate the weight using material properties across the entire structure. This method requires that the component of the structure be fully defined relative to the specified level of detail. This means that the assigned material density can be applied to the entire volume of the component to calculate the weight.

Each contributing weight component requires the weight to be calculated using one of these categories. The deciding factor for which method is used is typically based upon information available and the level of detail required. Often times these metrics are not consistent among the components that contribute to the weight. In early stages of designing a wing the ribs and spars may be well defined while the joints and attachments have been omitted. Therefore, most structural design problems use a combination of these methods to perform weight estimation.

#### *3.1.3.2 Cost Analysis*

Although cost analysis is not as tightly coupled as the other aerospace disciplines are, it is still a vital part of airplane design problems. As competition among airplane manufacturers rises it becomes more important that accurate cost modeling is used to predict life cycle cost and what drives it. There are many different methods for cost modeling that rely on a mix of expertise, vehicle parameters, and hard methodical accounting. Three traditional methods used in aerospace engineering are: Analogous, Parametric, and Bottom-up [50, 52]. A brief description of each one is given below.

**Analogous:** costing methods use the cost breakdowns of previous similar aircraft and adjust them based upon the target size and price of the current aircraft. The initial guess for the price typically comes from historical comparisons to previous aircraft. This method is the most widely used in the aerospace industry but requires a lot of expert opinion especially when incorporating new technologies [174, 178].

**Bottom-up:** is by far the most labor intensive of the three methods. It uses the size of a part and the process by which it will be manufactured to estimate the cost of everything associated with that part. It then estimates the aggregate cost of all the parts and sums them up based on the number of each part to get an overall estimate. This method produces the most detailed information but requires both time and detailed design knowledge.

**Parametric:** cost methods establish cost estimates based upon relationships between cost and aircraft parameters. These parameters vary in detail from the exact dimensions of the part to just the weight. Also, the parameters used aren't necessarily the drivers of the cost; therefore, unlike the previous two, it may be more difficult to trace cause-and-effect through the method. In addition, it is difficult to set up the model; however, after the model has been established it is fairly rapid and automatic to

calculate the cost.

For the purpose of including life cycle cost and manufacturing consideration early in the conceptual design the bottom-up cost methods are the most desirable. The advantage of this method is that it uses the details of the substructure to implement cost analysis so that key drivers of the life cycle cost can be identified. Additionally, the calculation of the cost is dependent on manufacturing information. Therefore, manufacturing considerations are taken into account. The disadvantage of bottom-up methods is the long run times associated with them. This can make them prohibitively expensive to use if multiple repetitions are required. If the run time ends up prohibiting the use of the bottom-up method, parametric models will present several of the same benefits, but not to the extent that bottom-up methods will. Parametric methods are generally considered lower fidelity than bottom-up methods. Therefore, if a long run time or the cost analysis or the number of repetitions required is small for the cost analysis then bottom-up methods should be used.

## *3.2 Structural Analysis*

Structural analysis is an important sub-problem of the structural design problem. During structural design a concept is proposed; however, structural analysis is required in order to assess whether the structure will fail. **Structural Analysis** is evaluating the deformations and stresses within a solid object due to applied loads for the purpose of assessing whether the structure fails [4,17]. There are four steps necessary to perform structural analysis:

1. Define the structural boundary and material properties
2. Apply boundary conditions and externally applied loads
3. Evaluate the resulting internal loads
4. Assess failure modes

As shown in Figure 26 the first step is a result of the structural design problem. The remaining steps are unique to structural analysis; thus, they will be discussed in further detail in this section. First a general description of structural analysis is given. Next, several metrics will be proposed to compare the methods. Finally, each of the steps will be elaborated on and several techniques used in each step will be introduced. By the end of this section several alternatives will have been proposed that could satisfy the overall research objective.

Two metrics that will be used to differentiate between the methods are fidelity and run time. Several simplifying assumptions are made to solve the structural analysis problem. For example, during structural analysis of thin walled structures the stress is assumed to be uniformly distributed across the wall thickness [17]. As a result of the simplifying assumptions, the analysis does not represent the system as well which reduces the accuracy of a model. The metric that describes the level at which structural analysis represents the physics of the system is called **fidelity**. The more difficult the structure is the more assumptions need to be applied; however, there are methods to reduce the number of simplifying assumptions by decomposing it into smaller portions (i.e. decomposing structure into simple components or the Finite Element Method). Yet, as the problem is decomposed into smaller portions the DOF that need to be solved increases. The increased number of DOF means a longer **run time** is required. Thus, the result is an inherent trade-off in the two metrics, run time and fidelity. Assuming no change in computational power, an increase in fidelity requires more sophisticated tools with longer run times, and to shorten run time less sophisticated tools need to be used with lower fidelity [3, 206]. This trade-off will be pivotal when selecting among the following methods.

### 3.2.1 External Loads

For structural design of an aircraft there are several external loads that can be applied to aircraft due to airloads, inertial loads, landing, takeoff, engine, and more [174]. These loads encompass many aerospace disciplines such as aerodynamics, aeroelasticity, thermodynamics, engine sizing, and controls. The purpose of this section is not to detail each load and its application. Instead, this section will focus on the methods used to apply the external loads to the structure. A symmetric load factor maneuver flight condition will be used to illustrate the process of applying external loads for structural analysis.

The external loads typically are not given for most structural analysis problems in aircraft design. Instead, some flight conditions or regulations have been specified in the requirements portion of the structural design problem. Thus, the first step is to assess the external loads for the specified load condition. Often this requires different aerospace disciplines. The symmetric load factor maneuver flight condition requires the aerodynamics discipline. There exist many different methods to generate the required external loads in the aerodynamics discipline such as:

- *Empirical Methods:* Empirical methods use data from previous aircraft or wind tunnel testing of similar airfoil or wing shapes to define an assumed load across the span of the wing [7, 124, 174, 178].
- *Panel Methods:* Panel methods divide the wing into straight lines with panels in between that are represented surface integrals or vortexes. These methods are limited to incompressible flow, although several methods modify these methods to correct for compressibility and viscous effects [131].
- *Computational Fluid Dynamics:* Computational fluid dynamics solves governing partial differential equations of fluid flow (typically using the NavierStokes equation) using a combination of numerical methods and finite element or finite difference techniques to obtain a numerical definition of the complete flow

field [8].

This chapter is focused solely on the structures discipline; therefore, these methods will not be discussed further. However, the selection of these methods, as well as any methods required by other aerospace disciplines for other load conditions, will have an impact on the run time and fidelity of the overall structural analysis problem.

The external loads must be applied to the existing substructure. There are many methods to accomplish this task, however, two methods are common for wing structures. The first method is to estimate all the external loads as shear, moment, and torque data (VMT data) along a specified axis and then apply beam theory at sections normal to the wing box [124]. This method can either be limited to spanwise loads only or the moment and torque can also be distributed chordwise along the cross sections. The second methods is to discretize the continuous external loads according to the substructure layout in order to apply them to a similarly discretized geometry model. Deciding between these two methods is dependent on the geometry model as well as the methods proposed in the next section.

### 3.2.2 Internal Loads

Calculating the internal loads involves satisfying three sets of equations: equilibrium equations that are a result of the applied and internal forces, constitutive laws that result from material science, and the kinematics of the problem that are the result of simple geometry [17]. These equations are solved using either linear elasticity, analytical mechanics, or energy methods. However, these methods have limitations in that they can only be applied to simple structures [17]. In order to implement structural analysis, the structure must be simplified so that a solution can be found. Three common methods are equivalent theories, simplified structures, and the finite element method. The manner in which the structure is represented is what determines the run time and fidelity of the structural analysis.

**Equivalent theories:** Equivalent theories involve simplifying the characteristics of a structure into a basic structural element like a beam [21] or a plate [83]. The simplification means that solutions for the displacements and stresses can be found using beam and plate theories. An advantages of using equivalent theories is that they have very fast run times and can provide a continuous solution across the equivalent structure. A disadvantage with these methods is that the solutions are for the equivalent structure and results must be translated to the actual structure which makes interpreting effects of the results on the actual structure difficult. Of the three structural analysis methods, equivalent plate methods have the lowest fidelity and shortest run time.

**Classical structural analysis:** Classical structural analysis employs an analytic approach to calculating the internal loads. This approach requires decomposing the structure, either into individual parts or a cross section, to create simplified structural analysis problems that can be solved analytically [9]. Decomposing the problem increases the number of problems that need to be solved to analyze the entire structure. Also, by decomposing the structure the interactions may not be accounted for unless a multi-level design optimization problem is implemented. These last two observations result in increased run time. However, the geometry of the actual structure is being used; thus, the fidelity depends only on how many problems are solved. Of the three methods, classical structural analysis methods are a compromise between the other two methods in terms of run time and fidelity.

**Finite element analysis:** Finite element analysis (FEA) for structural analysis first decomposes the structure into elements where each element is defined by discrete points called nodes [17]. By decomposing the structure into elements a solution can be found for the displacement of the nodes and the stress within each element. However, the nodes are usually shared by more than one element. Thus, every node must be

solved for simultaneously which presents two problems. In addition to decomposing the problem into nodes and elements, which adds to the run time, the behavior of each element needs to be assembled into global matrices to solve for the nodes simultaneously [46]. All of these processes will require a lot of computational power. However, the advantages of FEA are: there is no restriction on geometry so the structure can be represented in the level of detail desired, FEA can be applied to multiple different types of structures (e.g. plates, beams, trusses), and the fidelity can be improved by increasing the number of elements and decreasing the size of each element (i.e. increasing the element density) [46]. Of the three methods FEA will have the highest fidelity but also the longest run time, even for low element density.

Any of these methods will apply the external loads to the geometric shape of the structure to calculate the internal forces and displacements, commonly expressed in terms of stresses and strains. Once these values have been determined the final step is to use these values to assess failure.

### 3.2.3 Failure Criteria

After the stresses and strains have been calculated, all that remains is to determine whether the structure will fail or not. Determining whether a structure fails is dependent upon how the structure is expected to fail, refereed to as a mode of failure. A portion of setting up the structural analysis problem is deciding which modes to test. As an example, a structural element is expected to fail via static strength if is subjected to tension only. Thus, the metrics associated with the static strength mode of failure need to be calculated while the other modes of failure can be ignored. Aerospace structures have several different modes of failure that need to be tested [73,153]. Below some of the most common will be described in more detail.

#### *3.2.3.1 Static Strength*

The strength of a material is its ability to resist a load without failure or permanent damage (i.e. cracks or permanent deflection). If the total stress at any point of the material exceeds the specified stress then it is assumed the structure will fail according to the static strength mode of failure [153]. There are many different load conditions that can result in the static strength mode of failure (i.e. tension, bending, shear, and torsion). However, all of these loads can be expressed in terms of the metrics for strength yield stress ($\sigma_y$), ultimate stress ($\sigma_y$), and allowable stress ($\sigma_{allow}$) [17]. Each of these will be discussed further.

Yield stress and ultimate stress are material properties of linear elastic materials, which most aerospace materials exhibit similar behavior. Figure 28 depicts a stress-strain diagram of a linear elastic material. The material has elastic behavior in the region up to the limit of proportionality ($\sigma_e$). At a stress greater than limit of proportionality, called the yield stress, the structure will undergo plastic deformation so that when the load is removed there will be a permanent deformation. These permanent deformation can lead to the structure failing; thus the yield stress can be used as a failure criteria for the static strength failure mode.

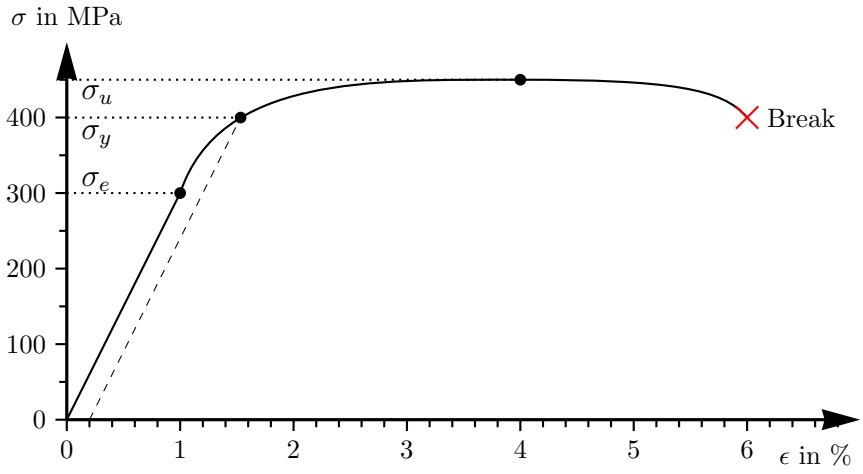


Figure 28: Stress-Strain Diagram

Some materials do not exhibit plastic deformation and thus the yield stress does not exist. The stress can be increased all the way to the ultimate stress without permanent deformation for these materials. However, once a structure is subjected to its ultimate stress it immediately breaks. Thus, in the absence of yield stress the ultimate stress can be used as a failure criteria for the static strength failure mode.

Allowable stress incorporates the concepts of yield stress or ultimate stress with a safety factor. In design it is good practice to include some margins to acknowledge uncertainty. Using the allowable stress reduces the maximum stress the structure is assumed to withstand before failure. The results is that the final structure is more robust to the static strength mode of failure.

$$\text{allowable stress} = \frac{\text{yield stress}}{\text{safety factor}} \qquad \text{allowable stress} = \frac{\text{ultimate stress}}{\text{safety factor}}$$

#### *3.2.3.2 Buckling*

While the static strength mode of failure occurs under multiple load conditions, buckling occurs when the structure collapses primarily under compression loads. The value of the load that causes the buckling failure mode is called the critical load [188]. The critical load is a result of elastic stability and depends upon both the material properties (i.e. stiffness) and the geometry of the structure. An example is the Euler buckling load for a beam which is depicted in Equation 13. In Equation 13 the Young's modulus ($E$) is a material property while the moment of inertia ($I$) and the length ($L$) are geometric properties of the beam.

$$P_{\text{Euler}} = \frac{\pi^2 EI}{L^2} \tag{13}$$

#### *3.2.3.3 Crippling*

Crippling is a specific type of buckling. While buckling is the collapsing of the entire structure due to compression loads, crippling is a local distortion in the cross-sectional shape [153]. As such, the structure can still withstand loads after crippling; however,

the load paths will be altered and can result in failure in other portions of the structure. No theory currently exists for the crippling mode of failure. However, through experiments and analytic studies several have addressed this problem by building empirical relationships for the crippling stress for common aerospace structures and materials [28, 29, 196].

An example of an empirical relationship is McCombs' equation for crippling of a flat plate [137] shown in Equation 14.

$$P_{cc} = C_1 \; F_{cy} \left[ \frac{F_{cy}}{E} \left( \frac{L}{t} \right)^2 \right]^{-C_2} \tag{14}$$

Equation 14 is a function of the material properties (the compression yield load ($F_{cy}$) and the Young's modulus ($E$)), the geometry of the plate (the length of the plate ($L$) and the thickness ($t$)), and two semi-empirical values based off experimentation and the orientation of the plate ($C_1$ and $C_2$).

#### *3.2.3.4 Damage Tolerance*

Damage tolerance refers to a structures ability to resist failure due to defects or partial failures (e.g. fatigue, cracks, and joint ruptures). Damage tolerance analysis is performed with extensive testing through experimentation or analysis during the later phases of design [153]; however, in early phases a maximum stress cutoff is specified based upon empirical data and material properties.

## *3.3 Structural Optimization*

Before introducing structural optimization, general optimization concepts need to be introduced. Optimization is the alteration of a set of **design variables** by some process in order to find the maximum or minimum values for some **objective function**. In optimization it is common to have certain conditions, known as **constraints**, that the design variables must satisfy. Vanderplaats defines optimization using the following equations [204]:

Minimize:

$$F(\bar{X}) \qquad \text{objective function} \tag{15}$$

Subject to:

$$g_j(\bar{X}) \leq 0 \qquad j = 1, m \qquad \text{inequality constraints} \tag{16}$$

$$h_k(\bar{X}) = 0 \qquad k = 1, l \qquad \text{equality constraints} \tag{17}$$

$$X_i^l \leq X_i \leq X_i^u \quad i = 1, n \qquad \text{side constraints} \tag{18}$$

Where:

$$\bar{X} = \begin{Bmatrix} X_1 \\ X_2 \\ X_3 \\ \vdots \\ X_n \end{Bmatrix} \qquad \text{design variables} \tag{19}$$

The optimization problem is typically solved iteratively [204]. The only exceptions are when discrete variables are present or certain heuristic optimization methods are used. Common iterative methods used in optimization include: Newton's method, quasi-newton's methods, finite difference, and numerical analysis. A general equation for the iterative optimization procedure is provided in Equation 20 [204].

$$X^q = X^{q-1} + \alpha S^q \tag{20}$$

In Equation 20 $q$ is the iteration number, $\alpha$ is a scalar quantity called step size, and $S^q$ is a vector of with $n$ dimensions (where $n$ is the same as in Equation 19) that is the direction between the current point and the next point. The manner in which these values are defined separates one optimization method from another and will have a large impact on the run time of the method.

In optimization the goal is to find the best possible solution across the entire design space, known as the **global optimum**. However, it is seldom possible to ensure that the optimal solution found is the global optimum for design problems of practical interest. Additionally, the global optimum of the objective function could be rendered

infeasible by the design constraints. Typically, the solution to the optimization is considered optimal within a local set of solutions. This known as a **local optimum**. While there is no way to ensure that a global optimum is found, there exists two conditions that ensure that an optimal value exists and is unique. The first is that the objective function is a convex function; the second is that the problem satisfies the KuhnTucker conditions [204]. If these two conditions are met, then a local optimum has been found. Thus, the best way to attempt finding the global optimum is to find as many local optimums as possible for comparison.

The metrics for optimization are different from those for modeling and analysis. One reason for the difference is that optimization is an iterative process. The iterative nature of optimization leads to the first metric used to assess the performance of the optimization routine, the number of **function calls** [55]. For every iteration of the optimization problem the objective function needs to be calculated at least once for the current set of design variables. If calculating the objective function is a trivial matter (i.e. it takes little time and needs little computational power) then the metric function calls is less important. However, for many optimization problems this is not the case and a single computation of the objective problem can take hours. In situations where calculating the objective function is not trivial, the number of function calls is used to assess the efficiency of the optimization technique to find an optimum value, where a lower value of function calls means that the optimization routine is more efficient.

The second reason for the difference is that optimization is a stochastic problem. In structural analysis a solution can be found and it is the only solution for the given inputs; however, this is not true for optimization. For optimization the solution, either the global optimum or the best local minimum within the constraints of the problem, is not guaranteed to be located. Instead there is only a probability that the solution will be found. Thus, the second metric to assess the performance of the optimization routine is the **hit rate** which is defined as the probability of finding the

best solution [156].

General optimization techniques have existed for a long time. However, they were not used in engineering design until Schmit applied nonlinear optimization to structural design [181]. Since its introduction, optimization has become a vital part of structural design and is commonly practiced among structural engineers. As a result, many important advances have been achieved over the years in order to solve optimization problems [192, 193]. As optimization has been used within structural engineering, a set of nomenclature and standard practices known as structural optimization has come to be. **Structural Optimization** is solving structural design problems through the use of numerical optimization methods [86]. The general ideas, practices, and nomenclatures of structural optimization will be discussed below in order to enhance understanding for future sections.

Before structural optimization can be performed the objective function, design variables, and constraints must be defined. The objective function is typically taken from the structural design problem. Either the overall design metric is used to evaluate the entire design for each iteration, or a smaller more manageable representation of the design metrics is used to reduce the dimensionality of the structural optimization problem. The other two tasks warrant further discussion which is given below. This section will conclude with a description of common numerical optimization strategies used in structural optimization.

### 3.3.1 Design Variables

For the numerical optimization the design variables are dependent on the type of structural optimization that is being performed. Structural optimization covers a wide variety of real world problems. These problems range from deciding the dimensions of small parts to arranging truss structures within a building. Structural optimization problems are sorted into three categories based upon the geometric features being

altered. These are known as sizing, shape, and topology optimization [86, 109]. A brief description of each is given below.

**Topology optimization** is the optimization of the layout within a given design space. It is the most general type of structural optimization. An example of topology optimization is selecting the cross-section of a beam or finding an initial conceptual shape.

**Shape optimization** refers to optimization of the boundaries of the structure. If a structure's outline was defined by two equations then the design variables for the optimization problem would be the variables in these equations. Unlike topology optimization, in shape optimization the boundaries are well defined before optimization and no new boundaries are formed.

**Sizing optimization** involves optimization in which the shape of the structure is already well known; thus the boundary is already defined with the exception of the dimensions of the structure (e.g. thickness and widths).

The selection of the design variables will depend heavily on which of these optimization problems are being used. For example, if the problem is limited to sizing then a structure has been assumed and only the dimensions and thicknesses are being optimized as the design variables.

### 3.3.2 Structural Optimization Constraints

Several constraint are used throughout structural optimization. The most common constraints used during structural optimization of an aerospace structure are discussed below.

#### *3.3.2.1 Margin of Safety / Factor of Safety*

The terms Safety Factor and Margin of Safety are two related values that are commonly used throughout the aerospace industry. As such they are contained in a majority of textbooks on the subject [34, 36, 161], recognized by major aerospace institutions (i.e. NASA [43] and AIAA [5]), and are used by the FAA to pass safety regulations [72, 73]. In order to understand what the definition of Safety Factor and Margin of Safety are we must first define some terms:

**Failure Strength:** The calculated stress or force at which point the material fails by some criteria, such as buckling or yielding, for the given structure.

**Limit Load:** The calculated maximum loads that the structure is subject to under designed conditions.

Failure strength comes from the material properties of the structure. It answers how much load can be handled by the given types, amounts, and arrangements of materials before failure occurs. The limit load comes from the internal loads calculated after applying the external loads to the structure. For aircraft, the external loads come from the design conditions such as the takeoff and landing field lengths or the loads experienced during a turn. Essentially, the two terms express the strength of the structure and the maximum loads the structure will be required to withstand. The ratio of these values is called the factor of safety [34].

$$\textbf{Factor of Safety} = \frac{\text{Failure Strength}}{\text{Limit Load}}$$

There are many variations of factors of safety. For instance, when the limit load is multiplied by 1.5 it is referred to as the ultimate load. Often the ultimate load is used in place of the limit load to account for any errors in calculating the limit load. Regardless of which variation is used, the factor of safety expresses whether there is enough material or if it is arranged properly in order to carry the necessary load.

A value of one means there is just enough material to carry the loads. A value less than one means the structure is likely to fail. Another way of expressing the failure condition is the margin of safety [34].

$$\textbf{Margin of Safety} = \frac{\text{Failure Strength}}{\text{1.5 Limit Load}} - 1$$

Instead of a ratio of the strength of the material and the load the material is subject to, the Margin of Safety is a measure of the structures ability to handle loads beyond the design loads. A negative value means that the structure cannot support the design loads. A value of zero means there is just enough material to support the loads. Thus, the factor of safety or margin of safety provide a simple and methodical way to assess whether or not the structure can adequately carry the loads.

An important assumption in the calculation of the factor of safety and margin of safety is that the limit loads are for the design loads only. The reason that only the design loads are used is to save on cost. Increasing the loads will result in increased weight and cost of the aircraft. Therefore, the structure is designed only for the loads that are known to drive the design. However, during its life the aircraft will experience loads greater than it was designed (e.g. increased loads due to turbulence or a hard landing). A proper selection of the factor of safety is a value greater than one, and a proper selection of the margin of safety is a value greater than zero. The increased margin results in extra material being used to ensure that the structure is robust enough to handle any additional load.

#### *3.3.2.2 Manufacturing Constraints*

There are several manufacturing constraints that need to be applied to the structural optimization problem. These constraints deal with the fabrication of the product and typically take on the form of upper and lower limits on the size of a feature or the dimensions of a structure [47, 95, 214]. The constraints vary depending upon the manufacturing method being used. For example, there are different constraints for

casting and extrusion [212]. Although the manufacturing constraints may have little effect during the design process, not accounting for all of them will have consequences when it comes time for fabrication. Therefore, these constraints should be accounted for even in the early stages of design.

#### *3.3.2.3 Other Constraints*

There exists a wide variety of other constraints that may need to be applied that do not fit into the previous two categories. Some examples of additional aircraft structural optimization constraints are:

- A maximum wing displacement during taxi so that the engine will have enough clearance [178]
- Minimum rib spacing to ensure there is enough room for maintenance workers to have access for repairs [153]
- Damage density requirements for accidental impacts (i.e. lightning, hail, or bird strikes [94])

Many more constraints exist, but as they tend to be problem specific, it is up to the structural engineer to decide which constraints need to be included in the structural optimization problem.

### 3.3.3 Numerical Optimization Methods

Numerical optimization is a highly established field with several different methods to solve an optimization problem [86, 118, 204]. As the current research does not require an in depth understanding of the mathematical concepts behind these methods, like consistency or convergence, a general review of useful methods will be presented. The review will cover the basic process behind categorized methods. Based upon a literature review, numerical optimization methods can be organized into four categories: search methods, gradient based methods, heuristic methods, and discrete methods.

For convenience Equation 20, which defines the iteration to the next design point specified for each iteration of the optimization, is displayed below for reference.

$$X^q = X^{q-1} + \alpha S^q$$

#### *3.3.3.1 Search methods*

Search methods are optimization methods that methodically search for the optimum point (except for the random search method) without the use of gradients. These methods include 1-D search methods (i.e. golden section algorithm [204] or midpoint) random search methods (i.e. Monte Carlo [42] and random search direction) and neighborhood search methods (i.e. Tabu search [84] and pattern search [204]).

The pattern search algorithm illustrates some of the advantages and disadvantages to using these methods. Pattern search is an iterative optimization problem that utilizes Equation 20. An initial point is selected at random. The next point is searched for by selecting a direction and step size to test for a better point. The direction is selected based upon an organized pattern. Once a better point is found the point becomes the current design point and the process is repeated. If a better point cannot be found then the step size is reduced and the directions are tested again. This is repeated until the step size is sufficiently small.

The pattern search method, like many search methods, is easy to implement. This is the major advantage of these methods. However, there are many disadvantages to using search methods. First, there is no guarantee that an optimum is found. Second the optimization routine is extremely inefficient. Thus, search methods are typically only used as a small portion of a more elaborate optimization routine.

#### *3.3.3.2 Gradient based methods*

Gradient based methods calculate the gradients at the design point, either directly or through polynomial approximations, and use the values to decide which direction

the next point will be via $S^q$ in Equation 20. The additional information provided by the gradients results in the optimization routine converging faster [204]. These optimization methods can be organized into methods that use first order derivatives (i.e. steepest descent and conjugate gradient) and methods that use higher order derivatives (i.e. Newton's method, quasi-newton methods, and sequential quadratic programming).

The steepest descent algorithm is one of the worst performing gradient based optimization methods, but it is also the easiest to understand so it will be used as an example. After an initial point is selected the gradient of the objective function at the point is calculated. Using Equation 20, the search direction $S^q$ is selected as the negative of the gradient of the objective function. A 1-D line search is then used to specify the step size by locating the minimum point along the search direction. The design point is then moved to the new point and the process is repeated until convergence.

Gradient based optimization methods are advantageous for two reasons. The use of gradients increases the efficiency of the optimization method which means that fewer function calls are needed. The increase in efficiency can save a lot of time for computationally expensive function calls. The second is gradient based methods guarantee that an optimum is found [204]. Although, only a local optimum is guaranteed and the only way that gradient based optimization can compare local optimums is through repetition with different initial points. Gradient based optimization assumes that the objective function is first or second order differentiable, which it may not be. Additionally, if the gradient can be calculated, the calculation of the gradient may be so burdensome that it becomes a bottleneck for the optimization problem [106]. The benefits of gradient based optimization are substantial. So long as a gradient can be calculated and the design space does not have a large amount of local optimums these methods are preferred.

If implementing a function call or calculating the gradient is impossible or too difficult, then gradient based methods either can not be used or are unfavorable. In this situation a potential solution is to create a surrogate model. The surrogate model will take numerous runs to set up, but once it has been created the execution of a single run is trivial and a gradient can be calculated easily. Other than the large number of runs needed to create the surrogate model, the only other drawback is that the surrogate model is only an approximate representation of the function and so additional uncertainty is introduced into the optimization. Despite the drawbacks, if finding a gradient or implementing a function call is prohibitive to using gradient based optimization then surrogate models should be considered as an alternative.

#### *3.3.3.3 Heuristic methods*

Heuristic optimization methods can be characterized as trial and error. Heuristic methods rely on evolutionary computation to converge on an optimum solution [118]. Examples of heuristic methods include simulated annealing, ant colony optimization, and genetic algorithms. The disadvantage of heuristic methods is that they require a large number of function calls. If implementing a function call takes too long, then use of heuristic methods might not be feasible. Additionally, heuristic methods do not guarantee that even a local optimum will be found. However, there are many benefits associated with heuristic methods. Heuristic methods are conceptually simple to implement, have broad applicability, can incorporate discrete variables, and can be implemented in parallel [118].

#### *3.3.3.4 Discrete methods*

Many design problems are faced with discrete variables. Discrete variables can not be optimized in the same iterative fashion as continuous variable. The only way to garuntee that all the discrete options have been explored is through some form of enumeration [110]. Several discrete optimization methods exist that enumerate

discrete variables as efficiently as possible [110]. However, rarely are optimization problems presented with just discrete variables. The combination of continuous and discrete variables requires either heuristic methods or hybrid methods of discrete optimization methods and non-discrete optimization methods. Although discrete methods will increase the number of function calls factorially, they are required to deal with the optimization of the discrete variables.

# CHAPTER IV

# STRUCTURES MODELING & SIMULATION

In Chapter 3, the basic concepts behind Structural Design, Structural Analysis, and Structural Optimization were introduced to partially fulfill Research Objective 2. In this chapter, Modeling & Simulation (M&S) in structural design will be discussed.

---

**Research Objective 2**

Compare current structural design, analysis, and optimization methods based upon metrics that will identify which methods are most appropriate for the conceptual design phase.

---

First, the research observations from Chapter 2 will be used to illustrate that an M&S environment is necessary to address the overall research objective. Second, a method to characterize the complexity of structural M&S environments will be introduced. Finally, the method will be used to characterize several existing wing box structure M&S environments to make observations that will aid in fulfilling the overall research objective.

## *4.1 Modeling & Simulation Environment*

The use of Modeling & Simulation (M&S) is found throughout the fields of science and engineering [35, 115]. There are many different types of M&S methods used for a variety of different purposes [115]. Because M&S takes on a wide variety of forms and definitions depending upon the problem it is being used to solve, a working definition of M&S is needed.

As defined by Murphy, a model is a device which is related to a system so that observations on the model can be used to predict the desired performance of the system [149]. Models are typically either physical models or mathematical models. An example of a physical model is a scale model of a wing for wind tunnel testing. Although physical models are still relevant in engineering [19, 136] they are not cost effective [190]; thus, their use is largely discouraged in complex design problems. The models considered will be limited to mathematical models. Mathematical models are models that represent a system through mathematical relations [159]. The following definition is proposed for modeling:

**Modeling:** Using a device which is related to a system mathematically so that observations can be made that predict the desired performances of the system.

Whether or not simulation is required depends on the type of model. For some models a solution can be found analytically. For example, a solution can easily be obtained analytically for models that calculate the volume of a sphere or the time it will take an object to fall from a fixed height. An analytical solution can be found for any model that uses a set of equations that is consistent and determinate. In some cases an analytical solution can be found for indeterminate solutions using certain assumptions [152]. If an analytical solution cannot be determined then simulation is needed. Simulation can be described as evaluating a model numerically based upon a given set of inputs to measure the response [115]. In many cases, simulation involves several models that are connected using outputs as inputs. Thus, a working definition for simulation is:

**Simulation:** The numerical evaluation of a model or several connected models to gather data in order to estimate the desired characteristics of the model.

The use of M&S is commonly the primary means of design evaluation and verification; this is referred to as simulation-based design [160, 187]. Simulation-based design presents several benefits [160, 187, 190]:

- Organizes the approach to solving complex systems
- Shortens the design cycle and reduces the cost of design
- Gives immediate feedback on design decisions
- Provides repeat-ability that allows for exploration of design alternatives

For these reasons, simulation-based design is common in aircraft design [99, 189, 197, 213].

In Chapter 2, a design space characterization on the wing box substructure design problem was performed. During the design space characterization, research observations were made that illustrate how difficult the structural design problem is. Research Observations 1 and 2 illustrate that the structural design problem is a combinatorially large multivariate problem with several discrete design decisions. Thus, an organized approach is needed to deal with the complex problem.

At the end of Chapter 2 several of the research observations were used to develop Framework Proposition 1 which states that due to the complex and discontinuous nature of the design space, a strategy of exploration requiring a large number of analysis executions is required. Thus, repeat-ability is necessary for the structures design problem.

Research Observation 3 illustrates that a large percentage of the design space is infeasible due to the highly constrained nonlinear analysis. The infeasible region makes an already indeterminate system of equations inconsistent because there is a high likelihood that a solution cannot be found. Therefore, an analytical solution is not possible.

In review, M&S addresses problems presented by the research observations in three ways. First, an M&S environment will provide an organized approach to solving the

problem for the combinatorially large number of design variables as well as managing the discrete design decisions. Second, M&S provides a repeatable way to perform structural design. Finally, as no analytical solution can be found simulation is required in order to navigate the highly constrained nonlinear design space. This leads to the conclusion that an M&S environment is needed to address the overall research objective.

## *4.2 Modeling, Analysis, and Optimization*

The previous section defined the need for an M&S environment to address the overall research objective. The M&S environment will need to implement the methods for structural design, analysis, and optimization described in Chapter 3. The methods from Chapter 3 can be implemented in a massive number of different combinations. Additionally, several combinations of concepts will be impractical and should not be considered: full weight computation is not possible with equivalent plate analysis because the substructure is simplified to a plate, Finite Element Analysis requires a structural mesh and cannot be used with a simplified structural layout, or parametric weight estimation is illogical to use with a detailed fabrication structural layout model. Thus, experimentally testing each combination is untenable.

Instead of conceiving the M&S environment through experimentation, a literature survey of similar M&S environments for wing box substructure design is used to evaluate current methods. The literature survey will illustrate several common trends among the M&S environment because several combinations of structural design, analysis, and optimization are impractical. A structured method of comparison is needed to identify trends among the wing box structural design M&S environments.

### 4.2.1 Structural Optimization Complexity

The method used to compare the wing box structural design M&S environments will be based on Venkataraman and Haftka's literature survey of structural optimization M&S

environments [206]. In the paper the structural design, analysis, and optimization procedure is expressed in terms of three quantities: the **modeling complexity**, the **analysis complexity**, and the **optimization complexity**.

Venkataraman and Haftka define the modeling complexity as the computational cost associated with defining the geometry, loading, and material. For modeling complexity the degrees of freedom (DOF) of the model often has the largest impact on the computational cost associated with modeling. Topology or the shape of the structure is another factor of modeling complexity. A slender beam will be easier to analyze than a compact three-dimensional structure with the same DOF [206]. Additionally, the material properties will affect the modeling complexity. If the material is isotropic then no additional work is required for the modeling after the material properties have been defined. However, if the material specifies composite laminates the properties will need to be smeared for the stiffness matrix. In the paper the authors analyze several other structural M&S environments and rate them in terms of the model complexity (Figure 29).

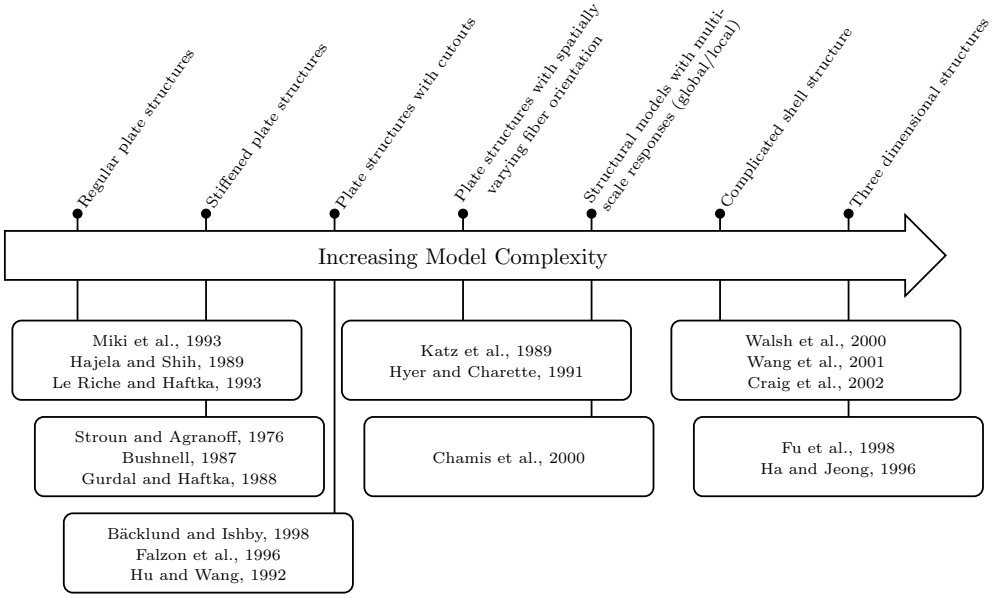


Figure 29: Modeling Complexity [206]

Venkataraman and Haftka define analysis complexity as the computational cost of performing the analysis procedure and specify three levels of analysis complexity: linear static analysis, eigenvalue analysis, and non-linear transient analysis. Linear static analysis is the simplest requiring simple methods such as matrix inversion. Eigenvalue analysis requires more complex linearization algorithms to solve the governing equation repeatedly. The most complex of the three is non-linear transient analysis which requires the equivalent of hundreds or thousands of linear static analysis executions. The authors provide examples of each in terms of increasing analysis complexity (Figure 30).

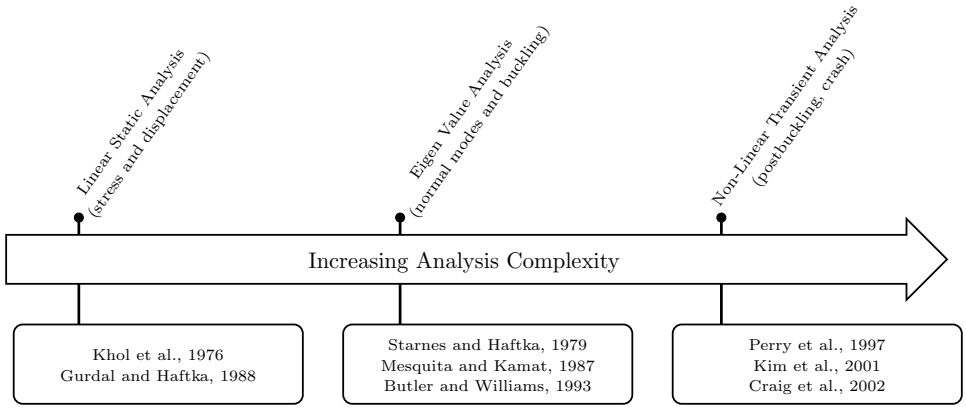


Figure 30: Analysis Complexity [206]

The number of objective function evaluations is typically how optimization complexity is defined but is an incomplete representation of analysis complexity. For example gradient based optimization seeks to minimize the number of analyses by using the sensitivities; however, calculating the gradients can be the dominating factor in computation cost of an optimization routine [206]. Thus, optimization complexity is defined in terms of the number of analyses required, the number of design variables, and the type of optimization. The authors provide several examples of structures M&S environments with increasing optimization complexity (Figure 31).

Although it is difficult to define the modeling complexity, the analysis complexity,

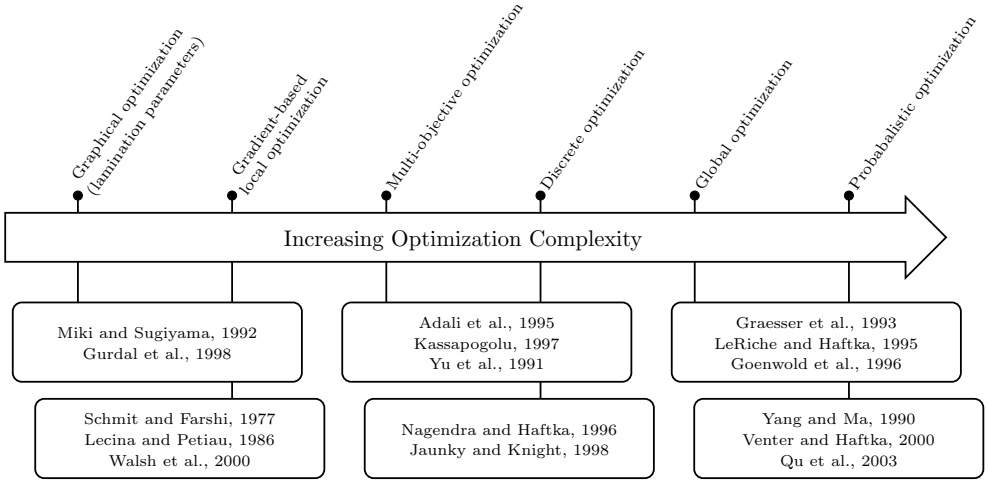


Figure 31: Optimization Complexity [206]

and the optimization complexity there is an important property of all three that makes them useful in assessing structural M&S environments. In the paper, the computational power required to perform the modeling, analysis, and optimization are used as surrogates for the respective complexities. All of these complexities are competing for a limited amount of computational resources. The three complexities form a Pareto Frontier where no value can be improved without the detriment of another (Figure 32).

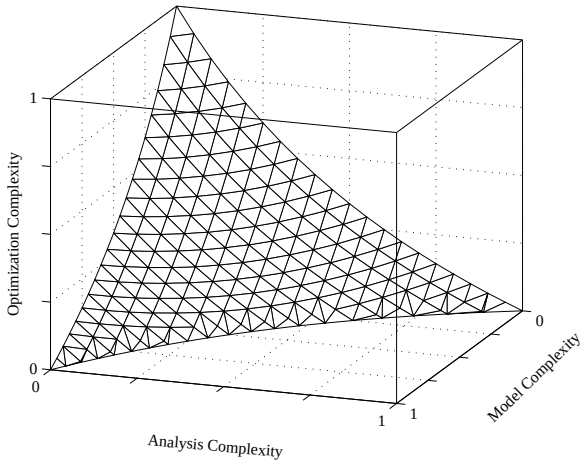


Figure 32: Modeling, Analysis, and Optimization Pareto Frontier

### 4.2.2 Quantify Model, Analysis, & Optimization Complexity

The previous subsection described a method of classifying structure M&S environments based on model complexity, analysis complexity, and optimization complexity. These three values will provide the basis of comparison for the literature survey of current wing box structure M&S environments in the next section.

However, there are some important differences between Venkataraman and Haftka's method and the method that will be used in this dissertation. First, for the dissertation the only structures considered will be wing structures which will alter how model complexity is defined. Second, wing box structural analysis typically focuses on linear static analysis. However, there are varying levels of analysis complexity used to perform linear static analysis that were not captured in Figure 30. Finally, Venkataraman and Haftka define the scale for optimization complexity based on the type of optimization used. For wing box structural optimization many of these methods are used in conjunction making it difficult to use Figure 31. Although the paper provides a basis for the comparing M&S environments, additional steps will have to be made to adapt the methods for the literature search to be performed in the next section.

To address the differences between the definitions of model, analysis, and optimization complexity, a method is proposed in which the model complexity, analysis complexity, and optimization complexity are quantified. The first step is to quantify the model and analysis complexity by decomposing each into different metrics. The majority of metrics that effect the model complexity and analysis complexity are qualitative values. These values will be made quantitative by using concepts from a house of quality [60]. Each metric will be ranked (high, medium, low, N/A) and each rank will carry a quantitative value (9, 3, 1, 0). The values will be summed and then normalized based on a theoretical maximum. Thus, the method will be able to quantify analysis complexity and modeling complexity based off of quantitative values.

The second step of the method is to compute the optimization complexity. Optimization complexity is unique in that several different methods can be used simultaneously. The fact that these methods can be used simultaneously makes it difficult to quantify metrics associated with model complexity. Instead, the optimization complexity will be calculated based on the analysis complexity and model complexity. An important feature of model complexity, analysis complexity, and optimization complexity is that they form a Pareto Frontier. Thus, the theoretical maximum optimization complexity available can be calculated using the quantified values for model and analysis complexity. This value will be used to represent optimization complexity during the literature survey in the next section.

#### *4.2.2.1 Quantify Model Complexity*

The model complexity, as defined by Venkataraman and Haftka, is a function of: the DOF, the topology of the structure, and the material used. These will also be used to quantify the model complexity, with one minor change. For the literature survey the model complexity will be a function of the DOF, the material selected, and the level of detail.

**Degrees of Freedom:** The structure geometry must be pre-processed into a form the governing equations can use to perform structural analysis. The difficulty of pre-processing the geometry is often dependent on the analysis selected. For example, to use Finite Element Analysis the geometry must be meshed into finite elements, while classical structural analysis methods only require dimensions of the idealized structure being analyzed. Rather than confounding the model complexity with the analysis complexity the effect of the type of pre-processing will be ignored (i.e. it is assumed that the time to create a mesh is equivalent to the time needed to estimate the geometry into beam characteristics). However, the computational cost required to perform the pre-processing will be affected by the DOF of the structural analysis

problem (i.e. creating a 100 node mesh requires little time but creating a 100,000 node mesh can take a long time). Thus, the DOF affects the model complexity.

The DOF is already a quantified value. Yet, large changes can have minimal effect on the computational cost. It is only when the DOF increases by many factors that there is a significant change in the computational cost. Thus, the DOF is broken down into ranges based on the low, medium, high scale. In additional to differentiating between DOF ranges, this allows the DOF metric to be treated similar to the other qualitative values. The final ranges are shown in Table 8.

**Material Selection:** To understand the effect of the material selected consider the compliance form of Hooke's law (Equation 21). The large matrix in Equation 21 is called the compliance matrix. To perform structural analysis this matrix, or systems of equations similar to it, need to be calculated. There are 36 individual components each of which has to be calculated for the material selected and the orientations. Several of these components can be eliminated through symmetry or simplifying assumptions depending on the type of material; thus, material selection effects model complexity.

$$\begin{Bmatrix} \epsilon_x \\ \epsilon_y \\ \epsilon_z \\ \gamma_{yz} \\ \gamma_{zx} \\ \gamma_{xy} \end{Bmatrix} = \begin{bmatrix} C_{11} & C_{12} & C_{13} & C_{14} & C_{15} & C_{16} \\ C_{21} & C_{22} & C_{23} & C_{24} & C_{25} & C_{26} \\ C_{31} & C_{32} & C_{33} & C_{34} & C_{35} & C_{36} \\ C_{41} & C_{42} & C_{43} & C_{44} & C_{45} & C_{46} \\ C_{51} & C_{52} & C_{53} & C_{54} & C_{55} & C_{56} \\ C_{61} & C_{62} & C_{63} & C_{64} & C_{65} & C_{66} \end{bmatrix} \begin{Bmatrix} \sigma_x \\ \sigma_y \\ \sigma_z \\ \tau_{yz} \\ \tau_{zx} \\ \tau_{xy} \end{Bmatrix} \tag{21}$$

The simplest form of the compliance matrix is for isotropic materials (Equation 22). Because isotropic materials are uniform in all directions there is no orientation. The result is that the 36 components can be defined with only 2 values (the Young's modulus ($E$), the Shear modulus ($G$), or Poisson's ratio ($\nu$)). Isotropic materials are

so simple they are often solved using a system of equations rather than the compliance matrix; hence, isotropic materials are assigned a low value for material complexity (Table 8).

$$\begin{Bmatrix} \epsilon_x \\ \epsilon_y \\ \epsilon_z \\ \gamma_{yz} \\ \gamma_{zx} \\ \gamma_{xy} \end{Bmatrix} = \begin{bmatrix} \frac{1}{E} & \frac{-\nu}{E} & \frac{-\nu}{E} & 0 & 0 & 0 \\ \frac{-\nu}{E} & \frac{1}{E} & \frac{-\nu}{E} & 0 & 0 & 0 \\ \frac{-\nu}{E} & \frac{-\nu}{E} & \frac{1}{E} & 0 & 0 & 0 \\ 0 & 0 & 0 & \frac{(1+\nu)}{E} & 0 & 0 \\ 0 & 0 & 0 & 0 & \frac{(1+\nu)}{E} & 0 \\ 0 & 0 & 0 & 0 & 0 & \frac{(1+\nu)}{E} \end{bmatrix} \begin{Bmatrix} \sigma_x \\ \sigma_y \\ \sigma_z \\ \tau_{yz} \\ \tau_{zx} \\ \tau_{xy} \end{Bmatrix} \tag{22}$$

Orthotropic materials are similar to isotropic materials except that the material properties are directional (Young's Modulus = $[E_x, E_y, E_z]$). This increases the affect on the model complexity by increasing the number of values from 2 to 6, and direction now needs to be accounted for. However, the increase in model complexity compared to isotropic materials is marginal; thus, orthotropic materials are assigned a low value for material complexity as well (Table 8).

Anisotropic materials are the most complex materials, unless they are designed to be symmetric (i.e. $C_{ij} = C_{ji}$) (Equation 23). In symmetric cases the number of components required for the stiffness matrix reduces from 36 to 21. The reduction in the components of the compliance matrix reduces symmetric anisotrpic materials effect on the model complexity. Additionally, several methods to smear properties for symmetric anisotropic materials exist that will reduce the computational power required to model the material. For these reasons symmetric anisotropic materials are assigned a medium value for material complexity (Table 8).

$$\begin{Bmatrix} \epsilon_x \\ \epsilon_y \\ \epsilon_z \\ \gamma_{yz} \\ \gamma_{zx} \\ \gamma_{xy} \end{Bmatrix} = \begin{bmatrix} C_{11} & C_{12} & C_{13} & C_{14} & C_{15} & C_{16} \\ & C_{22} & C_{23} & C_{24} & C_{25} & C_{26} \\ & & C_{33} & C_{34} & C_{35} & C_{36} \\ & & & C_{44} & C_{45} & C_{46} \\ & sym & & & C_{55} & C_{56} \\ & & & & & C_{66} \end{bmatrix} \begin{Bmatrix} \sigma_x \\ \sigma_y \\ \sigma_z \\ \tau_{yz} \\ \tau_{zx} \\ \tau_{xy} \end{Bmatrix} \tag{23}$$

Non-symmetric anisotropic materials require the full 36 components of the compliance matrix. Additionally, non-symmetric anisotropic materials require difficult and computationally expensive procedures to develop the compliance matrix (i.e. ply layup). For these reasons non-symmetric anisotropic materials are assigned a high value for material complexity (Table 8).

**Level of Detail:** In the previous section, one of the factors of model complexity was the structure topology (i.e. a slender beam will be easier to analyze than a compact three-dimensional structure with the same DOF). However, only wing box structures will be considered for the literature survey to be performed in the next section. All the structures will have a similar topology, only with different levels of detail. Thus, the final contribution to model complexity is the level of detail of the structure.

Four levels of detail were defined in Section 3.1.1: Equivalent, Simplified, Preliminary, and Fabrication. Only conceptual or preliminary level M&S environments will be considered during the literature search; hence, no M&S environments with a fabrication level of detail will be considered. If we apply the logic that a structure with simpler topology will be less complex, then it is easy to assign the three remaining levels of detail to the low, medium, high scale (Table 8).

Table 8: Quantifying Model Complexity

| | Low | Medium | High |
|---|---|---|---|
| Degrees of Freedom | DOF< $10^2$ | $10^2 \leq$ DOF $\leq 10^4$ | $10^4 <$ DOF |
| Material Selection | Isotropic + Orthotropic | Symmetric Anisotropic | |
| Level of Detail | Equivalent (i.e. beam or plate) | Substructure Layout | Substructure Layout + Detailed Features |

#### *4.2.2.2 Quantify Analysis Complexity*

In the previous section analysis complexity is defined only in terms of three structural analysis methods: linear static analysis, eigen value analysis, and non-linear transient analysis. For the purposes of wing box structural design the analysis complexity rarely goes beyond linear static analysis. However, there is a significant difference in analysis complexity depending upon the methods used (Section 3.2.1 and Section 3.2.2). Additional factors that will affect the analysis complexity are: degrees of freedom, number of iterations, and number of matrices.

**Degrees of Freedom:** As an example of analysis complexity, consider the governing equation for linear static analysis using Finite Element Analysis (Equation 24).

$$\{u\} = [K]^{-1}\{\sigma\} \tag{24}$$

The most computationally expensive part of executing Finite Element Analysis is inverting the element stiffness matrix ($[K]$) [46]. The size of the stiffness matrix, and the computational cost of inverting it, increases as the DOF increase. Thus, DOF will affect the analysis complexity. This is also true for non Finite Element Methods. As the DOF increase the size of the system of equations increases for classical structural analysis and equivalent methods which increases the analysis complexity.

The DOF is a quantitative value. However, due to the logic discussed in the previous section, the degrees of freedom is broken down into the low, medium, high qualitative values that all the other metrics use (Table 9).

**External Loads:** Structural analysis focuses on converting external loads applied to a structure into the internal loads of the structure. Thus, the method used to calculate the external loads will impact the analysis complexity. Section 3.2.1 describes several methods to generate the external loads of a wing structure based on fidelity. For the purpose of quantification, analysis complexity is synonymous with fidelity. The three methods are ranked in Table 9.

**Internal Loads:** Similar to the external loads, the method to calculate the internal loads affects the analysis complexity. Section 3.2.2 describes several methods to generate the external loads of a wing structure based on fidelity. For the purpose of quantification, analysis complexity is synonymous with fidelity. The three methods are ranked in Table 9.

**Number of Iterations:** Occasionally, the governing equations used to solve the structural analysis problem require iterations to solve. For example, if the problem being solved focuses on the aerostructural correlations, then an iterative method is necessary to account for the fact that the aerodynamic loads will change as the structure bends. Additionally, some structure M&S environments implement structural dynamics methods with governing equations that require iterative linear analysis methods to solve. An important distinction is that the only iterations being considered are those necessary to solve the governing equations. If the M&S environment includes sizing optimization then these iterations do not contribute to the analysis complexity. The number of iterations is a quantitative value but is broken into ranges as shown in Table 9.

**Number of Matrices:** As previously mentioned the most computationally expensive portion of the analysis process is the mathematics dealing with matrices (e.g. Gaussian elimination, multiplication, inversion). Thus, the number of matrices affects the analysis complexity.

Structural analysis for wing box structural design rarely goes beyond linear static analysis. Solving linear static equations with classical structural analysis is done with a system of equations that are independent and require no matrix inversions. If the linear static analysis implements finite element method then the system of equations are dependent and one matrix will need to be inverted. For some designs it is necessary to perform structural dynamics which require two or three matrices [92]. Any analysis that requires more than 3 matrices is considered highly complex. These values are reflected in Table 9.

Table 9: Quantifying Analysis Complexity

| | Low | Medium | High |
|---|---|---|---|
| Degrees of Freedom | DOF < $10^2$ | $10^2 \leq$ DOF $\leq 10^4$ | $10^4$ < DOF |
| Material Selection | Isotropic + Orthotropic | Symmetric Anisotropic | |
| External Loads | Empirical + Semi-Empirical | Panel Methods | Computational Fluid Dynamics |
| Internal Loads | Equivalent Theories | Classical Structural Analysis | Finite Element Analysis |
| Number of Iterations* | 2 -- 10 | 10 -- 100 | 100+ |
| Number of Matrices* | 1 | 2 -- 3 | 4+ |

#### *4.2.2.3 Calculate Optimization Complexity*

Optimization complexity is the most difficult of the three complexities to define. As previously mentioned, the number of function calls is not a perfect representation of the optimization complexity. There are additional considerations such as the type of optimization and the number of design variables. However, this formulation still ignores the fact that many of the concepts used in Figure 31 can be used simultaneously (i.e. using gradient based optimization with multi-objective optimization to find the global optimum). Instead of defining the optimization complexity for each method, the optimization complexity will be calculated based upon the analysis complexity and the model complexity using the fact that the model complexity, analysis complexity, and optimization complexity form a Pareto Frontier (Figure 32). Thus, if it is assumed that the modeling, analysis, and optimization methods are as efficient as possible (i.e. the point lies on the surface of the Pareto Frontier) then the optimization complexity ($x_o$) can be calculated from the analysis complexity ($x_a$) and the model complexity ($x_m$) using Equation 25.

$$1 = x_m + x_a + x_o + x_m\ x_a + x_a\ x_o + x_o\ x_m \tag{25}$$

## *4.3 Current Methods*

This section will perform a literature survey of existing wing box structural M&S environments used for design purposes using the method developed in the previous section to quantify the complexities. Seven papers are presented below and a description of each paper will be accompanied by a table consisting of the qualitative observations made based off of Tables 8 and 9. The qualitative observations will be used in the next section, along with the method from the previous section, to quantify the model, analysis, and optimization complexities for each M&S environment.

### 1. Equivalent Plate Analysis of Aircraft Wing Box Structures with General Planform Geometry [83]

The M&S environment uses equivalent plate analysis based on the Ritz method to perform both linear static analysis and vibration analysis. The equivalent plate representation of the wing structure is broken down into multiple trapezoids and requires a minimal amount of iteration. The external loads are calculated use empirical tables of pressure coefficients and the governing equations are based on isotropic materials.

| Degrees of Freedom | Material Selection | Level of Detail | Internal Loads | External Loads | Number of Iterations | Number of Matrices |
|---|---|---|---|---|---|---|
| Medium | Low | Low | Low | Low | Low | Medium |

### 2. Enabling Rapid and Robust Structural Analysis During Conceptual Design [63]

This M&S environment was created to analyze a low-boom supersonic aircraft. Therefore, the external loads are calculated using advanced CFD analysis. The structures module uses NASTRAN static analysis on a substructure layout. The M&S environment can include any material in the analysis but is assumed to use symmetric composites.

| Degrees of Freedom | Material Selection | Level of Detail | Internal Loads | External Loads | Number of Iterations | Number of Matrices |
|---|---|---|---|---|---|---|
| High | Medium | Medium | High | High | N/A | Low |

### 3. High-Fidelity Aerostructural Design Optimization of a Supersonic Business Jet [129]

The goal of this paper is to develop an M&S environment for high-fidelity analysis and optimization of aircraft configurations. The external loads are calculated using a parallel flow solver based on CFD. The structural analysis uses FESMEH, a finite

element solver, to solve aerostructural problems. To account for the aerostructural coupling several iterations are needed. The finite element model consists of a mesh of the substructure layout consisting of 640 finite elements. The M&S environment can include any material in the analysis but is assumed to use symmetric composites.

| Degrees of Freedom | Material Selection | Level of Detail | Internal Loads | External Loads | Number of Iterations | Number of Matrices |
|---|---|---|---|---|---|---|
| Medium | Medium | Medium | High | High | Medium | Low |

### 4. On the Static Aeroelastic Tailoring of Composite Aircraft Swept Wings Modelled as Thin-Walled Beam Structures [121]

The author creates a thin-walled beam equivalent model for the purpose of aeroelastic tailoring of swept aircraft wings. The equivalent beam model allows for the inclusion of several interactions (e.g. transverse shear effects, non-uniform torsion, in plane warping) that make the governing equations complex. The materials are fiber reinforced laminate composites which are assumed to be orthotropic; however, special cases are presented where the method can be adapted to anisotropic fiber reinforced laminate composite materials. The external loads are calculated using strip-theory aerodynamics, which is solved in a manner similar to panel methods.

| Degrees of Freedom | Material Selection | Level of Detail | Internal Loads | External Loads | Number of Iterations | Number of Matrices |
|---|---|---|---|---|---|---|
| Low | Medium | Low | Low | Medium | N/A | High |

### 5. Development and Implementation of an Advanced, Design-Sensitive Method for Wing Weight Estimation [64]

The M&S environment known as EMWET (Elham Modified Weight Estimation Technique) performs classical structural analysis on portions of the substructure layout. Classical structural analysis methods solve governing equations with few DOF; however, several components are analyzed making the total number of DOF large.

The external loads are calculated from empirical models. The methods used can only use isotropic and orthotropic materials.

| Degrees of Freedom | Material Selection | Level of Detail | Internal Loads | External Loads | Number of Iterations | Number of Matrices |
|---|---|---|---|---|---|---|
| Medium | Low | Medium | Medium | Low | N/A | N/A |

### 6. Enhanced Conceptual Wing Weight Estimation Through Structural Optimization and Simulation [163]

The author created an Excel based M&S environment that uses classical analysis methods to size each component individually based on linear static analysis. The classical analysis methods represent only a handful of DOF; however, each component is represented increasing the DOF significantly. The classical methods size each component of the substructure using simplified features. The loads are calculated using several semi-empirical methods that assume an isotropic material.

| Degrees of Freedom | Material Selection | Level of Detail | Internal Loads | External Loads | Number of Iterations | Number of Matrices |
|---|---|---|---|---|---|---|
| Medium | Low | High | Medium | Low | N/A | N/A |

### 7. Multilevel Structural Optimization for Preliminary Wing-Box Weight Estimation [21]

The author uses a two step multilevel procedure to perform structural design. The first-level procedure utilizes a beam model of the wing optimized by MSC/NASTRAN SOL200 to perform initial estimates for the wing static and dynamic behavior. The beam model makes few assumptions about the details of the wing. The second-level procedure uses MSC/NASTRAN to implement linear static FEA on the defined substructure layout. The second level is more complex, and so the model, analysis, and optimization complexities will be based on this M&S method. The external loads are calculated using CFD analysis. The author mentions that the method can handle

composite materials with some minor changes; however, the example shown focuses on isotropic materials.

| Degrees of Freedom | Material Selection | Level of Detail | Internal Loads | External Loads | Number of Iterations | Number of Matrices |
|---|---|---|---|---|---|---|
| Medium | Low | Medium | High | High | N/A | Low |

## *4.4 Summary*

This chapter has focused on comparing existing structural design M&S environments to make meaningful observations to aid in the overall research objective. A method was developed based upon observations made during a previously executed literature survey [206] to quantify three values: model complexity, analysis complexity, and optimization complexity. Qualitative observations made in Section 4.3 are used in the method proposed in Section 4.2.2 to generate the quantified model complexity, analysis complexity, and optimization complexity. The results are shown in Table 10.

Several different methods for structural design, analysis, and optimization are presented in Chapter 3. These methods can be combined in a very large number of combinations to develop a structure M&S environment. However, several of the methods are impractical to use together. Thus, the purpose for quantifying the model,

| Paper | Optimization Complexity | Model Complexity | Analysis Complexity | Internal Loads |
|---|---|---|---|---|
| 1 | 0.6333 | 0.1481 | 0.1235 | EQ |
| 2 | 0.0033 | 0.4444 | 0.4506 | FE |
| 3 | 0.1411 | 0.2963 | 0.4444 | FE |
| 4 | 0.6868 | 0.0988 | 0.1296 | EQ |
| 5 | 0.5184 | 0.2469 | 0.1235 | CA |
| 6 | 0.4645 | 0.2963 | 0.1235 | CA |
| 7 | 0.2271 | 0.2716 | 0.3765 | FE |

Table 10: Quantified Model, Analysis, and Optimization Complexity

analysis, and optimization complexity is to make observations based upon existing M&S environments. The result of the literature survey is that despite the large number of combinations the majority of existing structural M&S environments can be divided into three categories based upon how the internal loads are generated: using Finite Element Analysis (FE), using classical structural analysis methods (CA), or using equivalent methods (EQ). Thus, the method of internal load calculation dictates the model, analysis, and optimization complexities for structural M&S environments.

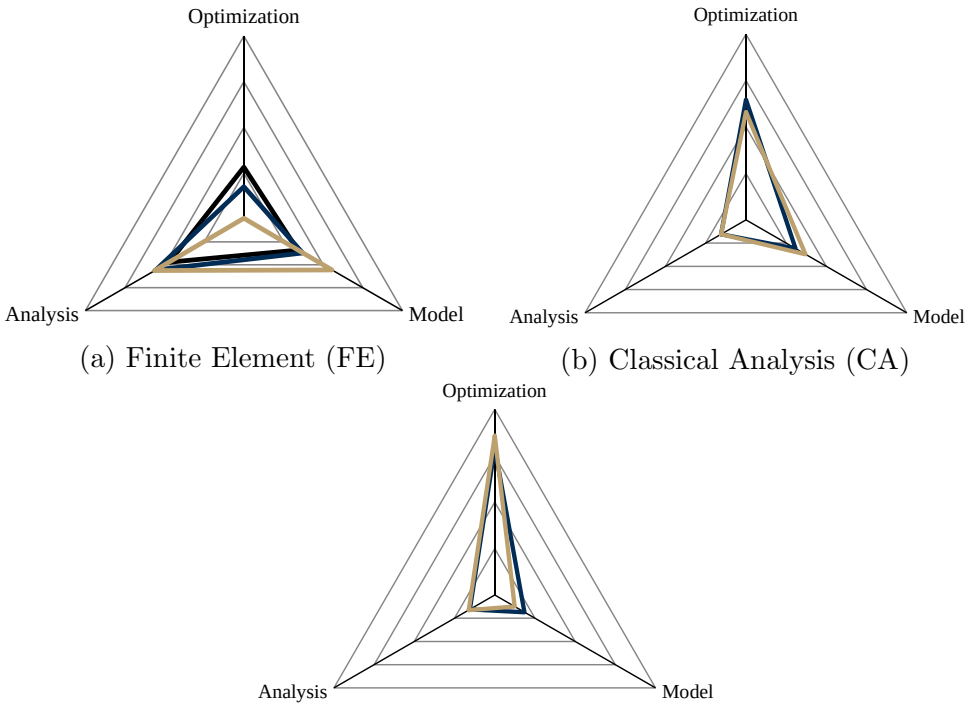


(a) Finite Element (FE)

(b) Classical Analysis (CA)

(c) Equivalent Methods (EQ)

Figure 33: Quantified Model, Analysis, and Optimization Complexities

Figure 33 presents three radar plots. Each axis of the radar plot represents either the model, analysis, or optimization complexity. The values from Table 10 are broken up according to the manner in which the internal loads are generated (see the final column).

Figure 33a illustrates the three M&S environments from the previous section that use Finite Element Analysis [21, 63, 129]. Structural M&S environments that utilize

Finite Element Analysis are characterized by larger model and analysis complexities. In one case [63] the number of elements is much larger (i.e. increased DOF) than the other two making the modeling complexity and analysis complexity larger. The large number of DOF makes the model and analysis complexity so large that the optimization complexity is near zero. Still, even for M&S environments that seek to reduce the number of elements the process of creating the mesh and then performing the analysis uses the majority of the computational cost available leaving little left for the optimization.

Figure 33b illustrates the two M&S environments from the previous section that use classical structural analysis to calculate the internal loads [64, 163]. Classical structural analysis (e.g. Bernoulli buckling, thin-walled shear flow, etc.) uses governing equations that can be solved analytically. For this reason the analysis complexity is much lower than Finite Element Analysis. The modeling is also much simpler as no meshing is required. However, M&S environment that use classical structural analysis tend to break the substructure layout into the components and then analysis each component separately. Extracting the necessary dimensions from the substructure layout increases the model complexity. The analysis and model complexities are much smaller for classical structural analysis methods; thus, there is enough computational power left over to have an increased optimization complexity.

Figure 33c illustrates the two M&S environments from the previous section that use equivalent methods to calculate the internal loads [83, 121]. Equivalent methods simplify the wing geometry to a simple structure that can be easily solved using classical structural analysis; thus, the analysis complexity is similar to those in Figure 33b. However, the simplification of the wing structure reduces the model complexity significantly; thus, M&S environments that use equivalent methods have the most optimization complexity of the three.

As discussed at the beginning of the chapter, an M&S environment will be required

to fulfill the overall research objective. Part of creating the M&S environment will involve selecting from the three categories: using Finite Element Analysis (FE), using classical structural analysis methods (CA), or using equivalent methods (EQ). In Chapter 1 the motivation for the research is laid out. Part of the motivation is implementing physics-based structural analysis to capture the effect of the substructure details on cost and weight. Equivalent methods are efficient at estimating structural behaviors of the entire wing structure; however, using equivalent methods makes it difficult to differentiate between substructure design decisions. Thus, according to the problem motivations in Chapter 1 the M&S environment should not use equivalent methods to calculate the internal loads.

Framework Proposition 1 is proposed at the end of Chapter 2. This observation is based on the design space characterization and states that due to the complex and discontinuous nature of the physics-based structural analysis design space, a strategy of exploration requiring a large number of analysis executions will be required. In terms of the model, analysis, and optimization complexities a strategy of exploration means reducing the model and analysis complexities to increase optimization complexity. Of the three categories (Finite Element Analysis (FE), classical structural analysis methods (CA), or equivalent methods (EQ)) the M&S environments that used Finite Element Analysis have the lowest optimization complexity (Figure 33); therefore, according to Framework Proposition 1 the M&S environment should not use Finite Element Analysis to calculate the internal loads.

If both equivalent methods and Finite Element Analysis are poor choices, then classical structural analysis methods are the most appropriate methods to use in the structural M&S environment used to satisfy the overall research objective. Using classical structural analysis will allow the M&S environment to differentiate between substructure design decisions while having low enough model and analysis complexity to explore the complex and discontinuous design space. This is expressed in Framework

Proposition 2 below.

---

**Framework Proposition 2**

If a strategy of exploration requiring a large number of analysis executions is necessary, then the structural analysis sub-problem should be executed using lower fidelity classical structural analysis methods.

---

# CHAPTER V

# DEVELOPING A WING BOX SUBSTRUCTURE DESIGN FRAMEWORK

---

**Overall Research Objective**

Develop a physics-based structural design method to incorporate new concepts, technologies, and materials into the conceptual design phase.

---

The overall research objective for this thesis is to develope a design method to implement physics-based structural design in the conceptual design phase. The previous chapters have addressed Research Objective 1 and Research Objective 2 by making gathering information and making observations regarding what the design method will need to succeed. This information was synthesized in order to make general propositions for the eventual framework that will be required. The resulting information, observations, and propositions will be used during the next three chapters to address Research Objective 3.

---

**Research Objective 3**

Develop a framework using the previously identified structural analysis and optimization methods based upon research observations made from characterizing the design problem.

---

This chapter is the first of three chapters that address Research Objective 3. In

this chapter the overall design framework will be laid out. First an existing framework will be introduced and will be used as a guide for the developed framework. Next several key features that the framework will require will be introduced. Finally, the basic concepts needed to implement each feature will be introduced. Implementation of the framework will be discussed in the following two chapters.

## *5.1 Previously Existing Framework*

In early 2011, Triumph Aerostructures - Vought Aircraft Division approached Aerospace Systems Design Laboratory (ASDL) at the Georgia Institute of Technology with a project involving one of their frameworks for substructure configuration. The framework developed by Triumph [180] is meant for use in the initial stages of substructure layout. It sizes a wing box substructure for a given wing and wing box configuration based on minimum feasible weight.

Triumph's framework is depicted in Figure 34. It uses several classical structural analysis routines to size the individual parts (i.e. ribs, covers, spar segments) in a serial fashion. There is an iterative loop after the Spar Analysis routine to account for the

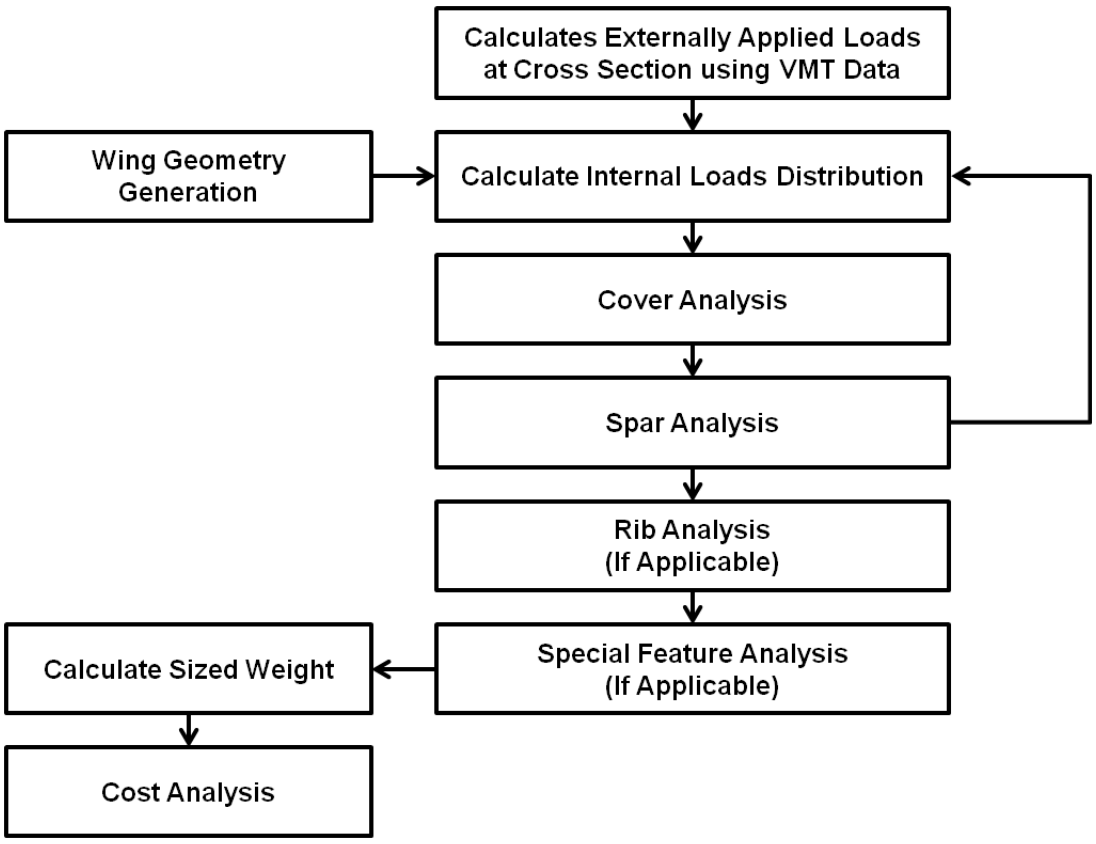


Figure 34: Triumph Substructure Design Method

The method used to size the substructure involves separate excel based analysis routines with inputs that are entered manually. The sizing process itself is an iterative process, meaning long and arduous tasks are often repeated. The result of this iterative and manual process is a long and tedious design cycle.

Additionally Triumph's framework assumes a fixed outer mold line (OML) and typically gathers the necessary geometric information from a previously existing CAD file. Because Triumph's framework is intended for the preliminary design phase this is not a problem. However, in the conceptual design phase the OML is fluid and numerous different substructure configurations need to be investigated. Relying on manually imputing the geometric information makes it difficult to explore the numerous alternatives mentioned in Framework Proposition 1.

The current framework has several problems that make it difficult to use to solve

the overall research objective. The proposed framework must improve the current framework so that it can investigate the numerous alternatives and explore the complex and discontinuous design space presented by physics-based wing box substructure design problem.

In order to accomplish this the framework must have several key features. The framework must be completely **autonomous** so that a single alternative can be investigated without human interaction, the framework must be **rapid** so that several alternatives may be investigated, and the framework must be **parametric** so that the system responses can be explored with fewer variables.

These key aspects result in the need for a M&S environment. The next section will introduce the M&S environment that will be used in the proposed design framework and how it will address each one of the key features required. The following section will discuss how the key features of the design framework and M&S environment are important to solving the substructure configuration design problem.

## *5.2 Wing Box Substructure Sizing Modeling & Simulation Environment*

The Overall Research Objective is to create a physics-based structural design method which will implement structural design, structural analysis, and structural optimization (see Chapter 3). The wing box substructure sizing problem focuses on the structural analysis and structural optimization portion of the method.

The wing box substructure sizing problem entails performing structural analysis and structural optimization on a given configuration. The configuration has a fixed wing outer mold line (OML), wing planform, external loads, and substructure layout. The wing box structural sizing problem uses structural analysis and optimization to size each feature (i.e. web, upright, cap) for every part (i.e. rib, stringer, spar, skin panel) of the given configuration. The dimensions could be sized using both weight and cost. However, including cost during substructure sizing is rarely done.

In sizing optimization problems for simple structures, where the material and part count is fixed and the only design variables are the dimensions, reducing the weight is equivalent to reducing cost. Also, including cost would increases the number of executions substantially and make the optimization problem more difficult; therefore, to simplify the optimization and reduce run time only the weight of each part will be considered.

The beginning of Chapter 4 laid out an argument that an M&S environment is required to solve a physics-based structural design problem; specifically, the structural analysis and optimization portion of the structural design problem. The wing box substructure sizing problem focuses on the structural analysis and structural optimization portion of the structural design problem; thus, the wing box structure sizing problem is solved using the required M&S environment. The structures M&S environment will consist of the methods laid out in Chapter 3 and will use classical structural analysis methods as suggested by Framework Proposition 2.

There are three concepts that are important to the wing box substructure sizing problem: the classical structural analysis methods, multi-level optimization, and sizing optimization. All three methods aid in the Overall Research Objective by addressing Research Observation 1, Research Observation 3, and Framework Proposition 2. These three concepts are discussed below.

### 5.2.1 Classical Structural Analysis Routines

Chapter 4 used a literature survey of wing box structures M&S environments to develop Framework Proposition 2. Framework Proposition 2 states that the structural analysis sub-problem should be executed using classical structural analysis methods. Many assumptions are required to use classical structural analysis during the wing box substructure sizing problem; these assumptions are discussed below.

Section 3.2 introduced the basic concepts of structural analysis. One of the basic

concepts of structural analysis is the need to simplify the structure so that the governing equations can be applied. All forms of structural analysis follow this basic principle (i.e. wing simplified to a plate, the substructure decomposed into elements). It is impractical to perform structural analysis on the entire wing box using classical structural analysis methods; therefore, the wing box is decomposed into components (i.e. spars, ribs, covers) and the components are simplified to their most basic features (i.e. caps, webs, uprights). The decomposition will allow the geometry to be simplified enough that linear elastic governing equation can be applied.

Additionally, several assumptions are made to further simplify the structural analysis problem. Examples of simplifying assumptions include: constant thicknesses across the feature, loads applied uniformly across the component, and the absence of detailed features, like bolts. The resulting geometries are the most basic form of each of the substructure components that can still capture the effect of the wing box design variables on the substructure configuration.

Several classical structural analysis routines were created to apply classical structural analysis to the simplified substructure components. These routines include: the Torque Box Analysis Routine, the Cover Panel Sizing Routine, the Spar Segment Sizing Routine, and the Rib Sizing Routine. The Torque Box Analysis Routine is responsible for estimating the internal loads for each substructure component based upon a cross-section of the wing box configuration and the external loads. These internal loads are then used to size each of the components using the respective sizing routine (i.e. the Cover Panel Sizing Routine, the Spar Segment Sizing Routine, and the Rib Sizing Routine). The classical analysis routines are detailed further in Chapter 7.

### 5.2.2 Multi-Level Optimization

As discussed in the previous section, the classical structural analysis and sizing routines require decomposing the wing box substructure into the components. By decomposing the substructure into components the structural analysis problem is simplified so that classical analysis methods can be used. However, decomposing the problem means that only the component level objective functions are being optimized. An optimum at the system level may not be found because only the component level objective functions are optimized and interactions between the components may not be accounted for [56, 128]. Thus, a strategy that can optimize the system level objective functions based upon the component level objective functions is required.

Structural sizing problems that require decomposition typically use multi-level optimization. Multi-level optimization (MLO), which is mathematically similar to multidisciplinary optimization (MDO) [55, 128], decomposes a complex system into individual elements and then synthesizes the results of the optimization of the individual elements to find the optimum of the system. MLO is also useful for solving structural sizing problems because these problems tend to have an excessively large number of design variable and constraints [193, 194]. By decomposing the problem into a hierarchy of smaller more manageable problems, the optimization problem is simpler at both the component and system level. Thus, MLO helps address both Research Observation 1 and Research Observation 3.

Solving MLO problems require mathematical architectures to incorporate the interaction between the elements into the optimization of the sum of the elements. Several methods already exist to solve MLO problems [15, 49, 55, 128, 192]. Below is a discussion that characterizes these methods as well as identifies the advantages and disadvantages of each.

As defined by Martins [128], the general MLO and MDO problem is expressed below.

Minimize:

$$f_0(\bar{y}_0, \bar{y}_i, \bar{x}_0, \bar{x}_i) + \sum f_i(\bar{y}_0, \bar{y}_i, \bar{x}_0, \bar{x}_i) \qquad \text{objective function} \tag{26}$$

With respect to:

$$\bar{y}_0, \bar{y}_i, \bar{x}_0, \bar{x}_i, \hat{y}_i \tag{27}$$

Subject to:

$$c_0(\bar{y}_0, \bar{x}_0) \qquad \text{global constraints} \tag{28}$$

$$c_i(\bar{y}_0, \bar{x}_0, \bar{x}_i) \qquad \text{discipline constraints} \tag{29}$$

$$c_i^c = \hat{y}_i - \bar{y}_i = 0 \qquad \text{consistency constraints} \tag{30}$$

The MDO problem is solved in the same iterative fashion as a normal numerical optimization problem except MLO uses an objective function that is a summation of the objective functions from the individual elements as well as the global objective function. Additional differences are: the state variables $y$ (also known as the responses) come from several different analyses instead of one, the constraints are also separated into global constraints (applied at the system level) and discipline constraints (applied at the component level), and the introduction of consistency constraints. There are several different methods for solving MLO/MDO problems. These methods differ based upon where the constraints are enforced, how the constraints are enforced, and where the optimization occurs. The differences between architectures will be discussed in detail below.

The consistency constraint is used in several MLO and MDO architectures to enforce consistency in the problem. It accomplishes this by using two sets of state variables, $\bar{y}_i$ and $\hat{y}_i$. One of the state variables is estimated at the system level while the other is the result of the individual analyses. Enforcing the constraint that these two values be equal forces the MDO problem towards consistency.

There are two underlying decisions that are made during selection of an MLO architecture. The first is the execution of the optimization problem. The MLO strategy is *monolithic* if each individual analysis routine is executed and then the results are

used to solve one optimization problem at the top level (i.e. the system level). A monolithic architecture is shown in Figure 35. Monolithic architectures, also known as simultaneous analysis and design (SAND), tend to be more difficult to solve because they only have one optimizer that is responsible for solving the design variables and enforcing the constraints [15].

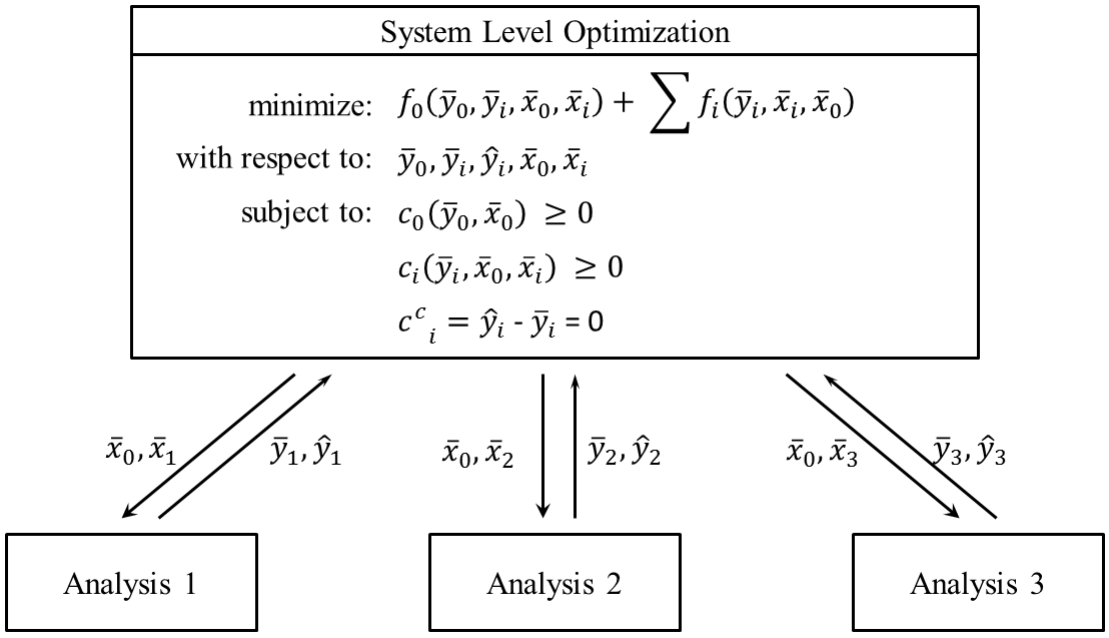


Figure 35: Monolithic Optimization Problem [128]

If the optimization problem is decomposed among the individual elements then the MLO strategy is said to be *distributed* (Figure 36). Distributed architectures tend to have simpler optimization problems with fewer design variables and constraints to account for; however, the cost is that there are more optimization problems to solve during one system optimization iteration. The increased number of optimization problems causes a growth in the number of executions of the individual analysis routines. Thus, given the same problem a distributed architecture will usually have longer run times than a monolithic architecture [201].

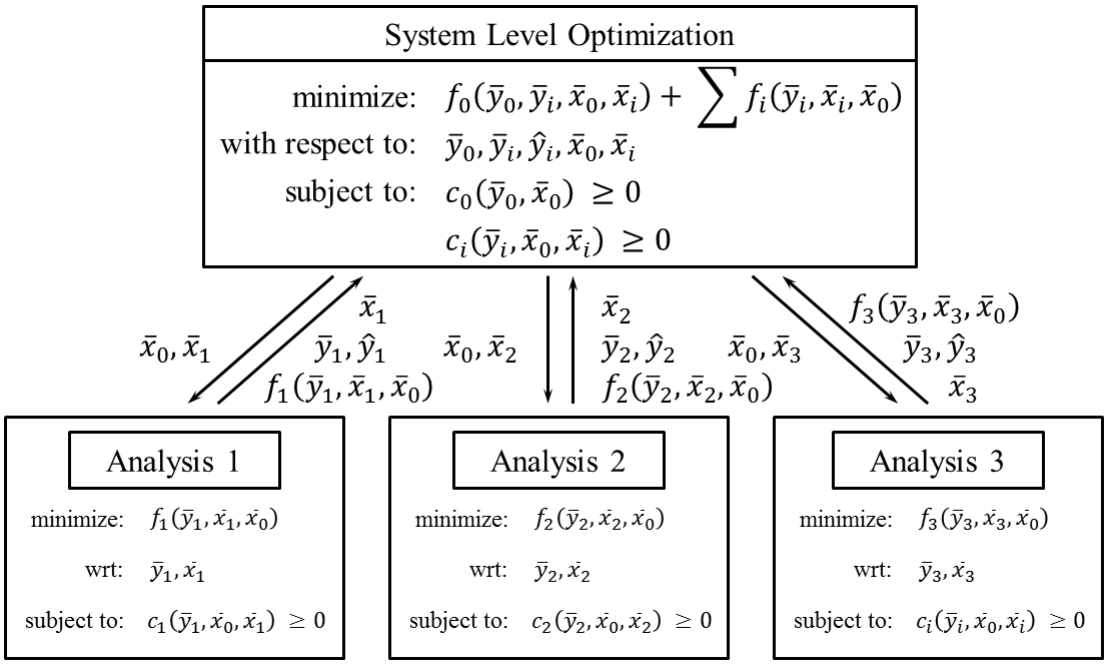


Figure 36: Distributed Optimization Problem [128]

The second underlying decision that is being made during the selection of an MLO architecture is the enforcement of the consistency constraints. The consistency constraint is used in several MLO and MDO architectures to enforce consistency between the optimums of the system level and the component level. It accomplishes this by using two sets of state variables, $\bar{y}_i$ and $\hat{y}_i$. One of the state variables is estimated at the system level while the other is the result of the individual analyses. Enforcing the constraint that these two values be equal forces the MDO problem towards consistency.

To comprehend decision being made based on enforcing the consistency constraint, two terms need to be defined:

| | |
|---|---|
| **Individual discipline feasibility:** | The problem has converged to a solution that produces a feasible solution for each individual element [49]. |
| **Multidisciplinary feasibility:** | In addition to being individual discipline feasible, the problem also converges to a design where the input state variables for each analysis matches the outputs of the other analyses via the interdisciplinary mappings [49]. |

*Multidisciplinary feasible methods* (MDF), also known as nested analysis and design (NAND) [15], utilizes multidisciplinary analysis (MDA) to solve the governing equations for each individual analysis to ensure that all consistency constraints are satisfied [128, 201]. The constraints and objective functions are calculated for the system level optimization after the MDA is implemented; thus, MDF methods ensure that the design is multidisciplinary feasible. An MDF architecture is diagrammed in Figure 37.

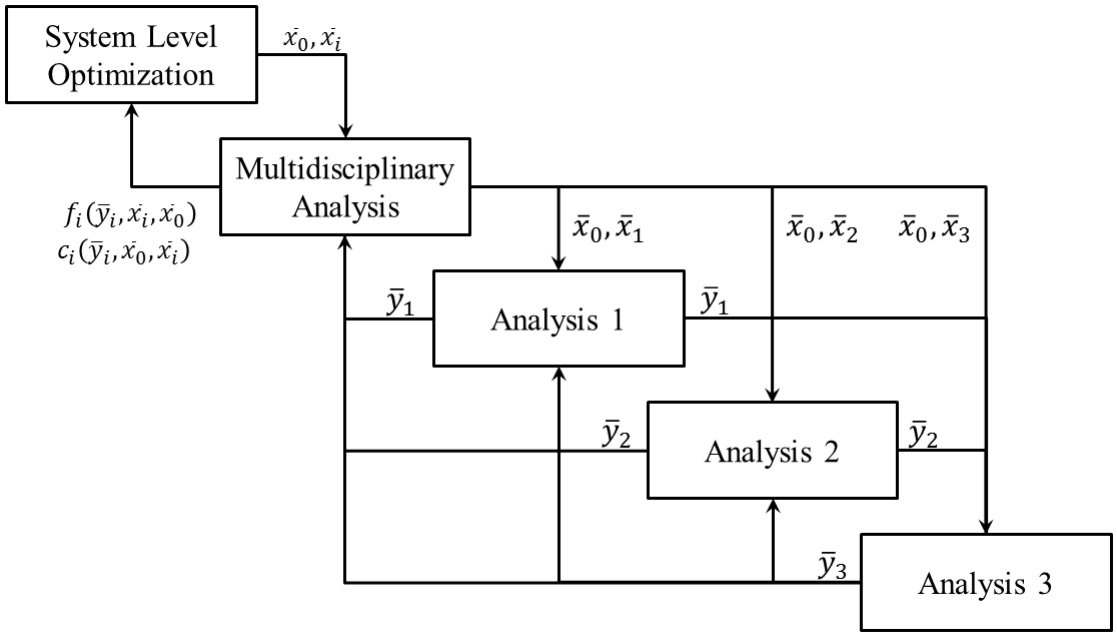


Figure 37: Multidisciplinary Feasible Method

*Individual discipline feasible* methods do not utilize MDA. Instead, the individual elements are decoupled so that no consistency constraints are enforced during analysis

[128, 201]. IDF methods ensure that the design will always be individual discipline feasible at every iteration (Figure 38); however, more must be done to ensure that the result is multidisciplinary feasible. To accomplish this, the system level optimization creates an estimate of analysis responses. These values are then compared to the results of the individual analyses via the consistency constraint [128]. Assuming the consistency constraints can be satisfied, the system level optimization will converge to a solution that is multidisciplinary feasible.

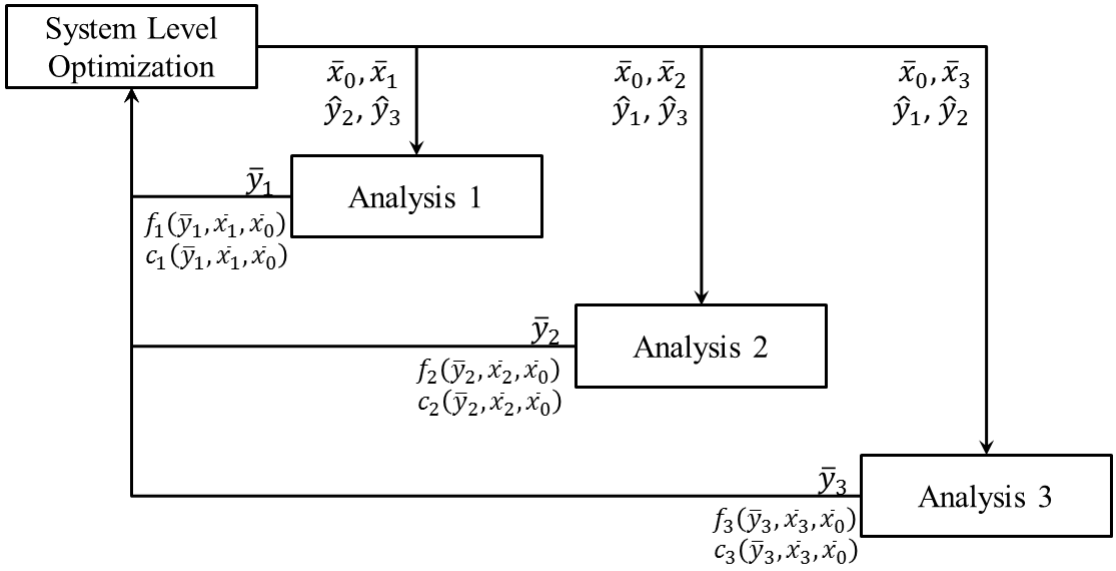


Figure 38: Individual Discipline Feasible Method

Selecting between MDF and IDF will be done on the basis of how important multidisciplinary feasibility is to the problem and whether extra time needed to implement MDA is necessary. The major difference between MDF and IDF is the execution of the MDA to ensure the design is multidisciplinary feasible at every iteration; however, implementing MDA will increase the time it takes to converge on a solution [128] and limits the use of parallel computing [201].

IDF methods do not guarantee multidisciplinary feasibility at every iteration, but

instead attempt to converge on a multidisciplinary solution. IDF methods typically have shorter run times per iteration because MDA is not required; however, IDF methods risk not be multidisciplinary feasible if the consistency constraints cannot be converged, or if the execution of the optimization routine ends prematurely.

Other considerations for selecting between MDF and IDF include: the number of coupling variables because too many consistency constraints might affect the efficiency of an IDF optimizer [128], whether or not gradients will need to be calculated as gradients are easier to calculate using IDF [128], and whether the architecture is going to be distributed or monolithic.

### 5.2.3 Sizing Optimization

The final portion of the wing box substructure sizing problem is the sizing optimization. The previous section introduced MLO. MLO will be used to include the interactions between the decomposed components in the system level optimization. However, two decisions must be made when selecting the MLO method: distributed or monolithic, and MDF or IDF. These two questions must be addressed to solve the wing box sizing problem.

An understanding of the structural optimization problem is necessary to decide between monolithic and distributed. The structural optimization problem was discussed in section 3.3. During structural optimization several constraints are applied to the structure. The most important and numerous of these constraints are the Margins of Safety and the dimension constraints due to manufacturing. The Margins of Safety and dimension constraints are typically applied on the component level. Thus, it is more convenient to use a distributed architecture.

An example will help illustrate why a distributed architecture is more convenient. The Rib Sizing routine contains two margin constraints which pertain to the rib web and rib caps. The only variables that effect these margins are the internal loads and

rib dimensions. The rib sizing problem is to minimize the rib dimensions for given rib under a given load. The sizing of each rib could be combined to include all the ribs, covers, and spar segments sized monolithically; however, doing so would provide no benefit to sizing the rib. Using a distributed method, where the rib sizing problems are handled independently, provides the benefit of a simpler optimization problem with few negatives.

The final decision is to decide whether the decomposed wing box substructure sizing problem will need to be solved with a MDF method or an IDF methods. However, the structural sizing problem is different from most other MLO and MDO problems in that an IDF method will also produce an multidisciplinary feasible design. Each decomposed sizing problem is to minimize the weight. While performing each sizing problem does not guarantee that the minimum wing box weight is found, it does guarantee that the entire wing box substructure is a feasible design. Thus, the substructure sizing will be performed along with the classical analysis method in the Cover Sizing Routine, the Spar Sizing Routine, and the Rib Sizing Routine.

## *5.3 Wing Box Configuration Design Problem*

The wing box structures sizing problem focuses on the structural analysis portion and the structural optimization portion of the Overall Research Objective. The remaining structural design portion of the Overall Research Objective is solved during the wing box configuration design problem.

The wing box configuration design problem utilizes the M&S environment to perform design space exploration of the wing box substructure configuration. The available design variables include the wing shape (OML and planform), the substructure configuration, and the load cases. The wing box configuration design problem captures the effect of the design variables on the total wing box weight and the total wing box cost so that design decisions can be made.

There are two concepts that are important to the wing box configuration design problem: multi-objective optimization and design space exploration. Both methods aid in the Overall Research Objective by addressing Research Observation 2, Research Observation 4, Research Observation 5, Research Observation 6, and Framework Proposition 1. These concepts are discussed below.

### 5.3.1 Multi-Objective Optimization

One of the motivations for using physics-based structural design is to incorporate the structural layout so that more accurate cost data can be used during the structural design problem. The cost could be addressed by optimizing the wing box substructure for both weight and cost; however, to simplify the wing box substructure sizing problem the substructure is only optimized for minimum weight. The cost will be incorporated into the wing box configuration design problem to satisfy Research Objective 4.

Multi-Objective Optimization (MOO) is required to incorporate cost into the wing box configuration design problem. MOO methods attempt to find optimal solutions when presented with more than one objective. Unlike single-objective optimization problems, multi-objective problems have more than one solution. Instead MOO problems solve for a set of solutions known as a Pareto frontier. The terms Pareto optimal and Pareto frontier are defined below.

**Pareto optimal:** An optimal solution where it is impossible to improve upon one objective without detriment to the other objectives

**Pareto frontier:** A set of Pareto optimal solutions

The existence of the Pareto frontier means that MOO problems have two phases; the first is to identify the Pareto optimal points, and the second is to identify a preferred solution from the Pareto frontier [57]. MOO methods are categorized by their approach to the two phases.

The MOO problem as defined by Marler and Arora [126] is given below.

Minimize:

$$F(\bar{X}) = [F_1(\bar{X}), F_2(\bar{X}), \ldots, F_k(\bar{X})]^T \qquad \text{objective function} \tag{31}$$

Subject to:

$$g_j(\bar{X}) \leq 0 \qquad j = 1, m \qquad \text{inequality constraints} \tag{32}$$

$$h_k(\bar{X}) = 0 \qquad k = 1, l \qquad \text{equality constraints} \tag{33}$$

$$X_i^l \leq X_i \leq X_i^u \quad i = 1, n \qquad \text{side constraints} \tag{34}$$

In the first phase of the MOO problem Pareto optimal points, or an estimate of Pareto optimal points, must be identified; therefore, a strategy that assesses the multiple objective functions is needed. There exist three general strategies to find a Pareto optimal solution: combine objective functions, rank objective function, and establish objective function goals.

**Combine objective functions:** The first strategy is to combine the objective functions into one equation. An example of this strategy is the weighted sums method [127]. The weighted sums method combines the individual objective functions into the multi-objective function in Equation 35.

$$F(X) = \sum_{i=1}^{n} w_i F_i(X) \tag{35}$$

Other methods similar to this include the exponential weighted criterion and the weighted product method [126]. Methods that utilize a general strategy of combining the objective functions into one are common because it is easy to implement and do not require multiple function calls.

**Rank objective functions:** The second general strategy for assessing the multiple objective functions to find a Pareto optimal solution is to rank the objective functions by importance and then minimize the functions sequentially. The lexicographic method is an example of one of these strategies [126].

Minimize:

$$F_i(\bar{X}) \tag{36}$$

Subject to:

$$F_j(\bar{X}) \leq F_j(\bar{X}_j^*) \tag{37}$$
$$j = 1, 2, \ldots, i-1 \tag{38}$$
$$i = 1, 2, \ldots, k \tag{39}$$

During each subsequent optimization a constraint is added so that the objective functions with higher importance cannot be increased. This process is repeated for every objective function so that the final objective function will have to take into account every other objective function as a constraint.

Methods that use the general strategy of ranking objective functions and then minimizing them one at a time are not used as much as the other two methods. These methods require the execution of multiple optimization problems so they take longer than methods that use the other two strategies.

**Establish objective function goals:** The final strategy for assessing the multiple objective functions is to specify goals for each objective function and then evaluate design points based upon how well it achieves these goals. The goal programming method utilizes this strategy [126]. The method establishes a goal for each objective. Then an optimization problem is solved to minimize the total deviation from these goals. Methods that use a goal specifying strategy have the benefit of only having to solve one optimization problem. However, specifying the goals of an objective function is much harder than selecting a weighting for each function. Therefore, methods that use a goal specifying strategy are more difficult and less common than methods that combine the objective function into one equation with weightings.

To this point only the first phase of solving an MOO problem, identifying Pareto optimal points, has been considered. The second phase is to select a final solution from the Pareto frontier. There are three ways for the decision-maker to articulate a

preference: a priori articulation of preferences, a posteriori articulation of preferences, and no preferences [126]. The weighted sum method in equation 35 is used to illustrate each approach below.

Using an **a priori articulation of preferences** means the decisions that specify the preferences are made before the Pareto optimal points are found. In terms of the weighted sums method, implementing an a priori articulation of preferences amounts to selecting the weightings $w_i$ before any analysis is done. Under the circumstances, the MOO problem is solved easily and only one run of the optimization problem is required. However, without a well-defined problem it is difficult to identify these weightings and arbitrarily specifying the weightings amounts to randomly selecting a design from the Pareto frontier.

Applying an **a posteriori articulation of preferences** means that the selection of a design point from the Pareto frontier will occur after all the Pareto optimums have been assessed. This means that the points along the Pareto frontier will have to be mapped to the parameters that define the preference. The mapping is accomplished for the weighted sums method by calculating the Pareto optimums for a set of $w_i$s. An a posteriori articulation of preferences requires substantially more work but is justified as it allows for exploration of the Pareto frontier [126].

**Specifying no preferences** means locating the Pareto optimum point that satisfies each objective function equally. This is equivalent to an a priori articulation of preferences in that assumptions are being made before an analysis is completed. Thus, it will have the same advantages and disadvantages as an a priori articulation of preferences.

### 5.3.2 Design Space Exploration

At the end of Chapter 2 several of the research observations were used to describe the physics-based design space as complex and discontinuous. These observations

led to Framework Proposition 1 which states that s strategy of exploration is necessary requiring a large number of analysis executions. Framework Proposition 1 will be addressed in the wing box configuration design problem through design space exploration.

The concepts in design space exploration are very similar to those in optimization; however, there are differences between the two concepts. Optimization is focused on identifying a set of design variable that minimize a given objective function. The iterative nature of optimization means that only one point is being assessed with no consideration to correlation between the design variables. Furthermore, optimization methods are considered to be more efficient if they minimize the number of function calls. Minimizing the number of function calls is equivalent to reducing the number of alternatives explored.

Design space exploration seeks to capture the effect of the design variables on the responses across as much of the design space as possible. The emphasis of design space exploration is to explore as many alternatives as possible (as opposed to minimizing the number of function calls). Design space exploration also emphasizes capturing the correlations between the design variables through a systematic approach rather than the iterative approach of optimization. Optimization is still used extensively throughout design space exploration; however, the methodologies differ. The benefits that design space exploration provides over traditional optimization are required to solve the wing box configuration design problem.

There are three requirements to perform design space exploration: a representation of the design space, automated and rapid analysis of the alternatives, and an exploration method [102]. The first two requirements are satisfied by the M&S environment that will be created to solve the wing box substructure sizing problem; however, the wing box configuration design problem will have to select an exploration method. There are two common exploration methods used with design space exploration: heuristic

methods [70,158] and design of experiments [144]. Heuristic methods are less structured than design of experiments but offer the possibility of locating the best alternatives faster. Design space exploration methods that use design of experiments typically also require surrogate models [67, 142] to fill in the gaps between experiments or for visualization of the design space.

## *5.4 Summary*

The overall design methodology proposes decomposing the wing box substructure design problem into two sub-problems: the substructure sizing problem and the configuration design problem. The substructure sizing problem will be solved using an M&S environment. The M&S environment will implement classical structural analysis as proposed in Framework Proposition 2. The M&S environment will utilize MLO to address several problems presented by Research Observation 1 and Research Observation 3. A distributed MLO architecture is needed to implement classical structural analysis; however, the architecture can be either MDF or IDF. Further details about the M&S environment will be discussed in Chapter 6 and 7.

The wing box configuration design problem will utilize the M&S environment during the design process. The M&S environment will be used for both DSE and MOO. DSE will provide a systematic method to explore the discontinuous (Research Observation 2), multimodal (Research Objective 4), and discontinuous (Research Observation 6) wing box configuration design problem. MOO will enable the design problem to optimize for both the weight and cost (Research Objective 4).

# CHAPTER VI

# STRUCTURAL PRELIMINARY ANALYSIS AND DESIGN SPACE EXPLORATION TOOLKIT

---

**Research Objective 3**

Develop a framework using the previously identified structural analysis and optimization methods based upon research observations made from characterizing the design problem.

---

Chapter 5 introduced a design framework to address the Research Objective 3. The framework divides the wing box structural design problem into two sub-problems: the wing box substructure sizing problem and the wing box configuration design problem. The previous chapter established that the wing box substructure sizing problem is solved using an M&S environment and the wing box configuration design problem will be solved through design space exploration using the M&S environment. Therefore, the current chapter and Chapter 7 will document an M&S environment called SPANDSET (Structure Preliminary ANalysis and Design Space Evaluation Toolkit).

SPANDSET is an M&S environment built for structural sizing and configuration optimization of a wing box using classical structural analysis, as proposed by Framework Proposition 2, and multi-level optimization. The use of classical analysis methods to carry out structural analysis and sizing reduces the run time of the M&S environment; thus, more alternatives can be explored, as proposed by Framework Proposition 1.

The structural analysis method was developed by Triumph Aerostructures - Vought Aircraft Division for use in preliminary wing box sizing. Aerospace Systems Design Laboratory (ASDL) at the Georgia Institute of Technology developed a framework to integrate a parametric geometry tool, manufacturing cost analysis, and the Triumph developed tools and methods so that rapid exploration of the substructure design space can be performed to solve the wing box configuration design problem.

SPANDSET performs rapid structural sizing for a substructure configuration of a wing box. Given an initial wing planform and OML, SPANDSET calculates the necessary geometric information, distributes the geometric information to the analysis routines, automatically runs optimization on several of the substructure dimensions, then uses the results of the optimization to generate weight and cost estimates for the entire wing. The structural analysis modules SPANDSET uses include the wing geometry tool, external loads module, internal loads distribution analysis, upper and lower cover analysis, spar analysis, rib analysis, and recurring manufacturing cost analysis.

SPANDSET is implemented using Microsoft Excel routines. The sizing for each structural analysis routine is performed using the Excel Solver Add-In. Integration and automation of the analysis routines is accomplished through Visual Basic for Applications (VBA) code. The routine converges to a solution within several iterations and takes on the order of 30 minutes to complete a single design concept evaluation.

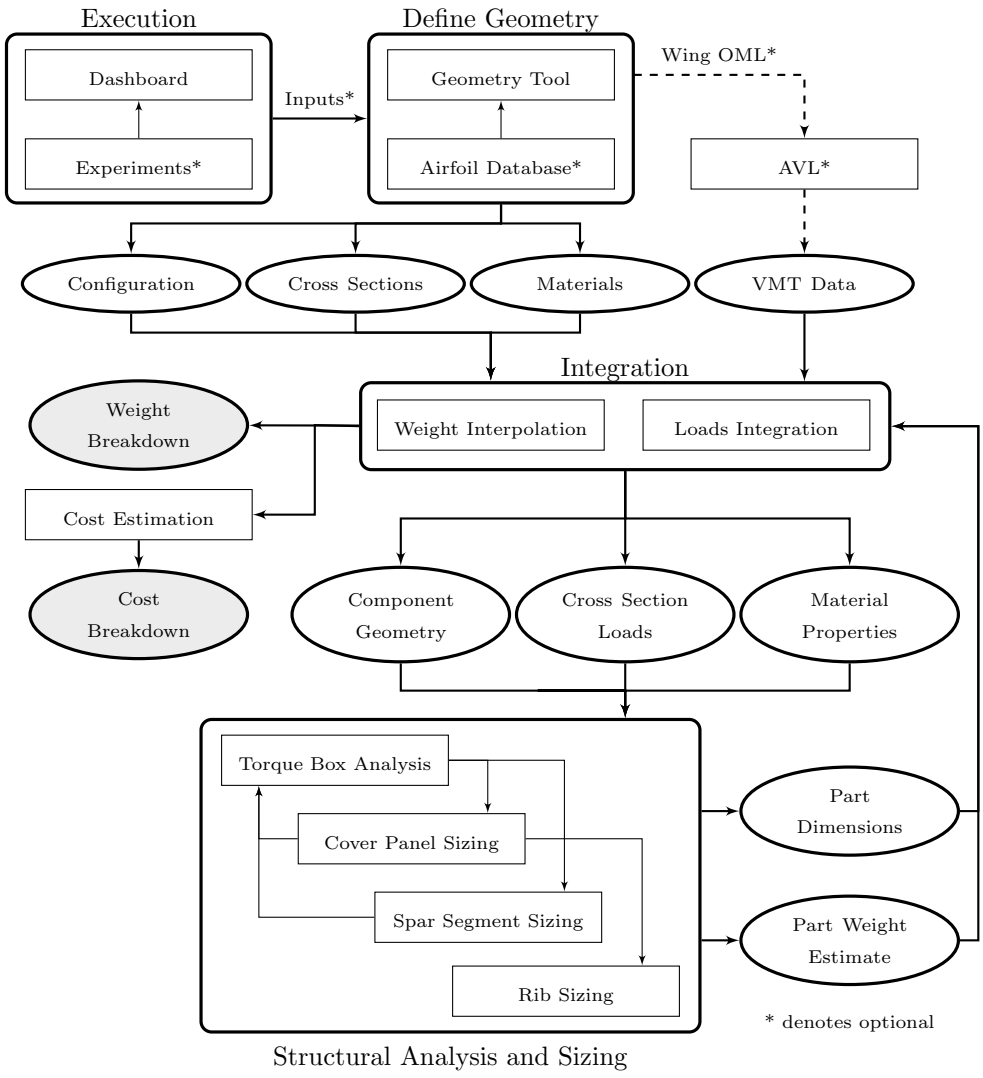


Figure 39: SPANDSET Flow Chart

SPANDSET's process is divided into four phases and is depicted in Figure 39.

- Phase 0: User Inputs
- Phase 1: Generate Geometry and External Loads
- Phase 2: Structural Analysis and Sizing Routines
- Phase 3: Weight and Cost Breakdown

The first phase (Phase 0: User Inputs) requires the user to define the wing OML, wing box substructure, and several important optimization settings that need to be

defined before SPANDSET can be executed. *Dashboard* executes SPANDSET and contains the majority of the VBA macros required to execute the analysis and transfer data. *Experiments* is an optional file that is only used by *Dashboard* that stores all the inputs required for the different design alternatives. *Geometry Tool* is the file primarily responsible for defining the geometry. A wing OML and substructure configuration needs to be defined before SPANDSET can be executed. The remainder of this chapter will describe the three remaining phases of SPANDSET.

## 6.1 Phase 1: Generate Geometry and External Loads

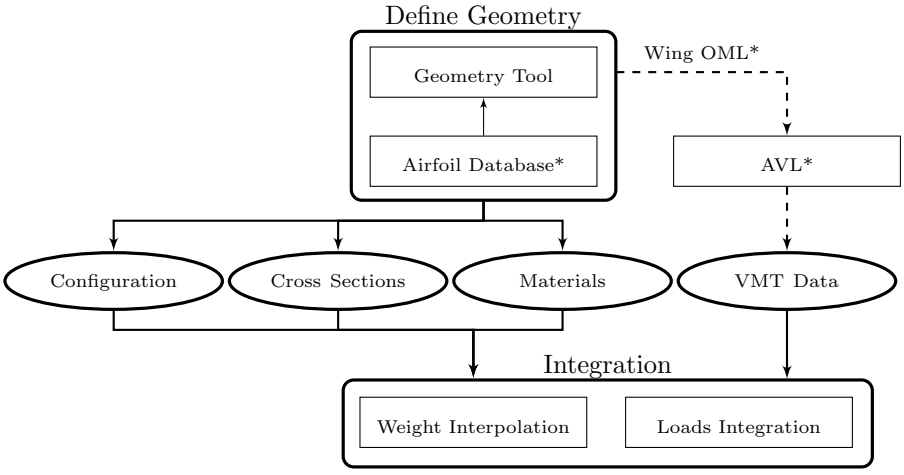


Figure 40: Phase 1 of SPANDSET

Chapter 3 established that the geometry and external loads must be defined to perform structural analysis. Phase 1, which is outlined in Figure 40, illustrates how SPANDSET accomplishes this. *Geometry Tool* contains a parametric geometry model that translates the user inputs (Phase 0) into the geometric data required by the structural analysis and sizing routines. Additionally, *Geometry Tool* is used to set the material properties for each part. The output from *Geometry Tool* is the substructure configuration, the cross section data, and the material properties. The parametric geometry model is discussed further in section 6.1.1.

The second part of Phase 1 is to generate the external loads. SPANDSET uses VMT (Shear, Moment, Torque) data along a specified reference axis to apply external loads to the substructure. SPANDSET gathers this data in one of two methods: either the data is manually input into SPANDSET or SPANDSET inputs the wing geometry from *Geometry Tool* into AVL (Athena Vortex Lattic) [61] which calculates the VMT data. The calculation of the external loads are discussed further in section 6.1.2.

### 6.1.1 Parametric Geometry Model

The original structural analysis methods used by SPANDSET and developed by Triumph require a large amount of geometric information. Originally the geometric information was gathered by hand from 3D CAD models; a task that prohibited automation and made the design cycle time burdensomely long. To mitigate these problems a parametric geometry model (PGM) was developed.

The PGM aids in addressing the overall research objective by providing the geometric information and material properties required for structural analysis in an automated and rapid fashion, and by reducing the dimensionality of the problem through parametric relationships. A major drawback to the PGM is that it limits the design alternatives that can be explored by making assumptions about the substructure layout. For example, an assumption used by the PGM is that the ribs have equal spacing; however, better alternatives likely exist that do not have evenly spaced ribs. Even still, SPANDSET reduces the combinatorially large number of variables required to define the entire wing box geometry to less than 50 by using the PGM combined with the sizing and analysis routine. Thus, the PGM is an important feature of SPANDSET that aids in addressing Research Observation 1.

The PGM also aids in addressing the discrete design decisions discussed in Research Observation 2. Chapter 2 describes two common discrete design decisions made during structural design problems: configuration selections and material selections. The PGM

aids SPANDSET in dealing with both of these discrete design decisions. The effects of discrete configuration decisions are automatically accounted for in the parametric geometry model. For example, if intermediate spars are added to the configuration then the stringers and covers are automatically adjusted accordingly. Additionally, the parametric geometry model allows for material selection for each part feature. Thus, the PGM allows SPANDSET to addresses Research Observation 2.

As discussed above, the parametric geometry model makes several assumptions to reduce the dimensionality of the problem as well as automate the process of creating the geometric information for a given alternative. These assumptions will have a large effect on the overall design space; thus, the assumptions and parametric relationships that define the PGM need to be documented.

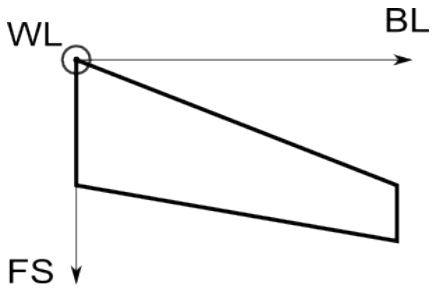


Figure 41: Parametric Geometry Model Coordinate System

The coordinate system that the PGM uses is shown in Figure 41. The dimensions are the Fuselage Station ($FS$), the Butt Line ($BL$), and the Water Line ($WL$). The origin is at the intersection of the wing planform leading edge and the root of the wing.

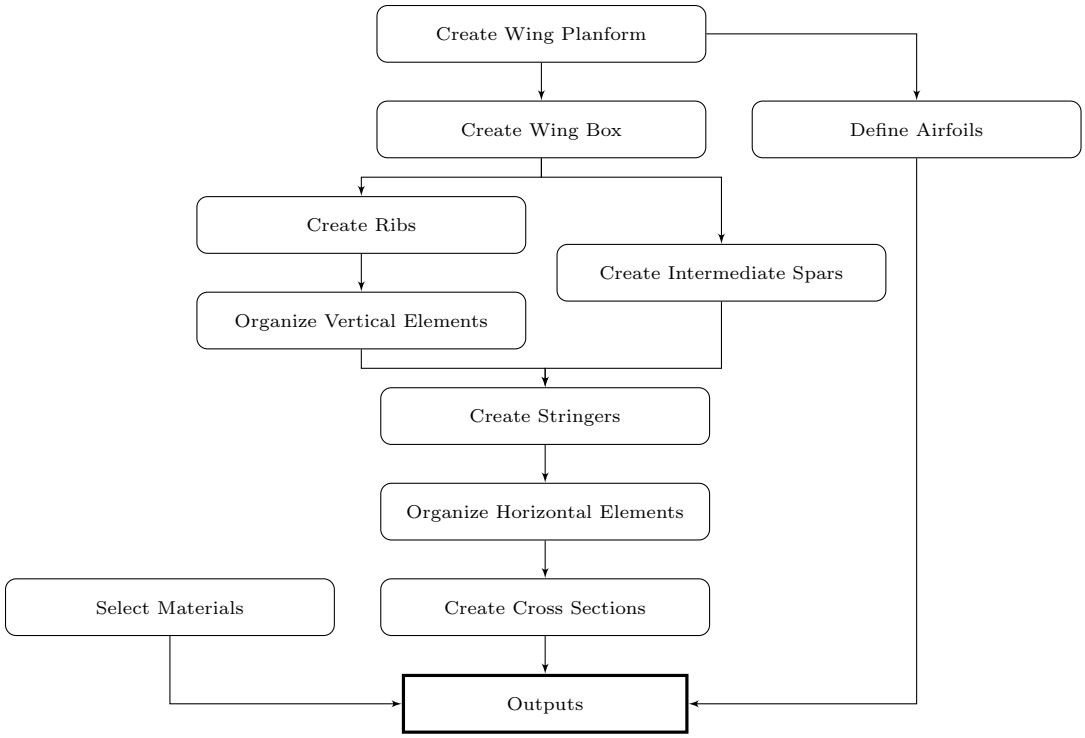


Figure 42: Geometry Tool Flow Chart

Part of defining parametric relationships is defining a hierarchy of decisions. Figure 42 illustrates the hierarchy the PGM uses. The hierarchy works so that any changes made to elements in Figure 42 propagate down through the other elements. For example, everything is derived from the wing planform, shown at the top of Figure 42. Any changes made to the wing planform will affect all the other elements in the PGM. However, the reverse is not true as a change to the ribs will not affect the wing planform. Each of these elements is described below.

*Wing Planform*

The wing planform is defined in the ($BL$, $FS$) plane at $WL = 0$. The planform is assumed to be a trapezoid so that traditional wing planform variables (e.g. Aspect Ratio, Span, Sweep, Taper Ratio) [174, 178] can be used to calculate the four points of the trapezoid.

The wing planform defines the bounds of the entire wing box geometry. All the

parametric relationships are defined so that no substructure can exist outside of the wing planform.

*Define Airfoils*

The substructures are defined in the ($FS$, $BL$) plane; however, the ($WL$) must still be accounted for. To define the third dimension the PGM calculates the intersection of the substructures defined in the ($BL$, $FS$) plane with the upper and lower surface of the wing Outer Mold Line (OML). The parametric geometry tool assumes that all of the substructures are normal to the ($BL$, $FS$) plane.

The OML is defined by airfoils along the span of the wing. The airfoils are defined either using predefined parametric airfoils (i.e. NACA airfoils) or through user defined airfoils stored in *Airfoil Database*. The user defined airfoils are defined with three dimensions (Figure 43): the distance along the chord of the airfoil ($x$), the upper thickness ($t$), and the lower thickness. To parameterize the airfoil dimensions, each dimension is normalized by the chord length ($c$) so that the airfoil changes sizes based upon its location along the span of the wing. A finite number of airfoils are used to define the wing OML; thus, the PGM calculates the $WL$ values as needed using linear interpolation between the airfoils.

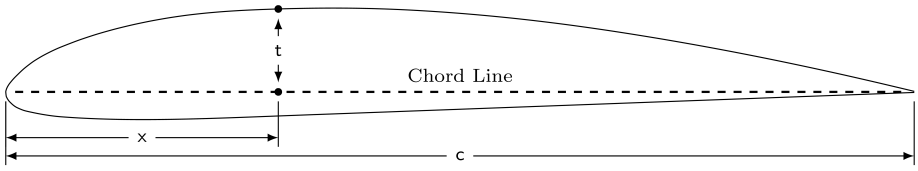


Figure 43: Airfoil Dimensions

*Create Wing Box*

The wing box is defined as the area between the front spar, rear spar, root rib, and tip rib. The front and rear spar are assumed to be be straight (i.e. there are no spar kinks) and continuous so that they both intersect the wing planform root and tip.

The root rib is assumed to be at the root chord of the wing planform and the top rib is assumed to be along the tip chord. The four components are all defined using four percent chord values which define the intersection of the front and read spar with the root and tip chord as a percent of the chord from the leading edge of the wing planform. These percent chords are assumed to be greater than 0% and less than 100% so that they all exist on the wing planform.

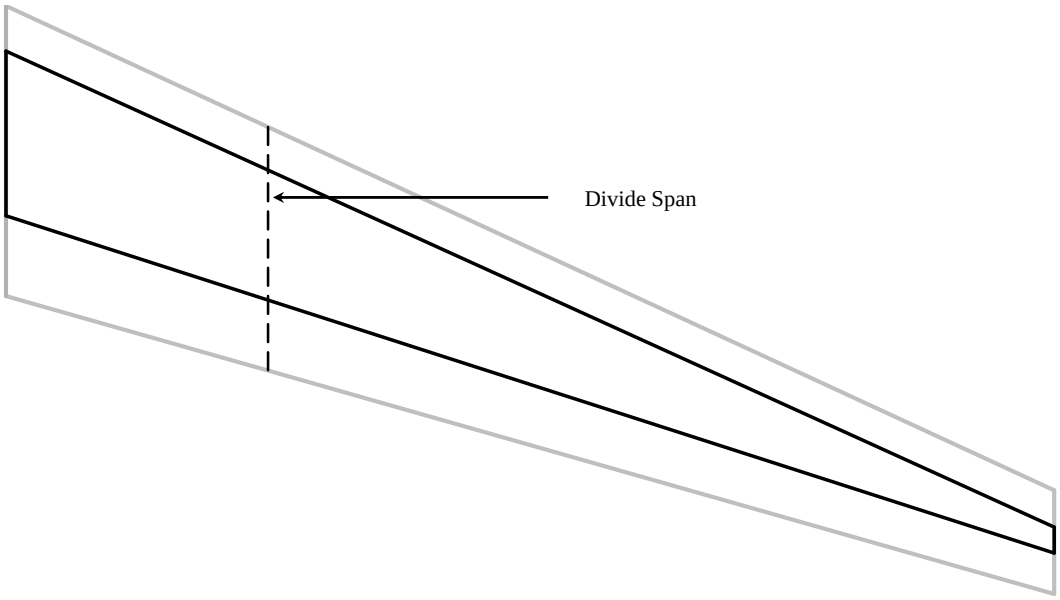


Figure 44: Wing Box Geometry

It is assumed that all the substructures exist within the wing box, meaning the wing box defines the bounds of all other substructures. For example, a rib is assumed to exist between the front spar and the rear spar and therefore can be defined by its intersection with the two spars. The result of this assumption is that every element of the substructure can be defined using only a single point and an orientation. This reduced the dimensions required to define each substructure components to two; however, the dimensionality is reduced further by specifying specific patterns for the remaining substructure elements.

*Create Ribs*

In various substructure layouts it is common to have several ribs with similar orientations. Often, these groups of parallel ribs fall into two sets of orientations: those parallel to the fuselage and those perpendicular to some reference (e.g. the leading edge, the front spar, the quarter chord). In SPANDSET these groups of ribs have been given names. The stub ribs are the inboard ribs that are oriented parallel to the fuselage. The main ribs are the outboard ribs that are oriented perpendicular to a specified reference axis. The ribs are separated at a point along the span specified by the user called the divide span (Figure 44).

The ribs are assumed to be placed in a pattern an equal distance from one another to further reduce the dimensions used to define the ribs from a point and orientation for each rib to a single variable. The variable can either be the rib spacing or the number of ribs. There exists a finite area in which the stub ribs and main ribs can exist based upon the boundaries defined by the wing box and the divide span. When the ribs are placed based upon rib spacing, an initial rib is placed at the furthest inboard point and then each additional rib is placed a set distance from the previous one until there is no more room. When the ribs are placed based upon the number of ribs, the ribs are placed so that they fill the entire area and are an equal distance apart.

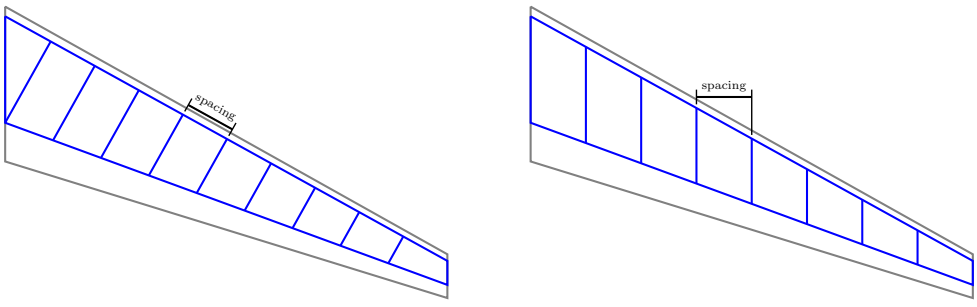


(a) Main Rib Spacing (b) Stub Rib Spacing

Figure 45: Rib Types

The PGM uses two methods to orient the main ribs. Either the angle is specified, or a horizontal element is specified (e.g. front spar, rear spar, leading edge) and the main ribs are all perpendicular to the horizontal element. The stub ribs are assumed to be oriented perpendicular to the $FS$ axis.

One of the discrete configuration decisions made in SPANDSET is how to transition from main ribs to stub ribs. There exist three methods to accomplish the transition: no transition, fan ribs, and divide rib. Selecting no transition will position the first main rib at the location of the divide span. Selecting fan ribs creates a new set of ribs called fan ribs. These ribs transition between the stub ribs and main ribs by gradually altering their orientation and spacing over a specified number of ribs. Selecting divide rib creates an additional stub rib at the divide span. Additionally, the main ribs can be modified so that they intersect the divide rib instead of the wing box boundaries.

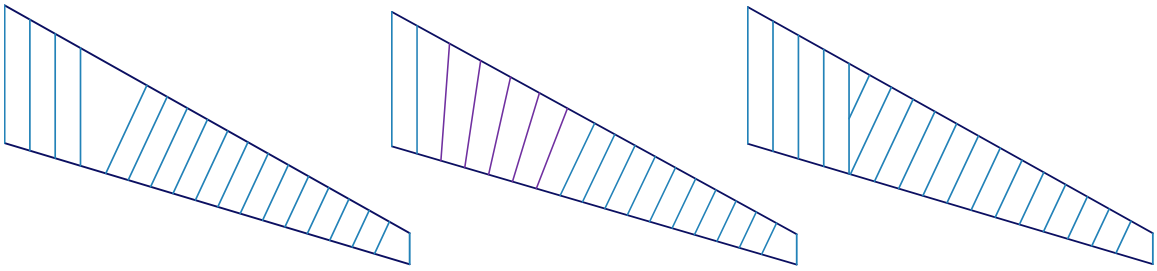

(a) None (b) Fan Ribs (c) Divide Rib

Figure 46: Rib Transition

An additional variable that is not reflected in the PGM but is important to the structural analysis and sizing routine is the rib upright spacing. SPANDSET models all ribs as web stiffened ribs which consist of the rib web, rib caps, and web uprights. The rib web can be defined using the rib intersection with the wing OML and the rib caps are assumed to exist on the top and bottom of the rib web. The rib upright locations are defined along the length of the rib web by the rib upright spacing. An initial rib upright is placed in the center of the rib web and the remaining uprights

are placed based upon the rib upright spacing value. All rib uprights are assumed to be vertical based upon the $WL$ axis.

The final step of creating the ribs is to organize all the ribs into a table called vertical elements. The vertical elements are used to define the covers which will be discussed later in this section.

*Create Intermediate Spars*

The front and rear spar are defined by the wing box; however, the PGM allows for additional spars, called intermediate spars, to be specified between the front and rear spar. These spars are assumed to be evenly spaced throughout the area provided and are all parallel to one another. Intermediate spars are assumed to intersect the root rib and then extend until it reaches either the front spar, rear spar, or tip rib. These spars are created by specifying the number of intermediate spars and the location of the outside spars in relation to the front and rear spars.

All the intermediate spars are parallel to one another with a specified orientation. The PGM uses one of three methods to orient the intermediate spars: either the user specifies an angle, the intermediate spars are parallel to a referenced horizontal element (e.g. front spar, rear spar, leading edge), or the intermediate spars are parallel to a percent chord from the leading edge.

The intermediate spars are created by placing a specified number of spars within a boundary defined by user inputs and the spar orientation. The boundary is defined in terms of the distance inward from the front and rear spars. It is not assumed that the intermediate spars are parallel to either the front of rear spar; thus, there is no constant spacing that exists from which to define the distance between the intermediate spars and the front or rear spar. Instead the root chord is used as a common reference so that the intermediate first and last intermediate spars can be placed specified distances from the front and rear spars, called the front offset and

rear offset receptively (Figure 47).

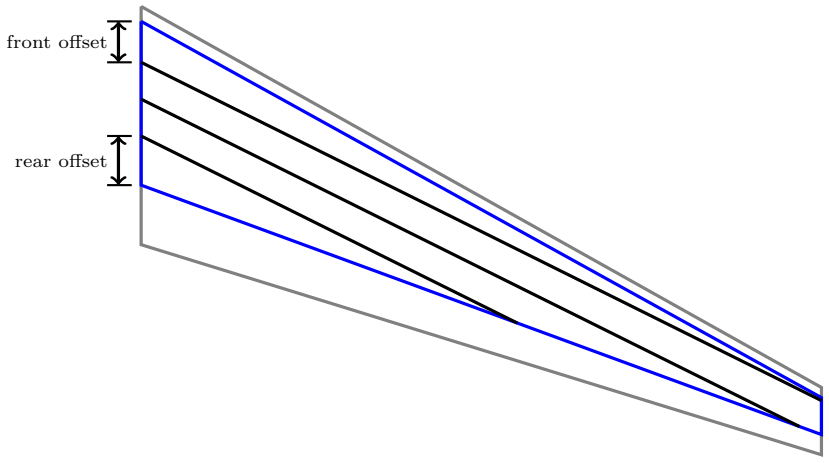


Figure 47: Intermediate Spar Dimensions

The final portion of the spars that need to be defined are the spar uprights. All the spars (including the front and rear) are assumed to be web stiffened spars made up of the spar web, spar upper and lower cap, and the web uprights. The spar web uprights are assumed to be evenly spaced along the spar web sections located between two adjacent ribs. This presents a problem because there are different rib spacings between the main ribs, stub ribs, and fan ribs. Additionally, the spar sections between the stub ribs will typically need more uprights due to the larger web heights and larger loads that are a result of being further inboard. Instead of specifying a single upright spacing value, as is the case for the rib uprights, two separate number of uprights are specified for the spar sections between main ribs and spar sections between stub ribs. For each spar section the adjacent ribs are used to identify which value to use and the number of uprights are placed between the adjacent ribs so that they are spaced evenly.

*Create Stringers*

The PGM defines the stringer similarly to the intermediate spars with a few key differences. The first difference is that the stringers do not have to intersect with the root chord. The stringers extend the length of the wing that it can. The second difference is that the stringers start and end at a rib due to the assumption that the covers are quadrilaterals. Like the intermediate spars, the stringers are assumed to be parallel to one another with an orientation specified by the user. However, if any intermediate spars exist then the stringers are assumed to be parallel to the intermediate spars. Another difference is that the stringers are placed using spacing and not number. Two sets of stringers exist, one for the upper surface and one for the lower surface; thus, the stringers are defined using two different spacings (upper stringer spacing and lower stringer spacing).

Another problem unique to the stringers is that the upper stringer spacing and lower stringer spacing are only estimates of the perpendicular distance between the stringers. The reason these values are only an estimate is that the stringers are placed between existing spars and the available space between the spars is unlikely to match the stringer spacings specified by the user; thus, the stringers will not be perfectly spaced through the areas between the stringers. There are two different arrangements of the stringers that can mitigate this problem. If the stringers are arranged so they are 'centered' then the stringers will be placed from the center out using the defined stringer spacing until no more stringers can be placed with that spacing. A result of the centered arrangement is that the outer two stringers will be placed further away from the spars than the user defined spacing. If the stringers are placed so that they are 'distributed' then the stringers are placed evenly throughout the available area, but at a larger spacing than is defined by the user. The difference between the two arrangements are illustrated in Figure 48. Table 11 shows the stringer spacing of the stringers at the root of the configurations depicted in Figure 48.

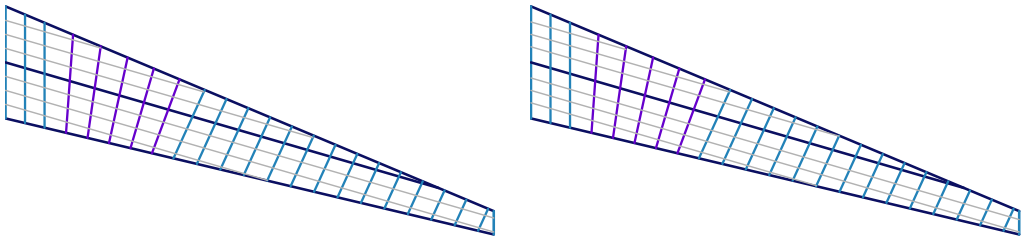

(a) Distributed (b) Centered

Figure 48: Stringer Arrangement

Table 11: Stringer Spacings for Different Arrangements

| **Distributed (in.)** | **Centered (in.)** |
|---|---|
| 16.91 | 18.83 |
| 16.91 | 15.00 |
| 16.91 | 15.00 |
| 16.91 | 18.83 |
| 16.91 | 18.83 |
| 16.91 | 15.00 |
| 16.91 | 15.00 |
| 16.91 | 19.20 |

After the stringers have been created, they are organized into horizontal elements along with the spars. The horizontal elements are arranged in order with the front spar first and the rear spar last. The horizontal elements are created to create the covers.

*Covers*

The PGM defines the covers based upon the ribs, spar, and stringers so no additional inputs are needed. The covers are assumed to be quadrilaterals defined span-wise as between adjacent vertical elements (ribs) and chord-wise as between adjacent horizontal elements (stringer or spar). The stringers are assumed to begin and end at each rib in order to enforce the quadrilateral cover requirement (Figure 49). However, additional assumptions are needed to enforce the requirement. If an intermediate spar

terminates at the front or rear spar it will form a triangular cover. This is rectified by ignoring the portion of the intermediate spar that extends beyond the final rib it intersects (Figure 49). A similar situation exists between ribs if a main rib intersects the divide rib. The cover defined on the inboard of the main rib will be a triangle and the outboard section a pentagon. This is rectified by combining the two covers into one.

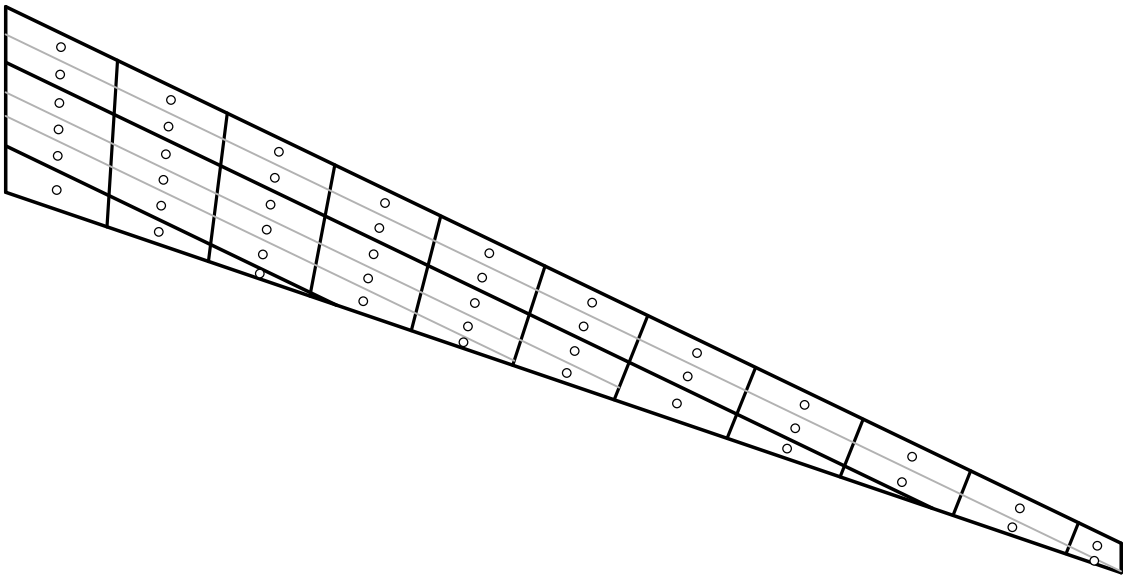

Figure 49: Lower Cover Centroids

*Create Cross Sections*

The cross sections are used to define the geometry used by the structural analysis and sizing routines. The geometry of the cross section is specified using a reference axis that defines the VMT data. Each cross section is assumed to extend from front spar to rear spar. Thus all that is needed to define a cross section is a reference position and orientation. The orientation of all the cross sections are assumed to be parallel while the position of the cross section is defined as the $BL$ of the point where the cross section and reference axis intersect.

There are two methods to define the cross sections. The first method is by pattern. A cross section pattern is defined with a user specified number of cross sections that

are placed evenly along the span of the wing. The second method is by creating custom cross sections where the location is specified by the user. The custom sections allow for analysis at specific areas of interest along the span (e.g. engine mount, landing gear, etc.).

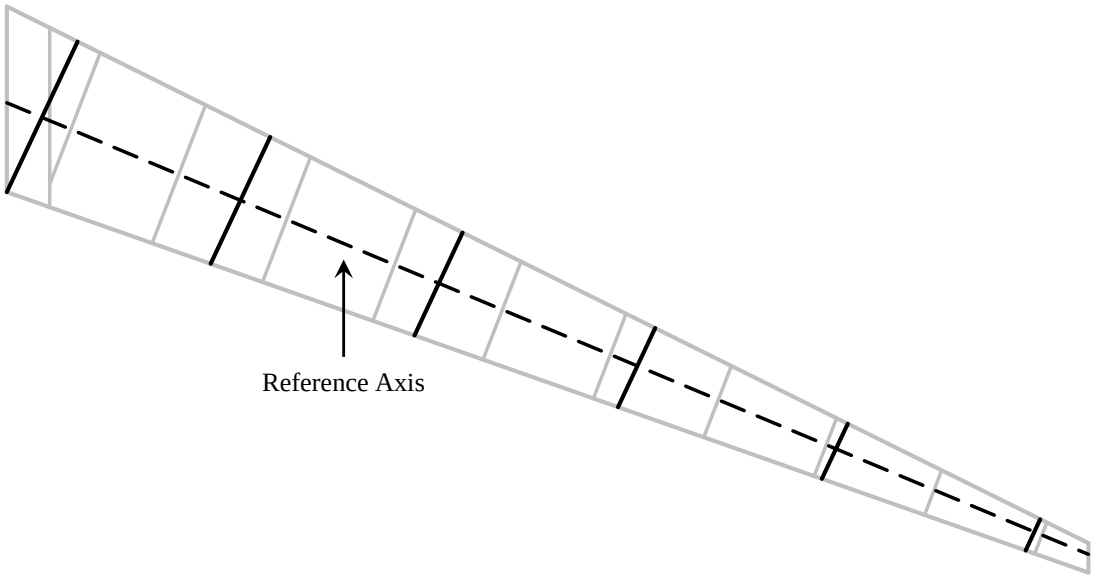


Figure 50: Cross Sections

*Select Materials*

In addition to creating the geometric information for the wing box substructure layout, the PGM is also responsible for distributing the material properties to the required routines in Phase 2 and Phase 3. The PGM contains a library of several different materials where the material properties listed in Table 12 are defined for each material. The parametric geometry tool lets the user assign a material to each of the part features listed below:

- Spar Webs
- Spar Web Stiffeners
- Spar Upper Chord
- Spar Lower Chord
- Upper Cover Skin
- Upper Cover Stringer
- Lower Cover Skin
- Lower Cover Stringer
- Rib Webs
- Rib Web Stiffeners
- Rib Chords

Every similar component is assumed to have the same features, and each feature has the same material properties for all the similar components. For example, all the stub ribs and main ribs are assumed to have webs made of the material specified.

Table 12: SPANDSET Material Properties

| | | | |
|---|---|---|---|
| Young's Modulus | $E$ | $\text{lb/in}^2$ | Ratio of the stress divided by strain for materials when normal stress is applied [17] |
| Shear Modulus | $G$ | $\text{lb/in}^2$ | Ratio of the stress divided by strain for materials when shear stress is applied [17] |
| Poisson's Ratio | $\nu$ | | Ratio of the lateral strain measured normal to the loading direction to the normal strain measured in the direction of the load [153] |
| Ultimate Tensile Load | $F_{tu}$ | $\text{lb/in}^2$ | Maximum load a material can sustain under tensile stress [153] |
| Tensile Yield Load | $F_{ty}$ | $\text{lb/in}^2$ | Load at which the material begins to yield under tensile stress [153] |
| Compression Yield Load | $F_{cy}$ | $\text{lb/in}^2$ | Load at which the material begins to yield under compression [153] |
| Ultimate Shear Load | $F_{su}$ | $\text{lb/in}^2$ | Maximum load a material can sustain under shear stress [153] |
| Density | $\rho$ | $\text{lb/in}^3$ | Mass per volume of a material |

### 6.1.2 External Loads

SPANDSET uses a common classical technique to apply the external loads to the substructure [93,124]. The classical technique maps shear, moment, and torque (VMT) data across a wing reference axis. The VMT data represents the maximum positive and negative shear, moment, and torque values calculated along the reference axis for all of the load cases. The VMT data is then applied at local load points defined by the intersection of the reference axis and the cross sections. Example VMT data is shown in Figures 51, 52, and 53.

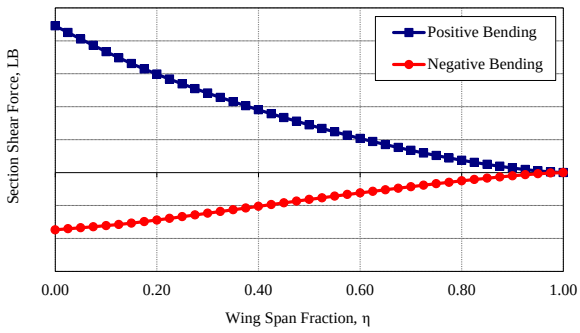


Figure 51: Wing Shear Data

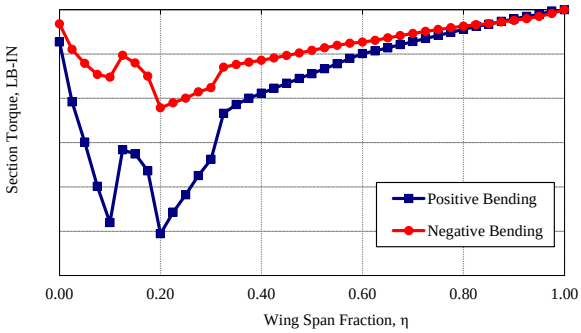


Figure 52: Wing Torque Data

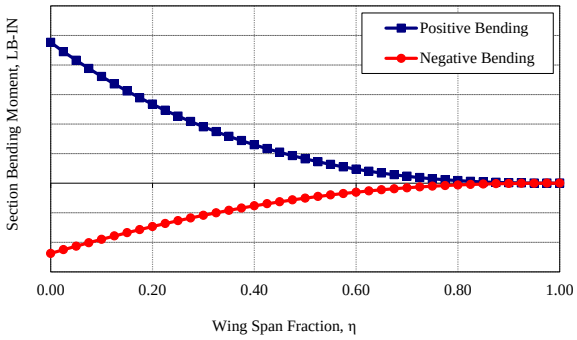


Figure 53: Wing Bending Moment Data

SPANDSET uses two loading conditions to perform structural analysis on the wing box substructure: a 2.5g up bending condition (+2.5g) and a 1.0g down bending condition (-1.0g). These two conditions will adequately capture the minimum and maximum VMT values that will be used by the Margins of Safety in the structural analysis and sizing routines.

The VMT data SPANDSET uses is stored in *VMT* in three tables. The tables contain three columns: the first column contains the wing span fraction ($\eta$) and the second and third contain either the shear, moment, or torque values for the +2.5g or -1.0g load conditions.

As previously mentioned there are two methods to defining the VMT data. VMT data is typically provided to SPANDSET using higher fidelity aerodynamic analysis tools. The VMT data generated by the higher fidelity tools can then be copied manually into *VMT* assuming the wing planform, wing OML, and loading conditions

remain constant. However, if any of these variables are altered then the external loads will change and updating the VMT data manually becomes infeasible. Therefore, SPANDSET provides a second method that uses AVL to calculate the VMT data.

AVL (Athena Vortex Lattice) [61] is an aerodynamic and flight-dynamic analysis tool used for aircraft configuration development. AVL is based on the vortex-lattice method and therefore implies certain limiting assumptions. The analysis assumes quasi-steady flow for thin lifting surfaces at small angles of attack due to its inability to model separated flow. AVL uses Prandtl-Glauert transformations to account for compressibility effects; thus, AVL should not be used to estimate aerodynamic effects in the transonic region or higher ($M \leq 0.7$). These assumptions notwithstanding, AVL provides a reliable way to generate the VMT data SPANDSET requires for various wing shapes and sizes.

AVL is a command line executable that requires a number of input files to execute the analysis. SPANDSET automates the creation of these input files and the execution of AVL. When AVL is implemented by SPANDSET the necessary geometric data is extracted from *Geometry Tool* to run AVL, and the resulting VMT data is automatically input into *VMT*. However, some inputs required by AVL can not be calculated by existing elements of SPANDSET. Thus, and additional file was created that manages the inputs required by AVL for SPANDSET. A description of these inputs is given below.

**Wing Data** The wing planform defined in SPANDSET uses the same trapezoidal assumption as the PGM; thus, the majority of the wing data required by AVL is extracted directly from the PGM. The only difference is that the PGM assumes a flat 2D planform while AVL includes the 3D variables: wing incidence, wing dihedral, and wing twist. These values can be specified by the user to be used by AVL. However, these values will not be represented in the PGM. If these values are used the aerodynamic

wing model will not match with the structures wing model; thus, these values should only be used if necessary to capture the wing loading.

**Reference Axis** AVL defines the shear, moment, and torque data at either the leading edge (LE) or the quarter-chord (c/4). However, SPANDSET allows the user to specify the location of the reference axis. Therefore, post-processing is required to transfer the pitching moment from the leading edge to the desired reference axis.

The strip lift is given by Equation 40, where $S_i$ is the $i$th strip.

$$L_i = q_{\text{inf}}\ S_i\ (C_l)_i \tag{40}$$

For each strip in the discretized geometry, the moment about the leading edge is given by Equation 41. In Equation 41, $S_i$ is the area and $c_i$ is the chord of the $i$th strip.

$$(M_{c/4})_i = q_{\text{inf}}\ S_i\ c_i\ \left((C_m)_{c/4}\right)_i \tag{41}$$

In Equation 41, the moment coefficient is about the quarter chord. To calculate the moment about the specified reference axis a new moment of coefficient is plugged into Equation 41. The new moment coefficient is calculated using Equation 42.

$$\left((C_m)_{ref}\right)_i = \left((C_m)_{c/4}\right)_i - (C_l)_i\left(\left(\frac{x}{c}\right)_{ref} - \frac{1}{4}\right) \tag{42}$$

**Airfoils** Two or more airfoils need to be specified for AVL to define a wing. The root and tip airfoils must always be defined; otherwise, airfoils should be specified at chord and dihedral breaks, control surface ends, or anywhere else that represents discontinuities in the OML. AVL assumes a thin-lifting surface so that the the wings are represented by a sheet along the mean chamber line of the airfoil sections. The midpoints between the upper and lower surfaces are used to define the surface sheet. SPANDSET generalizes the airfoil data required by AVL in *Geometry Tool* automatically.

**Flight Conditions** As previously mentioned, SPANDSET uses the 2.5g up bending and -1.0g down bending conditions. AVL requires several additional values that are not specified by any other component in SPANDSET; thus, these values must be defined by the user in SPANDSET before AVL is executed. These values are listed below.

- The air density ($\rho$)
- The freestream values ($V_{inf}$, $q_{\text{inf}}$)
- The air density ($M$)
- Weight load factor ($n$)
- Initial TOGW estimate ($W$)
- Aerodynamic coefficients ($C_L$, $C_D$)
- Non-dimensional roll, pitch, and yaw rates ($p_{rate}$, $q_{rate}$, $r_{rate}$)

**Vortex-Lattice Distribution** The final set of inputs AVL requires define the distribution of the vortex-lattice. AVL decomposes the planform geometry into panels to perform vortex-lattice analysis (Figure 54).

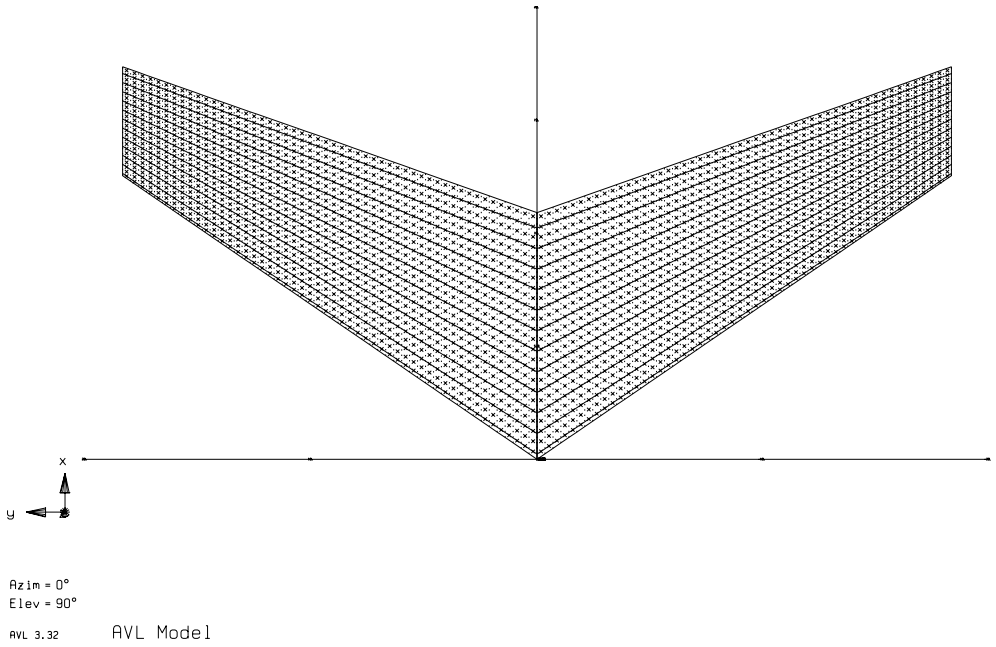


Figure 54: Vortex Lattice Distribution

There are four values that define the vortex-lattice; Nchord, Cspace, Nspan, Sspace. These values are defined in Table 13.

Table 13: Vortex Spacing Parameters

| **Parameter Name** | **Description** |
|---|---|
| Nchord | Number of chordwise horseshoe vortices placed on the surface |
| Cspace | Chordwise vortex spacing parameter |
| Nspan | Number of spanwise horseshoe vortices placed on the surface |
| Sspace | Spanwise vortex spacing parameter |

The vortex spacing distribution in both the spanwise and chordwise direction is controlled by the spacing parameters: Sspace and Cspace. The spacing parameter is a value between +3.0 and -3.0. The values change the distribution from between equal spacing (3.0, 0, -3.0), sine spacing (2.0, -2.0), cosine (1.0, -1.0). SPANDSET assumes equal spacing (Cspace=3 and Sspace=3).

The Nchord and Nspan parameters define the number of vorticies in the spanwise and chordwise directions. However, there are two different values for each: section and surface. The surface Nchord and surface Nspan values specify the number of vortices across the entire surface. The section Nspan parameter specifies the number of vortices located in the interval between the section and the next outboard section. For certain cases, using the section Nspan allow the user more control over the vortex distribution. There is no difference between surface Nchord and section Nchord; however, section Nchord must be used with section Nspan. These values are set to default values; however, before using SPANDSET they should be tailored to the specific problem.

## 6.2 Phase 2: Structural Analysis and Sizing Routines

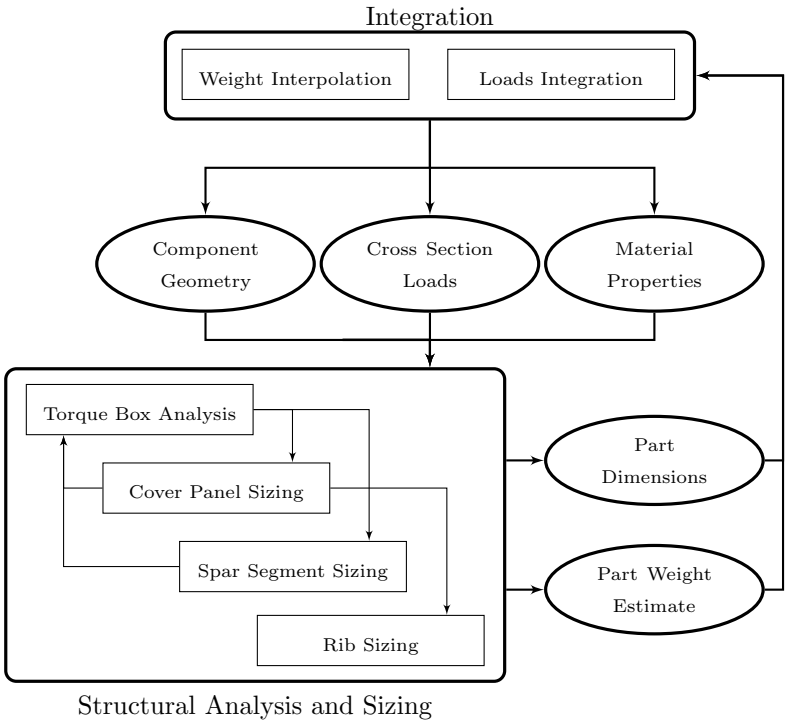


Figure 55: Phase 2 of SPANDSET

Phase 2 of SPANDSET (Figure 55) implements the structural analysis and sizing routines. After the wing box substructure is laid out and the external loads data is calculated, several cross sections are specified by the parametric geometry model for the purpose of structural analysis. At each cross section, the VMT data is applied to the wing box structure using *Torque Box Analysis* which executes modified thin walled multi-cell torque box analysis to calculate the internal loads distribution.

The internal loads are then passed to the *Cover Panel Sizing*, *Spar Segment Sizing*, and *Rib Sizing* routines. Each sizing routine performs component level sizing using classical closed-form solutions as well as semi-empirical relationships. Thus, the analysis is straight forward and computationally efficient. Each element is sized for minimum weight subject to constraints on minimum margins of safety on various

structural failure modes as well as geometric considerations such as minimum gauge. Each routine sizes its respective component and outputs a part weight estimate and part dimensions to be used for the weight and cost breakdown.

The structural analysis and sizing routines aids in addressing the overall research objective by automatically performing structural analysis on the wing box substructure as well as solving for several of the component dimensions with sizing optimization. When combined with the PGM, the structural analysis and sizing routines reduce the combinatorially large number of design variables that are required to define the entire wing box substructure to fewer than 100. Thus, the structural analysis and sizing routine helps address Research Observation 1.

Chapter 5 describes two important characteristics of the sizing optimization: the sizing optimization is distributed and IDF (see Chapter 5). The justification for making the sizing optimization this way has to do with structural analysis implementation and feasibility; however, these two characteristics also aid in addressing Research Observation 2. By making the sizing routines so that they are distributed and IDF they become modular so that a new sizing and analysis routine can be inserted into Phase 2. Having a modular form allows for the remaining discrete design decisions (i.e. the form of the feature and the components) to be accounted for in interchangeable sizing routines. For example, the *Cover Panel Sizing* routine assumes that the stringers are z-shaped stringers. If the stringers were changed to hat-stiffened stringers then a new *Cover Panel Sizing* routine can be inserted into the rest of the structural analysis and sizing routines and few adjustments would need to be made to the other routine.

The structural analysis and sizing routines are sufficiently complicated that a more detailed description required its own chapter. Thus, Chapter 7 provides further description of the structural analysis and sizing process in SPANDSET.

## 6.3 Phase 3: Cost and Weight Breakdown

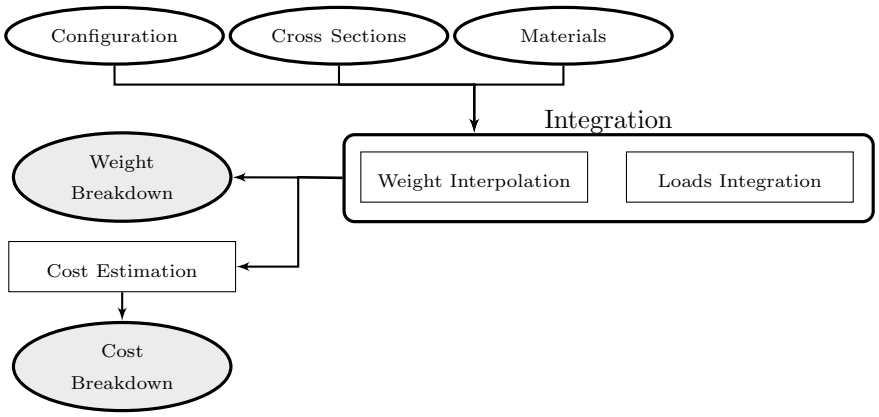


Figure 56: Phase 3 of SPANDSET

Phase 3 of SPANDSET (Figure 56) combines the results of the structural analysis and sizing routines (Phase 2) with the geometric data from the substructure layout (Phase 1) to develop weight and cost estimates of the wing box substructure. The results from the structural analysis and sizing routines are for the cross sections only. *Weight Interpolation* calculates the weight of the entire wing box structure by interpolating the cross section results for each component set (e.g. upper covers, lower covers, individual spars) over the entire span of the wing using geometric data (e.g. heights, lengths, areas) from the *Geometry Tool*. The linear interpolation used to calculate the weight breakdown is discussed further in Section 6.3.1.

The final step of SPANDSET is to estimate the cost breakdown of the wing box substructure using the recurring manufacturing costs analysis in *Cost Estimation*. The recurring manufacturing cost analysis uses surrogate models created from previously performed proprietary research. The surrogate models use the estimated weights of the components (Phase 3), the final dimensions of the components (Phase 2), and the geometry of the components (Phase 1) to estimate the cost of manufacturing the wing box structure. The surrogate models were created using an activity based cost model

called SEER-MFG [78] to estimate the cost based on the physics of the structure and the manufacturing process required to build each part. The recurring manufacturing costs analysis in *Cost Estimation* is discussed further in Section 6.3.2.

### 6.3.1 Weight Estimation

Chapter 3 describes several methods to estimate the weight of a wing substructure. The first step of any weight estimation method is to decide which components of the weight are being measured. The only weight estimates that will be considered are those of the wing box structure: upper and lower covers (skin panel and stringer segment), the spars, and the ribs.

One of the motivations of this thesis is to increase designer knowledge through implementing physics-based structural analysis. Doing so will allow the designer to make decisions based upon the captured physics of the problem. This motivation leads to the conclusion that the weight should be estimated based upon the entire substructure (identified as Full Weight Computation in Chapter 3). However, estimating the weight based on the entire substructure is not feasible using SPANDSET due to the limiting nature of the structural analysis. The use of classical analysis requires that the wing box substructure be divided into the cross sections. Thus, the weight will be estimated by interpolating the results of the part weight estimates that are the result of Phase 2. The partial weight estimates will be iterated across the entire wing box geometry using the geometric information provided by Phase 1.

**Spar Weight Estimation** The structural analysis and sizing routines create a weight per unit length estimate for each spar at every cross section. The spar segment lengths are calculated by the PGM. An estimate for the weight of a spar segment is calculated by performing linear interpolation on the weight per unit length estimates from the cross sections and then multiplying the interpolated value by the segment length. The location used for the linear interpolation is the segment

midpoint (represented as circles in Figure 57). The segments are summed to get a weight estimate for an individual spar. This process is repeated for each spar and then SPANDSET sums the estimated spar weights into one Total Spar Weight value.

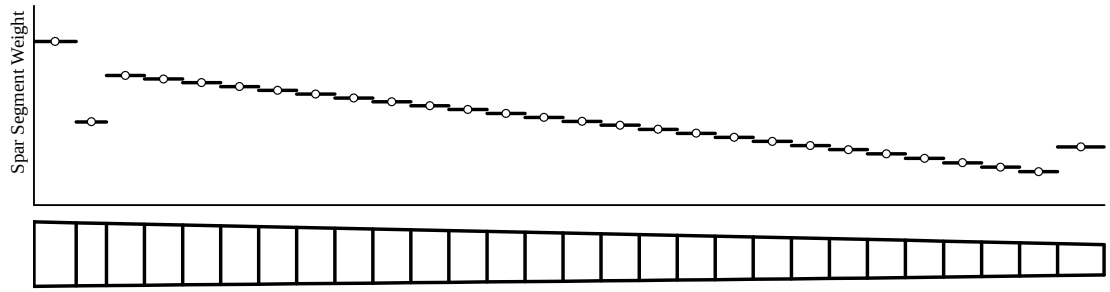


Figure 57: Spar Weight Estimate

**Cover Weight Estimation** To estimate the full cover weight the geometry of each cover section and stringer is required. The PGM calculates the area and centroids of each cover sections for both the upper and lower surface (Figure 49). Additionally, the structural analysis and sizing routine outputs an estimate of the cover weight per unit area for each cover along all of the cross sections. The weight per unit area for all the covers that are not on the cross section are estimated by performing two linear interpolations using the values from the nearest two cross sections using the cover centroid location ($FS_c$,$BL_c$). The first linear interpolations are to calculate a value along each of the cross sections at the $FS_c$ location on the cross sections. The second linear interpolates the previous two values to match the $BL_c$ location. In Figure 59 the blue circles represent the values calculated at the cross sections while the black circles represent the values calculated at the cover centroids. Once a weight per unit area value has been estimated for the cover the value is then multiplied by the cover area, estimated by the PGM, to get an estimate for the cover weight. This process is repeated for every cover on both the upper and lower surfaces. SPANDSET sums all the cover weights for each cover into a Total Upper Cover Weight value and a Total Lower Cover Weight value.

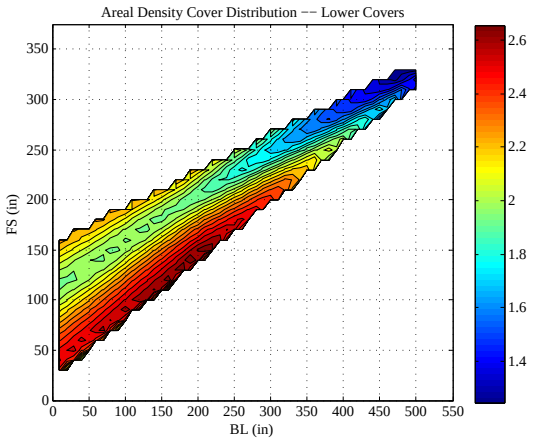


Figure 58: Cover Density Interpolation

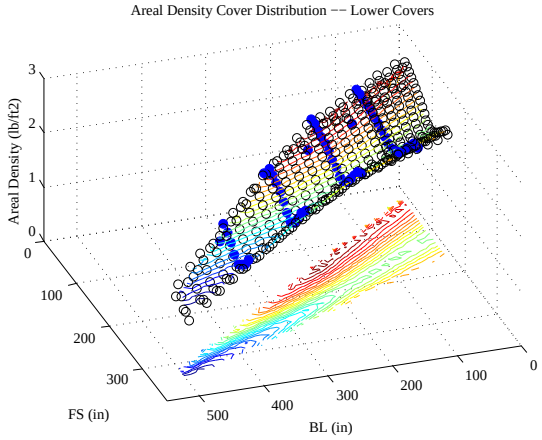


Figure 59: Cover Density Centroids

**Skin Panel Weight Estimation** The skin panel weight is estimated exactly the same as the cover weight. It uses the same areas from the PGM and the same interpolation routine between the cross sections. The only difference is that instead of the weight per unit area of the entire cover, the weight per unit area of the skin panel is used.

**Stringer Weight Estimation** The stringer weight estimated is using data from the Cover Panel Sizing routine and the PGM. To estimate the stringer weight the PGM decomposes each stringer into stringer segments, where a stringer segment is the portion of the stringer that intersects each cover panel. During the Cover Panel Sizing routine the weight per unit length of the stringer segment associated with each cover is estimated. The weight per unit length is only estimated for the stringer segments that intersect covers on the cross sections. The same interpolation routine used to calculate the cover weights is used to get an estimate of the weight per unit length for each stringer segment. SPANDSET combines the weight per unit length estimate and the length of each stringer segment to calculate the weight of each stringer segment. Then, SPANDSET sums all the stringer segments on the upper and lower surface to get the total stringer weight.

**Rib Weight Estimation** The rib weights are calculated directly by the structural analysis and sizing routines. As explained in Chapter 7 the ribs do not always intersect a cross section; thus, the rib weights can not be calculated through interpolation. SPANDSET sums the rib weights from the structural analysis and sizing routines into one Total Rib Weight value

SPANDSET gathers the resulting weight estimations into the weight breakdown. The weight breakdown organizes all the weight information that is used to assess the wing box substructure. The final weight outputs are listed in Table 14.

Table 14: SPANDSET Weight Breakdown

| Outputs | Description |
|---|---|
| Front Spar Weight (lb) | The weight of the front spar |
| Rear Spar Weight (lb) | The weight of the rear spar |
| Intermediate Spar Weight (lb) | The weight of all the intermediate spars |
| **Total Spar Weight** (lb) | The sum of all the spar weights |
| Upper Skin Weight (lb) | The sum of all the skin panel weights on the upper surface |
| Lower Skin Weight (lb) | The sum of all the skin panel weights on the lower surface |
| **Total Skin Weight** (lb) | The sum of all the skin panel weights |
| Upper Stringers Weight (lb) | The sum of all the stringer segment weights on the upper surface |
| Lower Stringer Weight (lb) | The sum of all the stringer segment weights on the lower surface |
| **All Stringers Weight** (lb) | The sum of all the stringer segment weights |
| Upper Cover Weight (lb) | The sum of all the cover (skin panel + stringer segment) weights on the upper surface |
| Lower Cover Weight (lb) | The sum of all the cover (skin panel + stringer segment) weights on the lower surface |
| **All Cover Weight** (lb) | The sum of all the cover (skin panel + stringer segments) weights |
| Ribs Weight (lb) | The sum of all the rib weights |
| **Total Wing Box Weight** (lb) | The weight of the entire wing box substructure |

### 6.3.2 Cost Estimation

Chapter 3 described three general methods used to estimate wing manufacturing costs: Analogous, Bottom-up, and Parametric. Since the Overall Research Objective is to introduce physics-based methods to increase overall design knowledge, Analogous methods which estimate the cost based on empirical data will not be a suitable choice. Parametric cost models are an improvement over Analogous cost models. They create semi-empirical relationships based on the substructure layout. However, the physical parameters typically are not the main drivers of the cost which makes it difficult to trace cause-and-effect relationships between the design decisions and the manufacturing cost. Therefore, a Bottom-up method is the best choice.

Bottom-up methods, also called Activity Based Cost modeling, attempts to model the process used to create the substructure. Bottom-up methods can calculate the amount of hours spent, and thus the labor cost, to create the substructure by modeling the process. This allows Bottom-up methods to calculate the labor costs as well as the material costs. However, Bottom-up methods can be extremely complex and time consuming. Additionally, they might require geometric detail that is not available in the PGM (i.e. fastener locations, adhesive areas, number of drilled holes). Ideally a Bottom-up cost method exists that can estimate the costs associated with the manufacturing process based on the physical parameters without having to model each step.

All these features exist in a commercially available software package called SEER-MFG [78]. SEER-MFG allows the user to create parametric models based on the physical structure. These models recreate the manufacturing process based upon an existing library of manufacturing processes to generate labor hours and costs as well as raw material costs. Most of the manufacturing processes required for aircraft wings are included in the pre-existing library of manufacturing processes; thus, SEER-MFG is commonly used in the aerospace industry [105, 119]. Incorporating SEER-MFG will

allow SPANDSET to generate manufacturing cost estimates and address Research Objective 4.

SEER-MFG requires a lot of setup, designer knowledge, and manufacturing details. This information is typically not available outside of industry. However, Triumph allowed ASDL access to their existing SEER-MFG models to build a parametric cost model based on the PGM. These models are discussed below.

#### *6.3.2.1 SEER-MFG Models*

The SEER-MFG model developed by Triumph breaks down the process of creating the wing box into the following sub processes: skin panel fabrication, stringer fabrication, spar components fabrication, spar sub assembly, rib components fabrication, double and single sided rib sub assembly, and the major component assembly. Each of these models is discussed further below. The section concludes with a description of the outputs for all the SEER-MFG models.

**Skin Panel Fabrication** The SEER-MFG model for skin panel fabrication models the process of manufacturing the skin panels from raw materials to finished product. The model assumes that each skin panel is a rectangular panel with uniform thickness. These values are represented as the maximum values of the skin panel. There are several pockets built into the skin panel. The SEER-MFG model evaluates each skin panel using the following skin panel specific variables:

- Length (in) - maximum length of the skin
- Width (in) - maximum width of the skin
- Thickness (in) - maximum thickness of the skin
- Pocket Quantity - number of pockets machined into the skin
- Pocket Volume ($in^3$) - average volume of the pockets machined into the skin
- Periphery - periphery of the finished wing skin
- Finished Weight (lb) - weight of the finished machined skin

- Surface Area ($in^2$) - surface area of the finished skin (both top and bottom sides)

The skin panel fabrication model required additional variables that are not associated with the individual skin panels. These values are manufacturing specific values provided by Triumph. These are listed below:

- Skin Installation Auto Drill % - the % of fasteners that attach the skins that are automatically drilled and fastened (the rest are installed by hand)
- Skin Installation Hiloc % - the % of fasteners that attach the skins that are hilocs (the rest are rivets)
- Maximum Thickness of Upper Skin (in) - The maximum thickness of all the upper skin panels (this value is used to calculate the raw material cost for the upper skins)
- Maximum Thickness of Lower Skin (in) - The maximum thickness of all the lower skin panels (this value is used to calculate the raw material cost for the lower skins)
- Number of Lower Skin Access Panels - number of removable hatch access panels on the lower skin (note: if there are access panels on the upper skin include them in this value but keep in mind the lower skin cost will seem inflated)

**Stringer Fabrication** The SEER-MFG model for skin panel fabrication models the process of manufacturing the skin panels from raw materials to finished product. The model assumes that each stringer is a Z-shaped stringer and is attached to the skin panels. The SEER-MFG model evaluates each stringer using the following stringer specific variables:

- Length (in) - length of the stringer
- Raw Cross Section Area ($in^2$) - cross section surface area of stringer before machining (area of part that comes out of extrusion machine)
- % Material Removed - estimate of the % of the material removed

- Surface Area ($in^2$) - surface area of all sides after machining
- Weight (lb) - weight of stringer after being machined

The stringer fabrication model required additional manufacturing specific variables that were provided by Triumph. These are listed below:

- Stringer to Skin Auto Drill % - the % of fasteners that attach the stringer to the skin that are automatically drilled and fastened (the remaining fasteners are done by hand)
- Stringer to Skin Hiloc % - the % of fasteners that attach the stringers to the skins that are hilocs (the rest are rivets)

**Spar Fabrication** The SEER-MFG model for spar fabrication models the process of manufacturing the entire spar from raw materials to finished product. Unlike the ribs, the spar fabrication includes assembling the spar components into a completed spar. There are several pockets built into the spar components. The variables that SEER-MFG requires for each spar are:

- Length (in) - length of the spar
- Width (in) - maximum width of the spar (i.e. width of the spar cap)
- Height (in) - maximum height of the spar (from upper surface to lower surface)
- Datum Area ($in^2$) - area of spar as viewed from top of aircraft ($Length \times Height$)
- Periphery (in) - periphery of the finished spar ($2\ Length + 2\ Height$)
- Pocket Quantity - number of pockets machined into the spar components
- Pocket Length (in) - average length (along length of spar) of the pockets machined into the spar components
- Pocket Width (in) - average width (from cap to cap) of the pockets machined into the spar components
- Pocket Depth (in) - depth of pockets
- Finished Weight (lb) - weight of the finished machined spar components

- Surface Area ($in^2$) - surface area of the finished spar components (after assembly and including pockets)

**Double Sided and Single Sided Rib Fabrication** There exist two SEER-MFG models for fabricating the rib components. Double sided rib are those ribs that include unique web uprights on both sides of the web. These spars will also have unique rib caps due to the web uprights on both sides. Single sided ribs do not have any features on one side of the spar. Each model is unique; however, the inputs are the same for both models. A variable called 'Single or Double Sided' specified whether the single sided model is used or the double sided model is used.

The SEER-MFG model for both single sided rib fabrication and double sided rib fabrication model the process of manufacturing the rib components (chords, web, web uprights) from raw materials to finished product. There are several pockets built into both the single sided ribs and the double sided ribs. The variables that SEER-MFG requires for each rib are:

- Length (in) - length of the rib
- Width (in) - maximum width of the rib (i.e. width of the rib cap)
- Height (in) - maximum height of the rib (from upper surface to lower surface)
- Profile Area ($in^2$) - area of rib as viewed from top of aircraft ($Length \times Height$)
- Periphery (in) - periphery of the rib ($2\ Length + 2\ Height$)
- Pocket Quantity - number of pockets (double sided ribs have pockets on both sides of the web, single sided only has then on one)
- Pocket Length (in) - average length of pockets (along length of rib)
- Pocket Width (in) - average width of pockets (from cap to cap)
- Pocket Depth (in) - depth of pockets
- Finished Weight (lb) - weight of the finished machined rib components
- Surface Area ($in^2$) - surface area of the finished rib components (after assembly

and including pockets / not including shear ties, baffle clips, butterfly clips, or fasteners)

**Rib Sub Assembly** The SEER-MFG model for rib sub assembly estimates the time and cost required to assemble the rib components into a completed rib. The rib sub assembly is the same for both the double sided ribs and the single sided ribs; however, the number of parts will be different. The model is repeated for each rib and the results are summed in SPANDSET to get the entire cost of assembling all the ribs. The inputs for the SEER-MFG model are listed below:

- Assembly Size ($in^2$) - area of rectangular box the completed rib occupies on shop floor (i.e. $Length \times Height$)
- Number of Parts - number of parts in rib sub assembly (excluding fasteners)
- Join Length (in) - length of joints in rib sub assembly (approximately $2 \times Length$)
- Join Width (in) - average width of points in rib sub assembly
- Number of Fasteners - Number of fasteners used in rib sub assembly
- Thickness of Rib Web (in) - average thickness of rib web
- Thickness of Shear Tie (in) - thickness of a shear tie

**Spar Sub Assembly** The SEER-MFG model for the spar sub assembly estimates the time and cost required to assemble the necessary components to attach the spars and the ribs (i.e. attaching rib posts to the spar). The model is repeated for each spar and the results are summed in SPANDSET to get the entire cost of assembling all the spars. The inputs for the SEER-MFG model are listed below:

- Number of Parts - number of parts in spar sub assembly (excluding fasteners)
- Raw Weight (lb) - raw weight of a single rib post
- Thickness of Stiffener (in) - thickness of a rib post
- Periphery (in) - periphery of a rib post

- Finished Weight (lb) - finished weight of a rib post
- Cut Length (in) - Cut length of a rib post (finished length of a rib post)
- Join Length (in) - length of joint that attaches all rib posts to all spar webs ($qty\ of\ rib\ posts \times length\ of\ rib\ post$)
- Join Width (in) - width of joint that attaches all rib posts to spar web
- Thickness of Spar Web (in) - average thickness of the spar web
- Part Area (in) - surface area of rib post
- Assembly Area (in) - area of a rectangular space that the spar occupies on shop floor ($SparLength \times SparWidth$)
- Number of Fasteners - Number of fasteners used in rib sub assembly

**Major Component Assembly** The process of aligning the spars, inserting the ribs, attaching the stringers to the skin, and installing the skin have all been combined into one model called the major component assembly model. SEER-MFG does not require the full details of the substructure layout. Instead SEER-MFG estimates the time and cost required to assemble the wing box off the size of all the parts and all the joint lengths summed together. Additionally, two representative thicknesses are used rather than specifying the thickness of the two parts at each fastener. The inputs for the SEER-MFG major component assembly are listed below.

- Assembly Area ($in^2$) - area of a rectangular space that the wing box occupies on shop floor
- Number of Parts - number of parts in wing box assembly (spars, ribs, skins, stringers)
- Number of Fasteners - number of fasteners used in wing box assembly (excludes rib and spar sub assemblies)
- Join Length (in )- length of joints in wing box assembly
- Join Width (in )- average width of joints in wing box assembly

- Thickness of Part 1 - thickness of a representative part in a wing (maximum skin thickness used)
- Thickness of Part 2 - thickness of a representative part in a wing (maximum skin thickness used)
- Auto Drill % - percent of fasteners in wing box assembly (excluding spar and rib sub assembly) that are automatically drilled and installed (remaining are done by hand)
- Hiloc % - percent of fasteners in wing box assembly (excluding spar and rib sub assembly) that are hilocs (remaining are assumed to be rivots)

**Model Outputs** All the SEER-MFG models have the same set of outputs. The outputs can be divided into two categories: the labor time outputs and the manufacturing cost outputs. The labor time outputs are listed in Table 15. These outputs are calculated by SEER-MFG's manufacturing process estimation capabilities.

Table 15: SEER-MFG Labor Time Outputs

| Outputs | Description |
|---|---|
| Setup Time (min) | The time it takes to get the tooling, carry it to the machine, and install it into the equipment. |
| Direct Time (min) | The time to pick up the part, place the part into the tool, perform manual and machining operations, then remove the part. It also includes idle time (waiting on raw material, lost time to breaks, sick-time, etc.). |
| Inspection Time (min) | The time it takes to inspect finished work pieces. |
| Rework Time (min) | The time it takes to correct deficiencies found during inspection. |
| Total Labor Time (min) | The total time spent on a part (including setup, direct, inspection, and rework). |

SEER-MFG requires the user to specify the labor rates (Table 16) and material costs (Table 17) to calculate the costs.

Table 16: Labor Rates

| User Inputs | Description |
|---|---|
| Fabrication Direct Labor Rate ($/hr) | Labor rate for direct fabrication. |
| Assembly Direct Labor Rate ($/hr) | Labor rate for assembly. |
| Fabrication Setup Labor Rate ($/hr) | Setup labor rate for fabrication. |
| Assembly Setup Labor Rate ($/hr) | Setup labor rate for fabrication. |

Table 17: Material Costs

| User Inputs | Description |
|---|---|
| Upper Skin Material Cost ($/lb) | Cost of raw materials required to build the upper skin panels. |
| Upper Stringer Material Cost ($/lb) | Cost of raw materials required to build the upper stringers panels. |
| Lower Skin Material Cost ($/lb) | Cost of raw materials required to build the lower skin panels. |
| Single Sided Rib Material Cost ($/lb) | Cost of raw materials required to build single sided ribs. |
| Double Sided Rib Material Cost ($/lb) | Cost of raw materials required to build double sided ribs. |
| Spar Material Cost ($/lb) | Cost of raw materials required to build spars. |

SEER-MFG outputs the manufacturing costs for each model by combining the labor time, the labor rates, and the material costs. The manufacturing costs outputs are listed in Table 18.

Table 18: SEER-MFG Manufacturing Cost Outputs

| Outputs | Description |
|---|---|
| Setup Labor Cost ($) | The labor cost of getting the tooling, carrying it to the machine, and installing it into the equipment. |
| Direct Labor Cost ($) | The labor cost associated with the direct fabrication of the part (i.e. placing and removing parts and manual or machining operations). |
| Inspection Labor Cost ($) | The labor cost for inspecting finished work pieces. |
| Rework Labor Cost ($) | The labor cost for correcting deficiencies found during inspection. |
| Total Labor Cost ($) | The sum of the setup, direct, inspection, and rework labor costs. |
| Material Cost ($) | Purchase cost of raw materials (fabrication) and components (assembly). |
| Total Cost ($) | Total variable cost (sum of total labor cost and material cost). |

#### *6.3.2.2 Excel Cost Tool*

Incorporating SEER-MFG directly into SPANDSET is impractical. The run time for SEER-MFG is longer than is practical for conceptual design. Additionally, the SEER-MFG models contain proprietary information which creates difficulties in using the model on computers outside of Triumph. Surrogate models (specifically Response Surface Equations) of the SEER-MFG models are created to mitigate these problems.

The PGM does not create all the geometric values required by the SEER-MFG Response Surface Equations (RSEs). Additional processing is required; thus, the Excel Cost Tool was created. The surrogate models were incorporated into an Excel file using VBA. Excel is used to make the cost tool portable, adaptable, and user-friendly. The Excel cost tool takes inputs from the user, PGM, and structural sizing and analysis routines. Then, the excel cost tool uses rules of thumbs to determine the required inputs to the RSEs.

The inputs required by the Excel Cost Tool can be divided into user inputs, inputs from the PGM, and inputs from the structural analysis and sizing routines.

**User Inputs** These inputs are values from the SEER-MFG models that are input directly by the user. These variables are listed below.

- Fabrication Direct Labor Rate
- Assembly Direct Labor Rate
- Fabrication Setup Labor Rate
- Assembly Setup Labor Rate
- Material Cost
- Skin Pocket Depth Removed
- Stringer % Material Removed
- Single or Double Sided (for each rib)
- Shear ties? (for each rib)
- Butterfly clips? (for each rib)
- Baffle Clips? (for each rib)
- Stringer to Skin Auto Drill %
- Stringer to Skin Hiloc %
- Skin Installation Auto Drill %
- Skin Installation Hiloc %
- # Access Panels in Lower Skin

**Inputs from PGM** Several inputs for the SEER-MFG models can be taken directly from the PGM. These variables define the number and sizes for several of the components. These variables are listed below. All lengths are in inches.

- Wing Span, Root Chord Length, and Tip chord Length
- Front Spar % Chord (average of percent chord values that define the front spar)
- Rear Spar % Chord (average of percent chord values that define the rear spar)
- Number of Covers (calculated for both the upper and lower surfaces)
- Average Area of Cover (calculated for both upper and lower surfaces)
- Number of Ribs, Upper Stringers, Lower Stringers, and Spars
- Upper and Lower Stinger Lengths (for each upper stringer)
- Rib Lengths & Heights (for each rib)
- Spar Lengths & Heights (for each spar)

**Inputs from Structural Analysis and Sizing Routines** The final set of inputs for the Excel cost tool are the values from the structural analysis and sizing routines. These values consist of the weights and dimensions. The skin panel values are input as an average or a sum of all the skin panels due to the large number of skin panels. These values are listed below.

- Average Upper Skin Thickness and Average Lower Skin Thickness
- Total Upper Skin Weight and Total Lower Skin Weight

The stringer dimensions for both the upper and lower stringers are the averages of the stringer segment values across the entire length of the stringers. The stringer weight is calculated during the weight estimation. The Excel cost tool requires the following inputs for each stringer on the upper and lower surface.

- Stringer Height ($h$)
- Stringer Base Width ($b_{base}$)

- Stringer Thickness (uses web thickness $t_{web}$)
- Stringer Weight

The spar dimensions are the average of all the spar segment dimensions in the structural analysis and sizing routines. The weight is calculated during the weight estimation. The Excel cost tool inputs are listed below.

- Spar Cap Width ($w_1 + w_2$) (calculated using the average of both the upper and lower caps)
- Spar Upright Spacing ($S$)
- Average Spar Stiffener Length (calculated using the average length of all the upright on the spar segment)
- Spar Web Thickness
- Spar Weight

The rib dimensions and rib weights are already calculated for each rib by the structural analysis and sizing routine. The values required by the Excel cost tool are listed below.

- Rib Cap Width ($w_1$) for each rib
- Rib Upright Spacing for each rib
- Rib Web Thickness ($t_{web}$) for each rib
- Rib Cap Thickness ($t_1$) for each rib
- Rib Weight for each rib
- Average Rib Post Thickness (calculated as average spar upright thickness of all spar uprights)

After these values have been gathered, the Excel cost tool then translates the inputs into values that can be used by the SEER-MFG RSEs. Not all values that are required by the RSEs have been gathered in the inputs. The Excel cost tool uses several rules of thumb to fill in these knowledge gaps. For example, there are no

inputs for the number of fasteners. Instead the Excel cost tool uses an estimated value for number of fasteners per length of an edge for a specific part (i.e. rib, spar, or stringer); therefore, the number of fasteners required to attach a stringer to the skin is the length of the stringer multiplied by the estimated number of fasteners per length for the stringers. Triumph has developed several of these estimates and allowed them to be input into the Excel cost tool.

The Excel cost tool assesses each surrogate model for the given inputs using a VBA version of the RSE. The outputs of each RSE are given in the previous section; however, the Excel cost tool reorganizes the outputs based upon the overall costs of the wing box. The final cost outputs are listed in Table 19.

Table 19: SPANDSET Cost Breakdown

| Outputs | Description |
|---|---|
| Skin Fabrication Cost ($) | The cost to fabricate all the skin panels on the upper and lower surface from raw material to completed skin panel |
| Stringer Fabrication Cost ($) | The cost to fabricate all the stringers on the upper and lower surface from raw material to completed stringer |
| Spar Fabrication Cost ($) | The cost to fabricate all the spars from raw material to completed spar |
| Spar Fabrication Cost ($) | The cost to fabricate all the rib components from raw material to completed components |
| Rib Assembly Cost ($) | The cost to assemble the rib components into the completed ribs |
| Spar Assembly Cost ($) | The cost to install the rib posts on all the spars |
| Major Assembly Cost ($) | The cost assemble all the components into completed wing box |
| Labor Hours (hr) | Total time spent manufacturing the wing box (including setup, direct, inspection, rework, and assembly). |
| Labor Cost ($) | The cost of the labor associated with manufacturing the wing box |
| Material Cost ($) | The cost of the raw materials required to manufacture the wing box |
| Total Cost ($) | The total cost of manufacturing the wing box |

# CHAPTER VII

# STRUCTURAL ANALYSIS AND SIZING ROUTINES

Chapter 6 introduced SPANDSET (Structure Preliminary Analysis and Design Space Exploration Toolkit). SPANDSET is a parametric wing box structural analysis and sizing M&S environment that uses classical structural analysis to individually size the elements of the wing box substructure. In Chapter 6 the sizing and analysis routine was described but not in sufficient detail. This chapter seeks to explain the entire structural analysis and sizing process used by SPANDSET.

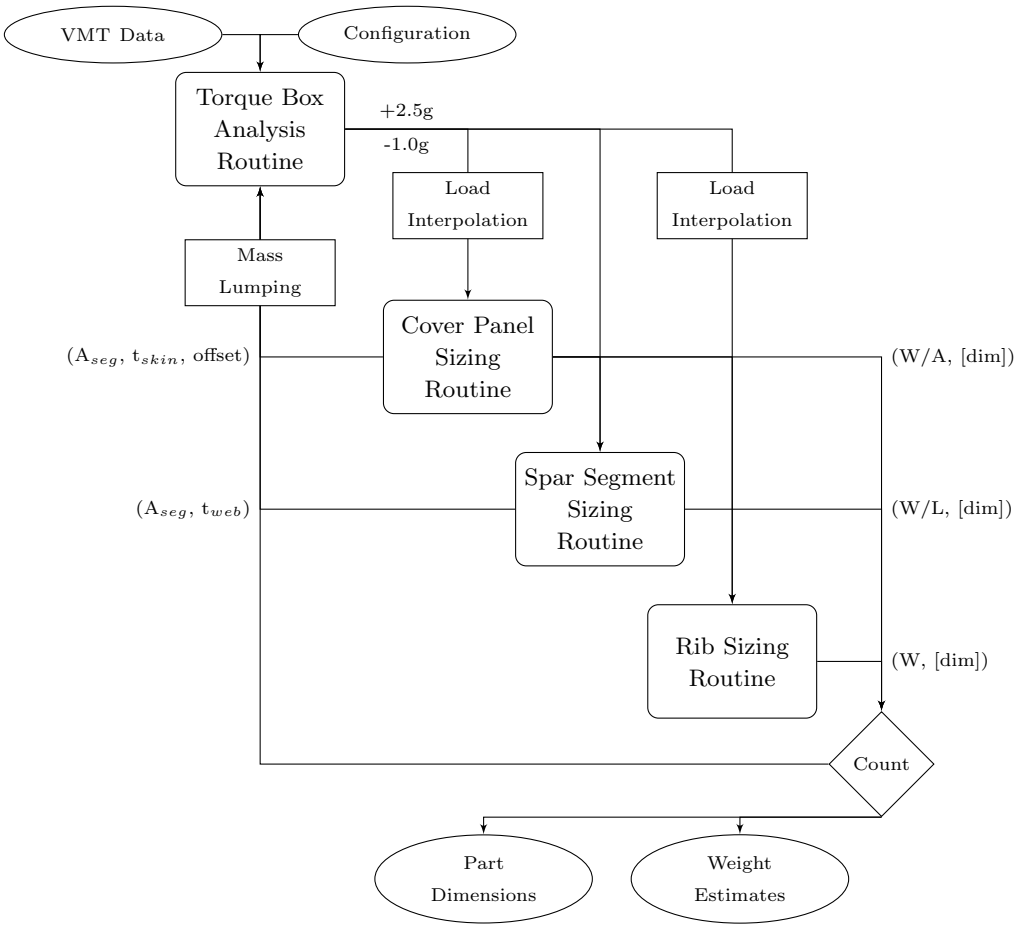


Figure 60: Structural Analysis & Sizing

Figure 60 illustrates the structural analysis and sizing process used in SPANDSET. SPANDSET converts the externally applied loads to internal loads using the torque box analysis routine (Section 7.1). The torque box analysis routine uses the shear, moment, and torque (VMT) data generated from the external loads and the substructure configuration to generate the internal loads (shear stresses and axial stresses) for several specified cross-sections. These internal loads are then sent to the part analysis and sizing routines (note that some loads need to be interpolated). The cover panel sizing routine (Section 7.1.4), spar segment sizing routine (Section 7.2.4), and rib sizing routine (Section 7.3.4) then use the internal loads to perform structural analysis and sizing on the cover panels, spars, and ribs respectively. The final result of the structural analysis and sizing portion of SPANDSET is the part dimensions and weight estimates used for the final wing box weight.

## *7.1 Thin Walled Torque Box Analysis*

SPANDSET calculates the internal loads by performing common multi-cell torque box analysis on several cross-sections specified by the parametric geometry tool. The parametric geometry tool gives the torque box analysis routine the necessary geometric data and material properties. The torque box analysis then performs multi-cell shear flow analysis as well as calculates the axial loads due to the bending moment in several lumped masses along the cross-section. The Torque Box Analysis will provide the bending stiffness of the cross-section, the shear distribution along the cross-section, and the axial loads at each of the lumped masses for the other sizing routines.

### 7.1.1 Inputs

The torque box analysis requires several inputs from other portions of SPANDSET. These inputs are organized into: cross-section nodes, part dimensions, external loads data, and material properties.

#### 7.1.1.1 Cross-Section Nodes

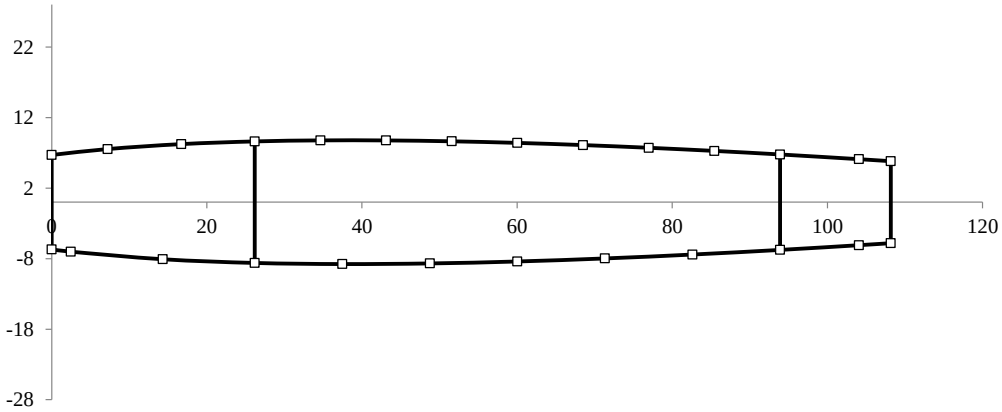


Figure 61: Cross-Section Intersections

The first step in executing the torque box analysis is to calculate the intersections of all the spars and all the stringers with the cross-section for each cross-section. Figure 61 illustrates an example. In Figure 61 the outline represents either the skin panels or spar webs that intersect the cross-section, while the squares represent either the stringers or spar chords that intersect the cross-section. These points are calculated in both the $[BL, FS, WL]$ coordinate system and an $[y, z]$ coordinate system in the plane of the cross-section where $y$ runs the length of the cross-section, $z$ is parallel to the height of the cross-section, and the origin is at the intersection of the front spar and the cross-section.

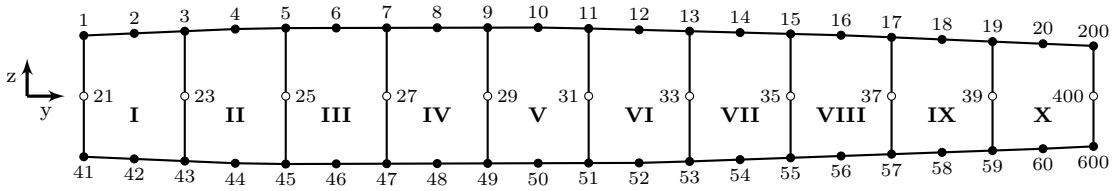


Figure 62: Torque Box Points

After the cross-section intersections are calculated they need to be transformed into the nodes for the torque box analysis routine. The torque box analysis assumes a specific form with 10 cells formed by spars and covers, as well as 53 nodes representing

lumped masses (Figure 62). The number of cross-section intersections is unlikely to match the number of nodes required. Figure 61 depicts a cross-section geometry from the parametric geometry tool. The cross-section in Figure 61 has only 2 spars and fewer stringers and spar chords (represented by the squares) than the torque box analysis routine requires. Therefore, additional steps are required to match the cross-section intersections with the torque box analysis nodes.

A generalization of the process to alter the intersections to match the nodes can be described in the following steps. First, create a set of evenly spaced points on the upper and lower surface. Next, points are added to the top and bottom surfaces at the exact location of each spar and one point is deleted from the previous step for each spar (i.e. the points closest to the spar location). Finally, adjust the remaining points so that they are evenly spaced without moving the points located on a spar. Due to the mass lumping and matching the spar locations the process is more difficult than the generalization described above. However, the generalization will suffice for this dissertation.

#### *7.1.1.2 Part Dimensions*

The torque box analysis routine requires several dimension values from the subcomponents to calculate the internal loads distribution. However, the torque box analysis is executed before any of the subcomponents are sized. For this reason the analysis and sizing portion of SPANDSET is iterative. For the first iteration the torque box analysis routine assumes initial values for the dimensions. As the iterations progress, the torque box analysis uses the sized values from the previous iteration. The analysis and sizing process continues until a reasonable convergence criteria is met.

The thicknesses of the cell walls ($t_{seg}$) are required to perform the shear flow portion of the torque box analysis. These thicknesses correspond to the skin thicknesses in the cover analysis routine and the spar web thicknesses from the spar segment analysis

routine.

The nodes represent lumped masses and are defined by two dimensions. The first nodal dimension is the segment area ($A_{seg}$). If the node lies on the intersection of the upper or lower surface and a spar, then the segment area is the segment area of the spar cap (Equation 43) from the previous iteration for the specified spar. The calculation of segment areas for the reaming nodes is more difficult because these segment areas are calculated based upon the lumped masses. Because the number of nodes is unlikely to line up with the number of stringers, the stringer masses need to be distributed across the nodes. For each node the segment area is calculated by multiplying the average of the cover segment areas from the previous iteration by several ratios (Equation 44). These ratios are based upon the cover segment areas and node segment areas from the previous iteration as well at the spacing between nodes and the stringer spacing. The calculation of the segment loads is complex and the general explanation will suffice for this dissertation.

$$\text{Spar node: } [A_{seg}]_{node} = [A_{seg}]_{spar\ cap} \tag{43}$$

$$\text{Cover node: } [A_{seg}]_{node} = \frac{\sum [A_{seg}]_{cover}}{n_{covers}} \frac{\sum [A_{seg}]_{cover}}{\sum [A_{seg}]_{node}} \frac{s_{node}}{\sum b_{covers}/n_{covers}} \tag{44}$$

The second nodal dimension is the offset ($\bar{z}_{i,o}$). The offset represents the distance between the OML of the cross-section (where the intersections are calculated) and centroid location of the lumped skin/stringer area or spar cap areas at each of the 21 nodes along the upper and lower wing box surface. The offset is assumed to be oriented so that a positive direction is vertically along the z-axis from the surface toward the cross-section interior. If the node lies on the intersection of the upper or lower surface and a spar, then the offset is the centroid of the specified spar cap calculated by the spar analysis during the previous iteration (Equation 45). For the remaining nodes linear interpolation is performed on the cover centroids from the

previous iteration based upon the $FS$ coordinate of the cover and node (Equation 46).

$$\text{Spar node: } [\bar{y}]_{node} = [\bar{y}]_{spar\ cap} \tag{45}$$

$$\text{Cover node: } [\bar{y}]_{node} = \frac{(FS_i - FS_1)(\bar{y}_2 - \bar{y}_1)}{(FS_2 - FS_1)} + \bar{y}_1 \tag{46}$$

As previously mention the internal loads analysis is based on a fixed number of nodes. Converting the actual cross-section geometry (Figure 61) to the fixed number of nodes (Figure 62) is likely to result in several nodes that do not represent a subcomponent. For example, if only the front and rear spar exist the nodes that pertain to the other spars (i.e. 23, 25, 27, 29, 31, 35, 37, 39) are still used in the torque box analysis. In the case that one such node represents a spar the segment is negated by setting the thickness to a very small value (0.0001in). Additionally, if the node pertains to a lumped mass that has no stringer associated with it, the segment is negated by setting the area to zero.

#### *7.1.1.3 External Loads Data*

SPANDSET provides the externally applied shear, moment, and torque (VMT) distribution along the wing span to the torque box analysis routine. The VMT distribution is supplied via an input table consisting of the shear ($V_z$), moment ($M_y$), and torque ($T$) loads for the positive (+2.5g) and negative (-1.0g) bending conditions as a function of the wing span fraction. The positive and negative bending loads are envelope conditions and establish the critical sizing conditions for the wing box. The load distribution is one dimensional and located along the load reference axis. The load reference axis is specified along with the external loads inputs with the VMT data and the location the load reference axis intersects the cross-section is calculated by the geometry tool. The VMT data can be specified for any number of points along the load reference axis.

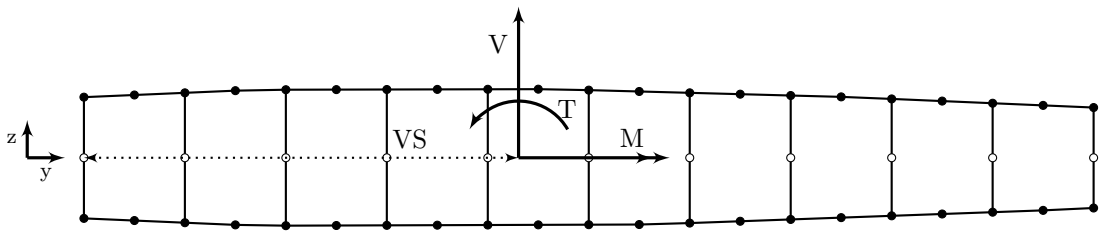


Figure 63: Torque Box Loads

The VMT data needs to be applied to each cross-section before the torque box analysis can be used. However, the VMT data is supplied at a limited number of points. Thus, linear interpolation is used to calculate the shear ($V_z$), moment ($M_y$), and torque ($T$) loads at the intersection of the loads reference axis and the cross-section. The intersection of the load reference axis and the cross-sections are calculated by the parametric geometry tool in both the $[BL, FS, WL]$ coordinate system (to be used for the VMT interpolation) and the $[y, z]$ coordinate system (to be used for the torque box analysis). The intersection is also the point along the cross-section that the loads are applied. The distance along the cross-section from the intersection to the front spar is $VS$ (Figure 63). All these values are required inputs for the torque box analysis routine.

Each load case is applied one at a time so that the torque box analysis can determine the distribution of the internal loads for both the up bending and down bending external load cases. The internal load distribution will then be used by to the sizing analysis routines.

#### *7.1.1.4 Material Properties*

The material properties required by SPANDSET are listed in Table 12. Not all of these properties are required for the torque box analysis. The material properties required by the torque box analysis are the Young's modulus ($E$) for the spar chords, stringers, spar webs, and skin panels as well as the shear modulus ($G$) for the skin panels and spar webs.

The points in the Torque Box Analysis routine do not match the exact location of the intersections of the cross-section with the subcomponents. Thus, the geometry being analyzed by the Torque Box Analysis routine is not the same as the geometry of the cross-section. A result of the difference in geometries is a need to calculate lumped material properties for each of the skin panels and lumped masses. These lumped masses are calculated based upon area weighted material properties of the components that each lumped node represents.

### 7.1.2 Pre-processing

There exist several values that are used in multiple phases of the torque box analysis. These values will be discussed below.

#### *7.1.2.1 Bending Stiffness*

The sectional stiffness is calculated using only the nodal properties of the lumped masses. The spar web thickness is assumed to be small enough that the spars webs have no effect on the bending stiffness. The spar chords, stringers, and covers are accounted for by the lumped masses.

The centroid of the cross-section must be calculated before the sectional stiffness can be calculated. The nodal properties ($E_i$ and $A_i$), nodal coordinates ($y_i$ and $z_i$), and the offset ($\bar{z}_{i,o}$) are used to calculate the centroid coordinates in Equation 47 and Equation 48.

$$\bar{y} = \frac{\sum y_i E_i A_i}{\sum E_i A_i} \tag{47}$$

$$\bar{z} = \frac{\sum (z_i - \bar{z}_{i,o}) E_i A_i}{\sum E_i A_i} \tag{48}$$

After the centroid is located the centroid coordinates ($\bar{y}$ and $\bar{z}$), the nodal properties ($E_i$ and $A_i$), nodal coordinates ($y_i$ and $z_i$), and the offset ($\bar{z}_{i,o}$) are used to calculate

the bending stiffness in Equation 49, Equation 50, and Equation 51.

$$(EI)_y = \frac{\sum (z_i - z_{i,o} - \bar{z})^2 E_i A_i}{\sum E_i A_i} \tag{49}$$

$$(EI)_z = \frac{\sum (y_i - \bar{y})^2 E_i A_i}{\sum E_i A_i} \tag{50}$$

$$(EI)_{yz} = \frac{\sum (y_i - \bar{y})(z_i - z_{i,o} - \bar{z}) E_i A_i}{\sum E_i A_i} \tag{51}$$

#### *7.1.2.2 Segment Properties*

A segment is defined as the portion of the cross-section between the lumped masses. These segments are considered to be equivalent to the spar webs or the cover skin panels. Each segment has a thickness ($t_{seg}$), shear modulus ($G_{xy}$), and Young's modulus ($E_x$) associated with it. The length of each segment is calculated in Equation 52.

$$d_{seg} = \sqrt{(\Delta y_{seg})^2 + (\Delta z_{seg})^2} \tag{52}$$

$$\Delta y_{seg} = y_{i+1} - y_i \quad \text{and} \quad \Delta z_{seg} = z_{i+1} - z_i$$

Additionally, the displacement constant to be used during the closed cell shear flow analysis is calculated in Equation 53.

$$\alpha_{seg} = \frac{d_{seg}}{Gt} \tag{53}$$

#### *7.1.2.3 Cell Areas*

The cell areas are calculated using the nodes in Figure 62. Each cell has nine points associated with it. The coordinates of the nine points that make up each cell ($[y_i, z_i] : i = 1, 2, ..., 9]$) can be used to calculate the cell area using coordinate geometry and Equation 54.

$$A_c = \frac{\sum_{i=1}^{8} (y_i z_{i+1} - z_i y_{i+1})(y_9 z_1 - z_9 y_1)}{2} \tag{54}$$

### 7.1.3 Shear Flow Analysis

The torque box analysis performs shear flow analysis on a multi-cell thin walled box. The multi-cell shear flow analysis uses the principle of super position to sum together the shear flow of the closed cells with the shear flow of an open section. For both the open and closed shear flow analysis the masses are assumed to be lumped at the intersections. This assumption means that the cover skins and spar webs can be treated as shear panels with uniform shear flow across each panel.

#### *7.1.3.1 Open Section Shear Flow*

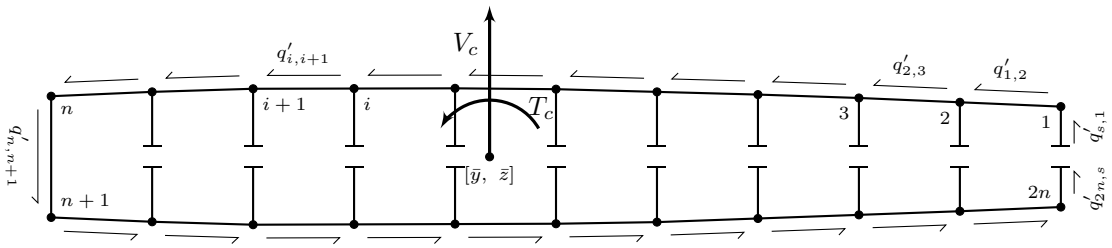


Figure 64: Open Section Shear Flow

The open section shear flow analysis assumes that there are several cuts on all of the spars except for one. The resulting shear flow along a cut spar web is zero. The spars that are cut are arbitrary with regard to the final shear flow calculations. SPANDSET assumes the form for the open section illustrated in Figure 64.

SPANDSET calculates the shear flow in a counterclockwise direction (Figure 64). The first shear flow is zero ($q'_{s,1} = 0$) because it is part of a cut spar web. The remaining open shear flows are calculated using Equation 55.

$$q'_{i,i+1} = q'_{i-1,i} + VE_iA_i\frac{y_c(EI)_{yz} - z_c(EI)_z}{\Delta(EI)} \tag{55}$$

Where:

$$\Delta(EI) = (EI)_y(EI)_z - (EI)^2_{yz}$$

$$y_c = (y_i - \bar{y}) \text{ and } z_c = (z_i - z_{i,o} - \bar{z})$$

The upper surface shear flow and lower surface shear flow will sum to zero due to no horizontal force being applied to the cross-section. Additionally, the final shear flow should be equal to zero ($q'_{22,s} = 0$).

#### *7.1.3.2 Closed Cells Shear Flow*

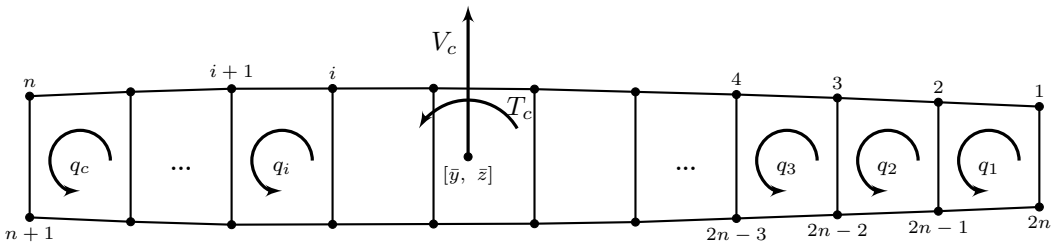


Figure 65: Closed Cells Shear Flow

The closed shear flow for each cell is depicted in Figure 65. The closed shear flows for each cell are calculated simultaneously by solving a system of equations. The equations are a result of enforcing compatibility conditions where the physical condition that the angle of twist of each cell in the cross-section must be equal. Enforcing the compatibility condition results in $c-1$ equations where $c$ is the number of cells and the unknowns are the closed cell shear flows ($q_i$).

The final step of the shear flow analysis is to superpose the closed cell shear flows over the open section shear flows. For instance the closed shear flows ($q_i$) are in the same direction as the upper surface open shear flows (i.e. $q'_{1,2}$, $q'_{2,3}$,...); thus, they should be added together. However, the closed shear flows ($q_i$) are in the opposite direction as the lower surface (i.e. $q'_{n+1,n+2}$, $q'_{n+2,n+3}$,...).

#### *7.1.3.3 Shear Center*

By definition, the shear center location is where the vertical shear load will produce bending without twisting. The shear flow of the open section creates an unbalanced torque. Thus, the shear center location can be calculated by summing the moments

of the open section shear flow and the shear force applied at the shear center to zero. For the shear center calculation the torque box analysis assumes the covers are flat to simplify the moment calculations. The result is shown in Equation 56.

$$e_{sc} = -\frac{1}{V}\left[\sum_{i=1}^{n} q'_{i,i+1} d_{seg} z_i + \sum_{i=n+1}^{2n} q'_{i,i+1} d_{seg} z_i\right] \tag{56}$$

Only one coordinate of the shear center is required because the shear is assumed to be applied along the z-axis and not the y-axis.

### 7.1.4 Axial Segment Loads

The final set of loads calculated by the torque box analysis are the segment loads. These loads are the axial loads in the lumped mass nodes due to the bending of the wing. From Euler-Bernoulli beam bending theory [17] the axial load of each segment is calculated using Equation 57.

$$P_{seg} = \sigma_x A_{seg} = A_{seg}\left[\frac{y_c (EI)_{yz} - z_c (EI)_z}{\Delta(EI)}\right] \tag{57}$$

Where:

$$\Delta(EI) = (EI)_y (EI)_z - (EI)_{yz}^2$$

$$y_c = (y_i - \bar{y}) \text{ and } z_c = (z_i - z_{i,o} - \bar{z})$$

In Figure 63, the bending moment ($M$) is positive so that a positive moment puts the upper surface in compression ($P_{seg}$ is negative) and the lower surface is in tension ($P_{seg}$ is positive).

## 7.2 Stiffened & Unstiffened Cover Panels Sizing

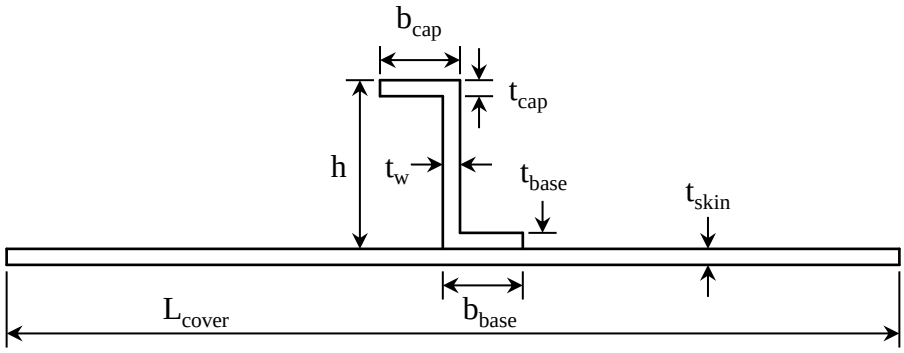


Figure 66: Cover Features

SPANDSET uses the cover analysis routine to perform sizing on several cover panels. SPANDSET does not size all the cover panels; instead, the cover analysis sizes several panels along the length of each cross-section to get an estimate for weight per unit area. SPANDSET then uses the estimated weight per unit areas to estimate the entire weight of the upper covers and lower covers.

The covers sections are either stiffened skin panels or unstiffened skin panels based upon their location in the configuration. If the cover section is located over a spar it is unstiffened, otherwise it is stiffened. For the stiffened cover panels the features are the skin and a Z-section stiffener (Figure 66). For the unstiffened cover the feature is just the skin panel.

**Stiffened Cover**
Minimize:

$$F(\bar{X}) = \frac{W_{skin} + W_{stringer}}{L_{cover}} \tag{58}$$

Subject to:

$$\begin{aligned} &2.1 \geq h \geq 1.0 && t_{skin} \geq 0.065 \\ &b_{cap} \geq 0.6 && t_w \geq 0.09 \\ &b_{base} \geq 1.08 && t_{base} \geq 0.05 \\ &1.25 \geq \frac{b_{cap}}{b_{base}} \geq 0.25 && t_{cap} \geq 0.125 \\ & && t_{cap} \geq t_w \end{aligned} \tag{59}$$

$$\begin{aligned} &\text{M.S. Section Crippling} \geq 0 \\ &\text{M.S. Damage Tolerance} \geq 0 \\ &\text{M.S. Skin Compression + Shear Buckling} \geq 0 \\ &\text{M.S. Column Stability Johnson-Euler} \geq 0 \\ &\text{M.S. Euler-Johnson + Shear Interaction} \geq 0 \end{aligned} \tag{60}$$

Where:

$$\bar{X} = \left\{ t_{skin},\ h,\ t_w,\ b_{cap},\ t_{cap},\ b_{base},\ t_{base} \right\} \tag{61}$$

**Unstiffened Cover**
Minimize:

$$F(\bar{X}) = \frac{W_{skin}}{L_{cover}} \tag{62}$$

Subject to:

$$t_{skin} \geq 0.04 \tag{63}$$

$$\begin{aligned} &\text{M.S. Durability and Damage Tolerance} \leq 0 \\ &\text{M.S. Skin Buckling} \leq 0 \end{aligned} \tag{64}$$

Where:

$$\bar{X} = \left\{ t_{skin} \right\} \tag{65}$$

The cover analysis routines uses numerical optimization to solve one of the optimization problems listed above for each cover panel along the specified cross-section. If the cover is stiffened ythen the objective function (Equation 58) is minimized using the dimension of the features (Figure 66) as the design variables (Equation 61) subjected to the constraints (Equation 59 and Equation 60).

If the cover is unsitffened then the number of design variables is reduced (Equation 65), the number of dimension constraints are reduced (Equation 63), and the weight component due to the stiffener is eliminated in the objective function (62). However, the elimination of the stiffener also changes the way the cover panel handles the loads. Instead of designing the stiffener to carry the majority of the weight, the skin panel must carry all the loads. Thus, the margins of safety are different as well (64).

### 7.2.1 Inputs

Each analysis routine requires three sets of inputs beyond the design variables: the material properties for each feature, geometric information from the configuration, and the internal loads calculated from the torque box analysis.

#### *7.2.1.1 Material Properties*

The material properties required by SPANDSET are listed in Table 12. Not all of these properties are required for each feature. The material properties that are required for the cover analysis are: the Young's modulus ($E$) and shear modulus ($G$) for the skin and stringer, the ultimate tensile load ($F_{tu}$) and tensile yield load ($F_{tu}$) for the skin, The compression yield load ($F_{cy}$) for both the skin and stringer, the ultimate shear load ($F_{su}$) for the skin, and the density ($\rho$) for both the skin and stringer.

#### *7.2.1.2 Configuration Geometry*

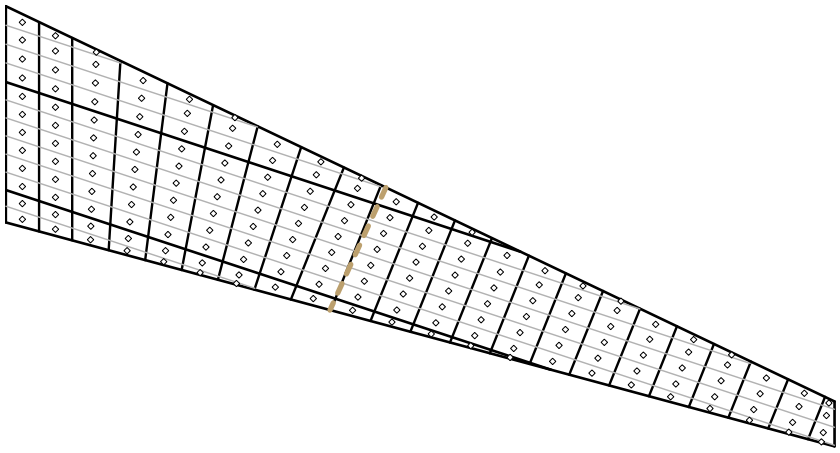

Figure 67: Surface Geometry

Several inputs required by the cover analysis come from the configuration. These variables are calculated by the parametric geometry tool. After the configuration has been defined the parametric geometry tool organized the components into horizontal elements (ribs) and vertical elements (spars and stringers). The parametric geometry tool then generates all the intersections between each horizontal elements and vertical element to generate the points that define each cover. Figure 67 illustrates all the covers for one of the surfaces (either upper surface or lower surface). The diamonds in the middle depict the centroid of each cover created. Figure 67 illustrates that every cover is defined between adjacent stringers or spars and adjacent ribs.

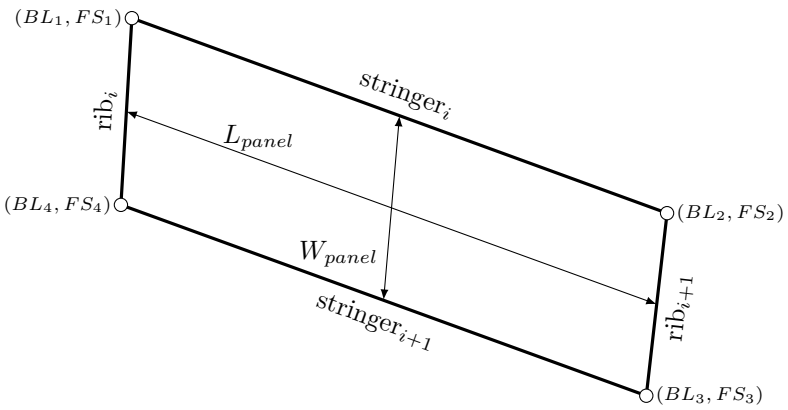


Figure 68: Cover Geometry

Figure 68 illustrates the cover geometry. The cover geometry is defined by the four points that result from the intersection of adjacent stringers ($\text{stringer}_i$ and $\text{stringer}_{i+1}$) and adjacent ribs ($\text{rib}_i$ and $\text{rib}_{i+1}$). Each cover is assumed to be flat and the points are defined in the $[BL,\ FS]$ coordinate system. The two dimensions that must be defined are the length and width of each cover panel. The width of the panel is synonymous with the stringer spacing. However, because the front spar and rear spar are not assumed to be parallel to all the other spars and stringer the panel width is defined as the length between the midpoints of the spars or stringers (Equation 66).

$$W_{panel} = \sqrt{\left(\frac{FS_1 + FS_2}{2} - \frac{FS_4 + FS_3}{2}\right)^2 + \left(\frac{BL_1 + BL_2}{2} - \frac{BL_4 + BL_3}{2}\right)^2} \quad (66)$$

Similarly, the length of the cover is synonymous with the rib spacing. However, because the ribs are not assumed to be parallel to one another (i.e. main ribs and stub ribs have different orientations) the panel width is defined as the length between the midpoints of the ribs (Equation 67).

$$L_{panel} = \sqrt{\left(\frac{FS_1 + FS_4}{2} - \frac{FS_2 + FS_3}{2}\right)^2 + \left(\frac{BL_1 + BL_4}{2} - \frac{BL_2 + BL_3}{2}\right)^2} \quad (67)$$

The length and the width of the cover panels do not need to be calculated for all the covers. The cover analysis only analyzes the covers that are closest to the

cross-section. In Figure 67 the dotted gold line represents one of the cross-sections. For this cross-section only the covers to the right will be analyzed. Therefore, the values $L_{panel}$ and $W_{panel}$ only need to be calculated for these covers as well as the cover associated with the other cross-sections.

#### *7.2.1.3 Internal Loads and Stiffness*

The cover analysis requires three loads for sizing the stiffened and unstiffened covers: the axial compression load ($N_{x\ comp}$) and the axial tension load ($N_{x\ tension}$). The analysis routine also uses an axial load for damage tolerance ($N_x\ DT$); however, this value is the same as the tension axial load ($N_xDT = N_{xtension}$).

There are two steps to calculating these loads. The first step is to transfer the nodal segment loads calculated by the torque box analysis to each individual cover. The difficulty is that rarely do the nodes (Figure 62) line up with the stringer locations (Figure 61). To calculate the cover loads from the segment loads linear interpolation is used based upon the $FS_c$ coordinates of the stringer intersection and the node coordinates. Therefore, the two nodes on either side of the cover and their associated loads ($P_1$ and $P_2$) and coordinates ($FS_1$ and $FS_2$) must be identified for interpolation. The second step is to identify whether to use the up bending loading condition or the down bending loading condition. If the cover is on the upper surface then the up bending condition will cause compression and the down bending will cause tension. It is the opposite for the lower covers. Thus, the equations for the axial compression

loads and axial tension loads are listed below.

Upper Cover

$$N_{x\ tension} = \frac{(FS_c - FS_2)(P_1^{[up]} - P_1^{[up]})}{FS_2 - FS_1)} + P_1^{[up]}$$

$$N_{x\ comp} = \frac{(FS_c - FS_2)(P_1^{[down]} - P_1^{[down]})}{FS_2 - FS_1)} + P_1^{[down]}$$

Lower Cover

$$N_{x\ tension} = \frac{(FS_c - FS_2)(P_1^{[down]} - P_1^{[down]})}{FS_2 - FS_1)} + P_1^{[down]}$$

$$N_{x\ comp} = \frac{(FS_c - FS_2)(P_1^{[up]} - P_1^{[up]})}{(FS_2 - FS_1)} + P_1^{[up]}$$

The cover analysis also requires the shear flow through the cover skin ($N_{xy\ comp}$). The cover skin shear flow is based upon the shear flow results ($q_i$) from the torque box analysis. The beginning and end of the shear panels used in the shear flow analysis do not line up with the beginning and end of the covers. Thus, the cover skin shear flow is the average of the two shear flows ($q_1$ and $q_2$) in the panels on either side of the stringer location on the cross-section. If the stringer is on the outer portion of the cross-section, then one of the shear flows will be the shear flow through the front spar web or the rear spar web. This logic is handled automatically by SPANDSET. Additionally, the shear flow is based on tension only; thus, either the up bending or down bending case must be used based upon whether the cover is on the upper surface or the lower surface. The cover analysis uses the magnitude of the shear flow, thus the absolute value of the average is used. The equation for the cover skin shear flow is

listed below.

$$\underline{\text{Upper Cover}}$$

$$N_{xy\ tension} = \frac{\left|q_1^{[down]}\right| + \left|q_2^{[down]}\right|}{2}$$

$$\underline{\text{Lower Cover}}$$

$$N_{xy\ tension} = \frac{\left|q_1^{[up]}\right| + \left|q_2^{[up]}\right|}{2} \tag{68}$$

### 7.2.2 Objective Function Calculation

The objective function for the cover analysis is the weight of the cover per unit area. The objective function for the stiffened cover sizing problem is shown in Equation 58, and the objective function for the unstiffened cover is shown in Equation 62. The weight per unit area is estimated by calculating the weight of a section of the cover normal to the stringer and dividing it by the length of the cover ($L_{cover}$). The weight of the section normal to the stringer is estimated by multiplying the area of the feature by the density of the material selected for that feature.

$$W_{skin} = t_{skin} L_{cover} \rho_{skin} \tag{69}$$

The portion of the weight due to the skin is shown in Equation 69. The area of the skin is the skin thickness multiplied by the length of the cover.

$$W_{stiff} = A_{stiff} \rho_{stiff} \tag{70}$$

$$A_{stiff} = b_{cap} t_{cap} + b_{base} t_{base} + (h - t_{cap} - t_{base}) t_w \tag{71}$$

The area of the stiffener calculated using the stiffener dimensions and Equation 71.

### 7.2.3 Constraints

The dimension constraints are listed in Equation 59. These constraints are the result of work at Triumph Aerostructures based on designer knowledge, manufacturing

requirements, and experience [180].

Additionally, there are several margin of safety constraints applied to the sizing optimization problem (Equation 60 and Equation 64). There are seven margins of safety constraints in total. Five are applied to stiffened covers and two are applied to the un-stiffened covers. Each is described in detail below.

#### *7.2.3.1 M.S. Section Crippling*

The margin of safety of section crippling sizes the stiffened cover to resist crippling under compression loads. The applied load that causes crippling for the segment is the compression axial load ($N_{x\ comp}$) multiplied by the stringer spacing ($b$). The effective section crippling load ($P_{cc}$) is the load at which point the structure will experience the crippling failure mode (see Chapter 3). Thus, the equation below is the equation for the margin of safety of section crippling.

$$\text{M.S. Section Crippling} = \frac{F_{cc}}{N_{x\ comp}\ b} - 1$$

The effective section crippling load is calculated by summing up the crippling loads of each section of the cover [153]. The sections of the cover are the straight segments of the stringer (i.e. stiffener cap, stiffener web, stiffener base) as well as the effective portion of the skin (with effective skin width $b_{eff}$) that also resists the compression load. The section crippling loads are multiplied by the area and summed up as shown in Equation 72.

$$F_{cc} = F_{cc,cap}\ A_{cap} + F_{cc,base}\ A_{base} + F_{cc,web}\ A_{web} + F_{cc,string}\ b_{eff}\ t_{skin} \tag{72}$$

The areas from equation 72 are shown in Equation 73.

$$A_{cap} = b_{cap}\ t_{cap} \qquad A_{base} = b_{base}\ t_{base} \qquad A_{web} = (h - t_{base} - tcap)\ t_{web} \tag{73}$$

The effective crippling load for the skin segment is assumed to be equal to the crippling load of the entire stringer. The crippling loads for the other segments are the minimum

of the compressive crippling yield load or the McCombs' crippling equation (Equation 14) and are shown in Equation 74.

$$F_{cc,cap} = min\left(F_{cy},\ (C_{1,cap})F_{cy}\left[\frac{F_{cy}}{E}\left(\frac{(b_{cap} - 0.5t_{web})}{t_{cap}}\right)^2\right]^{C_{2,cap}}\right) \tag{74}$$

$$F_{cc,base} = min\left(F_{cy},\ (C_{1,base})F_{cy}\left[\frac{F_{cy}}{E}\left(\frac{(b_{base} - 0.5t_{web})}{t_{base}}\right)^2\right]^{C_{2,web}}\right)$$

$$F_{cc,web} = min\left(F_{cy},\ (C_{1,web})F_{cy}\left[\frac{F_{cy}}{E}\left(\frac{h}{t_{web}}\right)^2\right]^{C_{2,web}}\right)$$

$$F_{cc,string} = \frac{F_{cc,cap}\ A_{cap} + F_{cc,base}\ A_{base} + F_{cc,web}\ A_{web}}{A_{cap} + A_{base} + A_{web}}$$

*7.2.3.2 M.S. Damage Tolerance*

$$\text{M.S. Damage Tolerance} = \frac{\sigma_{DT}}{b\ (N_xDT)/(A_{stiff} + b\ t_{skin})} - 1$$

The margin of safety for damage tolerance is a measure of the amount of tension load the stiffened cover can withstand before it is weakened by defects. As discussed in Chapter 2, there is no defined theory for damage tolerance so a damage tolerance stress cutoff ($\sigma_{DT}$) is specified based on designer experience. The applied load for damage tolerance is the axial tension load ($N_xDT = N_{xtension}$) divided by the stiffener area (Equation 71) and the skin area. Thus the margin of safety for the damage tolerance of the stiffened cover is presented below.

*7.2.3.3 M.S. Skin Compression + Shear Buckling*

$$\text{M.S. Skin Compression + Shear Buckling} = 2\left[n\ R_c + \sqrt{\left(n\ R_c\right)^2 + 4\ \left(n\ R_s\right)^2}\right]^{-1} - 1$$

A common form of the margin of safety for the buckling of a flat plat under combined shear and buckling form is given in Equation 75 [34].

$$\text{M.S.} = \frac{2}{R_L + \sqrt{\left(R_L\right)^2 + 4\ \left(R_S\right)^2}} - 1 \tag{75}$$

In Equation 75, $R_L$ is a ratio of the applied compression stress to the compression stress for buckling, and $R_S$ is the ratio of the applied shear stress to the shear stress for buckling.

The margin of safety of skin compression + shear buckling uses Equation 75 as a reference but makes some modifications; thus, it is a function of the compression ratio ($R_c$), the skin shear ratio ($R_s$), and a buckling load factor ($n$). These ratios capture the ability of the skin panel to resist buckling under the compression and shear respectively (Equation 76).

$$R_c = \frac{N_x}{N_{x\ cr}} \qquad\qquad R_s = \frac{N_{xy}}{N_{xy\ cr}} \tag{76}$$

The applied loads that result in buckling are the compression load ($N_x$) and shear load ($N_{xy}$). The loads at which point the structure experiences buckling are the compression critical load ($N_{x\ cr}$) and the shear critical load ($N_{xy\ cr}$). Solving for the compression critical load is an iterative process that uses the material properties ($E,\ F_{tu},\ F_{cy}$), the part dimensions ($t_{skin},\ W_{panel}$), a user specified buckling coefficient ($k$), and the Ramberg-Osgood parameter ($n_R$) [153]. The shear critical load is the minimum of the shear buckling stress, calculated from the material and geometry of the structure, or the shear yield stress, calculated from the material property.

$$\begin{aligned} N_{x\ cr} &= \text{Panel\_Buckling}\big(k,\ E,\ F_{tu},\ F_{cy},\ n_R, t_{skin},\ W_{panel}\big)\ t_{skin} \\ N_{xy\ cr} &= min\left(\frac{F_{cy}}{\sqrt{3}}\ ,\ 4.9\ E\left(\frac{t_{skin}}{W_{panel}}\right)^2\right)\ t_{skin} \end{aligned} \tag{77}$$

#### *7.2.3.4 M.S. Column Stability Johnson-Euler*

$$\text{M.S. Column Stability Johnson} = \frac{F_c}{N_x\ b_s} - 1$$

The margin of safety for column stability Johnson-Euler measures the ability of the stiffener to resist column buckling failure due to the compression load. The applied load for the margin is the compression load ($N_X$) and is divided by the length of the

stiffener which is estimated to be the stringer spacing ($b_s$). The allowable stress ($F_c$) is calculated using either Euler buckling theory or Johnson buckling theory depending upon the slenderness ratio ($L/\rho$). The slenderness ratio is a geometric property of the stringer calculated by Equation 78.

$$L/\rho = \frac{L_{panel}}{\sqrt{I/A}} \tag{78}$$

It has been shown through experimentation [153] that if the slenderness ratio exceeds a critical value then the buckling behavior deviates from Euler buckling theory to Johnson buckling theory. The critical slenderness ratio is calculated with Equation 79 using the crippling stress calculated for a previous margin of safety (Equation 72).

$$(L/\rho)_{crit} = \sqrt{\frac{2\ \pi^2 E}{F_{cc}}} \tag{79}$$

The allowable stress according to Johnson buckling theory is calculated using Equation 80. The allowable stress according to Euler buckling theory is calculated with Equation 81.

$$F_{Johnson} = F_{cc} - \left(\frac{F_{cc}^2}{E}\frac{(L/\rho)^2}{4\ \pi^2}\right) \tag{80}$$

$$F_{Euler} = \frac{\pi^2\ EI}{(L/\rho)^2} \tag{81}$$

*7.2.3.5 M.S. Euler-Johnson + Shear Interaction*

$$\text{M.S. Euler-Johnson + Shear Interaction} = 2\left[R_c + \sqrt{\left(R_c\right)^2 + 4\ \left(R_s\right)^2}\right]^{-1} - 1$$

The margin of safety for the Euler-Johnson and Shear Interaction measures the stiffened covers ability to resist buckling under both shear and compression. The margin of safety is based off of the buckling of a flat plate under compression and shear (Equation 75); thus, it is a function of both the cover compression ratio ($R_c$) and the cover shear ratio ($R_s$). The compression ratio is based on the applied compression

stress ($f_c$) and the allowable compression stress ($F_c$). The shear ratio is based on the applied shear load ($N_xy$) and the allowable shear load ($N_{xy\ allow}$).

$$R_c = \frac{f_c}{F_c} \qquad\qquad R_s = \frac{N_{xy}}{N_{xy\ allow}} \tag{82}$$

The applied compression force is the compression load ($N_x$) multiplied by the length of the section which is assumed to be the stringer spacing ($b_s$). To get the applied stress the applied force is divided by the segment area.

$$f_c = \frac{|N_x\ b_s|}{A_{seg}} \tag{83}$$

The allowable compression stress uses the same logic for the buckling as the previous margin of safety (either Equation 81 or Equation 80). The allowable shear stress is calculated using the material properties and the skin thickness.

*7.2.3.6 M.S. Durability and Damage Tolerance*

$$\text{M.S. Damage Tolerance} = \frac{\sigma_{DT}}{(N_{xtension})/(t_{skin})} - 1$$

The margin of safety for durability and damage tolerance (DADT) is a measure of the amount of tension load the un-stiffened cover can withstand before it is weakened by defects. The margin of safety for DADT of the un-stiffened cover is the same as the margin of safety for damage tolerance of the stiffened cover except there is no stiffener area. Also, the unstiffened and stiffened covers have their own individual values for the damage tolerance stress cutoffs ($\sigma_{DT}$). The applied load is the axial tension load ($N_{xtension}$) and is divided by the skin thickness to get the applied stress. Thus the margin of safety for DADT of the un-stiffened cover is presented below.

*7.2.3.7 M.S. Skin Buckling*

$$\text{M.S. Skin Buckling} = 2\left[n\ R_c + \sqrt{\left(n\ R_c\right)^2 + 4\left(\left(n\ R_s\right)^2\right)}\right]^{-1} - 1$$

The margin of safety is the same as the margin of safety of the skin compression + shear buckling for the stiffened panel. The margin of safety of skin buckling for the unstiffened cover is a function of both the skin compression ratio ($R_c$) and the skin shear ratio ($R_s$) as well as a buckling load factor ($n$). These ratios capture the ability of the skin panel to resist buckling under the compression and shear respectively (Equation 84). The applied loads are the compression load and shear load divided by the skin thickness and effective skin thickness ($t_{eff}$) (Equation 85).

$$R_c = \frac{f_c}{F_c} \qquad R_s = \frac{f_s}{F_s} \tag{84}$$

$$f_c = \frac{|N_x|}{t_{eff}} \qquad f_s = \frac{N_{xy}}{t_s} \tag{85}$$

The compression and shear buckling critical loads (Equation 86) are based off the geometry and material properties of the structure. The shear critical load chooses the minimum of either the shear buckling stress of the shear yield stress.

$$\begin{aligned} F_c &= \text{Panel\_Buckling}\big(k,\ E,\ F_{tu},\ F_{cy},\ n, t_{eff},\ W_{panel}\big) \\ F_s &= min\left(\frac{F_{cy}}{\sqrt{3}}\ ,\ 4.9\ E\left(\frac{t_s}{W_{panel}}\right)^2\right) \end{aligned} \tag{86}$$

### 7.2.4 Outputs

The cover analysis routine has three outputs: the sized part dimensions, the weight per unit area of the cover, and the part geometries used by the torque box analysis during the next iteration. The weight per unit area is the final value of the objective function and the part dimensions are the final values of the design variables. The part geometries required by the torque box analysis are the segment areas of the cover segment ($A_{seg}$), the location of the centroid from the surface OML ($\bar{y}$), and the cover skin thickness ($t_{skin}$). The segment areas of the stiffened covers are calculated during the cover analysis using Equation 73 recreated below and the skin panel segment area. The segment areas of the unstiffened covers includes only the skin panel segment area

$(t_{skin}L_{cover})$.

$$A_{seg} = A_{base} + A_{web} + A_{cap} + A_{skin}$$

$$A_{cap} = b_{cap}t_{cap} \qquad A_{base} = b_{base}t_{base}$$

$$A_{web} = (h - t_{cap} - t_{base})t_w \quad A_{skin} = L_{cover}t_{skin}$$

The locations of the centroids are also calculated during the cover analysis using the Equations below.

$$\bar{y} = \frac{E_{string}\left[A_{base}\bar{y}_{base} + A_{web}\bar{y}_{web} + A_{cap}\bar{y}_{cap}\right] + E_{skin}A_{skin}\frac{t_{skin}}{2}}{E_{string}\left[A_{base} + A_{web} + A_{cap}\right] + E_{skin}A_{skin}}$$

$$\bar{y}_{base} = t_{skin} + \frac{t_{base}}{2}$$

$$\bar{y}_{web} = t_{skin} + h - t_{cap} - \frac{(h - t_{cap} - t_{base})}{2}$$

$$\bar{y}_{cap} = t_{skin} + h - \frac{t_{cap}}{2}$$

The skin thickness is a design variable in the optimization problem; thus, no additional calculations are needed.

## 7.3 Spar Segment Sizing

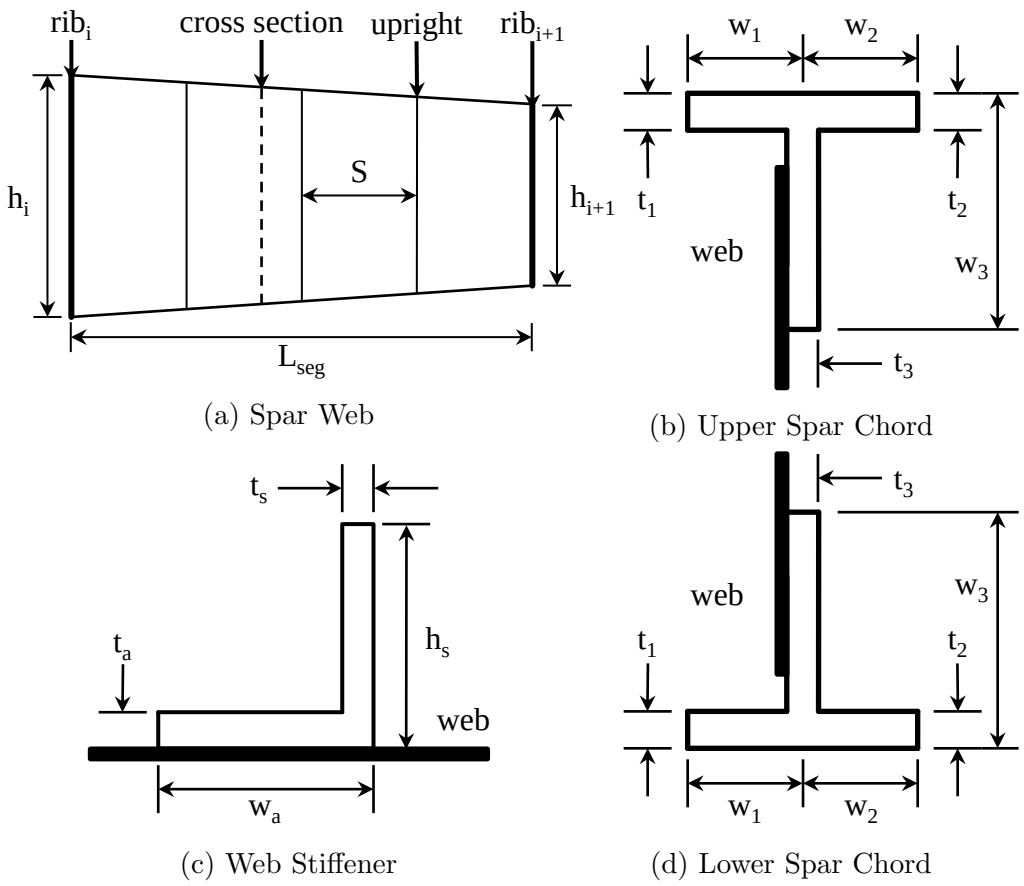


Figure 69: Spar Features

The spars are assumed to be web stiffened design. The spar features are the web, web stiffeners and rib posts, an upper spar cap, and a lower spar cap. These features are depicted in Figure 69. The web stiffeners are assumed to be a blade-section configuration. For simplicity the rib posts, which are responsible for attaching the ribs to the spars, are treated as web stiffeners by the spar analysis. The spar chords are T-section extrusions.

The spars are unique because each spar can span the entire wing. This means that the spar is subjected to very different loads at the root than at the tip. In terms of sizing the spar this means that the dimensions at the root should be different than at the tip. SPANDSET addresses this by sizing individual segments of the spar.

The segments are defined as the length of the spar between two ribs. Additionally, SPANDSET does not size every segments. Instead it uses the spar segments that intersect with the cross-sections to perform sizing on. In Figure 69a the cross-section is marked by the dotted line. It intersect the spar between $\text{rib}_i$ and $\text{rib}_{i+1}$. The portion of the spar between these ribs will be analyzed by the spar analysis routine. The results from the sized spar segments will be used to estimate the weight of the entire spar using interpolation.

Minimize:

$$F(\bar{X}) = \frac{W_{web} + W_{upright} + W_{lowerchord} + W_{upperchord}}{L_{seg}} \tag{87}$$

Subject to:

| Web & Stiffners | Cap (upper/lower) |
|---|---|
| $0.5 \geq t_{web} \geq 0.04$ | $1.6 \geq w_1 \geq 0.6$ |
| $0.8 \geq w_a \geq 0.6$ | $0.5 \geq t_1 \geq 0.06$ |
| $0.25 \geq t_a \geq 0.04$ | $w_1 \geq w_3 \geq 0.5w_1$ |
| $1.1 \geq h_s \geq 0.35$ | $1.1t_1 \geq t_3 \geq 0.5t_1$ |
| $1.25t_a \geq t_s \geq 0.75t_a$ | $w_2 = w_1 \quad t_2 = t_1$ |

(88)

| Web & Stiffeners | Cap (upper/lower) |
|---|---|
| M.S. Shear Rupture $\geq 0$ | M.S. Crippling $\geq 0$ |
| M.S. Force Crippling (Shear) $\geq 0$ | M.S. Durability and Damage Tolerance $\geq 0$ |
| M.S. Crippling Cutoff $\geq 0$ | M.S. Max Compression $\geq 0$ |
| M.S. Upright Column $\geq 0$ | M.S. Column Buckling $\geq 0$ |
| M.S. $\text{I}_{required} \geq 0$ | |

(89)

Where:

$$\bar{X} = \left\{ t_{web},\ h_s,\ t_s,\ w_a,\ t_a,\ [w_1,\ t_1,\ w_3,\ t_3]_{upper/lower} \right\} \tag{90}$$

The spar analysis routine uses numerical optimization to solve the optimization problem depicted above. The objective function (Equation 87) is minimized using the dimensions of the features (Figure 69) as the design variables (Equation 90) subjected

to the constraints (Equation 88 and Equation 89). In Equation 90 there are two sets of cap dimensions for the upper cap ($[w_1,\ t_1,\ w_3,\ t_3]_{upper}$) and the lower cap ($[w_1,\ t_1,\ w_3,\ t_3]_{lower}$). Additionally, to simplify the caps the two flanges are assumed to be symmetric ($w_2 = w_1$ and $t_2 = t_1$). All the units of length are in inches.

### 7.3.1 Inputs

Each analysis routine requires three sets of inputs beyond the design variables: the material properties for each feature, geometric information from the configuration, and the internal loads calculated from the torque box analysis.

#### *7.3.1.1 Material Properties*

The material properties required by SPANDSET are listed in Table 12. Not all of these properties are required for each feature. The material properties that are required for the spar analysis are: The Young's modulus ($E$) for the web, stiffeners, upper chord, and lower chord; and shear modulus ($G$) for the web only; the ultimate tensile load ($F_{tu}$) for the web only; the compression yield load ($F_{cy}$) for the stiffeners, upper chord, and lower chord; and the density ($\rho$) for all the features.

#### 7.3.1.2 Configuration Geometry

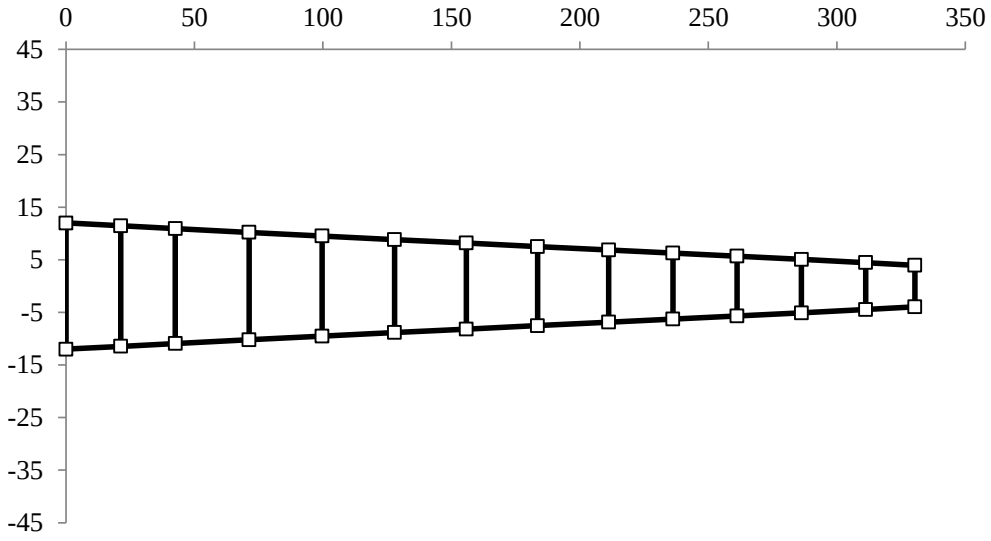


Figure 70: Spar Geometry

After the configuration has been defined the parametric geometry tool calculates the intersection of each spar with the intersection of each rib ($BL_i,\ FS_i$). These intersections define each spar segment. The length of each spar segment is calculated using Equation

$$L_{seg} = \sqrt{(BL_{i+1} - BL_i)^2 + (FS_{i+1} - FS_i)^2} \tag{91}$$

For each ($BL_i,\ FS_i$) the intersection of the spar with the upper surface and lower surface is calculated. These points are shown in Figure 70. The difference in these points (Equation 92) is the height of the intersection with the rib and spar ($h_i$) as depicted in Figure 69a.

$$h_i = WL_{upper}(BL_i,\ FS_i) - WL_{lower}(BL_i,\ FS_i) \tag{92}$$

The values $L_{seg}$ and $h_i$ are calculated across each spar because they are required for the weight estimation.

There are two additional values for the spar segments required by the spar analysis routine that are not required for the weight estimation. The first value is the average

height of the spar segment ($h_{avg}$). The top and bottom surfaces of the spar web are assumed to be close enough to linear that the average height of the spar segment is the average of $h_i$ and $h_{i+1}$. The second value is the spacing between the spar web stiffeners ($S$). The stiffener spacing is calculated in Equation 93 using the spar segment length ($L_{seg}$) and the number of stiffeners ($n$).

$$S = \frac{L_{seg}}{n} \tag{93}$$

The value of n depends upon the ribs that define the spar segment. The user defines two values for the number of spar stiffeners: one for the stub ribs and one for the main ribs. If the two ribs that define the spar segment are both stub ribs then the value of $n$ used is the first value specified by the user; otherwise, it is the second value. The reason two values are defined is because there are two different spacings defined for the stub ribs and the main ribs. If one is significantly larger than the other then the user can make sure that too many or too few spar stiffeners aren't created.

#### *7.3.1.3 Internal Loads and Stiffness*

The spar analysis routine required the ultimate shear flow ($q_{ult}$) to size the spar web. The ultimate shear flow is the resulting superimposed shear flow (closed cell shear flows and open section shear flows) for the specific spar web. This value is calculated in the shear flow analysis portion of the torque box analysis and no further calculations are needed.

The spar analysis routine requires three loads to size the upper spar cap and lower spar cap: the ultimate compression load ($P_{ult\ comp}$), ultimate tension load ($P_{ult\ tension}$), and the reference tension load ($P_{ref\ tension}$). The values for these three variables will be different for each spar cap due to the different loading cases. For the upper cap, the up bending load condition results in compression loads and the down bending load condition results in tension loads. Thus, for the upper cap the ultimate compression load is the corresponding nodal segment load from the up bending case, while the

ultimate tension load is the corresponding nodal segment load from the down bending case.

| Upper Cap | Lower Cap | |
|---|---|---|
| $P_{ult\ comp} = P_{seg}^{[up]}$ | $P_{ult\ comp} = P_{seg}^{[down]}$ | (94) |
| $P_{ult\ tension} = P_{seg}^{[down]}$ | $P_{ult\ tension} = P_{seg}^{[up]}$ | (95) |

The reference tension load is equal to the ultimate tension load for both the upper and lower cap ($P_{ref\ tension} = P_{ult\ tension}$).

### 7.3.2 Objective Function Calculation

The objective function for the spar analysis is the weight of the spar segment per unit length and is shown in Equation 87. The equation sums up the weights of the components and then divides the result by the length of the spar segment. The equations for each component of the weight are shown in Equation 96 and Equation 99. Each equation approximates the volume of each feature and multiplies the volume by the density of the material assigned to the feature.

$$W_{web} = h_c(2 + L_{seg}/S)A_{upright}\rho_{stiff} + A_{web}t_{web}\rho_{web} \tag{96}$$

$$A_{web} = H_{spar}L_{seg} \tag{97}$$

$$A_{upright} = w_a t_a + (h_s - t_a)t_s \tag{98}$$

The web component of the spar segment weight is shown in Equation 96. The equation sums the weight of the web, the web stiffeners, and the posts responsible for attaching the ribs to the spar. The web weight is the area of the web (Equation 97) multiplied by the thickness and the density. The weight of the stiffeners and posts are calculated by multiplying the area of the upright (Equation 98), the average segment height ($h_c$), and an estimate for the number of stiffeners and posts. The number of stiffeners is estimated by dividing the length of the spar segment ($L_{spar}$) by the upright spacing

($S$). There are two posts that are added to the number of stiffeners since the posts are treated the same as the uprights.

$$W_{chord} = A_{chord} L_{seg} \rho_{chord} \tag{99}$$

$$A_{chord} = w_1 t_1 + w_2 t_2 + (w_3 - t_1) t_3 \tag{100}$$

Equation 99 shows how the weight is calculated for each chord. The area of the chord is calculated from the dimensions (Equation 100) and multiplied by the length of the spar segment ($L_{seg}$) and the density. The dimensions of the upper chord can vary from the dimensions of the lower chord. Therefore Equation 99 must be used to calculate the upper chord weight and lower chord weight individually.

### 7.3.3 Constraints

The dimension constraints are listed in Equation 88. These constraints are the result of work at Triumph Aerostructure based on designer knowledge, manufacturing requirements, and experience [180].

#### *7.3.3.1 M.S. Shear Rupture*

$$\text{M.S. Shear Rupture} = \frac{F_s}{f_{s\ max}} - 1$$

The spar webs are large panels subjected to shear loading. One of the possible modes of failure is rupture due to the diagonal tension loads caused by the shear stress. The margin of safety for shear rupture is measures the ability of the structure to resist the rupture failure mode. The margin of safety is calculated using the allowable shear stress ($F_s$) and the corrected maximum web shear stress ($f_{s\ max}$). The diagonal tension due to shear is calculated based upon a curve fitting equation using the diagonal tension factor ($k_{dt}$). The diagonal tension factor is calculated using two other values: the corrected shear stress ($f_s$) and the critical shear buckling stress for the web ($F_{scr}$). The corrected shear stress calculates the applied stress over the web ($q_{ult}/t_{web}$) and

corrects it for the difference in the height measured by the geometry tool ($h$) and the actual web height ($h_c = h - \bar{y}_{cap}^{[u]} - \bar{y}_{cap}^{[l]}$).

$$f_s = \frac{q_{ult}}{t_{web}} \frac{h}{h_c} \tag{101}$$

The critical shear buckling stress is calculated based on elastic theory using: the Young's modulus ($E$), the web thickness ($t_{web}$), the upright spacing ($s$), and a correction factor ($K_s$) measured from empirical data.

$$F_{scr} = K_s^2 \; E\Big(\frac{t_{web}}{s}\Big)^2 \tag{102}$$

After the corrected shear stress and critical shear stress are calculate the value for the diagonal tension factor can be calculated using Equation 103.

$$k_{dt} = \tanh\Big[0.5 \; \log \frac{f_s}{F_{scr}}\Big] \tag{103}$$

However, if the corrected shear stress is greater than the critical shear buckling then the diagonal tension factor is zero ($k_{dt} = 0$). The allowable web shear stress is calculated by multiplying the material ultimate tension load by a curve fit (with coefficients $a_3$, $a_2$, $a_1$, $a_0$) based on the diagonal tension factor.

$$F_s = F_{tu}\Big[a_3 k_{dt}^3 + a_2 k_{dt}^2 + a_1 k_{dt} + a_0\Big] \tag{104}$$

The corrected maximum shear stress is a function of: the applied load divided by the web thickness ($q_{ult}/t_{web}$) corrected for the difference in the height measured by the geometry tool ($h$) and the actual web height ($h_c = h - \bar{y}_{cap}^{[u]} - \bar{y}_{cap}^{[l]}$), the diagonal tensor factor, and a correction factor ($C_1$) measured from empirical data.

$$f_{s\ max} = \frac{q_{ult}}{t_{web}} \frac{h}{h_c}\Big(1 + k_{dt} \; C_1\Big) \tag{105}$$

*7.3.3.2 M.S. Force Crippling (Shear)*

$$\text{M.S. Force Crippling (Shear)} = \frac{F_c}{f_{c\ max}} - 1$$

The margin of safety for force crippling measures the spar web uprights ability to resist forced crippling due to the diagonal tension load that results from the applied shear load. The margin of safety is calculated using the upright forced allowable crippling stress ($F_c$) and the peak upright compression stress ($f_{c\ max}$).

The calculation of the peak upright compression stress uses the effective area of the upright ($A_{eff}$). The effective area of the upright accounts for the eccentricity of the upright loading when the upright is attached to one side of the web.

$$A_{eff} = \frac{A_{upright}}{1 + \left[\frac{\bar{y}_{upright} + 0.5\ t_{web}}{\sqrt{I_{upright}/A_{upright}}}\right]^2} \tag{106}$$

The upright compression stress due to the diagonal tension is calculated in the equation below using the effective area, web thickness, upright spacing, and the previously calculated diagonal tension factor (Equation 103).

$$f_c = \frac{k_{dt}\ f_s\ t_{web}\ s}{A_{eff} + 0.5\ t_{web}\ s\ (1 - k_{dt})} \tag{107}$$

The peak upright compression stress is then estimated using a semi-empirical relationship and the diagonal tension factor.

$$f_{c\ max} = f_c\left[\frac{s}{h}(a_1\ k_{dt} - a_0) + b_1 - b_2\ k_{dt}\right] \tag{108}$$

The upright forced allowable crippling stress is estimated using a semi-empirical relationship between the geometry, material properties, and the diagonal tension factor.

$$F_c = min\left(a_1\ E\ F_{cy}^4\ k_{dt}^{2/3}\ \frac{t_a}{t_{web}}^{1/3},\ b_1\ E\ F_{cy}^{2/5}\right) \tag{109}$$

#### *7.3.3.3 M.S. Crippling Cutoff*

$$\text{M.S. Crippling Cutoff} = \frac{F_{cc}}{f_c} - 1$$

The margin of safety for crippling cutoff measures the spar webs uprights ability to resist conventional crippling due to the diagonal tension load that results from the applied shear load. The margin of safety is calculated using the upright allowable crippling stress ($F_{cc}$) and upright compression stress ($f_c$).

The allowable crippling stress is calculated by breaking the upright into three straight segments (cap, web, and base) and calculating the crippling stress for each segment based off McCombs' crippling equation (Equation 14) respectively.

$$F_{cc\ base} = min\left( (C_{1,base})\ F_{cy} \left[ \frac{F_{cy}}{E} \left( \frac{(w_a - 0.5\ t_s)}{t_s} \right)^2 \right]^{-C_{2,base}},\ F_{cy} \right) \tag{110}$$

$$F_{cc\ web} = min\left( (C_{1,web})\ F_{cy} \left[ \frac{F_{cy}}{E} \left( \frac{(h_s - 0.5\ t_a)}{t_s} \right)^2 \right]^{-C_{2,web}},\ F_{cy} \right) \tag{111}$$

The total allowable crippling stress is calculated by dividing the area weighted crippling stresses by the sum of the areas.

$$F_{cc} = \frac{w_a\ t_a\ F_{cc\ base} + h_s\ t_s\ F_{cc\ web}}{w_a\ t_a + h_s\ t_s} \tag{112}$$

The margin of safety for crippling cutoff uses the upright compression stress previously calculated in Equation 107.

#### *7.3.3.4 M.S. Upright Column*

$$\text{M.S. Upright Column} = \frac{F_c}{f_c} - 1$$

The margin of safety for the upright column measures the ability of the spar web upright to resist column buckling failure due to the diagonal tension applied to the spar webs. The margin of safety is calculated using the Euler-Johnson critical load ($F_c$) and the upright compression stress ($f_c$) previously calculated in Equation 107.

Either Euler buckling theory or Johnson buckling theory is used to determine the critical load. The slenderness ratio ($L/\rho$) is used to select which theory will be used. The slenderness ratio is calculated using the upright height ($h$), the area of the upright (Equation 98), and the moment of inertia of the upright.

$$(L/\rho) = \frac{h}{\sqrt{I_{upright}/A_{upright}}} \tag{113}$$

The slenderness ratio is compared against a critical slenderness ratio ($(L/\rho)_{crit}$).

$$(L/\rho)_{crit} = \frac{2\ \pi^2\ E}{F_{cc\ column}} \tag{114}$$

The crippling stress used to calculate the critical slenderness ratio is the column crippling stress which is calculated using the crippling stress from Equation 112 ($F_{cc}$) and the equation below.

$$F_{cc\ column} = F_{cc}\left(1 + \frac{4\ F_{cc}}{E}\right) \tag{115}$$

If the slenderness ratio exceeds the critical value then Johnson buckling theory is used to calculate the critical load. Otherwise, Euler buckling theory is used to calculate the buckling load. The allowable stress according to Euler buckling theory is calculated with Equation 81. The critical load according to Johnson buckling theory is calculated using Equation 80. The crippling stress used in Equation 80 is the column crippling stress.

#### *7.3.3.5 M.S. Moment of Inertia Required*

$$\text{M.S. I}_{required} = \frac{I_{upright}}{I_{req}} - 1$$

The spar upright is sized relative to the requirement that it possess sufficient stiffness to act as a panel breaker for shear web buckling. This leads to a moment of inertia requirement for the spar upright. The margin of safety is calculated using the moment of inertia of the spar upright ($I_{upright}$) and the required moment of inertia

($I_{req}$). The moment of inertia is calculated using the moment of inertia of each portion of the upright (base, web) and the parallel axis theorem.

$$I_{upright} = \frac{w_a\ t_a^3}{12} + \frac{t_s\ (h_s - t_a)^3}{12} + w_a\ t_a(\bar{y} - 0.5\ t_a)^2 + t_s(h_s - t_a)(0.5\ h_s - \bar{y})^2 \quad (116)$$

$$\bar{y} = \frac{0.5\ w_a\ t_a^2 + t_s(h_s - t_a)(\frac{h_s - t_a}{2} + t_a)}{A_{upright}} \quad (117)$$

The moment of inertia required is based on a semi-empirical relationship based upon the material properties of the web and uprights as well as the height of the spar ($h$), the upright spacing ($s$), and the web thickness ($t_{web}$).

$$I_{req} = h t_{web}^3 \frac{E_{web}}{E_{upright}} \left[ a_1 \left(\frac{s}{h}\right)^6 - a_2 \left(\frac{s}{h}\right)^5 + a_3 \left(\frac{s}{h}\right)^4 - a_4 \left(\frac{s}{h}\right)^3 + a_5 \left(\frac{s}{h}\right)^2 - a_6 \left(\frac{s}{h}\right) + a_7 \right]$$

#### *7.3.3.6 M.S. Crippling*

$$\text{M.S. Crippling} = \frac{F_{cc\ total}^{[u/l]}}{\left| f_{c\ total}^{[u/l]} \right|} - 1$$

The margin of safety of crippling measures the ability of the upper and lower spar caps to avoid the crippling failure mode under the total compression load due to the wing bending and spar web diagonal tension load. The upper and lower spar chords are not assumed to be symmetric; therefore, the margin of safety needs to be assessed for both the upper and lower spar. The margin of safety is calculated using the total allowable crippling stress ($F_{cc\ total}^{[u/l]}$) and the total compression stress ($f_c^{[u/l]}$) due to the wing bending and the diagonal tension of the spar web.

The total allowable crippling stress is calculated by summing up the area weighted crippling stresses of the straight segments that make up the spar chords (flange 1, flange 2, and vertical flange) based off McCombs' equation (Equation 14) and dividing

them by the total chord area (Equation 100).

$$F_{cc\ f1}^{[u/l]} = min\left( (C_{1,f1})\ F_{cy} \left[ \frac{F_{cy}}{E} \left( \frac{w_1^{[u/l]} - 0.5\ t_3^{[u/l]}}{t_1^{[u/l]}} \right)^2 \right]^{-C_{2,f1}},\ F_{cy} \right) \tag{118}$$

$$F_{cc\ f2}^{[u/l]} = min\left( (C_{1,f2})\ F_{cy} \left[ \frac{F_{cy}}{E} \left( \frac{w_2^{[u/l]} - 0.5\ t_3^{[u/l]}}{t_2^{[u/l]}} \right)^2 \right]^{-C_{2,f2}},\ F_{cy} \right) \tag{119}$$

$$F_{cc\ vf}^{[u/l]} = min\left( (C_{1,vf})\ F_{cy} \left[ \frac{F_{cy}}{E} \left( \frac{w_3^{[u/l]} - 0.5\ t_1^{[u/l]}}{t_3^{[u/l]}} \right)^2 \right]^{-C_{1,vf}},\ F_{cy} \right) \tag{120}$$

$$F_{cc\ total}^{[u/l]} = \left[ \frac{t_1\ (w_1 - 0.5\ t_3)\ F_{cc\ f1} + (w_2 - 0.5\ t_3)\ t_2\ F_{cc\ f2} + (w_3 - 0.5\ t_1)\ t_3\ F_{cc\ vf}}{A_{chord}} \right]^{[u/l]} \tag{121}$$

The total compression stress is the axial compression stress due to the wing bending ($f_c$) and the compression stress due to the diagonal torsion ($f_{dt}$). The compression stress due to the wing bending is the axial compression load from the torque box analysis (Equation 94) divided by the chord area.

$$f_c^{[u/l]} = \frac{P_{ult\ comp}^{u/l]}}{A_{chord}^{[u/l]}} \tag{122}$$

The compression stress due to the diagonal torsion is calculated using the shear stress from the torque box analysis ($q_{ult}$) and the previously calculated diagonal tension factor (Equation 103).

$$f_{dt}^{[u/l]} = k_{dt} \left( \frac{q_{ult}^{[u/l]}}{t_{web}} \right) \left( \frac{1.92}{(2\ A_{chord}^{[u/l]}) / (h\ t_{web}) + 0.5(1 - k_{dt})} \right) \tag{123}$$

The final compression load is the sum of the two compression loads.

$$f_{c\ total}^{[u/l]} = f_c^{[u/l]} + f_{dt}^{[u/l]} \tag{124}$$

*7.3.3.7 M.S. Max Compression*

$$\text{M.S. Max Compression} = \frac{F_{cy}}{\left| f_{sb}^{[u/l]} - f_{c\ total}^{[u/l]} \right|}$$

The margin of safety for maximum compression is a measure of the ability of the spar chords to handle the maximum compression load. Although Equation 124 is called the total compression load, there is an additional compression load due to a secondary bending moment ($f_{sb}^{[u/l]}$) induced in the spar chord by the diagonal tension of the spar webs. The margin of safety includes the additional compression loads in the applied stress and uses the material compression yield stress ($F_{cy}$) as the allowable stress. The margin of safety must be applied to both the upper and lower spar chords.

The value of the secondary moment induced by the diagonal tension is calculated using semi-empirical relationships. The moment equation includes the previously calculated diagonal tension factor (Equation 103), the shear load from the torque box analysis ($q_{ult}^{[u/l]}$), the effective length of each web shear panel which is estimated using the upright spacing ($s$), and a constant estimated from empirical data ($C_2$).

$$M_{sec} = \frac{(0.839)\ C_2\ k_{dt}\ q_{ult}\ s^2}{12} \tag{125}$$

The compression stress due to the secondary moment is calculated using elastic theory for beam bending.

$$f_{sb}^{[u/l]} = \frac{M_{sec}\bar{y}^{[u/l]}}{I_{chord}^{[u/l]}} \tag{126}$$

*7.3.3.8 M.S. Column Buckling*

$$\text{M.S. Column Buckling} = \frac{F_c^{[u/l]}}{\left|f_{c\ total}^{[u/l]}\right|} - 1$$

The margin of safety for column buckling measures the ability of the upper and lower spar chord to resist column buckling failure due to the wing bending and the diagonal tension due to the spar web shear. The margin is applied to both the upper chord and lower chord individually. The margin of safety is calculated using the Johnson critical buckling load ($F_c$) and the previously calculated total compression load (Equation 124).

The critical load for the spar cap is calculated using the previously discussed Johnson buckling theory. Equation 80 requires the slenderness ratio and the crippling stress. The slenderness ratio for the spar cap is calculated using the upright spacing ($s$) as the length.

$$(L/\rho) = \frac{s}{\sqrt{I_{chord}^{[u/l]}/A_{chord}^{[u/l]}}} \tag{127}$$

The crippling stress ($F_{cc}^{[u/l]}$) used to calculate the Johnson buckling critical load is estimated from the previously calculated crippling stress (Equation 121).

$$F_{cc}^{[u/l]} = F_{cc\ total}^{[u/l]}\left(1 + \frac{4\ F_{cc\ total}^{[u/l]}}{E}\right) \tag{128}$$

*7.3.3.9 M.S. Durability and Damage Tolerance*

$$\text{M.S. Durability and Damage Tolerance} = \frac{F_{cutoff}^{[u/l]}}{P_{ref\ tension}^{[u/l]}/A_{chord}^{[u/l]}} - 1$$

The margin of safety of durability and damage tolerance (DADT) is applied to the upper and lower spar chords. The upper and lower spar chords are not assumed to be symmetric; therefore, the DADT margin of safety needs to be assessed for both the upper and lower spar. The margin of safety is a measure of the amount of tension load the spar chords can withstand before it is affected by defects. As discussed in Chapter 3, there is no defined theory for damage tolerance so a damage cutoff stress ($F_{cutoff}^{[u/l]}$) is selected for both the upper and lower chord based off empirical data. The applied stress is the applied tension load from the torque box analysis routine (Equation 95) divided by the area of the chord (Equation 100).

### 7.3.4 Outputs

The spar analysis routine has three outputs: the final part dimensions, the weight per unit length of the spar, and the part geometries used by the torque box analysis during the next iteration. The weight per unit length is the final value of the objective

function and the part dimensions are the final values of the design variables. The part geometries required by the torque box analysis are the segment areas of the upper and lower spar chords ($A_{seg}$), the location of the centroid from the surface OML for the upper and lower spar caps ($\bar{y}$), and the spar web thickness ($t_{web}$). The segment areas of the upper and lower spar chords are calculated during the spar analysis using Equation 100 recreated below.

$$A_{seg} = w_1 t_1 + w_2 t_2 + (w_3 - t_1) t_3$$

The locations of the centroids are also calculated during the spar analysis using the equation below.

$$\bar{y} A_{seg} = w_1 t_1 \left( \frac{t_1}{2} \right) + w_2 t_2 \left( \frac{t_2}{2} \right) + (w_1 - t_1) t_3 \left( t_1 + \frac{(w_3 - t_1)}{2} \right)$$

The spar web thickness is a design variable in the optimization problem; thus, no additional calculations are needed.

## 7.4 Rib Sizing

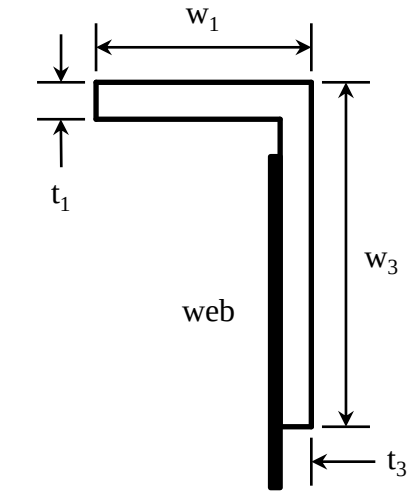


(a) Rib Cap

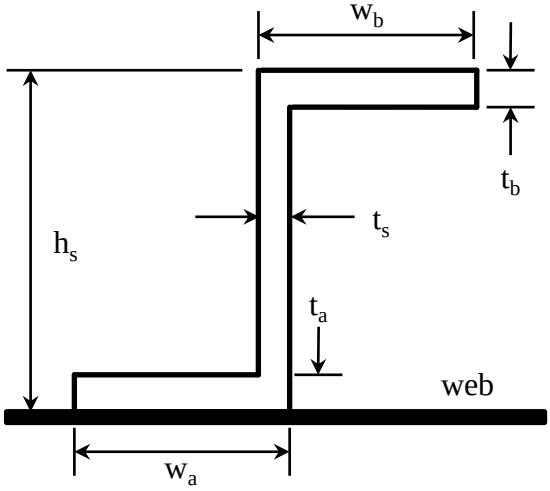


(b) Web Upright

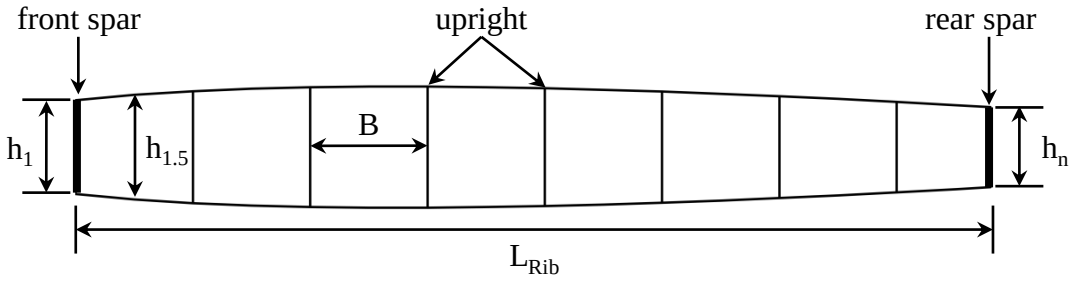


$H_{rib}=\max(\{h_x : x = 1,1.5,\ldots, n\})$

(c) Rib Web

Figure 71: Rib Features

The rib analysis assumes the rib is a web stiffened design. A web stiffened rib has three features: a web, a cap on both the upper and lower surface, and uprights to stiffen the rib web. These features are depicted in Figure 71. The rib serves three primary purposes: hold the cover to the contour, limit the effective length of the column stringers for column stability, and act as a load introduction and distribution structure. These requirements will dictate the margins of safety used to size the rib.

Minimize:

$$F(\bar{X}) = W_{chord} + W_{upright} + W_{web} \tag{129}$$

Subject to:

$$\begin{array}{lll} t_{web} \geq 0.04 & 1.5 \geq h_s \geq 0.5 & 1.5 \geq w_1 \geq 1.0 \\ 1.25t_a \geq t_{web} & 1.0 \geq w_a \geq 0.5 & 0.5 \geq t_1 \geq 0.07 \\ t_{web} \geq 0.75t_a & 1.25t_s \geq t_a \geq 0.05 & 1.5 \geq w_3 \geq 1.0 \\ w_a = w_b & t_a = t_b & 0.5 \geq t_3 \geq t_1 \end{array} \tag{130}$$

$$\begin{array}{l} \text{M.S. Web Upright Column} \geq 0 \\ \text{M.S. } I_{req} \geq 0 \end{array} \tag{131}$$

Where:

$$\bar{X} = \left\{ t_{web},\ h_s,\ t_s,\ w_a,\ t_a,\ w_1,\ t_1,\ w_2,\ t_2 \right\} \tag{132}$$

The rib analysis routine uses numerical optimization to solve the optimization problem depicted above. The objective function (Equation 129) is minimized using the dimensions of the features (Figure 71) as the design variables (Equation 132) subjected to the constraints (Equation 130 and Equation 131). For simplicity the upper cap and lower cap are considered symmetric so that $[w_1,\ t_1,\ w_3,\ t_3]_{lower} = [w_1,\ t_1,\ w_3,\ t_3]_{upper}$. Additionally, all the uprights are assumed to have the same dimensions $[\ h_s,\ t_s,\ w_a,\ t_a]$; thus only one set of design variables need to be solved. The two upright flanges are assumed to be symmetric meaning $w_a = w_b$ and $t_a = t_b$. All the units for length are in inches.

### 7.4.1 Inputs

Each analysis routine requires three sets of inputs beyond the design variables: the material properties for each feature, geometric information from the configuration, and the internal loads calculated from the torque box analysis.

#### 7.4.1.1 Material Properties

The material properties required by SPANDSET are listed in Table 12. Not all of these properties are required for each feature. The material properties that are required for the rib analysis are the compression yield load ($F_{cy}$) for the web stiffeners and web, the Young's modulus ($E$) for the web stiffeners and rib caps, and the density ($\rho$) for all three features.

#### 7.4.1.2 Configuration Geometry

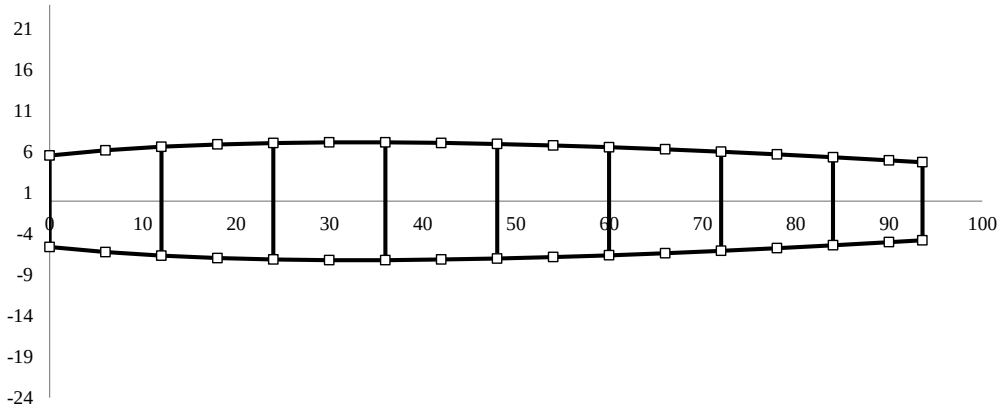


Figure 72: Rib Geometry

Several inputs required by the rib analysis come directly from the configuration. These variables are calculated by the parametric geometry tool. First, the user defines three values required by the rib analysis: the rib upright spacing for all the ribs ($B$) and the upper and lower stringer spacings. Next, the parametric geometry tool calculates the intersection of the each rib with the front spar ($BL_1$,$FS_1$) and the rear spar ($BL_n$,$FS_n$). Then, the length of the rib ($L_{rib}$) is calculated using the intersections by Equation 133.

$$L_{rib} = \sqrt{(BL_n - BL_1)^2 + (FS_n - FS_1)^2} \tag{133}$$

After the length of the rib is calculated, several points along the rib are selected based upon the upright spacing and the midpoints between the uprights. These points

include the intersections with the front and rear spar. At each of these points the intersection of the rib with the upper and lower surfaces are calculated ($WL_{upper}$, $WL_{lower}$), as illustrated in Figure 72. These points are used to calculate the height via Equation 134.

$$H = WL_{upper} - WL_{lower} \tag{134}$$

The height of the rib is assumed to be the maximum height from the previously calculated points (Equation 135). The reason only one height is used is that all the uprights are assumed to have the same dimensions. The failure criteria for the uprights is buckling and depends on the geometry of the feature and the load it is subjected to. All the uprights are assumed to be subjected to the same load so that the only difference between the uprights is the height ($H_x$). For the buckling failure criteria the longer the upright the more likely it is to fail; thus, only the longest upright needs to be sized.

$$H_{rib} = max(H_x : x = 1, 1.5, ..., n) \tag{135}$$

The final configuration value required for the rib analysis is the area of the web ($A_{rib}$). The points in Figure 72 are used to calculate this value. Each section between the points is assumed to be a trapezoid. Therefore, the area of each section can be calculated and all the areas can be summed up to get an estimate for the area of the web (Equation 136).

$$A_{rib} = \sum_{x=1}^{n} \frac{B}{2}(H_x + H_{x+\frac{1}{2}}) + \frac{B}{2}(H_{x+\frac{1}{2}} + H_{x+1}) \tag{136}$$

#### *7.4.1.3 Internal Loads and Stiffness*

The internal loads and section stiffness for the ribs are calculated differently from the other sizing routines due to the weight interpolation. This will be discussed further in the next section. Due to the SPANDSET weight estimation, each rib is sized

individually which means the internal loads need to be estimated for each rib. However, the torque box analysis only estimates the internal loads along the cross-sections. Thus, linear interpolation is used to calculate the loads. First the two cross-sections on either side of the rib are located. Next the intersections of the identified cross-sections and the rib with the reference load axis are calculated. Finally the $BL$ coordinates of the cross-section intersections ($[BL_1,\ BL_2]$) and the rib intersection ($BL$) are used to interpolate the wing bending stiffness for each cross-section ($EI_{y1}$ and $EI_{y2}$) and the wing bending moment at each cross-section ($M_1$ and $M_2$) to estimate the wing bending stiffness ($EI_{wing}$) and the wing bending moment ($M_{wing}$) used by the rib analysis.

$$EI_{wing} = \frac{(BL - BL_1)(EI_2 - EI_1)}{(BL_2 - BL_1)} + EI_1 \tag{137}$$

$$M_{wing} = \frac{(BL - BL_1)(M_2 - M_1)}{(BL_2 - BL_1)} + M_1 \tag{138}$$

Calculating the total segment load ($P_{seg}$) used in the rib analysis requires an additional step. Only one value for the segment load is input into the rib analysis. However, each cross-section has several values for the axial segment load. To combine all the cross-section axial loads into one value all the axial loads from the cross-section are summed. Two sets of axial loads exist for each cross-section, one due to the up bending loading condition and another for the down bending loading condition. For the rib analysis the larger set of axial loads (the up bending case) are used. The absolute value of the sum of the axial loads for each cross-section is interpolated via Equation 139.

$$P_{seg} = \frac{\left(BL - BL_1\right)\left(\left|\sum P_{seg}^{[up]}\right|_2 - \left|\sum P_{seg}^{[up]}\right|_1\right)}{(BL_2 - BL_1)} + \left|\sum P_{seg}^{[up]}\right|_1 \tag{139}$$

The cover stiffness for the upper surface ($EI_{cover}^{[u]}$) and lower surface ($EI_{cover}^{[l]}$) are also required by the rib analysis. These values have a similar problem to the total segment load in that there are several different covers with different stiffness across

the cross-section. A similar approach is used to interpolate the cross-section values to get a single value. For the cover stiffness the average cover stiffness for the entire cross-section is used.

$$EI_{cover}^{[u/l]} = \frac{\left(BL - BL_1\right)\left(\left(\sum EI_{cover}^{[u/l]}\right)/n\right)_2 - \left(\sum EI_{cover}^{[u/l]}\right)/n\right)_1\Big)}{(BL_2 - BL_1)} + \left(\sum EI_{cover}^{[u/l]}\right)/n\Big)_1 \quad (140)$$

### 7.4.2 Objective Function Calculation

The rib sizing calculates the objective function differently than the other sizing routines. For the cover sizing routine and the spar segment sizing routine the objective functions are the weight per unit area and weight per unit length respectively. The reason these weight were calculated per unit is that not every cover or spar segment will be sized. Instead, during the weight estimation portion of SPANDSET the sized weights per unit are interpolated across the entire span of the wing. Interpolating the weights over the span of the wing for the ribs makes less sense. The ribs are assumed to be relatively uniform across the length of the rib; thus, there is no reason to integrate a weight value across the length of the rib. Additionally, interpolating the rib weight across the span would be difficult because of the gaps between ribs and the different orientations of the stub ribs and the main ribs. Therefore, each rib is sized individually at the location of the rib and the objective function is the entire weight of the rib.

The objective function for the sizing problem is shown in Equation 129. The equations for each weight component are shown in Equation 141, Equation 142, and Equation 144. Each equation approximates the volume of the feature and multiplies the volume by the density of the material assigned to the feature.

$$W_{web} = t_{web} A_{web} \rho_{web} \quad (141)$$

The web volume is calculated based upon a value of the web area estimated by the parametric geometry tool multiplied by the web thickness which is one of the design

variables (Equation 141).

$$W_{chord} = 2A_{chord}\rho_{chord}L_{rib} \tag{142}$$

$$A_{chord} = w_1 t_1 + (t_3 - t_1)w_3 \tag{143}$$

The chord volume is estimated as the area of the chord (Equation 143) multiplied by the length of the rib. The upper and lower rib chords are assumed to be symmetric so this value is multiplied by two (Equation 142).

$$W_{upright} = (A_{upright}H_{rib})\lfloor L_{rib}/B \rfloor \rho_{upright} \tag{144}$$

$$A_{upright} = w_a t_a + (h_s - t_a)t_s \tag{145}$$

The upright volume for an individual upright is calculated as the area of the upright (Equation 145) multiplied by the height of the rib. The estimated volume of the individual upright is multiplied by an estimate of the number of uprights. The number of uprights is estimated by rounding to the lowest integer the rib length divided by the upright spacing. The total upright volume is then multiplied by the density of the material assigned to the web uprights (Equation 144).

### 7.4.3 Constraints

The dimension constraints are listed in Equation 130. These constraints are the result of work at Triumph Aerostructure based on designer knowledge, manufacturing requirements, and experience [180].

Two margin of safety constraints (Equation 131) are applied to the rib sizing. These margins of safety are the web upright column buckling margin of safety (M.S. Web Upright Column Buckling) and the moment of inertia required margin of safety (M.S. Moment of Inertia Required).

#### 7.4.3.1 M.S. Web Upright Column Buckling

$$\text{M.S. Web Upright Column} = \frac{F_{crit}}{P_{crush}/A_{seg}} - 1$$

The rib webs, which are reinforced by upright stiffeners, are sized to resist the crushing load ($P_{crush}$) that develops on the ribs due to the Brazier effect in wing bending. The margin of safety is calculated using the equation above. It is assumed that the crushing load is uniform over the entire rib. Additionally, the uprights all have uniform dimensions; thus, only the tallest upright needs to be sized. The critical loads ($F_c$) is calculated based on Euler-Johnson buckling (see Chapter 3).

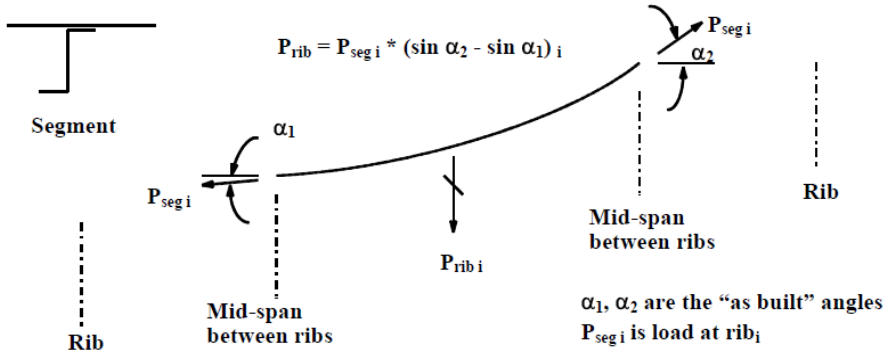


Figure 73: Rib Crush Loads [153]

The Brazier effect is when the upper and lower surfaces deflect to the neutral axis of the cross-section due to the flexure of the wing [166]. The deformation of the lower surface and upper surface are unequal causing a crushing load. Figure 73 illustrates that the crushing load is proportional to the segment load ($P_{seg}$). The geometric portion of the equation presented in Figure 73 can be estimated as half the curvature due to bending ($M_{wing}/EI_{wing}$) multiplied by the spacing between the ribs ($L_{rib}$). The crushing load is calculated with Equation 146.

$$P_{crush} = \frac{1}{2}\frac{P_{seg}\ M_{wing}}{EI_{wing}} \tag{146}$$

The margin of safety measures the crippling load based on the part geometry and material properties. The geometry of the part that withstands the crushing load is a web upright and a portion of the web defined by the length of the base upright base ($w_a$). The total critical load is calculated based on the areas of each portion (Equation 147) and the critical loads for each portion of the upright and web based on the buckling of a thin plate (Equation 148).

$$A_{cap} = w_b t_b \qquad A_{mid} = (h - t_a - t_b)h_s \qquad A_{base} = w_a t_a \tag{147}$$
$$A_{web} = w_a t_{web} \qquad A_{upright} = A_{cap} + A_{base} + A_{mid} \qquad A_{seg} = A_{upright} + A_{web}$$

$$F_{c,base} = min\left(F_{cy},\ (C_{1,base})F_{cy}\left[\frac{F_{cy}}{E}\left(\frac{(w_a - 0.5t_s)^2}{t_a}\right)^2\right]^{-C_{2,base}}\right) \tag{148}$$
$$F_{c,cap} = min\left(F_{cy},\ (C_{1,cap})F_{cy}\left[\frac{F_{cy}}{E}\left(\frac{w_b - 0.5t_s}{t_b}\right)^2\right]^{-C_{2,cap}}\right)$$
$$F_{c,mid} = min\left(F_{cy},\ (C_{1,mid})F_{cy}\left[\frac{F_{cy}}{E}\left(\frac{h_s - 0.5t_a - 0.5t_b}{t_s}\right)^2\right]^{-C_{2,mid}}\right)$$
$$F_{c,upright} = \frac{F_{c,cap}A_{cap} + F_{c,mid}A_{mid} + F_{c,base}A_{base}}{A_{cap} + A_{mid} + A_{base}}$$
$$F_{c,web} = min\left(F_{cy},\ (C_{1,web})F_{cy}\left[\frac{F_{cy}}{E}\left(\frac{w_a}{t_{web}}\right)^2\right]^{-C_{2,mid}}\right)$$

The crippling load of the entire part is calculated in Equation 149 using the areas calculated in Equation 147 and the crippling load of each portion of the upright and web based off McCombs' equation (Equation 14). They are calculated in Equation 148.

$$F_{crit} = \frac{F_{c,upright}A_{upright} + F_{c,web}A_{web}}{A_{upright} + A_{web}} \tag{149}$$

#### *7.4.3.2 M.S. Moment of Inertia Required*

$$\text{M.S. I}_{req} = \frac{I}{I_{req}} - 1 \tag{150}$$

The rib caps are sized relative to the requirement that they possess sufficient stiffness to enforce nodes for column buckling of stiffened skin segments. This leads to a moment of inertia requirement for rib caps. The margin of safety is the ratio of the moment of inertia of the rib caps ($I$) and the required moment of inertia ($I_{req}$). The upper and lower rib caps are assumed to be symmetric so only one rib cap is sized at a time. Thus, the moment of inertia is for one rib cap only. Equation 151 calculates the moment of inertia of a rib cap adjusted by the cap centroid ($\bar{y}_{cap}$) using the parallel axis theorem.

$$I = \frac{1}{12}\left[w_1 t_1^3 + w_1 t_1 \left(\frac{\bar{y} - t_1}{2}\right)^2 + t_3(w_3 - t_1)^3 + t_3(w_3 - t_1)\left(t_1 + \frac{(w_3 - t_1)}{2} - \bar{y}\right)^2\right] \tag{151}$$

The moment of inertia required ($I_{req}$) is calculated as a ratio of the stiffness of the covers to the stiffness of the rib caps. Equation 152 calculates the moment of inertia required using: the upper and lower cover stiffness ($EI_{cover}^{[u]}$), the spar cap Young's modulus ($E_{cap}$), the length of the rib ($L_{rib}$), the upright spacing ($B$), and the upper and lower stringer spacing ($b^{[u/l]}$). Additionally, anytime cover information is used the upper and lower cover values are averaged due to the symmetry requirement.

$$I_{req} = \left(\frac{1}{1.95}\right)\left(\frac{(EI_{cover}^{[u]} + EI_{cover}^{[l]})/2}{E_{cap} L_{rib}^3}\right)\left(\frac{B}{(b^u + b^l)/2}\right) \tag{152}$$

### 7.4.4 Outputs

The rib analysis routine has two outputs: the final part dimensions, the weight of the rib. The final weight of the rib is the final value of the objective function and the dimensions are the final values of the design variables. The ribs are not used in the torque box analysis; therefore, the part geometries are not output by the rib analysis routine.

## *7.5 Convergence Behavior*

As previously mention, the entire structural analysis and sizing method shown in Figure 60 is an iterative process. All iterative processes need some method to determine when to stop which is typically done with some sort of convergence criteria. SPANDSET elects not to use a convergence criterion and instead uses a specified number of iterations. This decision was made based off of experience with the Triumph developed method. It is assumed that the structural analysis and sizing routines will converge in a small number of iterations.

A small experiment was run to illustrate the convergence behavior with respect to the number of iterations. The error in the Total Wing Box Weight over a number of iterations is plotted in Figure 74 using a small business jet baseline (Chapter 8) and a single aisle airliner baseline (Chapter 9). Figure 74 shows that SPANDSET can be expected to converge in approximately 5 iterations. Both of the baselines have an approximate run time of less than 30 minutes with 5 iterations.

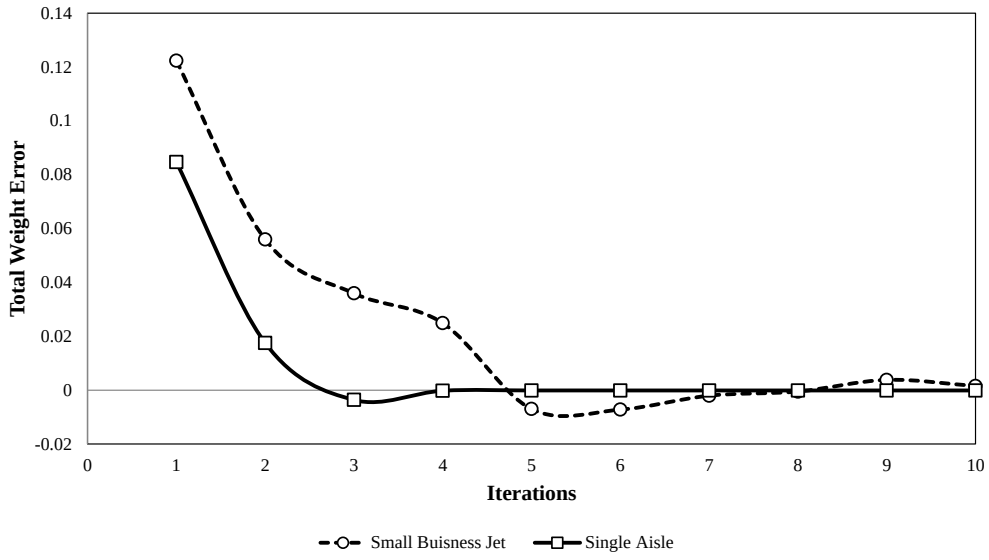


Figure 74: Iteration Convergence Behavior

An additional source of error convergence in SPANDSET is due to the number of cross sections. SPANDSET requires at least two cross sections be defined to estimate

the weights. Each cross section represents a data point to be used in the weights interpolation, so the more cross sections there are the more accurate the weights will be. This is especially true for wings with longer spans. Figure 75 represents the error in Total Wing Box weight with respect to the number of cross sections. As the number of cross sections increase the accuracy increases; however, as the number of cross sections increase the run time increases substantially. The trade in accuracy and run time will need to be considered when implementing SPANDSET. For the small business jet a total of 6 cross sections were used and for the single aisle 8 cross sections were used.

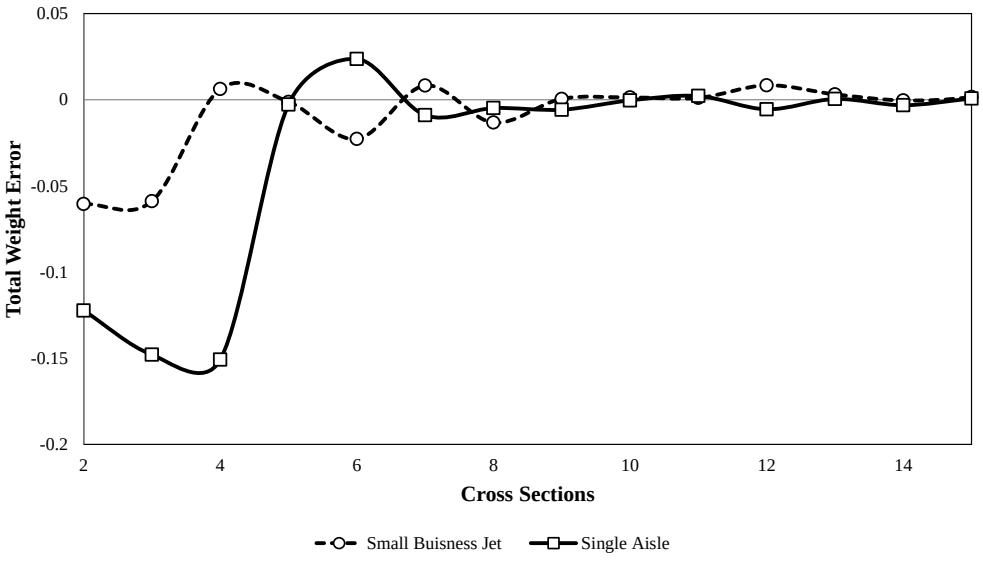


Figure 75: Number of Cross Sections Convergence Behavior

# CHAPTER VIII

# SUBSTRUCTURE CONFIGURATION EXPLORATION

During previous chapters, Framework Proposition 1 and Framework Proposition 2 were used as justification for decisions made while developing SPANDSET. This chapter seeks to verify these hypotheses using SPANDSET.

---

**Framework Proposition 1**

Due to the complex & discontinuous nature of the physics-based structural analysis design space, a strategy of exploration requiring a large number of analysis executions will be required.

---

---

**Framework Proposition 2**

If a strategy of exploration requiring a large number of analysis executions is necessary, then the structural analysis sub-problem should be executed using lower fidelity classical structural analysis methods.

---

The main clause of Framework Proposition 2 has already been verified in Chapter 4 through literature review. If the conditional clause is satisfied then Framework Proposition 2 can also be verified. However, the conditional statement can only be verified by verifying Framework Proposition 1. Thus, if Framework Proposition 1 is confirmed then Framework Proposition 2 is also confirmed.

Framework Proposition 1 states that a strategy of exploration requiring a large number of analysis executions is necessary to perform physics-based structural analysis. Experiment 1 will test Framework Proposition 1 using a canonical example of a wing

box substructure design problem. The canonical example will be used to disprove that the problem can be solved easily with few analysis alternatives through numerical optimization by illustrating that there is a correlation between the hit rate (i.e. the likelihood of the optimization locating the global optimum) and the number of alternatives evaluated (i.e. the number of objective functions evaluated). Framework Proposition 1 will be affirmed if fewer function calls results in a lower hit rate.

Experiment 1 will be divided into the following steps. First a simple two variable wing box substructure design problem will be set up. Then, each variable will be investigated independently to identify discontinuities and scope the ranges. Third, a two dimension design space exploration will be used to create surrogate models of the region of interest. Additionally, the local minima and global minimum of the surrogate models will be identified. Finally, several optimization algorithms will use the surrogate models and the minima to test Framework Proposition 1.

## *8.1 Canonical Example*

The canonical example is the study of the wing box design variables that result in discontinuous responses (Research Objective 6). The example uses a small business jet baseline. The small business jet is modified from and existing business. The reason this baseline is used is that SPANDSET has been validated against the existing business jet and the geometry is similar enough that the results can be trusted. Additionally, the VMT data from the existing business jet wing has been made available; thus, the external loads will be based off of higher fidelity analysis of an existing wing so long as the OML does not change.

The example will be limited to two design variables to simplify the problem. The two variables are change in rib spacing ($\Delta$ Rib Spacing) and change in stringer spacing ($\Delta$ Stringer Spacing). These two variables are applied uniformly to baseline values of the rib spacings (stub and main) and the stringer spacings (upper surface and

lower surface) using the parametric geometry tool. The ranges of these variables are shown in Table 20 and Table 21. To isolate the experiments from the rest of the wing sizing problem only one wing OML and one set of external loads will be used for each alternative investigated.

Table 20: Δ Rib Spacing Variable

| Variables | Base | Min | Max |
|---|---|---|---|
| Δ Rib Spacing (in) | 0 | -11.5 | 11.63 |
| MR Spacing (in) | 25 | 13.5 | 36.63 |
| SR Spacing (in) | 20 | 8.5 | 31.63 |
| Number of Ribs | 23 | 44 | 17 |

Table 21: Δ Stringer Spacing Variable

| Variables | Base | Min | Max |
|---|---|---|---|
| Δ Stringer Spacing (in) | 0 | -3.23 | 1.27 |
| Upper ST Spacing (in) | 8 | 4.77 | 9.27 |
| Lower ST Spacing (in) | 10 | 6.77 | 11.27 |
| Number of Ribs | 21 | 47 | 19 |

The responses of interest are Δ Total Wing Box Weight and Δ Total Wing Box Cost. These variables represent the percent difference in the total weight and total cost from the mean of all the values collected in the experiment, as shown in Equation 153 and Equation 154. This was done to protect the proprietary data shared to run these experiments.

$$\Delta\big(\text{Total Wing Box Weight}\big)_i = \frac{\big(\text{Total Wing Box Weight}\big)_i - \frac{\sum_{i=1}^{n} \text{Total Wing Box Weight}}{n}}{\frac{\sum_{i=1}^{n} \text{Total Wing Box Weight}}{n}} \tag{153}$$

$$\Delta\big(\text{Total Wing Box Cost}\big)_i = \frac{\big(\text{Total Wing Box Cost}\big)_i - \frac{\sum_{i=1}^{n} \text{Total Wing Box Cost}}{n}}{\frac{\sum_{i=1}^{n} \text{Total Wing Box Cost}}{n}} \tag{154}$$

## *8.2 1D Variable Exploration*

The first experiments run on the canonical example are the one dimension (1D) variable explorations. The purpose of these experiments is to identify the location of the discontinuities as well as investigate what the effects of the discontinuities on the responses are. Additionally, the 1D experiments are used to identify general trends so that the two dimensional design space can be scoped while still investigating a region

that contains the global minimum.

An iterative approach that uses the parametric geometry tool is used to identify the location of the discontinuities. First the ranges from Table 20 and StringVar are discretized and input into the parametric geometry tool. The parametric geometry tool then outputs the number of stringers and number of ribs. The two values on each side of a discontinuity (the points where the number of ribs or stringers change) are recorded. Next, the range between the values surrounding the discontinuity is discretized further. This process is repeated until the desired tolerance for the location of the discontinuities is reached. For these experiments the discontinuities are located to within one hundredth of an inch.

The next step is to map the continuous space between the discontinuities. The range between the discontinuities is divided into five equal parts (six points) so that the minimum and maximum values are within one hundredth of an inch of the discontinuities that bound the continuous space. This is repeated for each continuous space to create a full design of experiments (DoE). This DoE is then input into SPANDSET to map the responses ($\Delta$ Total Wing Box Weight and $\Delta$ Total Wing Box Cost) to the two variables ($\Delta$ Rib Spacing and $\Delta$ Stringer Spacing) one at a time. The results are discussed below.

### 8.2.1 1D Rib Spacing Total Weight Results

Figure 76 and 77 illustrate the $\Delta$ Total Wing Box Weight over the $\Delta$ Rib Spacing range given in Table 20. Research Observation 6 illustarted that there are discontinuities in the responses (i.e. weight and cost) due to a change in the number of parts that define the substructure. In both figures the dotted lines represent the approximate location (within 0.01 inches) of the discontinuities. The approximate locations of the discontinuities in terms of the $\Delta$ Rib Spacing are listed in Table 22.

In Figure 77 there is a gap at 38 ribs. This is due to the fact that two rib spacing

variables are altered by $\Delta$ Rib Spacing. The result of combining the two spacings is that the number of ribs jumps by two within 0.01 inches; thus, there are no points with 38 ribs. These dotted lines will also represent discontinuities in Figures 78.

There are two axis systems that will be used throughout the canonical example. The first is a **constant spacing** axis system where the x axis represents either the $\Delta$ Rib Spacing or the $\Delta$ Stringer Spacing. This axis system will be used to illustrate the general trend as the spacings are increased of decreased. This axis system is used in Figure 76.

The second axis system evenly spaces the discontinuities so that the x axis represents the **number of elements**. Between each set of adjacent discontinuities is a length of continuous response. The number of elements axis system gives equal length to each of these continuous regions regardless of its length on the constant spacing axis. This axis system allows for the observation of the effect of the discontinuities on the responses. Figure 77 uses the number of elements axis system.

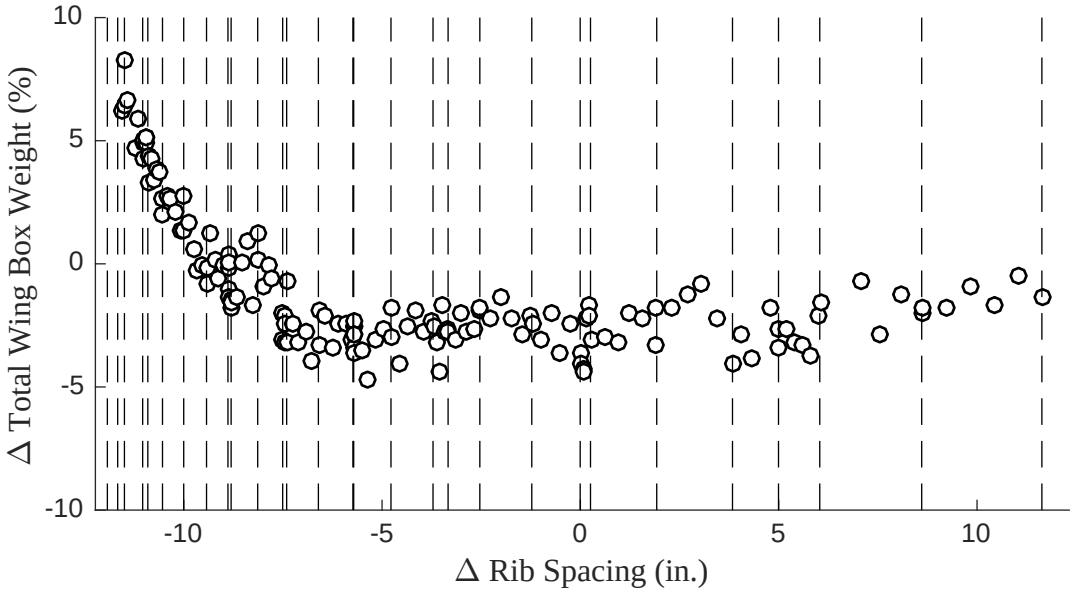


Figure 76: Rib Spacing Total Weight

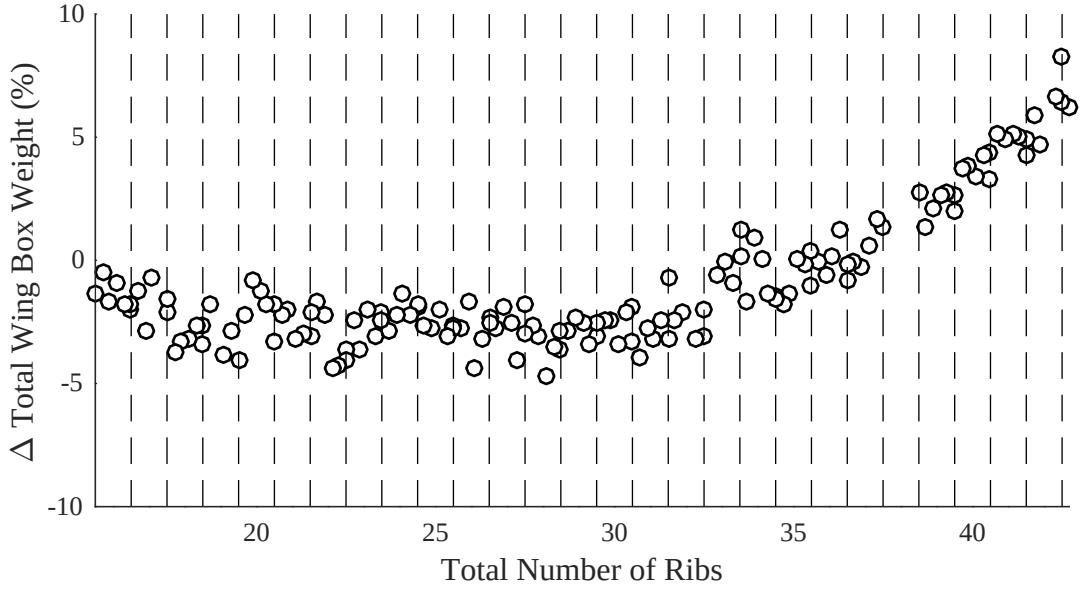


Figure 77: Number of Ribs Total Weight

Table 22: Rib Discontinuities

| Δ Rib Spacing | Number of Ribs |
|---|---|
| -12 | 46 |
| -11.93 | 46 |
| -11.92 | 45 |
| -11.67 | 45 |
| -11.66 | 44 |
| -11.5 | 44 |
| -11.49 | 43 |
| -11.04 | 43 |
| -11.03 | 42 |
| -10.91 | 42 |
| -10.9 | 41 |
| -10.54 | 41 |
| -10.53 | 40 |
| -10.001 | 40 |
| -9.999 | 38 |
| -9.43 | 38 |
| -9.42 | 37 |
| -8.89 | 37 |
| -8.88 | 36 |
| -8.81 | 36 |
| -8.8 | 35 |
| -8.14 | 35 |
| -8.13 | 34 |
| -7.51 | 34 |
| -7.5 | 33 |
| -7.41 | 33 |
| -7.4 | 32 |
| -6.61 | 32 |
| -6.6 | 31 |
| -5.74 | 31 |
| -5.73 | 30 |
| -5.72 | 30 |

| Δ Rib Spacing | Number of Ribs |
|---|---|
| -5.71 | 29 |
| -4.78 | 29 |
| -4.77 | 28 |
| -3.72 | 28 |
| -3.71 | 27 |
| -3.34 | 27 |
| -3.33 | 26 |
| -2.54 | 26 |
| -2.53 | 25 |
| -1.23 | 25 |
| -1.22 | 24 |
| -0.01 | 24 |
| 0 | 23 |
| 0.25 | 23 |
| 0.26 | 22 |
| 1.92 | 22 |
| 1.93 | 21 |
| 3.83 | 21 |
| 3.84 | 20 |
| 4.99 | 20 |
| 5 | 19 |
| 6.03 | 19 |
| 6.04 | 18 |
| 8.6 | 18 |
| 8.61 | 17 |
| 11.63 | 17 |
| 11.64 | 16 |
| 13.33 | 16 |
| 13.34 | 15 |
| 15.26 | 15 |
| 15.27 | 14 |
| 19.69 | 14 |
| 19.7 | 13 |
| 24 | 13 |

An interesting trend emerges in Figure 78 and 77. Initially the overall weight decreases as the rib spacing increases and the number of ribs decreases. The reduction of weight makes sense intuitively as a reduction in material results in a reduction of weight. However, the trend seems to flatten out between 20 and 34 ribs. The weight breakdown in Figure 78 explains what causes the weight to flatten. Figure 78 shows 6 graphs that pertain to a specific components contribution to the total wing box weight: the total spar weight, the rib weight, the upper skin weight, the upper stringer weight, the lower skin weight, and the lower stringer weight.

The rib weight trend needs to be explained in order to understand the total weight trend. In Figure 78 it can be seen that the rib weight increases as the rib spacing decreases and the number of ribs increases; however, at some point the rate of increase in the rib weight increases significantly. The cause of the change in the rate of rib weight increase is due to the constraints in the Rib Sizing routine used by SPANDSET. During the portion of the variable space that the rib weight increases gradually a smaller number of dimensions are at their minimum thickness. As the rib weight increases the percentage of dimensions at their minimum allowed thickness increases until nearly all of them are at their minimum value. When a new rib is added the sizing routine is once again restrained by the dimension minimums; thus, any new rib being added is adding redundant weight. Therefore, this portion of the variable space is not of interest nor will it contain the global minimum.

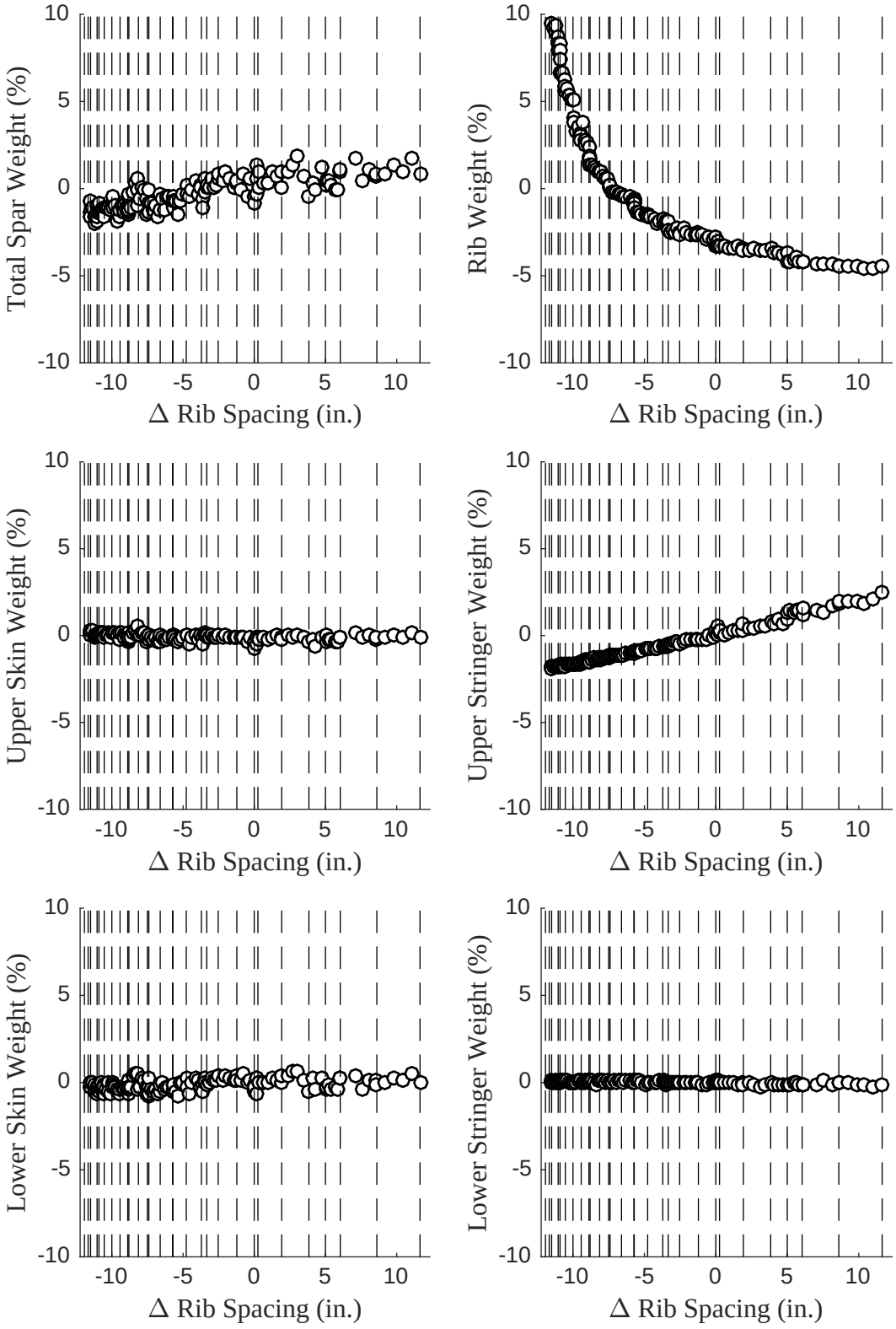


Figure 78: Rib Spacing Weight Breakdown

Although the trend in the rib weight is interesting it does not entirely explain the total wing box weight trend. If the region where redundant rib weight is being added is ignored, then the total weight is essentially flat despite the fact that the rib weight is still decreasing. The cause of the flattening of the total wing box weight is a trade in rib weight for upper stringer and spar weight. Figure 78 shows that the total spar weight and the upper stringer weight increase as the rib weight decreases. This is a result of the structural analysis and sizing portion of SPANDSET. SPANDSET sizes the stringers and spars before it sizes the ribs. As the Cover Sizing Routine and Spar Segment Sizing routine converge on larger spars and upper stringers, less weight is needed by the ribs to support the loads. The trade in weight from the ribs to the spars and upper stringers is nearly equal over the range of $\Delta$ Rib Spacing; thus, the total weight is flat.

### 8.2.2 1D Rib Spacing Total Cost Results

Figure 79 and 80 illustrate the $\Delta$ Total Wing Box Cost over the $\Delta$ Rib Spacing range given in Table 20. Figure 79 uses the constant spacing axis, while Figure 80 uses the number of elements axis. The dotted lines represent the discontinuities listed in Table 22. Once again there are no points with 38 ribs in Figure 80.

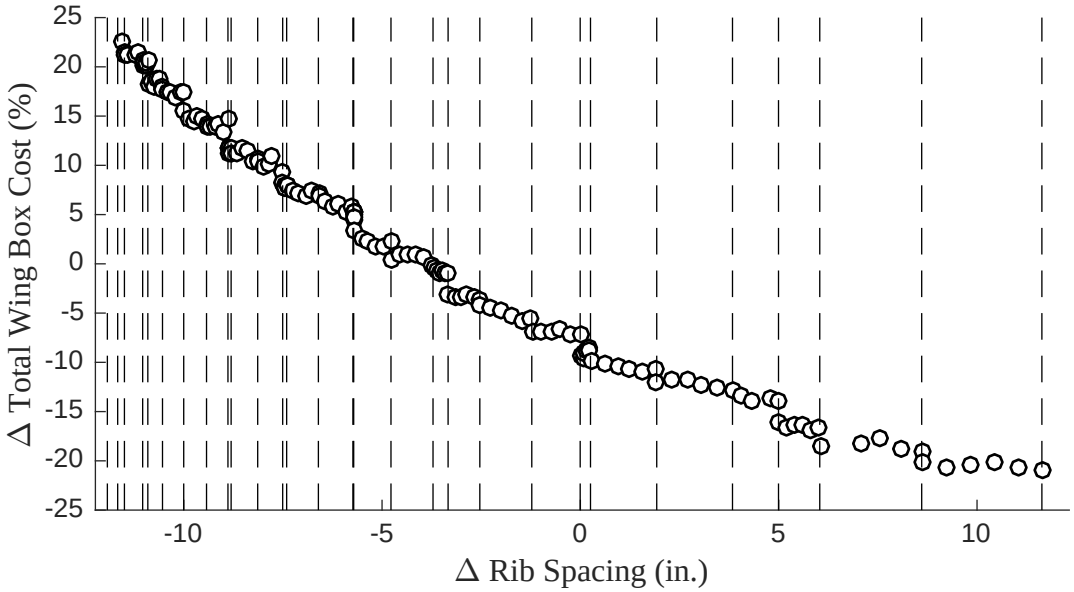


Figure 79: Rib Spacing Total Cost

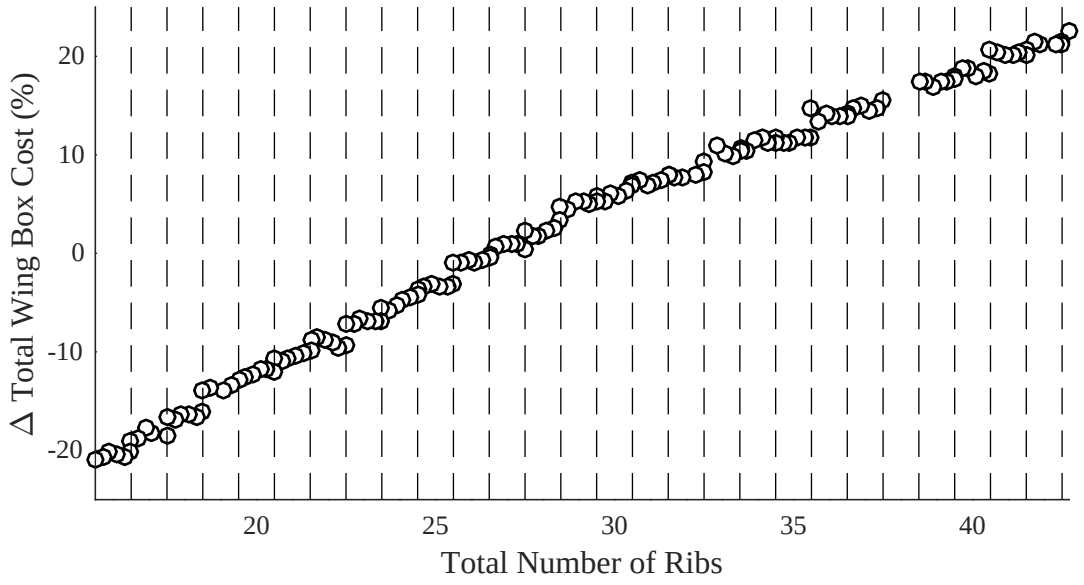


Figure 80: Number of Ribs Total Cost

The trend for Δ Total Wing Box Cost with respect to Δ Rib Spacing is simple to explain. As the number of ribs decreases the total cost decreases. Figure 81 illustrates a breakdown of the components that make up the wing box total cost and can be used to investigate further. The following observations are made.

Figure 81 shows a decrease in both the rib fabrication cost and rib assembly cost. This is obviously due to the reduction in the number of ribs.

Figure 81 also displays that the skin fabrication cost and the stringer fabrication cost decrease slightly as the number of ribs decreases. The number of skin panels and stringer segments is equal to the number of covers, and the covers are defined span-wise by the rib locations. Thus, as the rib spacing increases the size of the covers increase and the number of covers decreases. The decrease in the number of covers will reduce the setup time that is factored into both the skin fabrication and the stringer fabrication. Therefore, increasing rib spacing should decrease skin and stringer fabrication costs.

Finally, Figure 81 illustrates that the spar assembly cost decreases. The spar assembly cost only includes installing the rib posts. With fewer ribs fewer rib posts are required; thus the spar assembly decreases.

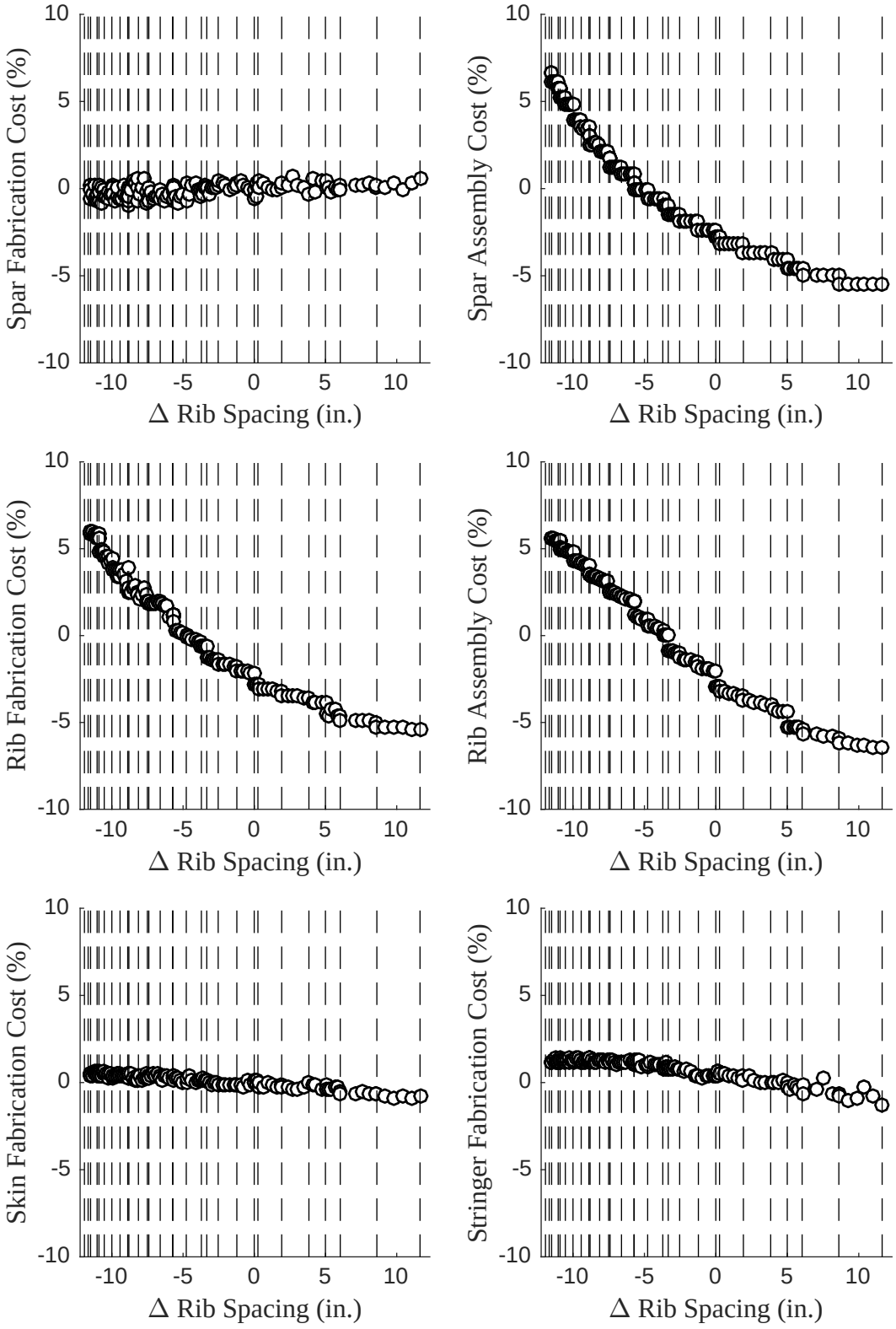


Figure 81: Rib Spacing Cost Breakdown

A final general observation about both the Δ Total Wing Box Weight response and the Δ Total Wing Box Cost response with respect to the Δ Rib Spacing is that the responses appear to be noisy. There are two reasons for the noise in the responses. The first is likely due to the large number of internal optimization problems solved in SPANDSET. Because solving optimization problems is a stochastic process there is room for small errors withing the optimization convergence. Thus, the large number of optimization problems in SPANDSET means that the cumulative effect of these errors can become significant.

The second reason is that the rib spacing affects several other parts in the parametric geometry tool. As previously discussed, the rib spacing affects the cover size, the spar upright spacing, the stringer length, as well as the number of ribs. The result is that a set of trend develops between the individual discontinuities. These trends alter the points from the overall global trend.

The final result of the 1D Δ Rib Spacing study identifies a region of interest (i.e. the most likely location of the global optimium) as the range between 25 and 35 number of ribs. This conclusion is reflected in the ranges of the two dimensional experiment in Table 24.

### 8.2.3 1D Stringer Spacing Total Weight Results

Figure 82 and 83 illustrate the Δ Total Wing Box Weight over the Δ Stringer Spacing range given in Table 21. Figure 82 uses the constant spacing axis to represent Δ Stringer Spacing, while Figure 83 uses the number of elements axis. The dotted lines represent the discontinuities listed in Table 23.

There are gaps in the number of stringers similar to the gap in the number of ribs. The gaps are the result of Δ Stringer Spacing combining the upper and lower stringer spacing into one variable. The gap at 25 stringers is the result of both the number of upper and the number of lower stringers changing within a 0.01 inch range.

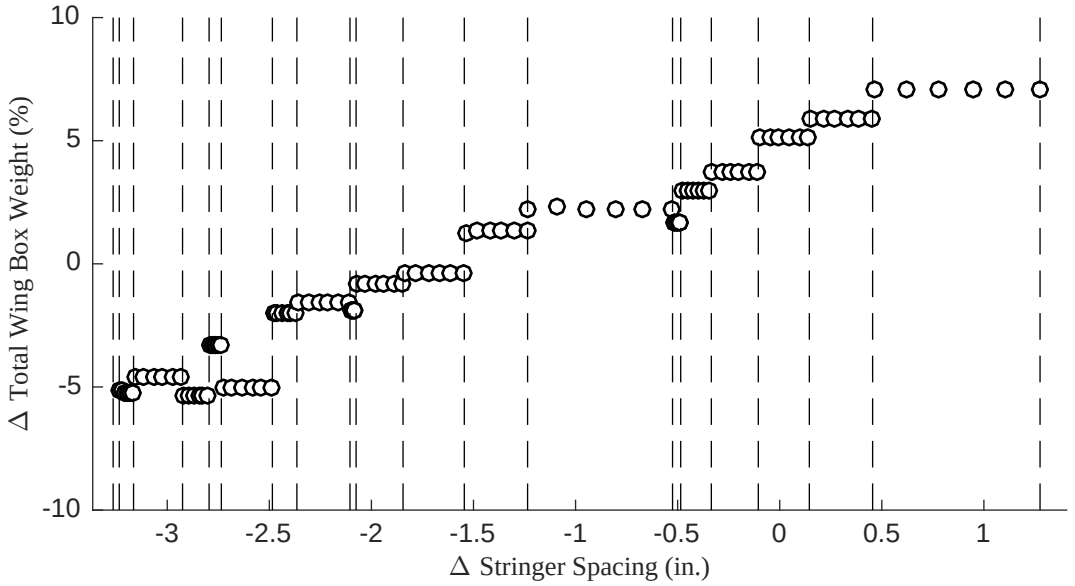


Figure 82: Stringers Spacing Total Weight

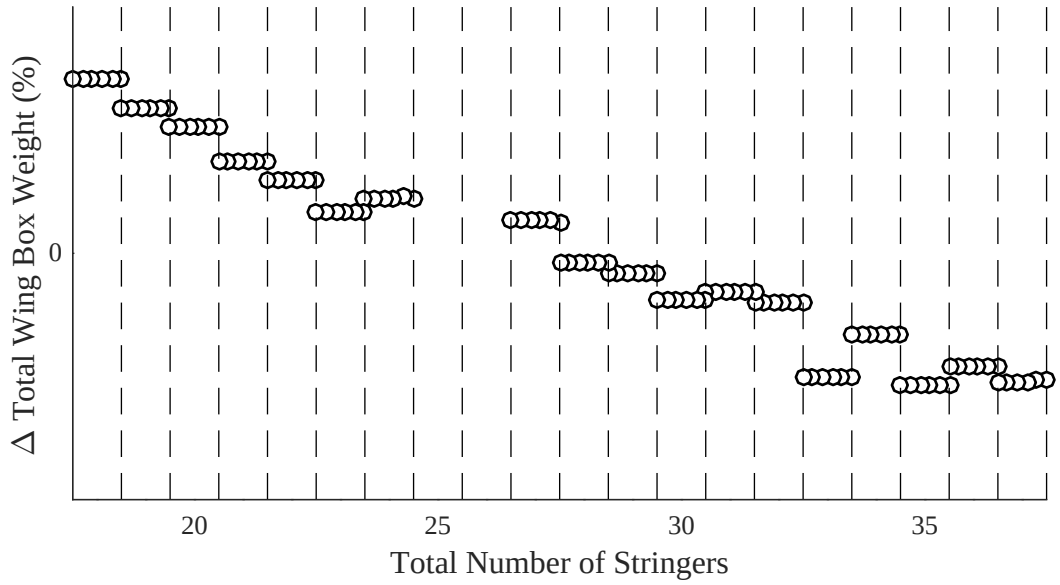


Figure 83: Number of Stringers Total Weight

Table 23: Stringer Discontinuities

| Δ Stringer Spacing | Number of Stringers | Δ Stringer Spacing | Number of Stringers |
|---|---|---|---|
| -4.00 | 47 | -0.52 | 24 |
| -3.95 | 47 | -0.49 | 24 |
| -3.94 | 46 | -0.48 | 23 |
| -3.85 | 46 | -0.34 | 23 |
| -3.84 | 45 | -0.33 | 22 |
| -3.78 | 45 | -0.11 | 22 |
| -3.77 | 44 | -0.10 | 21 |
| -3.70 | 44 | 0.14 | 21 |
| -3.69 | 43 | 0.15 | 20 |
| -3.49 | 43 | 0.45 | 20 |
| -3.48 | 42 | 0.46 | 19 |
| -3.27 | 42 | 1.27 | 19 |
| -3.26 | 41 | 1.28 | 18 |
| -3.24 | 41 | 1.47 | 18 |
| -3.23 | 38 | 1.48 | 17 |
| -3.17 | 38 | 1.66 | 17 |
| -3.16 | 37 | 1.67 | 16 |
| -2.93 | 37 | 1.84 | 16 |
| -2.92 | 36 | 1.85 | 15 |
| -2.80 | 36 | 2.14 | 15 |
| -2.79 | 35 | 2.15 | 14 |
| -2.74 | 35 | 3.27 | 14 |
| -2.73 | 34 | 3.28 | 13 |
| -2.49 | 34 | 3.53 | 13 |
| -2.48 | 33 | 3.54 | 12 |
| -2.37 | 33 | 3.84 | 12 |
| -2.36 | 32 | 3.85 | 11 |
| -2.11 | 32 | 5.53 | 11 |
| -2.10 | 31 | 5.54 | 10 |
| -2.08 | 31 | 5.78 | 10 |
| -2.07 | 30 | 5.79 | 9 |
| -1.85 | 30 | 6.91 | 9 |
| -1.84 | 29 | 6.92 | 8 |
| -1.55 | 29 | 7.78 | 8 |
| -1.54 | 28 | 7.79 | 7 |
| -1.24 | 28 | 8.91 | 7 |
| -1.23 | 25 | 8.92 | 6 |
| -0.53 | 25 | 12.00 | 6 |

The $\Delta$ Total Wing Box Weight exhibits an interesting behavior over the range of $\Delta$ Stringer Spacing. Figure 82 and 83 shows that the $\Delta$ Total Wing Box Weight exhibits a step like behavior where the response is constant over the continuous portion but jumps that coincide with the discontinuities. Thus, the discontinuities identified in Research Objective 6 dictate the behavior of the response. The physical explanation of this is that the stringers are very long and their weight is not effected by the stringer spacing except when the stringer spacing results in a change in the number of stringers.

The general trend of the $\Delta$ Total Wing Box Weight decreases as the stringer spacing increases and the total number of stringers increase. The reason for this behavior is illustrated in the weight breakdown (Figure 84).

In Figure 84 the rib weight and the spar weight remain nearly constant as the stringer spacing increases. This is expected as the number of ribs remains constant, and only small adjustments to the spar dimensions should be needed to account for the changing loads.

The upper skin weight and lower skin weight increase as the stringer spacing increases. The increase is a result of the reduction in the number of stringers. As the number of stringers that stiffen the skin panels decrease, the skin panel thickness must increase to withstand the crippling and buckling loads.

Figure 84 shows that the upper stringer weights decrease as the number of stringers decreases; however, the figure also shows that the lower stringer weight increases as the number of stringers decrease. While strange this is not impossible. Chapter 60 explains that the upper covers and the lower covers are sized with different loading conditions (tension and compression change based upon upper or lower surface). One of the active constraints in the cover routine is the stringer crippling. For this constraint the upper stringers are sized based on the larger +2.5g loads causing compression and the lower stringers are sized so that the -1.0g maneuver results in compression. The lower stringers are sized with smaller loads and as a result are defined by their dimension

constraints. However, as the number of stringers decrease the shear interaction with the skin panel becomes the active constraint. As a result the stringer base width is increased which results in an increase in the stringer weight as a whole.

The combined skin weight increases greater across the range of $\Delta$ Stringer Spacing than the combined stringer weight decreases. Thus, the weight breakdown explains the general trend of the increasing $\Delta$ Total Wing Box Weight across the range of $\Delta$ Stringer Spacing.

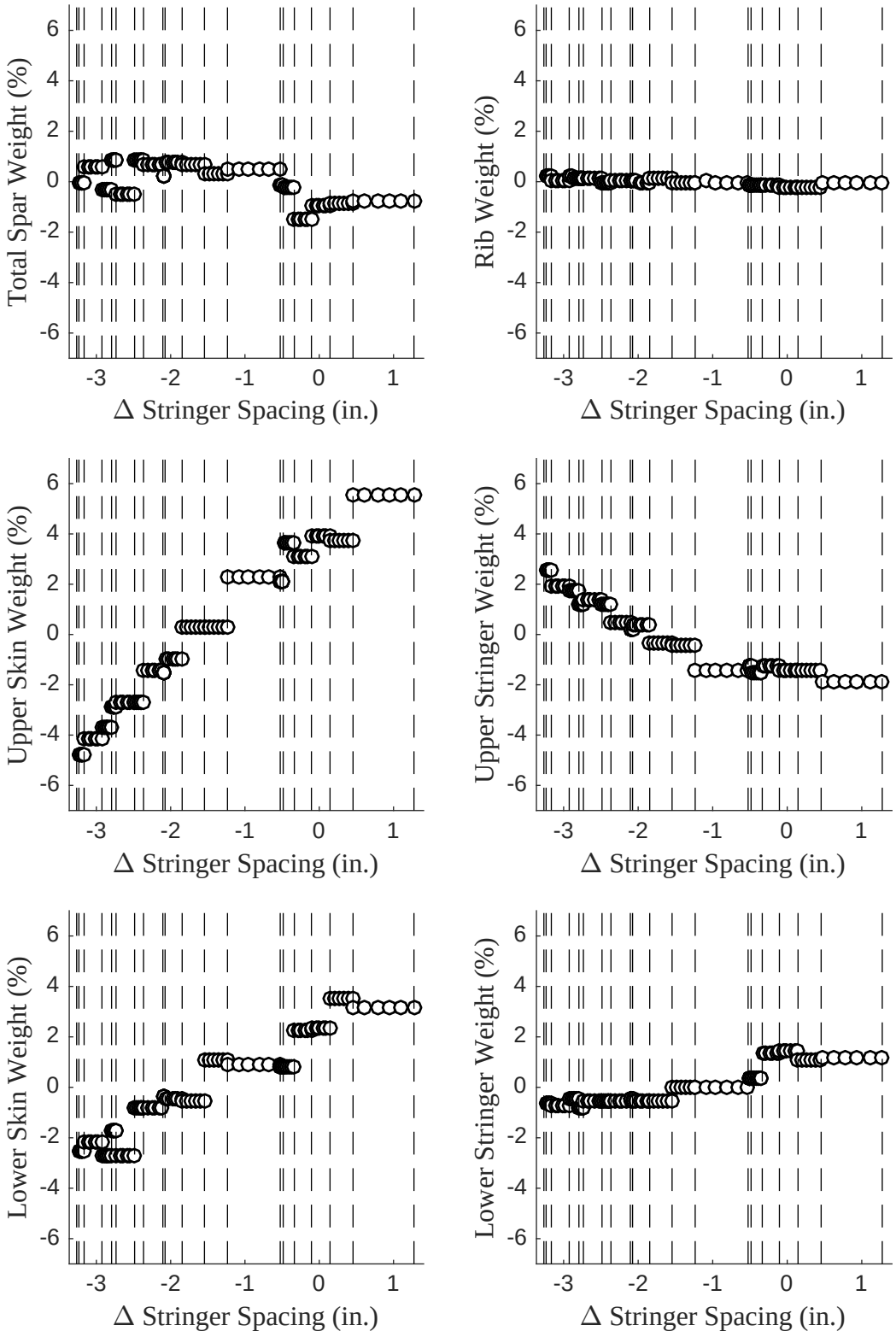


Figure 84: Stringer Spacing Weight Breakdown

### 8.2.4 1D Stringer Spacing Total Cost Results

Figure 85 and 86 illustrate the Δ Total Wing Box Cost over the Δ Stringer Spacing range given in Table 21. The x axes are the same as Figure 82 and Figure 83 receptively and the discontinuities from Table 23 are represented by the dotted lines.

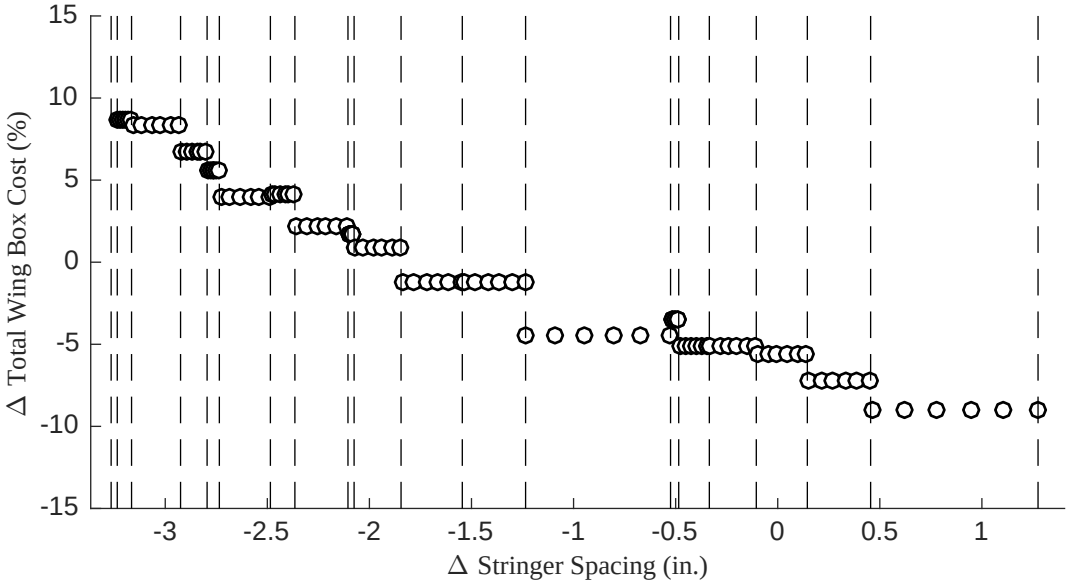


Figure 85: Stringer Spacing Total Cost

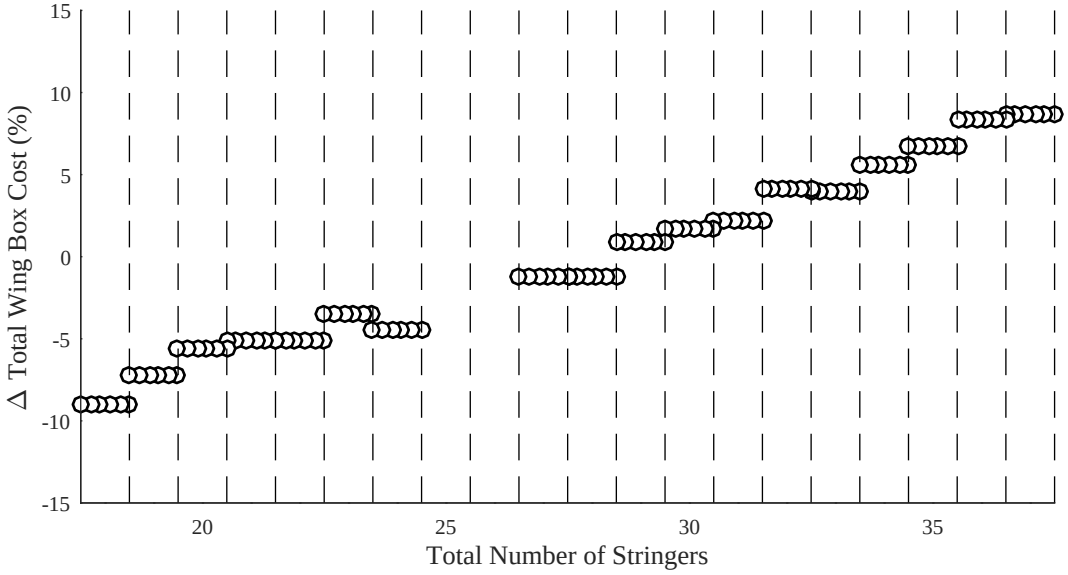


Figure 86: Number of Stringers Total Cost

The overall trend of the Δ Total Wing Box Cost decreases as Δ Stringer Spacing increases. The Δ Total Wing Box Cost also exhibits the same discontinuous behavior that was observed in the previous section. No cost breakdown is provided in this section because the results are easily explained; as the number of stringers increases the stringer fabrication cost increases while all the other costs remain constant. Thus, the minimum should be at the lowest number of stringers.

The results of the 1D Δ Stringer Spacing experiments show that the global minimum for the cost and the global minimum for weight are on the opposite sides of the range of Δ Stringer Spacing. This makes it difficult to identify a region of interest as a decrease in weight will result in an increase in cost. Ultimately the weight is prioritized over the cost so that the range of interest for the number of stringers is from 37 to 29 as shown in Table 24.

## *8.3 2D Design Space Exploration*

The next part of Experiment 1 is to run a two dimensional (2D) design space exploration of the ranges selected from the 1D experiments (Table 24). The purpose of the design space exploration is to develop a surrogate model that represents the design space of both the wing box weight and cost. The design space will be represented by a piecewise surrogate model so that the jump in the responses at the discontinuities can be accounted for. The model will consist of 99 individual Response Surface Equation (RSE). Once the RSEs have been created the global minima of the individual RSEs (called the local minima for the purpose of this experiment) will be located so that a global minimum of the design space can be found.

Table 24: Design Space Exploration Ranges

| Variables | Min | Max |
|---|---|---|
| $\Delta$ Stringer Spacing (in) | -3.16 | -1.55 |
| $\Delta$ Stringer Spacing (in) | -8.80 | -1.23 |
| Number of Stringers | 29 | 37 |
| Number of Ribs | 25 | 35 |

### 8.3.1 Create Surrogate Models

Surrogate models are analytic models that approximate the behavior of complex systems based on a limited number of computations. These models can be used to represent the design space for optimization and visualization. For the purpose of this experiment, surrogate models will represent the behavior of SPANDSET over the range of the design variables so that the computational time of the optimization function calls can be reduced.

The surrogate models are created by running a design of experiments (DoE) across the ranges of the variables. Each experiment will be applied to the baseline model which will then be assessed using SPANDSET. The results will then be used to create surrogate models for both the $\Delta$ Total Wing Box Weight and the $\Delta$ Total Wing Box Cost. However, the surrogate models should reflect the discontinuous nature of the design space. This is accomplished by using a piecewise surrogate model defined by the discontinuities identified during the 1D experiments. As a result, the piecewise surrogate model will consist of 99 RSEs that map the continuous space between adjacent discontinuities. This makes both the DoE and the process of creating the RSEs more difficult.

To create the DoE the ranges are divided into 99 sections, with each section residing between two adjacent discontinuities. For each section a a 33 point DoE is created to fit the surrogate model consisting of: the 4 corner points, a 9 point inscribed central

composite design, and a 20 point Latin Hyper Cube. The central composite design is inscribed so that no design point lies on or beyond the discontinuities. The Latin Hyper Cube captures the interior of the design space. The 4 corner points were added after an initial attempt to create the RSEs. The resulting RSEs without the corners caused a "dog-ear" effect so that the surrogate model gave large values with respect to the other points at the corners. Adding the 4 corner points fixed this problem. An additional 20 points randomly distributed within the section are added to test the representation of the model for each section.

After SPANDSET has executed all the experiments in the DoE, the RSEs are created using the results. a 4th order polynomial RSE is used to fit each continuous space between the discontinuities. Due to the large number of RSEs the model fitting is done using Matlab's 'fit' function.

After the RSEs are created the goodness of fit for each RSE is assessed based on the Sum of Squares Due to Error (SSE), the coefficient of determination ($R^2$), and the maximum error value. An example is shown in Figure 87.

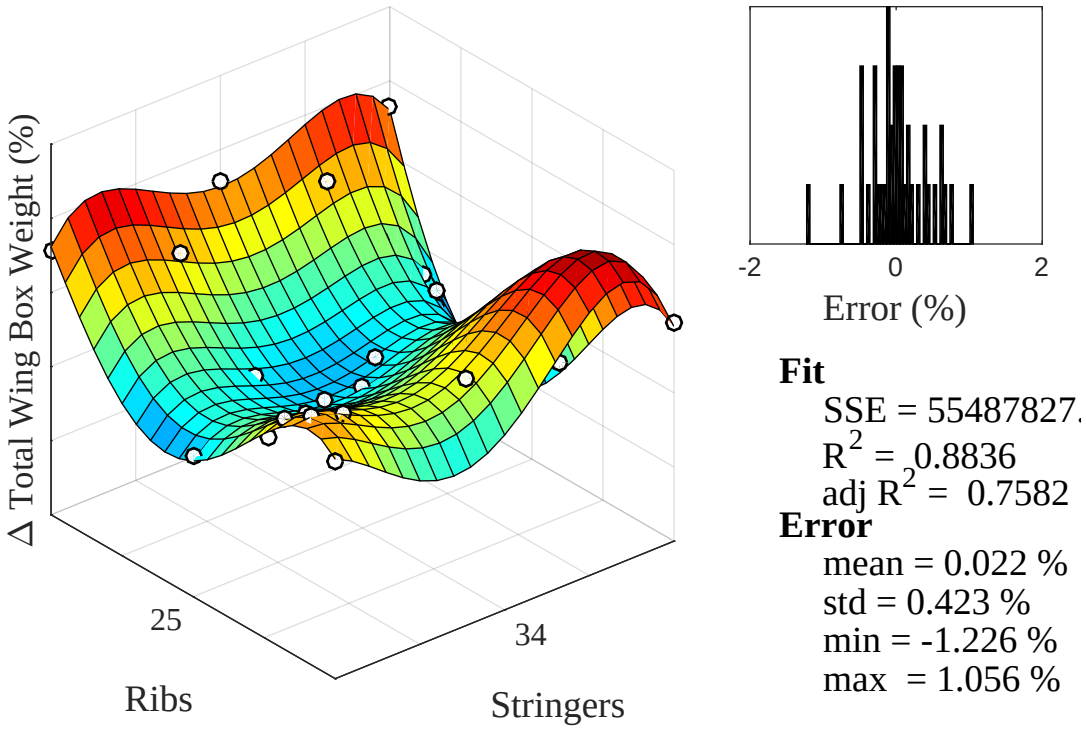


Figure 87: Example of 2D Regression

Figure 87 shows a section of the Δ Total Wing Box Weight surrogate model. The RSE created for the section is shown as the surface on the left, while the SPANDSET outputs are the white dots. This allows visual inspection of the surrogate model with respect to the outputs. The histogram on the upper right shows the distribution of the errors between the points and the RSE. The table on the lower right contains important metrics with respect to the goodness of fit and the model representation error. This figure can be recreated for each of the RSEs to create the surrogate model manually.

It is difficult to fit 99 RSEs manually in a timely manner; thus, the process was automated. Initially, all the RSEs are fit automatically and several values are used to assess the goodness of fit (i.e. the Sum of Squares Due to Error (SSE), the coefficient of determination ($R^2$), and the model representation error max/min and range). After the initial automatic runs the RSEs are judged and those that are not acceptable

are re-done manually using Figure 87. The RSEs are judged based upon closeness to an ideal fit which has an $R^2$ value as close to 1 as possible as well as small an error distribution as possible. These values are not achievable; therefore acceptable limits need to be set.

An acceptable limit on the errors is typically on the order of 1% to 5%. After the initial automated model fitting the surrogate models for both the $\Delta$ Total Wing Box Weight and $\Delta$ Total Wing Box Cost achieve error distributions such that none of the 198 RSEs having an error value greater than 2%. Thus, the error values are acceptable.

The $R^2$ values do not reflect a good fit as well as the errors do. The $R^2$ values are initially as low as 0.25. The poor $R^2$ values are a product of the piecewise nature of the surrogate model. Typically, the number of points used to create an RSE is on the order of 50 points per variables. For each individual RSE only 34 points are used because 99 RSEs are created. Yet, 0.25 is a poor $R^2$ value. The coefficient of determination is only one value used to assess the goodness of fit and the error values are sufficient for the purpose of the experiment; thus, an acceptable limitation on $R^2$ is greater than 0.5. 27 of the RSEs had to be re-done manually for the $\Delta$ Total Wing Box Weight surrogate model and 21 for the $\Delta$ Total Wing Box Cost to achieve acceptable $R^2$ values.

The results of the surrogate model fitting are displayed in Appendix A.

### 8.3.2 Identify Local Minimum

After the surrogate models are created, the minima of the design space are located. There are three types of minima: local minima, surrogate model local minima, and the global minimum. Local minima are the local optima as defined in Chapter 3. Each RSE will have at least one local minima; however, there are more than one local minima as the RSE is fourth order. There are likely over 400 local minima across the

entire design space.

Each RSE will have one global minimum. The global minimum of the surrogate model, called the surrogate local minimum for convenience, is defined as the minimum local minima of the RSE. Because RSEs are used to create the surrogate the local minima and the global minimum of each surrogate can be solved analytically; however, an automated process was used to find the surrogate local minima due to the large number of RSEs. The automated process utilized constrained gradient based optimization, which guarantees finding a local minimum, combined with a structured search pattern of 25 points to find the minimum local optimum (i.e. the surrogate local minima). The bounds of the optimization problem are the adjacent discontinuities so that only the RSE is being searched.

The final minimum is the global minimum of the entire design space. This minimum is found by comparing all of the surrogate local minima and selecting the smallest value.

The resulting surrogate local minima are displayed in Appendix B. The first set of columns identify each of the RSEs, the second set of columns contains the surrogate local minimum location and the percent change in the response from the baseline for the Total Wing Box Weight, and the final set of columns contains the surrogate local minimum location and the percent change in the response from the baseline for the Total Wing Box Cost. The global minimum is marked with an (*).

### 8.3.3 Surrogate Model Results

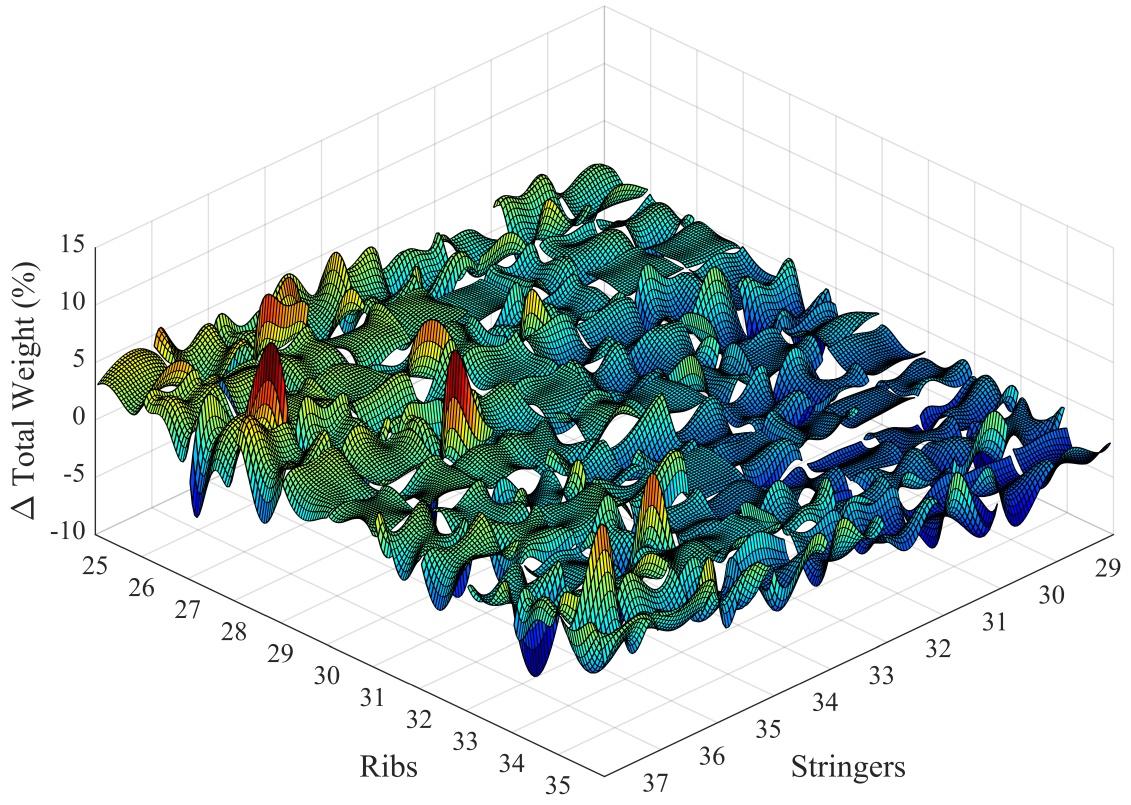


Figure 88: Δ Total Wing Box Weight Surface Plots

The surrogate models for the Total Wing Box Weight are depicted in Figure 88. Figure 88 depicts all 99 RSEs used to map the design space as surface plots. This figure allows for general observations about the overall design space. One observation is that the average weight value for each RSE does not change much across the design space. This means there is not a large difference between having 25 ribs and 35 ribs. This behavior is due in large part to the trade in weight between the ribs and spars discussed with Figure 77.

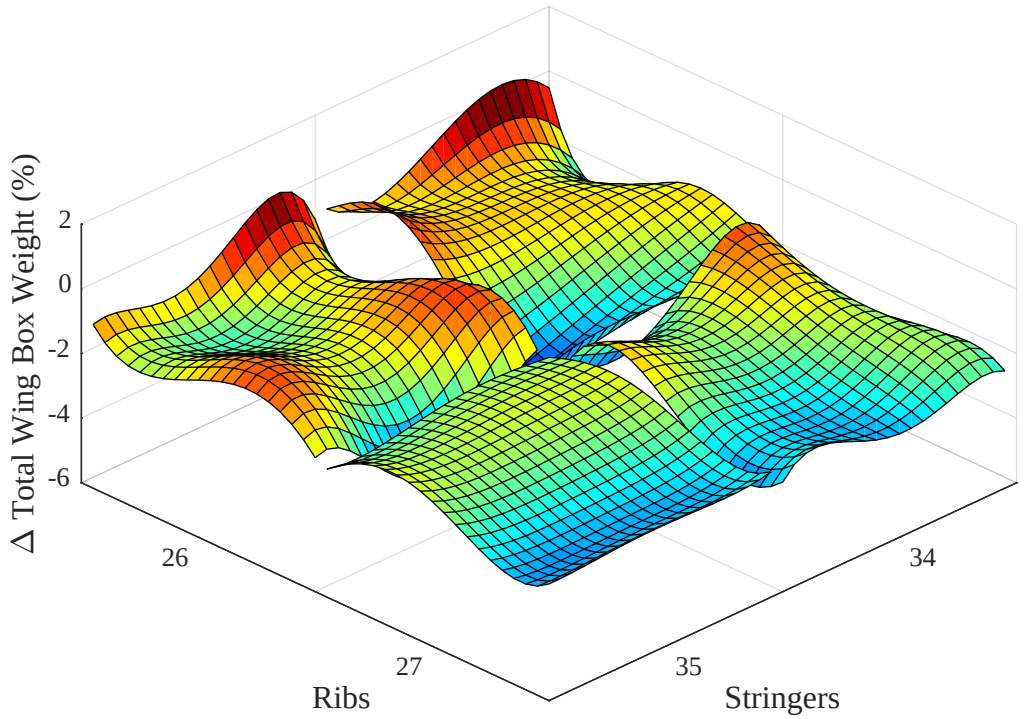


Figure 89: Δ Total Wing Box Weight Discontinuities

An important consequence of the discontinuities is a jump in the responses at the location of the discontinuities; however this is not easily observaed in Figure 88. Figure 89 contains four adjacent RSEs from Figure 88. Although the average weight value for each RSE does not change much across the design space there is still a large jump in the response values at the boundaries of the RSEs due to the discontinuities. Additionally, the gradients of each RSE are drastically altered across the discontinuity. This behavior is observed across the entire design space.

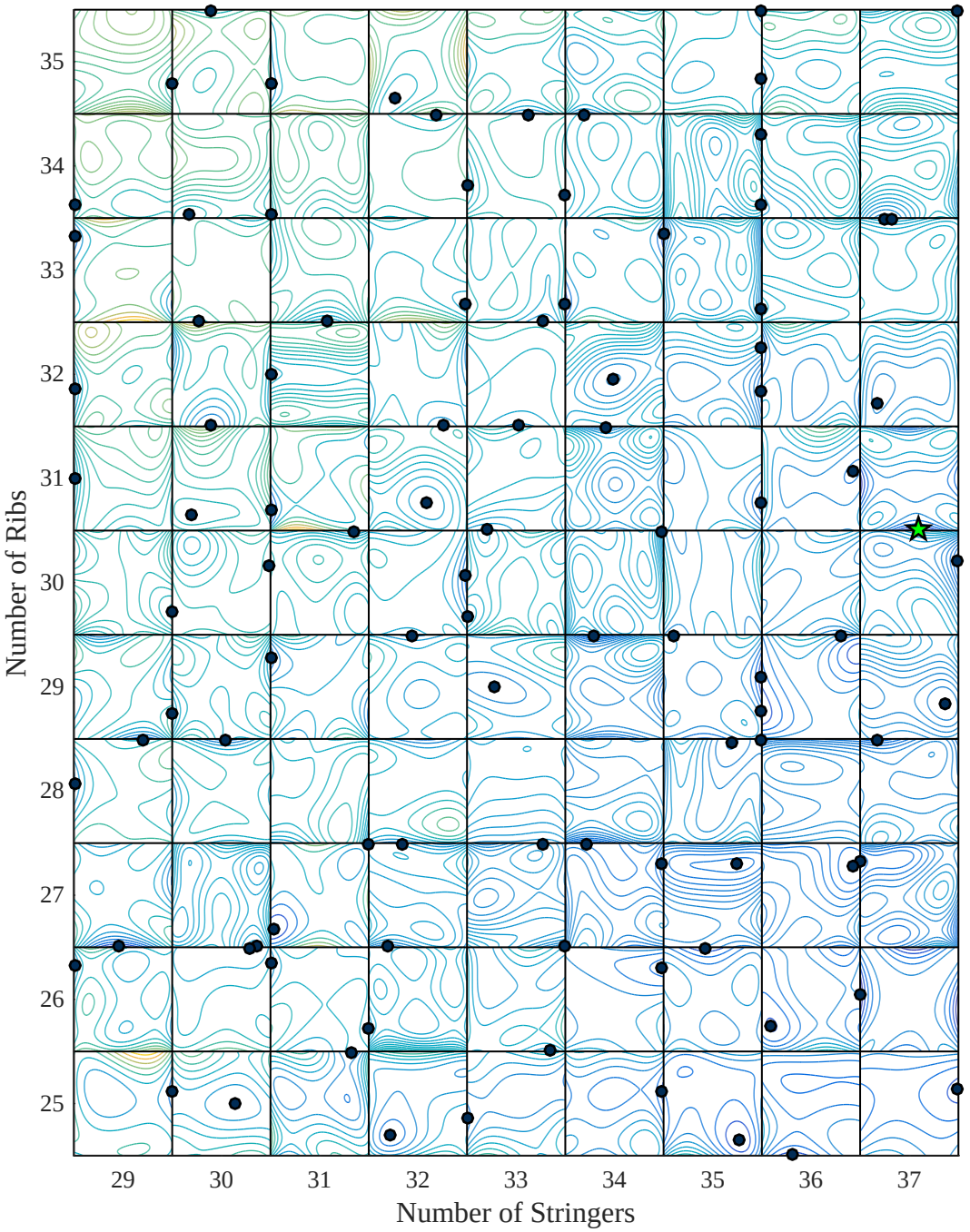


Figure 90: 2D Δ Total Wing Box Weight Contor Plots

The local minima for the Δ Total Wing Box Weight are located using the process discussed earlier. These minima are displayed on the contour plots of the RSEs shown in Figure 90. The x-axis and y-axis represent the continuous space for each

combination of the number of stringers and ribs respectively. The grid lines represent the discontinuity in the design space due to a change in the number of stringers or ribs. The RSEs are represented as the contours between the grid lines. The surrogate local minima are represented as blue dots except for the global optimum which is represented as a green star (ST=37, RB=31). The location of the global minimum is at the largest number of stringers which is consistent with Figure 83.

Figure 90 displays only a small portion of the local minima listed in Appendix B. The large number of local minima is due both to the fourth order equation required to represent the continuous spaces and also due to the discontinuities which create additional local minima on the boarders of each RSE. The large amount of local minima is consistent with the Research Observation listed in Chapter 2 and will likely present problems for the optimization algorithms tested in the next section.

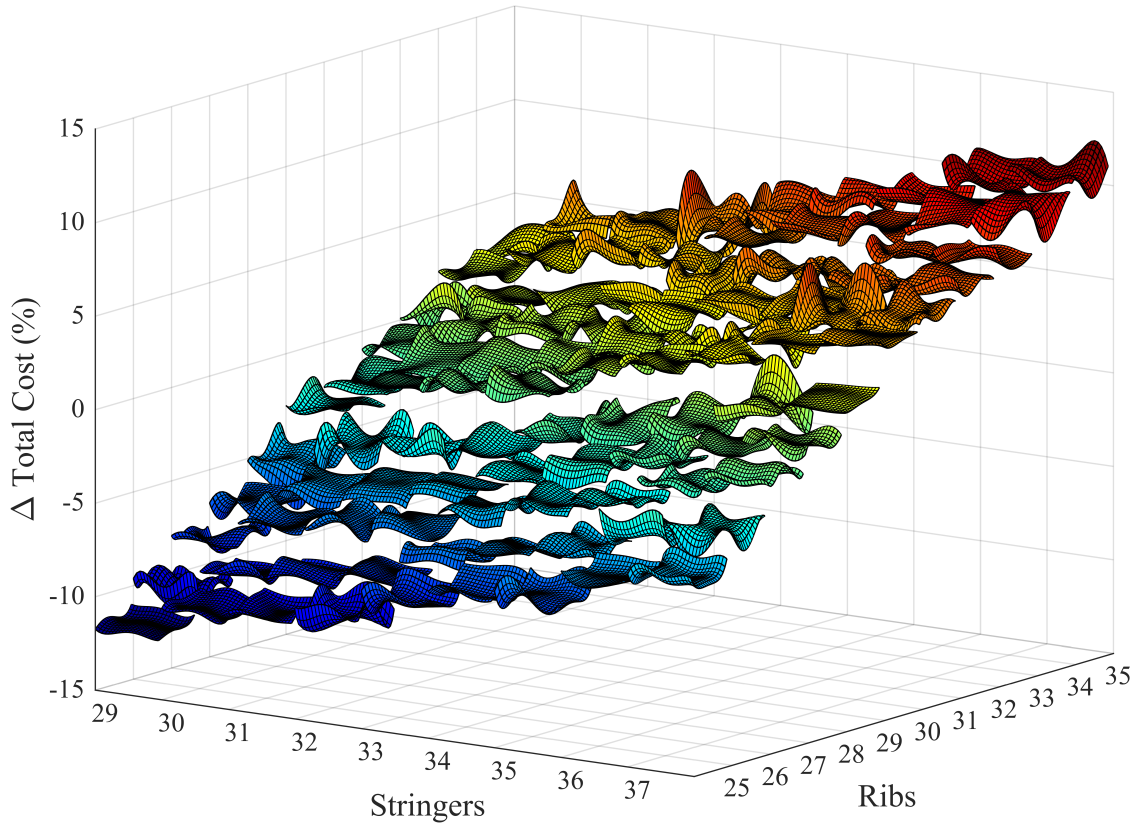


Figure 91: Δ Total Wing Box Weight Surface Plots

The surrogate models for the Δ Total Wing Box Cost are depicted in Figure 91 as surface plots. As with the Δ Total Wing Box Weight, all 99 RSEs that make up the design space are plotted in order to make observations about the overall trends of the design space. For the Δ Total Wing Box Cost there is an abvious trend where more parts is more expensive and less parts is less expensive. Another observation is that the continuous spaces are relatively flat between each discontinuity. This means that the change in spacing has little effect on the overall cost other than changing the number of ribs and stringers. These observations make sense intuitively as the cost is driven by the labor hours and the labor hours are driven by the number of parts. Any change in the size of the parts due to a change in the spacing is negligible as compared to the cost of an additional part.

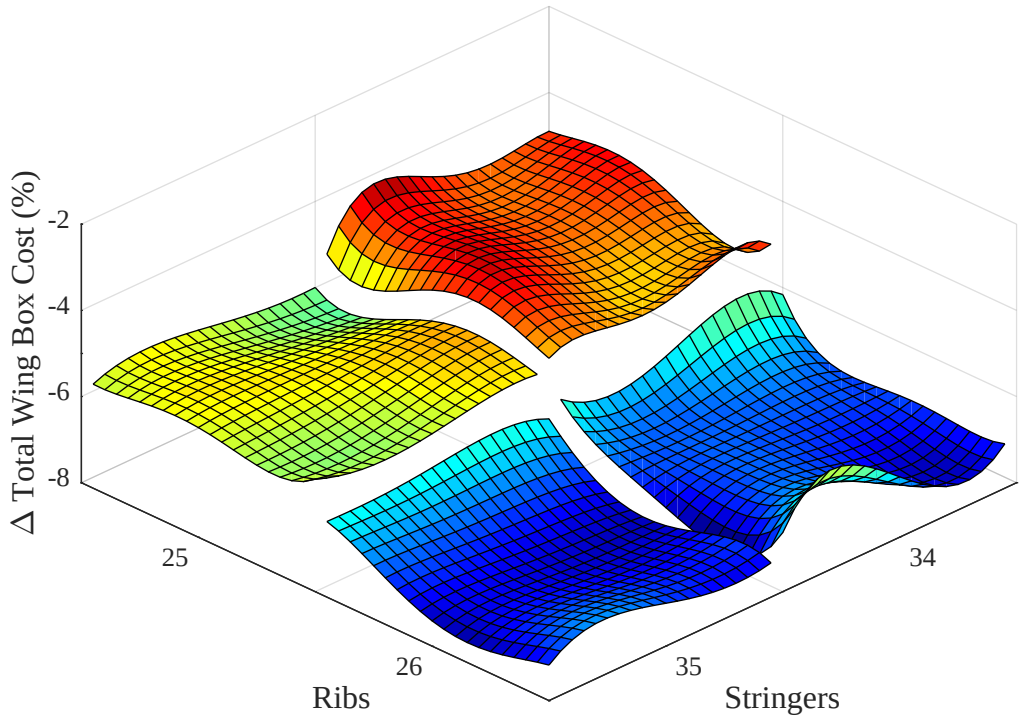


Figure 92: Δ Total Wing Box Weight Discontinuities

The effects of the discontinuities are easily observed in Figure 92. There are large jumps in the response and the gradients at each discontinuity. These jumps will make using gradient based optimization more difficult.

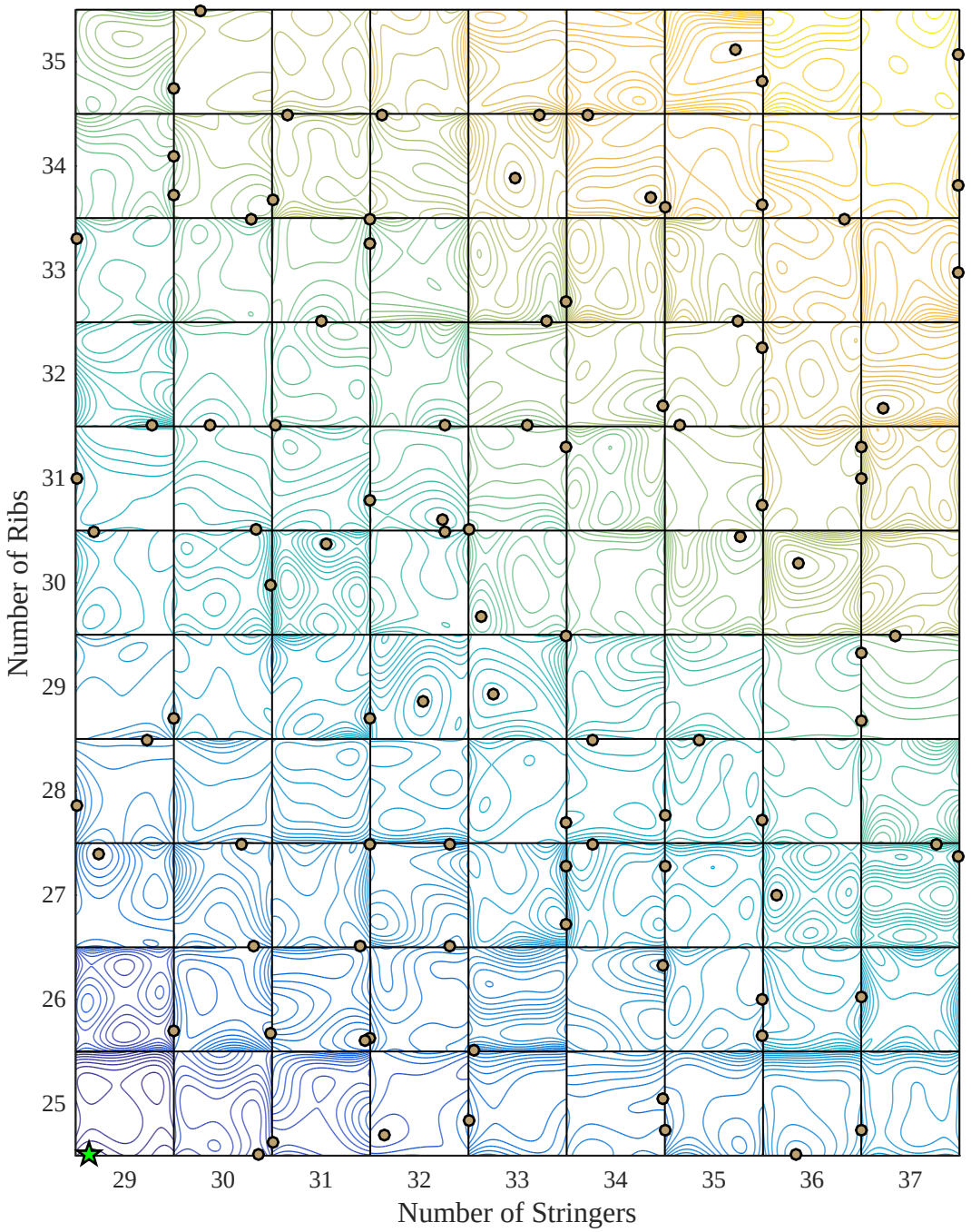


Figure 93: 2D Δ Total Wing Box Cost

The local minima for the Δ Total Wing Box Cost are displayed in Figure 93. The x-axis, y-axis, and grid lines are the same as Figure 90. The RSEs are again represented as the contours between the grid lines. The surrogate local minima are

represented as gold dots except for the global optimum which is represented as a green star (ST=29, RB=25). The Δ Total Wing Box Cost global minimum is at the fewest number of ribs and stringers which is consistent with Figures 80 and 86.

The same observations made for the Δ Total Wing Box Weight local minima also apply to the Δ Total Wing Box Cost local minima. However, because the wing box substructure design problem is a multi-objective problem the number of local minima essentially doubles.

### 8.3.4 Multi-Objective Optimization

The final portion of the design space exploration is to investigate the multi-objective design space using both the Δ Total Wing Box Weight surrogate and the Δ Total Wing Box Cost surrogate. The multi-objective optimization function uses the weighted sums function introduced in Equation 35. The equation will be modified to normalize the weight and cost values using the baseline weight ($W_0$) and cost ($C_0$) so that neither response dominates the solution (Equation 155).

$$F(X) = w_{weight} \times \frac{Weight(X)}{W_0} + w_{cost} \times \frac{Cost(X)}{C_0} \tag{155}$$

Where:

$$1 = w_{weight} + w_{cost} \tag{156}$$

An experiment is performed to identify the global optimum for several different weightings (Equation 156). The same process that was used to find the surrogate model local minima is used to identify the local minima of the combined Δ Total Wing Box Weight and Δ Total Wing Box Cost RSE for each set of discontinuities. Then, the surrogate local minima were compared to determine the multi-objective global optimum for the given weightings.

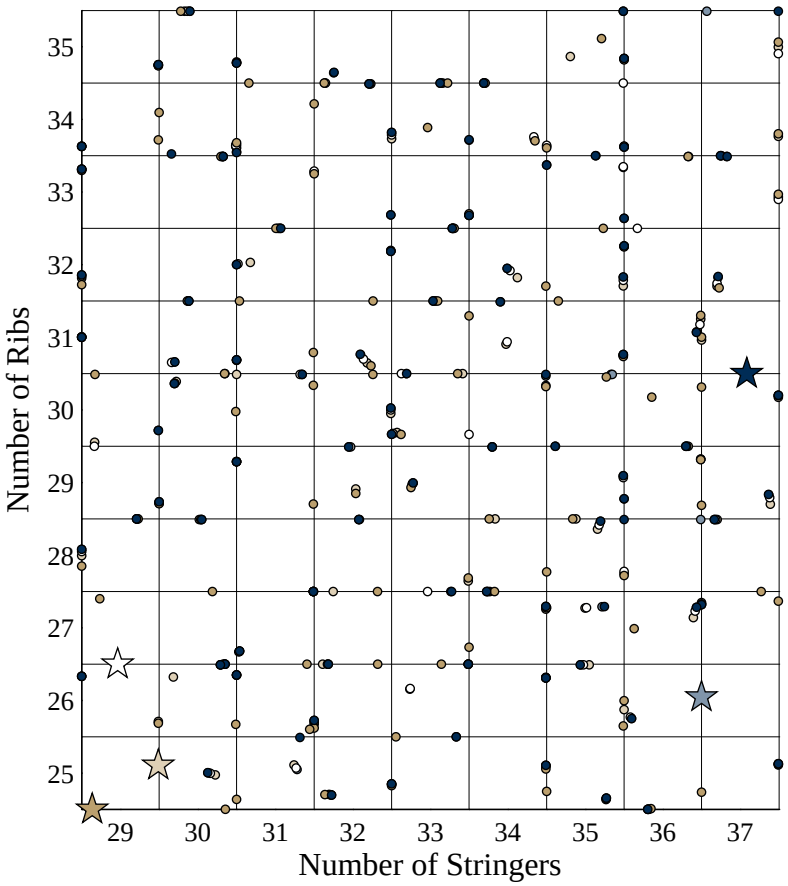


Figure 94: Multi-Objective Minima

The surrogate local minima (dots) and global minim (star) for different multi-objective weightings are shown in Figure 94. The color of the star corresponds to the weightings listed in Table 94 (i.e. dark blue is first option, light blue is second, white is third, light gold is fourth and dark gold is fifth). Figure 94 yields two observations. The first is that the multi-objective nature of the design problem significantly increases the number of local minima that must be explored in order to locate the global optimum. The second observation is that the optima, both local and global, move across the design space. For each RSE the location of the local minima shifts within the bounds. Also, the global optima shift across the entire design space drastically altering the optimized substructure configurations. Thus, the optimized wing box

substructure configuration is dependent on the trade between weight and cost.

The final global optimums are listed in Table 25. The first two columns identify the weightings used in the multi-objective function ($w_{weight}$, $w_{cost}$). The next two columns display the number of stringers and ribs. The third two show the final values of $\Delta$ Rib Spacing and $\Delta$ Stringer Spacing. The last two columns display the percent difference in weight and cost from the baseline weight and cost.

Table 25: Multi-Objective Global Minima

| $w_{weight}$ | $w_{cost}$ | Stringers | Ribs | $\Delta$ST | $\Delta$RB | $\Delta$ Weight % | $\Delta$ Cost % |
|---|---|---|---|---|---|---|---|
| 1.00 | 0.00 | 37 | 31 | -3.0644 | -5.7400 | -9.89 % | 4.77 % |
| 0.95 | 0.05 | 37 | 26 | -2.9300 | -2.9720 | -9.87 % | -4.16 % |
| 0.60 | 0.40 | 29 | 27 | -1.6849 | -3.3400 | -9.54 % | -7.50 % |
| 0.30 | 0.70 | 29 | 25 | -1.8371 | -2.0186 | -7.13 % | -11.03 % |
| 0.00 | 1.00 | 29 | 25 | -1.5900 | -1.2300 | -2.82 % | -11.52 % |

## *8.4 Optimization Experiments*

The final portion of Experiment 1 is to test the ability of several different optimization algorithms to locate the multi-objective global optima identified in Table 25. The purpose is to quantify the effect the discontinuities have on the optimization problem and to validate Framework Proposition 1. Each optimization algorithm will be repeated as necessary (i.e. different start points, larger population, etc.) in order to measure the hit rate (i.e. the likelihood of the algorithm to identify the global minimum) for each optimization algorithm so that the hit rate can be compared to the number of objective function calls.

### 8.4.1 Optimization Algorithms

Chapter 3 describes four types of optimization algorithms: search methods, gradient based methods, heuristic methods, and discrete methods. Of these four only gradient

based methods and heuristic methods will be tested as there are no discrete variables and search methods are known to perform worse than gradient based methods. Additionally, during Chapter 2 it was mentioned that the discontinuous nature of the design space will make the problem more difficult; thus, only one gradient based method will be tested as a proof of concept. The other methods tested will either be heuristic methods or a combination of heuristic and gradient based methods.

The following optimization algorithms are used in the optimization experiments:

**Sequential Quadratic Programming:** Sequential Quadratic Programming (SQP) is a constrained gradient based optimization algorithm that solves the search direction sub-problem using a quadratic approximation of the local objective function [204]. This algorithm was selected because it is a good representation of gradient based optimization methods.

**Genetic Algorithm:** Genetic Algorithm is a heuristic algorithm that mimics biological evolution [54]. A "population" of points is compared with only the best solutions being passed on to the next iteration. Additional evolutionary concepts such as reproduction and mutations are included to ensure that different alternatives are explored during each iteration.

**Particle Swarm Algorithm:** Particle Swarm Algorithm (PS) is a heuristic algorithm that mimics the behavior of a swarm [107]. A population of initial points is created that moves together across the search space. At each iteration the "swarm" moves with a direction and velocity based on the best solution from the previous iteration. The algorithm terminates once the swarm has no direction to go that improves the results.

***'GlobalSearch'* Algorithm:** 'GlobalSearch' is a commercial optimizer developed by MATLAB [133]. The optimization function combines heuristic search methods with a gradient based algorithm. This algorithm is included in the experiment to represent a hybrid algorithm that used both heuristic search methods and gradient based optimization.

### 8.4.2 Experiment Setup

The optimization algorithms will be used in the multi-objective optimization problem specified in Equation 155 using the previously created surrogate models. For this set of experiments the bounds of the optimization problem will include the entire design space and will not account for the discontinuities. Each algorithm will be tested with different weightings to account for the difficulty of both the weight and cost design spaces.

The SQP algorithm experiment needs to be executed differently from the other algorithms because it is a gradient based algorithm. While gradient based optimization mathematically guarantees finding a local minimum, there is no guarantee of finding the global optimum. Finding the global optimum becomes even more difficult due to the large number of local minimums identified in Appendix B. Thus, multiple initial conditions will be used to test the SQP algorithm.

Unlike gradient based methods, heuristic optimization does not mathematically guarantee that a local minimum will be found. However, heuristic optimization can find a close approximation of the global optimum through running a large number of cases and evaluating them for the minimum. Even still the minima identified by the GA and PS will likely not match the minima listed in Tables 25 exactly. Thus, the definition of finding the global optimum for the optimization experiments will be finding the correct number of ribs and stringers.

Each algorithm will be repeated multiple times to calculate the hit rate. The SQP

algorithm will be repeated 200 times with different initial points, and the while the GA and PS will be repeated 50 times with a different set of initial points each time. The hit rate will be calculated as the percentage of successes of all the runs, while the number of function calls will be the average of the number of function calls required for the algorithm to converge on a solution each time it is executed.

### 8.4.3 Optimization Experiments Results

The optimization results are listed in Tables 26 through 29. The first two columns of the table specify which multi-objective optimum is being tested ($w_{weight}$ and $w_{cost}$). The next two columns display the performance of the optimization algorithm in terms of the average number of function calls (F calls) and the hit rate percent (Hit Rate) for all the algorithm repetitions. The ST and RB columns specify the final substructure configuration determined by the optimization algorithm. The final two columns display the cost of missing the global optimum in terms of the change in weight ($\Delta$ Weight) and change in cost ($\Delta$ Cost) from the global optimum specified in Table 25.

Table 26: Sequential Quadratic Programming Results

| $w_{weight}$ | $w_{cost}$ | F Calls | Hit Rate | ST | RB | $\Delta$ Weight (lb.) | $\Delta$ Cost ($) |
|---|---|---|---|---|---|---|---|
| 1.00 | 0.00 | 92.43 | 3.0 % | 37 | 26 | 9.32 | -65573.10 |
| 0.95 | 0.05 | 93.31 | 5.5 % | 37 | 26 | 7.66 | 4549.04 |
| 0.60 | 0.40 | 96.56 | 0.0 % | 29 | 25 | 126.24 | -27483.03 |
| 0.30 | 0.70 | 91.10 | 22.5 % | 29 | 25 | 0.56 | 1.32 |
| 0.00 | 1.00 | 107.43 | 26.0 % | 29 | 25 | 0.02 | -0.01 |

Table 26 shows the results for the SQP algorithm. SQP algorithms are considered to be efficient at locating local minima; however, they do not guarantee that a global optimum is located (as the results show). The algorithm performed poorly for the given problem due to the large number of local minima. The hit rate is extraordinarily low despite the loose definition of finding global optimum. The SQP performance is

similar to the expected performance for a random search algorithm.

There are several benefits of the SQP algorithm. When the algorithm converges on the correct configuration (i.e. ST and RB) there are still several different local minima within the configuration; however, by locating a local minimum the SQP algorithm minimized the difference in weight and cost from the global optimum. Additionally, the SQP algorithm required a low number of function calls required to converge on a solution. However, executing even 100 objective function calls may become computationally burdensome to exploring the wing box substructure configuration design alternatives in the absence of surrogate models. Thus, the poor performance of the algorithm outweighs the benefits.

Table 27: Genetic Algorithm Results

| $w_{weight}$ | $w_{cost}$ | F Calls | Hit Rate | ST | RB | $\Delta$ Weight (lb.) | $\Delta$ Cost ($) |
|---|---|---|---|---|---|---|---|
| 1.00 | 0.00 | 3692.00 | 0.0 % | 37 | 26 | 1.68 | -70123.47 |
| 0.95 | 0.05 | 3616.00 | 24.0 % | 37 | 26 | 0.02 | 1.11 |
| 0.60 | 0.40 | 3504.00 | 4.0 % | 29 | 27 | 0.00 | 0.75 |
| 0.30 | 0.70 | 3234.00 | 100.0 % | 29 | 25 | 0.56 | 1.09 |
| 0.00 | 1.00 | 3018.00 | 100.0 % | 29 | 25 | 0.00 | -0.02 |

The results for the GA are shown in Table 27. The hit rate for the GA algorithm is significantly improved over the SQP algorithm. For the final two multi-objective global optima the GA had a 100% hit rate. For all the other global optima the hit rate is still significantly lower than desired. The increase in hit rate came at the cost of the number of function calls. Additionally, the GA does not guarantee a local minimum is found; thus, the difference in weight and cost from the global minima is much higher for the GA algorithm.

Table 28: Particle Swarm Results

| $w_{weight}$ | $w_{cost}$ | F Calls | Hit Rate | ST | RB | Δ Weight (lb.) | Δ Cost ($) |
|---|---|---|---|---|---|---|---|
| 1.00 | 0.00 | 747.20 | 0.0 % | 37 | 26 | 22.49 | -68055.30 |
| 0.95 | 0.05 | 788.00 | 84.0 % | 37 | 26 | 12.66 | 570.71 |
| 0.60 | 0.40 | 1321.60 | 0.0 % | 29 | 25 | 126.23 | -27482.03 |
| 0.30 | 0.70 | 559.20 | 100.0 % | 29 | 25 | 0.56 | 1.03 |
| 0.00 | 1.00 | 582.40 | 100.0 % | 29 | 25 | 0.00 | -0.02 |

The Particle Swarm algorithm performs more efficiently than the GA algorithm despite both being a heuristic algorithm. The difference in weight, the difference in cost, and hit rate are similar for both the GA algorithm and PS algorithm, but the number of function calls is reduced for the particle swarm optimization. The reduction in function calls is likely due to the directional nature of the PS as opposed to the sequential nature of the GA. Despite the reduction in function calls, the PS algorithm still required a large number of function calls to achieve the high hit rate.

Table 29: 'GlobalSearch' Results

| $w_{weight}$ | $w_{cost}$ | F Calls | Hit Rate | ST | RB | Δ Weight (lb.) | Δ Cost ($) |
|---|---|---|---|---|---|---|---|
| 1.00 | 0.00 | 4020.20 | 0.0 % | 29 | 27 | 20.66 | -96274.27 |
| 0.95 | 0.05 | 5044.90 | 80.0 % | 37 | 26 | 3.16 | 408.04 |
| 0.60 | 0.40 | 5307.20 | 10.0 % | 29 | 27 | 0.04 | -7.44 |
| 0.30 | 0.70 | 3745.80 | 100.0 % | 29 | 25 | 0.56 | 1.20 |
| 0.00 | 1.00 | 3512.40 | 100.0 % | 29 | 25 | -0.01 | 0.00 |

The 'GlobalSearch' algorithm exhibits benefits from both the heuristic algorithm and gradient based algorithm. The 'GlobalSearch' algorithm achieves a high hit rate (like the heuristic algorithm), and also achieves minimal difference in weight and cost (like the SQP algorithm). The cost of the improved results is that the number of function calls increases substantially. It required several thousand function calls

to locate the global optimum; however, it did not always find the global optimum. Meanwhile, the 2D design space exploration required 4851 analysis cases to develop the surrogate models which guarantee an approximation of the global optimum is found. Therefore, the function 'GlobalSearch' is considered to be less efficient than design space exploration.

## *8.5 Summary*

This Chapter used experimentation to perform a 2D design space exploration and to test the performance of different optimization algorithms. First, a 1D study of the design space was used to locate all the discontinuities and scope the ranges to a region of interest. Next, surrogate models of the 2D design space were created using 99 RSEs per to map the continuous space between the discontinuities for both the wing box weight and cost. Then, the surrogates were combined in a multi-objective function to locate the overall global minima for different weightings by comparing all of the local optima from each of the 99 RSEs. Finally, the surrogates were used to test several optimization algorithms ability to locate each of the global minimum for different multi-objective weightings.

The results of the 2D design space exploration confirm the logic used to create Framework Proposition 1. Research Observation 4 (i.e. multimodal design space), Research Observation 5 (i.e. multi-objective design problem), and Research Observation 6 (discontinuous design space) were all made independently based upon simple experiments. The experiments in this chapter were more robust and a better representation of the substructure design problem. The large number of local minima documented in Appendix B illustrate that a large number of design alternatives exist that need to be explored.

The result of the multimodal nature of the design space and the discontinuities result in a design space that is difficult to locate the global optimum. This is best

illustrated in the results of the optimization experiments. The linear optimization algorithm (i.e. SQP) had difficulty locating the global optimums identified by the 2D design space exploration. The reason SQP had difficulties is two part. First the discontinuities create large jumps in the responses as well as the gradient. These discontinuities in the gradient can result in the algorithm going in the wrong direction with respect to the global optimum due to SQP reliance on the gradient to select the direction of the next point. The second reason for the difficulties is that there exist over 400 unique local minima. SQP can guarantee that a local minimum is found. However, it does not guarantee that a global optimum has been found. Even though 200 different initial points were tested the SQP algorithm found the global optimums in a low percent of attempts.

The purpose of the experiments in this chapter was to test Framework Proposition 1 by establishing a correlation between the number of analysis executions (i.e. function calls) and the success of finding the global optimum. While the SQP struggled to locate the global optimum, the other algorithms located the global optimum more consistently. There are two reasons for the success of these algorithms. The first is that these algorithms do not rely on the griadients so the discontinuities did not impact the results. The second is due to their increased number of function calls: the GA evaluated the objective function around 3000 times, the PS evaluated over 500 function calls, and the 'GlobalSearch' used between 3500 and 5300 function calls. The SQP evaluated the objective function only 100 times per initial condition. However, it is important to note that none of the other algorithms guaranteed that the global optimum was found. To guarantee that the global optimum is found a strategy of exploration should be used focusing on a large number of evaluations. Thus, Framework Proposition 1 is supported.

**Conclusion 1**

The complex and discontinuous nature of the physics-based structural analysis design space requires a large number of analysis executions to differentiate between the numerous design alternatives.

The experiments in this chapter also tested Framework Proposition 2. Using SPANDSET proved to be an important factor in performing the 2D design space exploration. Hundreds of cases were required to locate the discontinuities and thousands of cases were required to create the RSEs. The computational costs to execute these cases would be too burdensome if higher fidelity FEA tools were used. By using classical analysis methods SPANDSET provided computationally efficient enough to explore the large number of alternative in a timely manner. Therefore, Framework Proposition 2 is supported.

**Conclusion 2**

Using classical structural analysis methods to solve the structural analysis subproblem enabled a strategy of exploration so that a large number of analysis executions could be tested.

One final observation is that the 2D design space exploration was set up to simplify the design space. There exist many variables of interest in substructure design, as well as the discontinuous design decisions, beyond the two that were investigated. Several of these variables will affect the outcome of the location of the discontinuities and so it will be non-trivial to locate these discontinuities. The strategies used in the 2d design space exploration would not be possible if the location of the discontinuities had not been previously known. Additionally, none of the algorithms could guarantee finding a global optimum for any of the simplified 2D multi-objective optimization cases. If the

optimization algorithms could not guarantee that the global optimum is found, then it is unlikely that optimization will work for larger design problems. Thus, it is likely that design space exploration will be the best option for wing box substructure design problems going forward; however, further testing is required before any conclusions can be made.

# CHAPTER IX

# DESIGN STUDIES

Thus far in this thesis dissertation the underlying theories behind SPANDSET have been supported through experimentation. This chapter will compare SPANDSET to best practices methods by performing design studies to both validate the results of SPANDSET as well as address Research Objective 4.

---

**Research Objective 4**

Test the developed methodology against previously used methods that use historical regressions to draw conclusions on using physics-based analysis in the conceptual design phase.

---

Three models will be compared in this chapter: SPANDSET, a Finite Element Analysis (FEA) wing box substructure model, and semi-empirical weight-based methods for wing weight estimation. Ideally, one experiment would be performed to compare the results of the three models; however, there are limitations for both the FEA model and weight-based methods that make this impractical. The weight-based model does not account for the substructure like the FEA model and SPANDSET; thus, there is no way to compare the substructure layout design variables between the weight-based method and the other two models. The FEA model is set up so that only one wing OML configuration is used; thus, there is no way to compare the wing planform design variables between the FEA model and the other two models. Therefore, two design studies are required: one to compare the FEA model and SPANDSET, and the other to compare SPANDSET and the weight-based methods. These experiments will be

based off a baseline case that is a variation of the Boeing 737.

## *9.1 Finite Element Analysis Design Study*

The FEA model uses a suite of commercial software to perform structural analysis and sizing optimization of a wing box substructure. A finite element model of the wing box is created and analyzed using MSC.NASTRAN/PATRAN [146,147]. The finite element model is loaded into HyperSizer [96]. HyperSizer is a computer aided engineering software interface for the optimization of composite and metallic structures. The wing box finite element model consists of the wing spars, ribs, and skin panels. The stringers are smeared into the skin panels using HyperSizer. HyperSizer executes the NASTRAN analysis for the external and internal loads, performs sizing optimization of several variables, and iterates so that the aeroelastic loop can be closed. The final result of the FEA model is a breakdown of the wing box weight by major components (i.e. spars, ribs, skin panels, and stringers).

Fidelity is defined in Chapter 3 as the level at which the structural analysis represents the physics of the system. This experiment compares two models with different fidelity: the higher fidelity FEA model and the lower fidelity SPANDSET. The difference in fidelity will result in an error between the responses of the models for the same inputs. The purpose of this experiment is to measure the error due to the different fidelity of the two models.

### 9.1.1 Modeling & Simulation Input Error

There are two sources of errors between the responses of the models: the error due to the inputs and the error due to fidelity. The purpose of this experiment is to measure the error due to the difference in model fidelity; thus, the error due to inputs needs to be minimized as much as possible.

There are two sets of inputs required by SPANDSET that could create an error in the weight: the wing and wing box substructure geometry and the external loads.

Several steps were taken to minimize the error due to the inputs. These steps are described below.

#### *9.1.1.1 Geometry Error*

To compare the results of SPANDSET with the results of the FEA model, the geometric data of the FEA model has to be recreated in SPANDSET. However, the geometry model used in the FEA model could not be matched exactly by the parametric geometry model used in SPANDSET. The difference in geometry models will result in differences in the geometric data used for structural analysis and thus there will be an error in the SPANDSET weight due to the geometric data.

A reason for the difference is the purpose of each model. SPANDSET was built to be a parametric M&S environment that can model a wide variety of wing shapes and sizes; therefore, several assumptions needed to be made in order to make the tool automatic, rapid, and robust. The FEM model was built to analyze a single wing configuration using a CAD program and only the substructures were parameterized so that the effect of the wing box substructure configuration can be studied. The resulting FEM model requires fewer assumptions be made and contains more user specified details that can not be recreated in SPANDSET. The geometric data from the FEA model was extracted from 2D drawings of the baseline geometry. Then, the extracted points were used to estimate inputs for the parametric geometry model in SPANDSET to reduce the error due to the geometric data.

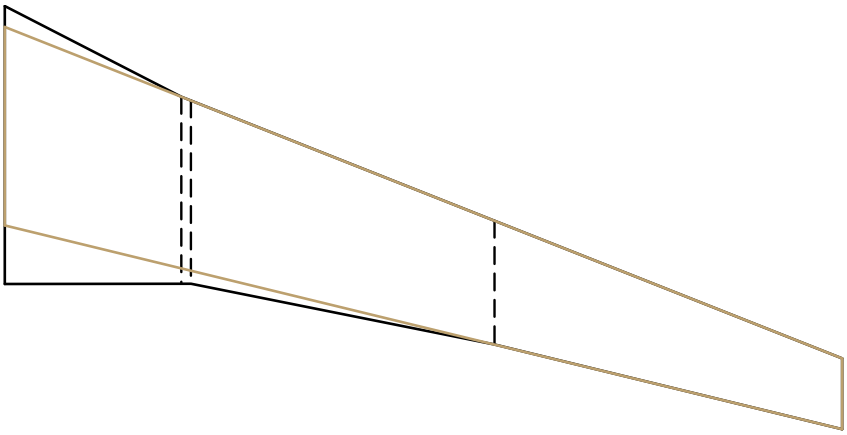

Figure 95: Geometry Error (Planform)

There are three sources for the error due to the geometric data: the wing planform, the airfoils, and the wing box. Figure 95 illustrates the different wing planform used by the FEA model (black) and SPANDSET (gold). The wing model used for FEA analysis is a multi-section wing with several breaks in the leading edge and trailing edge. One of the assumptions made by SPANDSET is that the wing is a single section. To rectify the difference the inputs for SPANDSET are selected so that the leading edge and trailing edge match those of the outboard section of the FEA model.

The FEA wing OML is defined using one airfoil across the entire span. The airfoil coordinates are normalized by the chord ($t/c$, $x/c$); this is also how the parametric geometry model defines airfoils. However, the airfoil heights are affected by the chord lengths which differ between the two geometry models due to the planform errors. A solution is to input different airfoil geometries ($t/c$, $x/c$) into SPANDSET based upon the wing OML of the FEA model. Thus, airfoils were created for SPANDSET at the root, tip, and at every break in the leading edge or trailing edge (i.e. the dotted lines in Figure 95) using the FEA OML. In the parametric geometry tool the third dimension of the wing OML ($WL$) is calculated through linear interpolation; therefore, the airfoils input into SPANDSET should reduce the error due to the airfoils to nearly zero.

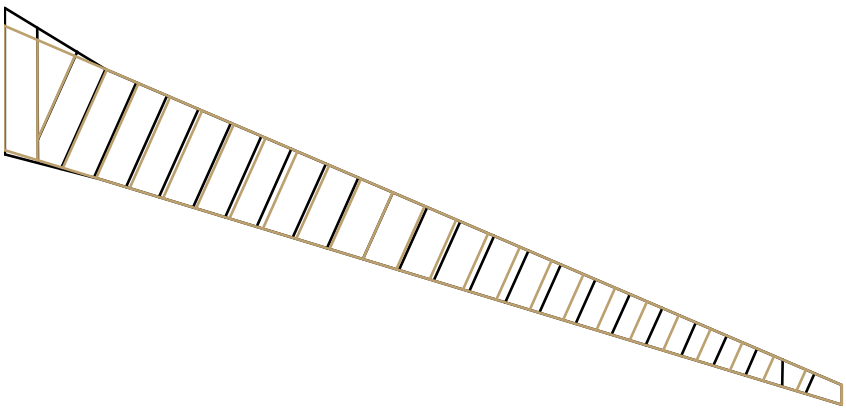

Figure 96: Geometry Error (Wing Box)

SPANDSET makes several assumptions to reduce the dimensionality of defining the wing box substructure. The FEA model does not have the same limitations; thus the following assumptions are not applied to the FEA geometry: even spacing between similar ribs, similar ribs are parallel, and no kinks in the spar. Figure 96 shows the two wing box substructure geometries used by the FEA model (black) and SPANDSET (gold). The different geometries result in errors in the spar lengths and wing box area (i.e. upper and lower cover areas) due to the spar kinks, as well as errors in the total rib lengths due to uneven spacing and a non-parallel rib.

Neither SPANDSET nor the FEA model account for the weights of the secondary structures (e.g. leading edge, trailing edge, control surfaces, winglet), so the error in the planform geometry can be ignored. Also, the airfoil geometry error has been sufficiently minimized. Therefore, the differences in the wing box geometries will be the only source of error that will affect the weight of the primary wing box structure. The differences in the lengths and area are the only source of error in the wing box substructure; thus, it can be assumed that the differences in the weights produced by the FEA model and SPANDSET will be proportional to the differences in the lengths and area. The differences in the lengths and area are measured using the extracted points and the outputs of the parametric geometry model. The resulting errors (Table

30) will be applied to the SPANDSET weight breakdown to account for the differences in the geometry.

Table 30: FEM Experiment Weight Errors

| Spar Error | Rib Error | Cover Error |
|---|---|---|
| 0.51 % | 1.89 % | 1.60 % |

#### *9.1.1.2 External Loads Error*

The external loads are created differently in the FEA model than the method used in SPANDSET (Chapter 6). The external loads calculation for the FEA model leverages the advantages that are inherent to FEA. A CAD drawing is used to create a mesh which is run through higher fidelity double lattice panel method analysis. The CFD results are then distributed among the structure mesh to apply the external loads without need to calculating the VMT data. Fortunately, an earlier iteration of the FEA model did not incorporate CFD analysis, and instead used AVL to generate VMT data. The wing geometry is the same for both the AVL results and the CFD results; thus, the AVL VMT data can be plugged directly into SPANDSET as a substitute for the CFD generated external loads. Any errors in the weight that result from the difference in loads data due to the use of AVL versus CFD will be considered part of the model fidelity error.

An additional source of error due to the external loads is that the FEA model includes the 3D deformation of the wing and the aeroelastic effects. SPANDSET does not include the capability to model the deformations in 3D; thus, it can not include the aeroelastic effects. This portion of the error due to the loads is directly related to the fidelity of the model and therefore the error due to the aeroelastic effects are considered to be part of the model fidelity error.

### 9.1.2 Measuring Model Fidelity Error

There are many possible sources of error when dealing with lower fidelity models such as: the equations do not accurately represent a physical phenomenon, the model made too many simplifying assumptions, or the dimensionality of the problem is reduced so that the actual behavior cannot be captured. The end result will be a significant difference in both the magnitude and form of the model responses. The differences can be expressed in terms of the scale of the model ($\gamma$) and the fidelity error ($\epsilon$). Accounting for the difference in scale of the model is relatively simple to account for as a scaling factor can easily be applied to low fidelity models based upon comparison to high fidelity models; however, the fidelity error is much more difficult to fix. If the fidelity error is large then it is likely that any design or optimization results will differ from results using higher fidelity analysis; therefore, it is important to make sure that the fidelity error is reasonably small.

The experiment for measuring model fidelity error is based off variable fidelity analysis methods. Variable fidelity analysis is a common solution to multi-fidelity problems and seeks to adjust the values of less costly lower fidelity analysis methods to match the results of computationally expensive higher fidelity analysis methods based off a small number of samples of the higher fidelity analysis [3]. There exist several scaling methods for variable fidelity analysis that can be used in this experiment to measure the error due to fidelity [79].

The scaling method selected to measure the fidelity error is based on a computational method for reliability assessment [175] which creates a reliability assessment parameter (Equation 157) to quantify the reliability of the model to represent the experimental data. This method was chosen because it is relatively simple and is not based on Hypothesis testing. However, this method only seeks to address how reliable a model is for a given error (i.e. measure $\gamma$). For the experiment, Equation 157 is modified so that the error can be measured through experimentation for a given

reliability.

$$r = Pr(-\epsilon < D < \epsilon) \tag{157}$$

The experiment will proceed as follows. Surrogate models of the low fidelity and high fidelity model will be created to compare the difference in the model responses. The model response of interest is the total wing box weight and will be mapped across the design variables and ranges in Table 31. The total wing box weight for SPANDSET will be adjusted using the errors in Table 30.

Table 31: FEA Experiment Design Variable Ranges

| Variables | Min | Max |
|---|---|---|
| Rib Spacing | 21.5 | 41 |
| Upper Stringer Spacing | 5 | 12 |
| Lower Stringer Spacing | 5 | 12 |

The resulting surrogate models will be used in Monte Carlo Simulation [145] to estimate the distribution for the difference in the model responses (Equation 158). The fidelity error ($\epsilon$) will be estimated using the 95% prediction interval of the distribution (Equation 160).

$$D = Y_{high} - Y_{low} \tag{158}$$

$$E = \frac{D}{Y_{low}} \tag{159}$$

$$95\% = Pr(\bar{E} - \epsilon_l < E < \bar{E} + \epsilon_h) \tag{160}$$

Additionally, the surrogate models will be used to perform optimization on the weight responses. The purpose will be to compare the final design variable values and draw conclusions based upon the outcome of the average difference ($\bar{D}$) and the fidelity error ($\epsilon$).

### 9.1.3 Results

Due to the discontinuous nature of the design space both surrogate models are made with Automated Neural Nets (ANN). Both the high fidelity and low fidelity ANNs represented the weight responses adequately ($R^2 = 0.97$ and $|\epsilon| < 2\%$).

The surrogate models were used to perform Monte Carlo Simulation. The experiment created 50,000 random points for each surrogate model. The 50,000 points all lie within the ranges in Table 31 offset by 1 inch (to account for surrogate errors at the edges). The error between the models was calculated for each point using Equation 159 to generate the distribution shown in Figure 97.

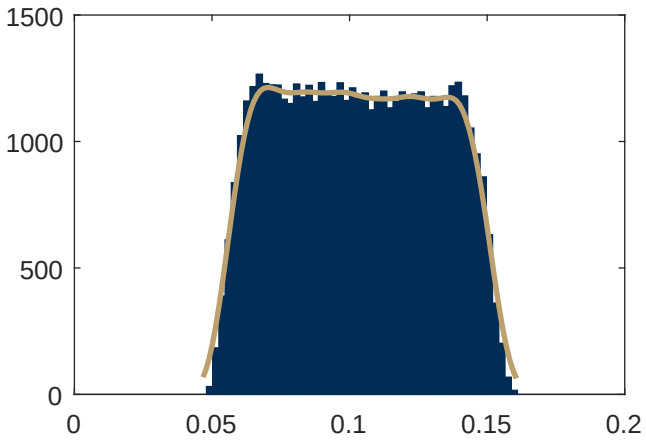


Figure 97: Fidelity Error Distribution

These results were input into a commercial statistics software package called JMP [101]. Using JMP the mean and 95 % prediction interval of the error was calculated. These values were then used to calculate the upper and lower fidelity errors in Table 32

Table 32: Multi-Fidelity Error

| | |
|---|---|
| Mean Error ($\bar{E}$) | 10.33 % |
| Upper Prediction Interval (95 %) | 15.77 % |
| Lower Prediction Interval (95 %) | 4.89 % |
| Upper Fidelity Error ($\epsilon_u$) | 5.44 % |
| Lower Fidelity Error ($\epsilon_l$) | 5.44 % |

The mean error is 10.33 % which is easily accounted for by applying a 10.33 % scaling factor to the calculated weight; however, the 5.44 % fidelity error is not easily accounted for. This error is a measure of the difference due to the form of the surrogate models and is likely due to some physical phenomenon not being accounted for by the lower fidelity model.

An optimization experiment is carried out to measure the effect of the fidelity error. For each surrogate model the previously mentioned 'GlobalSearch' algorithm is used to find the design variables that minimize the weight.

These results are shown in Table 33. The first column represents the FEA model, the second column represents SPANDSET, and the third column is the difference between the first and second column. The first three rows display the final optimized design variables for both surrogate models, the next three rows display the configuration information (i.e. number of ribs and stringers), and the last two represent the difference in the weight calculated by the surrogate models and the difference in weight after the scaling factor is applied. The FEA model is taken from proprietary research; thus, the weight values are left out.

Table 33: Multi-Fidelity Error

| | FEA | SPANDSET | Δ Values |
|---|---|---|---|
| Rib Spacing | 26.39 | 27.53 | -1.14 |
| Upper Stringer Spacing | 6.14 | 5.56 | 0.58 |
| Lower Stringer Spacing | 5.00 | 5.00 | 0.00 |
| Number of Ribs | 25 | 25 | 0 |
| Number of Upper Stringers | 14 | 15 | -1 |
| Number of Lower Stringers | 18 | 18 | 0 |
| Total Weight | - | - | 16.65 % |
| Scaled Total Weight | - | - | 6.32 % |

The weight results in Table 33 reflect the effect of the fidelity error on the optimization problem. Even though the error due to fidelity is 5.44 %, the error between the total weights (after the scaling factor is applied) is greater. The increase in error is because the fidelity error affects the form of the models as well as the accuracy. With different forms the models converge on different design variables. Therefore, the error in weight is due to the fidelity error and the difference in the optimized design variables.

Despite the difference in the weights, both optimization executions converged on similar substructure configurations (i.e. same number of ribs and stringers). Despite over 16% error in the weight the configurations only differed by 1 upper stringer.

### 9.1.4 Conclusion

This experiment sought to capture the effect of fidelity on two wing box substructure design models. Two important observations are made after the experiment has been performed. First, SPANDSET executed much faster than the FEA model. A single SPANDSET execution only required 25 minutes while an FEA execution took over an hour. This is consistent with what was proposed in Chapter 4. The large difference in execution time means that SPANDSET is better suited for use during early conceptual design.

The second observation is that the difference in fidelity caused a large difference in the total weight calculated by the model. These differences are so large that it raises concerns over the validity of SPANDSET. However, for the optimization SPANDSET returned nearly the same configuration as the FEA model despite the large differences in weight. This is an important outcome as SPANDSET is a design tool for early conceptual substructure design configuration. The final weight value does not matter as much as the final substructure configuration. A multi-fidelity strategy can easily be used to correct for the difference in weight after SPANDSET has formulated the initial configuration layout. Thus, the following conclusion is made about structural design methods that use classical analysis routines.

---

**Conclusion 3**

Despite the error in the calculated weight, Classical Analysis methods should be considered a viable option in future conceptual level structural design problems due to the lower run time and the ability to converge on the correct configuration.

---

## *9.2 Weight-Based Methods Design Study*

The overall research objective for this thesis is to develop a physics-based structural design method to incorporate new concepts, technologies, and materials into the

conceptual design phase. Chapter 1 listed the motivations for replacing methods that use weight-based historical regressions with methods that use physics-based structural analysis. Thus far, this thesis has developed a method to perform physics-based structural analysis, tested the underlying hypotheses used to develop the M&S environment, and validated the M&S environment against current state of the art. This final experiment will compare the proposed physics-based method against a weight-based method to illustrate the advantages of using physics-based analysis and validate the purpose of this thesis.

There exist two different methods for wing weight estimations. The first method involves using historical regressions to estimate the entire aircraft weight and then break down total aircraft weight into the components [174, 178]. The second method is an analytical-empirical method that attempts to estimate the required material to withstand the bending based upon empirical relationships and load distributions [202]. The second method is more sensitive to design parameters than the first; therefore, this method will be used for the experiment.

The physics-based model (i.e. SPANDSET) will be compared with an established system of computer programs called Flight Optimization System (FLOPS) [138]. FLOPS consists of several disciplinary specific modules. The only modules of interest to this experiment are the weights module and the aerodynamic module. The weight module used both of the previously discussed methods for wing weight estimation. It first uses empirical equations to predict the weight of each component group. Then it performs the more analytical estimate of the material required to resist bending [139]. The aerodynamic information required to estimate the bending moments is derived from parametric lift configurations.

FLOPS also integrates an additional module called Aircraft Life Cycle Cost Analysis (ALCCA) [77]. This module can estimate the aircraft manufacturing costs based upon data from FLOPS. Specifically, ALCCA can estimate the total manufacturing

cost and raw material cost of an airplane wing for a given materials (i.e. aluminum, composite, and titanium) based upon ratios used. For this experiment the wing will be all aluminum so the ratios do not need to be calculated.

### 9.2.1 Experiment

The experiment will proceed similar to the previous experiment. Surrogate models for both the physics-based and weight-based models will be created using the design variables in Table 34. One key difference between the two models is that weight-based models only represent the wing size and typically do not include substructures; thus the design variables for the physics-based model will include the wing size parameters (area and span) and three substructure variables (rib spacing, upper stringer spacing, and lower stringer spacing) while the weight-based method will only include the wing size parameters. The baseline case will once again be a variation of the Boeing 737.

Table 34: Weight-Based Experiment Design Variables

| | SPANDSET | | FLOPS | |
|---|---|---|---|---|
| Wing Area | 134390 | 164260 | 134390 | 164260 |
| Wing Span | 530 | 648 | 530 | 648 |
| Rib Spacing | 21.5 | 41 | - | - |
| Upper Stringer Spacing | 5 | 12 | - | - |
| Lower Stringer Spacing | 5 | 12 | - | - |

The response will be estimates for the total wing box weight and the total wing box manufacturing cost. To generate the weight FLOPS will used the weight module to compute the weights only (IANA = 1). The wing weight is broken down into three terms: the weight required to resist bending, the weight due to the spars, ribs, and

control surfaces, and miscellaneous weight. Ideally, the first and second term would both be used. However, there is no way to isolate the control surfaces from spar and rib weight; therefore, the first term will be used and a scaling factor will be applied to account for the rib and spar weights.

As previously mentioned FLOPS estimates the wing loads through an assumed load distribution and empirical relationships. SPANDSET, which requires more detailed VMT data, will have to use AVL to generate the external loads for the different wing sizes.

The surrogate models are created similar to previously discussed experiments. Firsta design of experiments is executed for each model. The the models are fit using the same methods as previous experiments. The FLOPS surrogate model for total wing box weight and total wing box cost are represented with a 2nd order Response Surface Equation ($R^2 > 0.99$ & $|\epsilon| < 0.01\%$ for both weight and cost), while the SPANDSET surrogate model took the form of an ANN. SPANDSET's total wing box weight surrogate model was fit easily ($R^2 = 0.97$ with $|\epsilon| < 2\%$); however, the total wing box cost required additional executions before an acceptable fit was achieved ($R^2 = 0.95$ with $|\epsilon| < 5\%$).

The surrogate models are then used in Monte Carlo simulations. The two models will be compared by plotting several random points on the weight-cost axes. These scatter plots are expected to yield several observations with regard to the advantaged of physics-based analysis.

### 9.2.2 Results

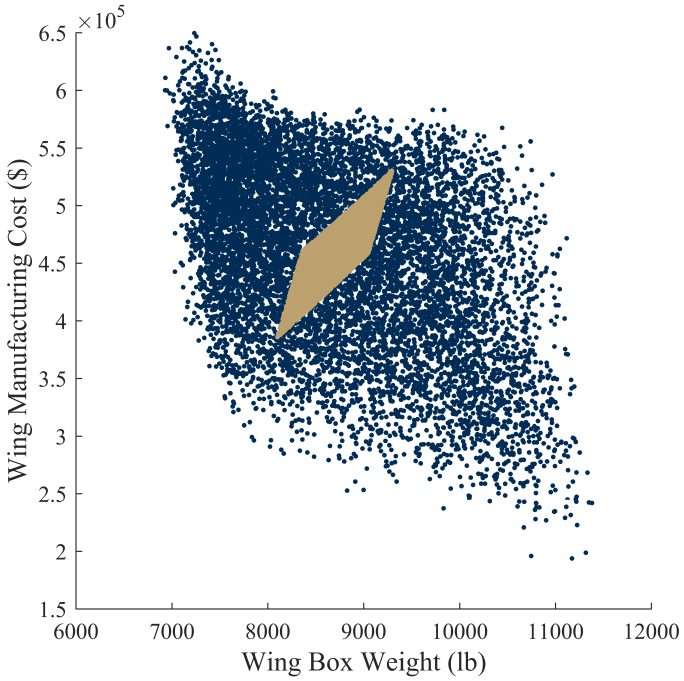


Figure 98: Pareto Frontier Scatter Plot

The results of the Monte Carlo Simulation are shown in Figure 98. The gold points represent the FLOPS results and the blue points represent the SPANDSET results. The figure shows that a much larger portion of the design space is investigated by SPANDSET. The maximum and minimum values are shown in Table 35 along with the correlation between weight and cost.

Table 35: Weight-Based Experiment Design Variables

| | max(Weight) | min(Weight) | min(Cost) | max(Cost) | corr(W,C) |
|---|---|---|---|---|---|
| FLOPS | 9295.86 | 8100.51 | 530314.99 | 6675.74 | 0.85 |
| SPANDSET | 11381.15 | 6928.59 | 649537.26 | 193842.94 | -0.48 |

The correlation between weight and cost yields and interesting observation. For FLOPS the correlation is large and positive. This is expected because the vast majority of the cost is calculated using semi-empirical equations based off the weight; thus, decreasing the weight also decreases the cost. However, the physics-based analysis had a low and negative correlation. The negative correlation between weight and cost suggests that there is a trade happening between the two. While consistent with Research Observation 4, this result is not predicted under current theories. Therefore, further investigation is required.

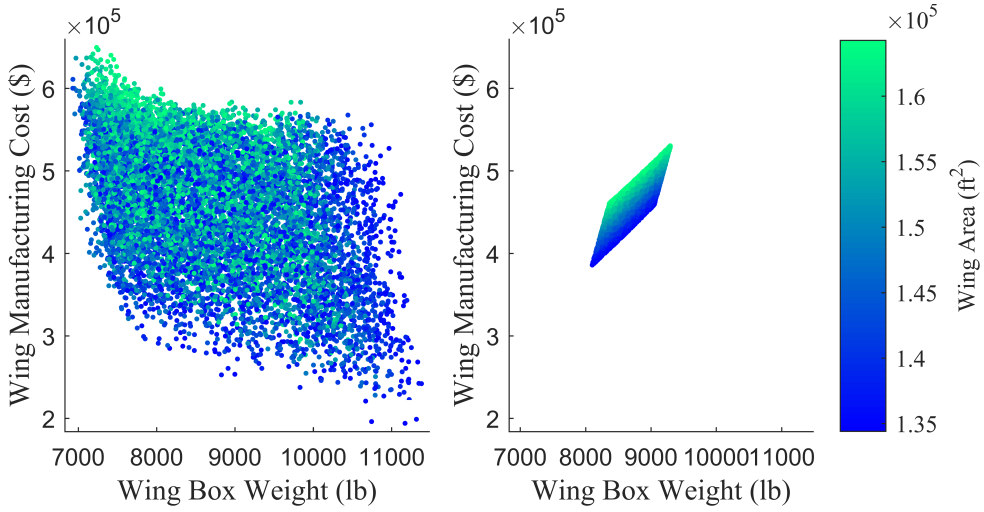


Figure 99: Wing Area Scatter Plot

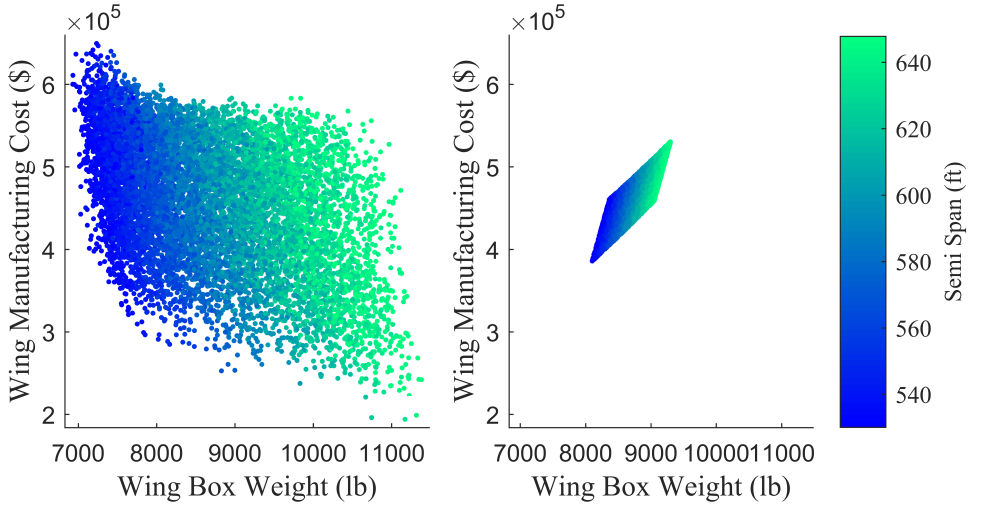


Figure 100: Wing Span Scatter Plot

Figure 99 and 100 compare both the FLOPS results and the SPANDSET results across the wing area and wing span. The same behavior is observed for both models across both variables. As the wing area is increased the wing manufacturing cost rises in both models (Figure 99). This matches intuition as a bigger wing will be more expensive to make. As the wing span increases the overall wing box weight increases in both the physics-based and weight-based model (Figure 100). Once again this matches intuition as a longer wing will experience a greater beding moment. It is unlikely the cause of the negative correlation can be related to the wing area or wing span; therefore it is likely due to the substructure variables.

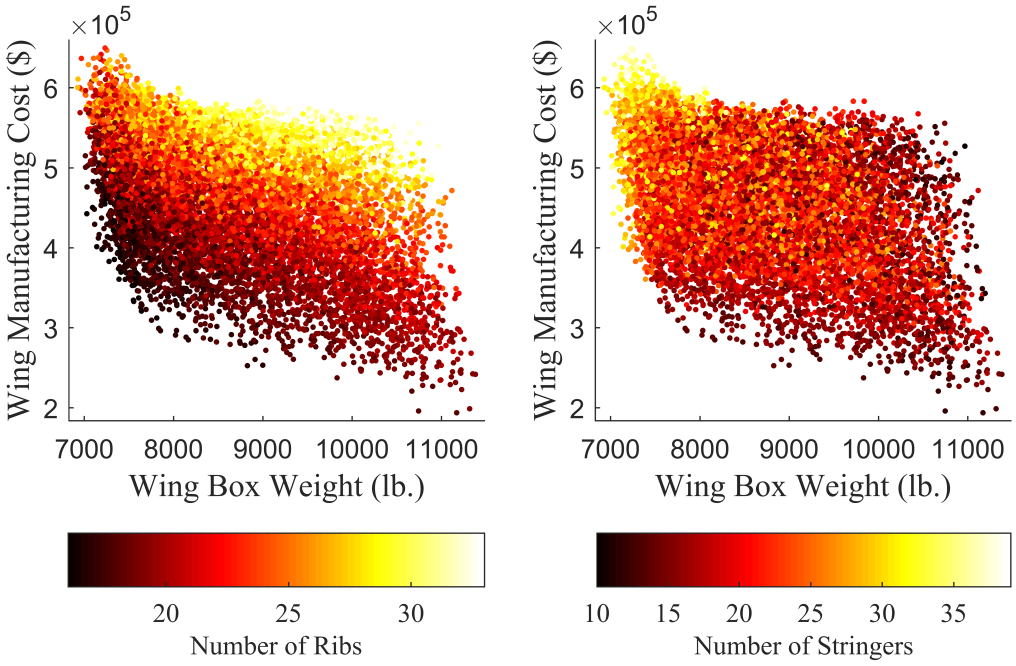


Figure 101: Quantity Scatter Plot

Figure 101 illustrates the effect the number of ribs and number of stringers has on the design space. The number of stringers seems to dictate the negative correlation between the weight and cost. As the number of stringers increases the cost increases and the weight decreases (this matches what was observed in Chapter 8). Meanwhile the number of ribs has little direct effect on the weight or cost (i.e. as the number

of ribs increases the weight and cost could go up or down) but instead dictates the feasible number of stringers For example, as the number of ribs increases from 18 to 23 there is an increases in the range of the number of stringers. These two behaviors combine to shape the overall behavior of the entire design space, and thus result in the negative correlation.

### 9.2.3 Conclusion

Figure 98 best represents the effect of adding physics-based structural analysis to the conceptual design problem. Current methods use historical regressions of previous aircraft rather than analyzing the substructure directly; however, this does not mean a substructure is not being analyzed. Instead of analyzing a new substructure it is merely altering previously created structures through statistical methods. While convenient, these methods have their limitations; hence the gold portion of the design space is much smaller than the blue portion.

Additionally, the physical representation allows for increased designer knowledge by incorporating classical structural analysis methods as well as activity-based cost modeling. Using these methods revealed several alternatives that the weight-based methods could not. Many of these new alternative lie on the Pareto Frontier and are thus of interest to the design problem. Thus the following conclusion is made.

---

**Conclusion 4**

Introducing physics-based structural analysis into the conceptual design problem significantly increases the design alternatives available.

---

The physics-based cost and weight analysis also unveiled a unique behavior dealing with the number of components across the design space. These behaviors ultimately lead to the design problem changing from a correlation between weight and cost

to a trade in weight and cost. These behaviors warrant future research before any conclusions are made.

# CHAPTER X

# SUMMARY OF THESIS STATEMENT

This thesis began by assessing the following challenges affecting the aerospace industry: rising demand for travel, international competition, emphasis on life cycle cost, government regulation on emissions, and global supply chains. All of these problems can be addressed by improving aircraft structural efficiency and manufacturing by introducing new concept, technologies, and materials to reduce weight, as well as using new design methods to increase design knowledge in early design phases. However, current practices which rely on empirical weight-based estimation technique prohibit the use of new concept, technologies, and materials while also limiting additional information from being generated. The proposed solution is to use physics-based structural design methods early in the design process. Chapter 1 concluded with the following overall research objective.

---

**Overall Research Objective**

Develop a physics-based structural design method to incorporate new concepts, technologies, and materials into the conceptual design phase.

---

## *10.1 Summary of Method Development*

For the duration of this thesis the problem was scoped to a wing box substructure design problem. The basic components of the primary wing box substructure were introduced as well as several design variables that affect the substructure configuration.

The first step of developing the method was to identify the challenges physics-based structural design will present through design space characterization. Chapter 2 reviewed literature and performed several small experiments to develop the following research observations:

- RO1: Combinatorially Large Design Space (Section 2.3)
- RO2: Discrete Design Decisions (Section 2.4)
- RO3: Highly Constrained Non-Linear Analysis (Section 2.5)
- RO4: Multimodal Design Space (Section 2.6)
- RO5: Multi-objective Design Problem (Section 2.7)
- RO6: Discontinuous Design Space (Section 2.8)

These research observations were used throughout the document to justify decisions made while developing the method. Several of the research observations resulted in the first Framework Proposition.

---

**Framework Proposition 1**

Due to the complex & discontinuous nature of the physics-based structural analysis design space, a strategy of exploration requiring a large number of analysis executions will be required.

---

Chapter 3 performed a literature survey of the methods that can be used during structural design, structural analysis, and structural optimization. The structural design problem is complex enough that a M&S environment, consisting of the methods in Chapter 3, is required. There exist enough different methods that can be used in the M&S environment for each sub problem so that testing the combinations through experimentation is impractical; thus, Chapter 4 performed a literature survey of existing physics-based wing box substructure M&S environments to make decisions regarding the overall design method.

Three metrics were identified to compare the wing box substructure M&S environments: model complexity, analysis complexity, and optimization complexity. These metrics capture the expected computational cost for each task. Using a method based on house of quality these three metrics were quantified for the existing M&S environment. The quantified values show that the method used to determine the internal loads determines the behavior of the M&S environment. Of the three most common methods used to define the internal loads (i.e. Finite Element Analysis, classical structural analysis, and equivalent methods) classical structural analysis provides the best balance of execution run time and fidelity. Thus, another proposition was made.

---

**Framework Proposition 2**

If a strategy of exploration requiring a large number of analysis executions is necessary, then the structural analysis sub-problem should be executed using lower fidelity classical structural analysis methods.

---

## *10.2 Summary of Method*

The substructure design problem could not be solved monolithically due to several negative effects of the research observation; thus, it is divided into two sub-problems: the wing box configuration design problem and the wing box substructure sizing problem. The wing box configuration problem is solved using design space exploration and multi-objective optimization. The wing box substructure sizing problem required creating a M&S environment based on multi-level optimization and classical structural analysis.

To solve the substructure sizing problem a M&S environment called SPANDSET (Structural Preliminary Analysis and Design Space Exploration Toolkit) was created. SPANDSET was specifically created to perform design space exploration on the wing

box configuration design sub problem. SPANDSET has three major phases:

- Phase 1: Generate Geometry and External Loads
- Phase 2: Structural Analysis and Sizing Routines
- Phase 3: Weight and Cost Breakdown

The first phase defines the geometry and external loads. The geometry is generated using a parametric geometry model (PGM). The PGM rapidly generates the entire wing geometry using parametric relationships to reduce the dimensionality of the problem as well as provides options to select discrete design decisions such as material properties or component configurations. To define the parametric relationships several assumptions had to be made which limit the design space. These assumptions are detailed in Chapter 6.

The external loads are defined as shear, moment, and torque (VMT) data along a user defined reference axis. SPANDSET provides an option to generate the external loads using a panel code called AVL. AVL gets all the required geometry data from the PGM and generates the necessary VMT data in a form SPANDSET can use.

The second phase performs structural analysis and sizing on the wing box substructure and is documented in Chapter 7. The structural analysis and sizing routines used in SPANDSET divide the wing box substructure into components (i.e. rib, spar segment, cover) to perform sizing optimization. Each component has a sizing routine which performs both classical structural analysis and constrained sizing optimization. The geometry for each routine is extracted from the PGM at user defined cross sections. At each cross section a routine performs thin walled torque box analysis to generate the internal loads from the applied external loads. The internal loads are then given to the individual structural analysis and sizing routines which then sizes the dimensions for each component based on constraints on the dimensions and the margins of safety. The results of the structural analysis and sizing routines are the final part dimensions and weight estimates.

The final phase of SPANDSET generates the weight breakdown and the cost breakdown. The weight breakdown separates the entire wing box weight into the total component weights. The total component weights are calculated using the weight estimates outputted from the structural analysis and sizing routines; however, these estimates are only calculated at the cross sections so interpolation is used to estimate the weights of the components that are not included in the cross section. These weight estimates are multiplied by the component sizes calculated by the PGM to get the final total component weights.

The cost breakdown uses surrogate models based off SEER-MFG. SEER-MFG is an activity based cost model that estimates the total time required to manufacture each portion of the wing box based upon the weight and size of the parts. The necessary weight data is gathered from the weight breakdown and the sizes are calculated by the PGM. The calculated labor hours are then multiplied by labor rates to calculate the total cost of manufacturing. The cost of manufacturing is combined with the cost of acquiring the raw material to estimate the total cost breakdown.

## *10.3 Summary of Experiments*

Two sets of experiments have been documented in this dissertation. The first set of experiments (Chapter 8) test the validity of Framework Proposition 1 and 2 using a canonical example. The second set of experiments (Chapter 9) performs design studies to validate SPANDSET against current state of the art methods as well as illustrate the effect of physics-based design on the wing box substructure design problem.

### 10.3.1 Canonical Example

Chapter 8 used a canonical example to perform 2D design space exploration and optimization to validate the need for a large number of analysis cases (Framework Proposition 1) and the use of classical analysis methods (Framework Proposition 2). The experiment explores wing box weight and cost design space for the rib spacing

and stringer spacing design variables. First, the responses are explored over each variable individually to observe general trends and scope the ranges to the area of the design space that likely contains the global minimum. Next, design space exploration is performed to create surrogate models of both the weight and cost for both design variables. These surrogate models are then used to locate all the possible local minima as well as the global optimum for the multi-objective design problem. Finally, several optimization algorithms are tested using the surrogate models. The purpose of these tests is to measure the probability of the algorithm to find the global optimum (i.e. hit rate) and compare these probabilities to the number of function calls required to converge to a solution.

The results from the first set of experiments illustrate how difficult the design space is to perform optimization on. There exist multiple discontinuities across the design space that cause jumps in the responses and the gradients for both weight and cost. Additionally, the discontinuities increase the number of local minima to over 400. The optimization algorithm that used gradient based optimization (Sequential Quadratic Programming) used less function calls but had a poor hit rate due to the discontinuous gradients and the large number of local minima. The other algorithms (Genetic Algorithm, Particle Swarm Algorithm, and 'GlobalSearch') used significantly more function calls and achieved better hit rates. Thus, Framework Proposition 1 was supported.

---

**Conclusion 1**

The complex and discontinuous nature of the physics-based structural analysis design space requires a large number of analysis executions to differentiate between the numerous design alternatives.

---

The canonical example also tested the use of classical structural analysis to solve the wing box substructure sizing problem. Using SPANDSET proved to be an

important factor in performing the 2D design space exploration. Thousands of cases were required to create the surrogate models and the more successful optimization algorithms required up to 5000 function calls. The computational cost to execute all the cases would have been too large had more sophisticated analysis been used. Therefore, Framework Proposition 2 is supported.

---

**Conclusion 2**

Using classical structural analysis methods to solve the structural analysis sub-problem enabled a strategy of exploration so that a large number of analysis executions could be tested.

---

### 10.3.2 Design Studies

Chapter 9 performed two design studies, one to compare SPANDSET to a similar wing box model that uses finite element analysis (FEA) and another to compare SPANDSET to an existing weight-based model.

The purpose of comparing SPANDSET to the FEA model is to validate the results of SPANDSET. Two surrogate models of the total wing box weight were created using the same baseline geometries, design variable, and ranges: one for SPANDSET and one for the FEA model. These models were then used in Monte Carlo simulation to calculate the error distribution between the two models. The error distribution was used to measure the mean error and the fidelity error. The results of the experiment showed a large mean error; however, this value can easily be accounted for by using a scaling factor. The fidelity error, which represents the error due to the difference in form between the two models, was higher than anticipated.

Next, the surrogate models were used to perform optimization on both models to observe the effect of the fidelity error on the optimum configuration (i.e. number of ribs and stringers) for the FEA model and SPANDSET. The results of the optimization

show a large difference in the final weights; however, the final configuration differed by only a single stringer. Accounting for the difference in run time between the models the results were acceptable. The difference in weight is not an issue so long as the configurations match because the final configuration can always be run through the higher fidelity analysis after exploration has been performed. Thus, classical analysis methods should be considered a viable option for structural design problems.

---

**Conclusion 3**

Despite the error in the calculated weight, Classical Analysis methods should be considered a viable option in future conceptual level structural design problems due to the lower run time and the ability to converge on the correct configuration.

---

The final experiment illustrated the effect that incorporating physics-based structural analysis can have on the design problem. While defining the substructure created some unique behaviors within the design space, it also lead to a significant increase in the number of design alternatives available. Several of these points lie along the Pareto Frontier. This is an example of increased designer knowledge earlier in the design process leading to more design freedom.

---

**Conclusion 4**

Introducing physics-based structural analysis into the conceptual design problem significantly increases the design alternatives available.

---

## *10.4 Contributions and Future Work*

Initial contributions of this thesis are to the field of structural design methods for aerospace structures. Several important observations about the physics-based substructure design problem through literature surveys and experimentation using a previously

existing framework. Although there may be disagreement about how to address these observations, the observations are inherent to the physics-based structural design problem. Thus, these observations will be a useful starting point for further research carried out in the field.

The primary contribution of this thesis is the framework developed for performing physics-based structural design of a wing box during the conceptual design phase of an aircraft called SPANDSET. SPANDSET is a framework with a unique set of features that enable for rapid and automated analysis and optimization of wing box substructure alternatives. The framework reduced the design cycle by using classical structural analysis methods based on first principles. This reduced design cycle time allows for implementation of a strategy of exploration which is important because normal optimization algorithms struggled to find the best alternative within the complex and discontinuous design space.

The final contribution is an example of incorporating physics-based structural analysis. This was accomplished by considering both material and geometry by representing and performing trades on the substructure configuration. By using physics-based analysis it was shown that more alternatives can be considered because the weight is no longer based on historical regressions of a single substructure configuration. Additionally, inclusion of geometric and material data enable activity based cost modeling so that cost and manufacturing considerations could be tied directly to the substructure configuration instead of relying solely on weight. Therefore, this thesis contributed an example of altering current design methods to increase knowledge earlier in the design process as well as facilitate considerations of cost and manufacturing in early design phases.

The majority of the effort in this thesis was committed to developing SPANDSET. To create the framework required three years of work from two people, thousands of lines of VBA code, incorporating AVL for aerodynamic loads, and several months

spent improving and debugging the existing framework. The largest challenges came from the automation requirement. Through the course of a single iteration hundreds of individual optimization problems need to be set up and solved automatically. Each optimization problem involves several constraints which are based on both the part geometry and the internal loads. Lots of information needs to be gathered before an optimization problem can be executed and the order in which the optimization is performed has to be managed.

Additionally the parametric geometry tool needed to be created. Lots of geometric information is required throughout the design cycle of SPANDSET. Previously this information was gathered manually or estimated using rules of thumb. This made it difficult to correlate the substructure geometry decisions (i.e. rib spacing, location of spars, orientation of stringers) to the system level metrics (weight and cost). By creating the parametric geometry tool this information is generated automatically in minutes; however, a significant amount of time and effort had to be spent creating and debugging the tool with no previously existing methods to call upon.

Furthermore, calculating the weight and cost required additional effort. The substructure was divided into cross sections to limit the amount of time required for analysis. To calculate the weight data information available at the cross-sections had to be interpolated across the span and projected onto the substructure geometry. Finally, all the weight and geometry information had to be converted into a form that the activity based cost model could use.

Although this thesis was able to make meaningful contributions, there are many shortcomings in SPANDSET that prevent it from being considered a state-of-the-art method for modern wing box substructure configurations. These shortcomings are a lack of aeroelasticity and limited use of multi-level optimization. These shortcomings are largely due to the difficulty of what was accomplished. The primary goal was to set up the framework to work from beginning to end automatically and accurately for

the simplest form of the design problem. This meant using collaborative optimization, which is simple to execute, rather than other multi-level optimization methodologies that have better performance. Future work should investigate new multi-level optimization strategies that will improve the overall system metrics and reduce run time.

The current state-of-the-art in wing box substructure design requires the inclusion of aeroelasticity. SPANDSET is not able to handle aeroelastic considerations. This is due in large part to the multi-level optimization methodology implemented. This method makes it difficult to apply constraints to the system level optimization problem. Including aeroelasticity to the design problem would require placing stiffness requirement on the wing that can be applied to each cross-section. SPANDSET does not allow for that; therefore, future work should be to incorporate aeroelasticity into SPANDSET.

Additional studies should also be performed that use composite materials. One of the motivations for using physics-based structural analysis is the inclusion of new concepts, technologies, and new materials. While including new concepts and materials may be difficult for the proposed framework, analyzing composite materials can be done by using new sizing routines that can account for composite material behavior.

# APPENDIX A

# SURROGATE FIT DATA

| **Reg.** | **Stringers** | **Ribs** | **SSE** | $\mathbf{R^2}$ | $\epsilon_{min}$ | $\epsilon_{max}$ |
|---|---|---|---|---|---|---|
| 1 | 37 | 35 | 19294.9 | 0.6917 | -1.00 % | 1.19 % |
| 2 | 37 | 34 | 5110.5 | 0.9038 | -0.97 % | 1.14 % |
| 3 | 37 | 33 | 725.6 | 0.8729 | -1.66 % | 0.82 % |
| 4 | 37 | 32 | 26901.2 | 0.6619 | -1.59 % | 1.16 % |
| 5 | 37 | 31 | 7799.3 | 0.9413 | -1.34 % | 1.25 % |
| 6 | 37 | 30 | 12591.9 | 0.7321 | -1.30 % | 1.11 % |
| 7 | 37 | 29 | 5009.7 | 0.7673 | -0.77 % | 0.58 % |
| 8 | 37 | 28 | 9096.1 | 0.8467 | -1.41 % | 0.91 % |
| 9 | 37 | 27 | 3113.3 | 0.8280 | -1.66 % | 0.79 % |
| 10 | 37 | 26 | 12424.3 | 0.6361 | -0.82 % | 1.08 % |
| 11 | 37 | 25 | 29503.9 | 0.7582 | -1.13 % | 1.32 % |
| 12 | 36 | 35 | 28688.6 | 0.7915 | -1.33 % | 1.03 % |
| 13 | 36 | 34 | 18806.6 | 0.7338 | -1.08 % | 1.76 % |
| 14 | 36 | 33 | 790.6 | 0.5367 | -1.23 % | 0.26 % |
| 15 | 36 | 32 | 26311.7 | 0.7564 | -1.59 % | 0.92 % |
| 16 | 36 | 31 | 14949.3 | 0.8435 | -1.12 % | 1.18 % |
| 17 | 36 | 30 | 5871.9 | 0.6124 | -0.81 % | 0.79 % |
| 18 | 36 | 29 | 12144.8 | 0.8220 | -1.24 % | 1.33 % |
| 19 | 36 | 28 | 3208.9 | 0.8270 | -1.44 % | 1.01 % |
| 20 | 36 | 27 | 3870.9 | 0.8614 | -0.95 % | 0.45 % |
| 21 | 36 | 26 | 23487.0 | 0.7815 | -1.33 % | 0.96 % |
| 22 | 36 | 25 | 31909.9 | 0.7261 | -1.36 % | 1.03 % |
| 23 | 35 | 35 | 11396.2 | 0.8456 | -0.81 % | 1.06 % |
| 24 | 35 | 34 | 15218.3 | 0.7441 | -0.82 % | 1.07 % |
| 25 | 35 | 33 | 24411.1 | 0.5967 | -0.92 % | 1.12 % |
| 26 | 35 | 32 | 21486.2 | 0.7838 | -1.13 % | 0.86 % |
| 27 | 35 | 31 | 26939.0 | 0.7397 | -1.55 % | 1.04 % |
| 28 | 35 | 30 | 16322.3 | 0.6549 | -1.16 % | 1.05 % |
| 29 | 35 | 29 | 23100.6 | 0.6447 | -1.68 % | 1.24 % |
| 30 | 35 | 28 | 13205.7 | 0.6916 | -1.09 % | 0.98 % |
| 31 | 35 | 27 | 19441.7 | 0.5289 | -1.49 % | 1.14 % |
| 32 | 35 | 26 | 3106.9 | 0.8978 | -0.77 % | 0.95 % |
| 33 | 35 | 25 | 13184.0 | 0.8949 | -1.09 % | 1.23 % |

| **Reg.** | **Stringers** | **Ribs** | **SSE** | $\mathbf{R}^2$ | $\epsilon_{min}$ | $\epsilon_{max}$ |
|---|---|---|---|---|---|---|
| 34 | 34 | 35 | 21113.2 | 0.7743 | -0.93 % | 1.15 % |
| 35 | 34 | 34 | 991.3 | 0.6154 | -1.39 % | 1.21 % |
| 36 | 34 | 33 | 24547.0 | 0.6331 | -1.25 % | 1.32 % |
| 37 | 34 | 32 | 19243.2 | 0.7307 | -1.11 % | 1.10 % |
| 38 | 34 | 31 | 18764.8 | 0.8044 | -1.60 % | 1.22 % |
| 39 | 34 | 30 | 928.2 | 0.7244 | -0.96 % | 0.31 % |
| 40 | 34 | 29 | 11083.8 | 0.6380 | -1.44 % | 0.67 % |
| 41 | 34 | 28 | 5866.6 | 0.8598 | -1.30 % | 1.14 % |
| 42 | 34 | 27 | 10686.6 | 0.7620 | -1.30 % | 1.18 % |
| 43 | 34 | 26 | 24471.9 | 0.7334 | -1.33 % | 1.82 % |
| 44 | 34 | 25 | 8179.8 | 0.9265 | -1.23 % | 1.06 % |
| 45 | 33 | 35 | 11304.8 | 0.8543 | -0.73 % | 1.06 % |
| 46 | 33 | 34 | 4912.4 | 0.6667 | -0.70 % | 0.45 % |
| 47 | 33 | 33 | 23581.5 | 0.6204 | -1.30 % | 1.10 % |
| 48 | 33 | 32 | 14288.8 | 0.8289 | -0.99 % | 0.85 % |
| 49 | 33 | 31 | 20616.5 | 0.6800 | -1.21 % | 1.64 % |
| 50 | 33 | 30 | 4520.9 | 0.6442 | -1.14 % | 0.81 % |
| 51 | 33 | 29 | 16744.3 | 0.7851 | -1.34 % | 0.82 % |
| 52 | 33 | 28 | 2555.6 | 0.7511 | -1.04 % | 1.07 % |
| 53 | 33 | 27 | 5773.5 | 0.6527 | -0.98 % | 0.99 % |
| 54 | 33 | 26 | 20143.2 | 0.7485 | -1.30 % | 1.11 % |
| 55 | 33 | 25 | 36081.9 | 0.7617 | -1.03 % | 1.26 % |
| 56 | 32 | 35 | 18215.4 | 0.7692 | -1.20 % | 0.96 % |
| 57 | 32 | 34 | 18758.8 | 0.5056 | -1.25 % | 0.90 % |
| 58 | 32 | 33 | 17853.2 | 0.6976 | -1.43 % | 0.96 % |
| 59 | 32 | 32 | 18561.7 | 0.7780 | -0.89 % | 1.00 % |
| 60 | 32 | 31 | 20468.1 | 0.7661 | -1.23 % | 1.10 % |
| 61 | 32 | 30 | 21341.4 | 0.6472 | -1.40 % | 1.88 % |
| 62 | 32 | 29 | 20765.3 | 0.6736 | -1.49 % | 1.19 % |
| 63 | 32 | 28 | 10102.7 | 0.8402 | -0.65 % | 0.93 % |
| 64 | 32 | 27 | 4391.9 | 0.7986 | -1.48 % | 1.22 % |
| 65 | 32 | 26 | 959.3 | 0.8449 | -1.27 % | 1.07 % |
| 66 | 32 | 25 | 27653.5 | 0.8265 | -1.40 % | 1.26 % |

| **Reg.** | **Stringers** | **Ribs** | **SSE** | $\mathbf{R}^2$ | $\epsilon_{min}$ | $\epsilon_{max}$ |
|---|---|---|---|---|---|---|
| 67 | 31 | 35 | 19279.1 | 0.7527 | -0.88 % | 1.27 % |
| 68 | 31 | 34 | 16539.1 | 0.7667 | -0.94 % | 1.13 % |
| 69 | 31 | 33 | 12440.0 | 0.7718 | -1.54 % | 1.55 % |
| 70 | 31 | 32 | 12607.7 | 0.8805 | -1.33 % | 0.89 % |
| 71 | 31 | 31 | 15701.8 | 0.8170 | -1.27 % | 1.27 % |
| 72 | 31 | 30 | 4508.9 | 0.7431 | -1.58 % | 1.50 % |
| 73 | 31 | 29 | 9102.2 | 0.6970 | -1.48 % | 1.17 % |
| 74 | 31 | 28 | 11928.5 | 0.8058 | -1.30 % | 1.30 % |
| 75 | 31 | 27 | 6844.4 | 0.7946 | -0.98 % | 0.92 % |
| 76 | 31 | 26 | 7326.3 | 0.7785 | -1.14 % | 0.87 % |
| 77 | 31 | 25 | 15426.9 | 0.8962 | -1.05 % | 2.35 % |
| 78 | 30 | 35 | 13870.0 | 0.8030 | -0.76 % | 1.24 % |
| 79 | 30 | 34 | 11731.1 | 0.8315 | -1.14 % | 1.08 % |
| 80 | 30 | 33 | 19672.9 | 0.6206 | -1.14 % | 1.60 % |
| 81 | 30 | 32 | 11077.5 | 0.8726 | -1.17 % | 1.42 % |
| 82 | 30 | 31 | 15301.9 | 0.6801 | -1.23 % | 0.94 % |
| 83 | 30 | 30 | 15380.0 | 0.5643 | -1.12 % | 0.79 % |
| 84 | 30 | 29 | 2785.8 | 0.7359 | -1.46 % | 0.87 % |
| 85 | 30 | 28 | 12393.5 | 0.6805 | -0.98 % | 0.93 % |
| 86 | 30 | 27 | 4022.0 | 0.7485 | -0.93 % | 1.68 % |
| 87 | 30 | 26 | 25278.4 | 0.7275 | -1.07 % | 1.30 % |
| 88 | 30 | 25 | 14415.1 | 0.8951 | -1.15 % | 1.58 % |
| 89 | 29 | 35 | 29100.7 | 0.5415 | -1.44 % | 1.16 % |
| 90 | 29 | 34 | 16431.8 | 0.8408 | -1.03 % | 1.17 % |
| 91 | 29 | 33 | 12086.5 | 0.8412 | -1.16 % | 1.49 % |
| 92 | 29 | 32 | 11849.5 | 0.8920 | -1.62 % | 0.83 % |
| 93 | 29 | 31 | 20022.6 | 0.7487 | -1.24 % | 0.82 % |
| 94 | 29 | 30 | 1084.1 | 0.5580 | -0.25 % | 0.76 % |
| 95 | 29 | 29 | 8332.7 | 0.8145 | -1.07 % | 0.98 % |
| 96 | 29 | 28 | 9258.9 | 0.7910 | -0.92 % | 0.98 % |
| 97 | 29 | 27 | 17378.3 | 0.6988 | -1.08 % | 1.28 % |
| 98 | 29 | 26 | 30004.5 | 0.7553 | -1.08 % | 1.27 % |
| 99 | 29 | 25 | 20614.3 | 0.8537 | -1.18 % | 1.41 % |

# APPENDIX B

# SURROGATE LOCAL MINIMA

| Response Surface Equations | | | Δ Total Wing Box Weight | | | Δ Total Wing Box Weight | | |
|---|---|---|---|---|---|---|---|---|
| **Reg.** | **Stringers** | **Ribs** | **Δ ST** | **Δ RB** | **Δ Weight %** | **Δ ST** | **Δ RB** | **Δ Cost %** |
| 1 | 37 | 35 | -3.16 | -8.79 | -4.16 % | -3.16 | -8.51 | 9.55 % |
| 2 | 37 | 34 | -2.99 | -7.51 | -5.72 % | -3.16 | -7.70 | 7.69 % |
| 3 | 37 | 33 | -3.01 | -7.50 | -4.11 % | -3.16 | -7.45 | 7.49 % |
| 4 | 37 | 32 | -2.97 | -6.79 | -5.66 % | -2.98 | -6.75 | 6.56 % |
| 5 | 37 | 31 | -3.06* | -5.74* | -9.89 %* | -2.93 | -6.17 | 4.52 % |
| 6 | 37 | 30 | -3.16 | -5.73 | -7.26 % | -3.01 | -5.71 | 3.19 % |
| 7 | 37 | 29 | -3.13 | -5.09 | -5.98 % | -2.93 | -4.95 | 2.33 % |
| 8 | 37 | 28 | -2.97 | -4.76 | -7.29 % | -3.11 | -3.72 | 0.41 % |
| 9 | 37 | 27 | -2.93 | -3.64 | -7.63 % | -3.16 | -3.66 | -0.57 % |
| 10 | 37 | 26 | -2.93 | -2.97 | -9.87 % | -2.93 | -2.96 | -4.16 % |
| 11 | 37 | 25 | -3.16 | -2.05 | -8.39 % | -2.93 | -1.54 | -4.93 % |
| 12 | 36 | 35 | -2.80 | -8.36 | -5.49 % | -2.80 | -8.35 | 9.65 % |
| 13 | 36 | 34 | -2.80 | -7.58 | -5.06 % | -2.80 | -7.59 | 7.93 % |
| 14 | 36 | 33 | -2.80 | -7.42 | -3.61 % | -2.90 | -7.50 | 6.75 % |
| 15 | 36 | 32 | -2.80 | -7.21 | -7.61 % | -2.80 | -7.20 | 5.96 % |
| 16 | 36 | 31 | -2.91 | -6.23 | -6.62 % | -2.92 | -6.43 | 4.19 % |
| 17 | 36 | 30 | -2.90 | -5.72 | -5.98 % | -2.84 | -5.73 | 4.35 % |
| 18 | 36 | 29 | -2.80 | -5.04 | -8.85 % | -2.92 | -5.54 | 0.26 % |
| 19 | 36 | 28 | -2.80 | -4.76 | -6.45 % | -2.79 | -3.95 | -1.26 % |
| 20 | 36 | 27 | -2.91 | -3.63 | -7.48 % | -2.82 | -3.52 | -1.57 % |
| 21 | 36 | 26 | -2.81 | -2.74 | -8.25 % | -2.80 | -2.93 | -4.08 % |
| 22 | 36 | 25 | -2.84 | -1.23 | -8.70 % | -2.84 | -1.24 | -5.34 % |
| 23 | 35 | 35 | -2.79 | -8.79 | -5.49 % | -2.78 | -8.54 | 8.44 % |
| 24 | 35 | 34 | -2.79 | -8.00 | -4.92 % | -2.74 | -7.58 | 6.86 % |
| 25 | 35 | 33 | -2.73 | -7.49 | -9.01 % | -2.78 | -7.41 | 4.33 % |
| 26 | 35 | 32 | -2.79 | -6.87 | -6.87 % | -2.75 | -6.61 | 4.13 % |
| 27 | 35 | 31 | -2.79 | -5.97 | -7.70 % | -2.79 | -5.94 | 2.20 % |
| 28 | 35 | 30 | -2.75 | -5.72 | -6.75 % | -2.78 | -5.73 | 2.87 % |
| 29 | 35 | 29 | -2.79 | -5.33 | -8.78 % | -2.76 | -4.78 | -0.83 % |
| 30 | 35 | 28 | -2.77 | -4.74 | -6.18 % | -2.74 | -4.00 | -1.48 % |
| 31 | 35 | 27 | -2.78 | -3.63 | -6.70 % | -2.74 | -3.63 | -3.08 % |
| 32 | 35 | 26 | -2.76 | -3.32 | -8.67 % | -2.79 | -2.66 | -5.18 % |
| 33 | 35 | 25 | -2.78 | -1.43 | -8.72 % | -2.74 | -1.55 | -7.29 % |

| Response Surface Equations | | | Δ Total Wing Box Weight | | | Δ Total Wing Box Weight | | |
|---|---|---|---|---|---|---|---|---|
| **Reg.** | **Stringers** | **Ribs** | **Δ ST** | **Δ RB** | **Δ Weight %** | **Δ ST** | **Δ RB** | **Δ Cost %** |
| 34 | 34 | 35 | -2.54 | -8.14 | -6.49 % | -2.54 | -8.14 | 7.05 % |
| 35 | 34 | 34 | -2.49 | -7.65 | -3.54 % | -2.69 | -7.64 | 7.02 % |
| 36 | 34 | 33 | -2.49 | -7.43 | -9.07 % | -2.49 | -7.43 | 4.10 % |
| 37 | 34 | 32 | -2.61 | -6.97 | -5.51 % | -2.73 | -6.77 | 3.26 % |
| 38 | 34 | 31 | -2.59 | -6.59 | -5.70 % | -2.49 | -6.42 | 2.36 % |
| 39 | 34 | 30 | -2.73 | -5.73 | -4.62 % | -2.48 | -5.72 | 1.84 % |
| 40 | 34 | 29 | -2.56 | -5.70 | -7.35 % | -2.55 | -4.77 | -1.75 % |
| 41 | 34 | 28 | -2.54 | -3.72 | -7.55 % | -2.55 | -3.72 | -4.42 % |
| 42 | 34 | 27 | -2.73 | -3.63 | -7.47 % | -2.49 | -3.43 | -3.72 % |
| 43 | 34 | 26 | -2.73 | -3.18 | -7.68 % | -2.73 | -3.19 | -5.58 % |
| 44 | 34 | 25 | -2.73 | -2.02 | -8.32 % | -2.73 | -1.95 | -7.14 % |
| 45 | 33 | 35 | -2.44 | -8.14 | -6.06 % | -2.45 | -8.14 | 5.82 % |
| 46 | 33 | 34 | -2.37 | -7.71 | -3.62 % | -2.42 | -7.75 | 5.88 % |
| 47 | 33 | 33 | -2.46 | -7.41 | -5.88 % | -2.46 | -7.41 | 3.06 % |
| 48 | 33 | 32 | -2.43 | -6.61 | -5.05 % | -2.44 | -6.61 | 2.40 % |
| 49 | 33 | 31 | -2.39 | -5.74 | -4.90 % | -2.36 | -5.75 | 0.60 % |
| 50 | 33 | 30 | -2.37 | -5.72 | -4.09 % | -2.38 | -5.72 | 1.35 % |
| 51 | 33 | 29 | -2.40 | -5.24 | -6.16 % | -2.40 | -5.18 | -1.78 % |
| 52 | 33 | 28 | -2.46 | -3.72 | -5.07 % | -2.48 | -3.92 | -3.28 % |
| 53 | 33 | 27 | -2.48 | -3.34 | -5.62 % | -2.48 | -3.63 | -4.50 % |
| 54 | 33 | 26 | -2.46 | -2.54 | -5.57 % | -2.38 | -2.54 | -6.30 % |
| 55 | 33 | 25 | -2.37 | -1.69 | -6.94 % | -2.37 | -1.65 | -8.61 % |
| 56 | 32 | 35 | -2.17 | -8.24 | -3.73 % | -2.14 | -8.14 | 4.07 % |
| 57 | 32 | 34 | -2.28 | -8.12 | -6.70 % | -2.11 | -7.50 | 3.06 % |
| 58 | 32 | 33 | -2.36 | -7.43 | -4.54 % | -2.11 | -7.48 | 1.87 % |
| 59 | 32 | 32 | -2.30 | -6.61 | -5.35 % | -2.30 | -6.61 | 0.72 % |
| 60 | 32 | 31 | -2.26 | -5.97 | -4.39 % | -2.29 | -5.83 | -0.08 % |
| 61 | 32 | 30 | -2.36 | -5.73 | -8.35 % | -2.30 | -5.73 | -0.50 % |
| 62 | 32 | 29 | -2.22 | -5.70 | -5.72 % | -2.24 | -5.11 | -2.89 % |
| 63 | 32 | 28 | -2.19 | -3.72 | -8.02 % | -2.31 | -3.72 | -4.52 % |
| 64 | 32 | 27 | -2.16 | -3.34 | -5.94 % | -2.32 | -3.34 | -5.85 % |
| 65 | 32 | 26 | -2.11 | -2.72 | -4.29 % | -2.11 | -2.63 | -7.87 % |
| 66 | 32 | 25 | -2.17 | -1.49 | -6.97 % | -2.14 | -1.50 | -9.98 % |

| Response Surface Equations | | | Δ Total Wing Box Weight | | | Δ Total Wing Box Weight | | |
|---|---|---|---|---|---|---|---|---|
| **Reg.** | **Stringers** | **Ribs** | **Δ ST** | **Δ RB** | **Δ Weight %** | **Δ ST** | **Δ RB** | **Δ Cost %** |
| 67 | 31 | 35 | -2.08 | -8.34 | -8.61 % | -2.08 | -8.14 | 4.24 % |
| 68 | 31 | 34 | -2.08 | -7.54 | -2.92 % | -2.08 | -7.62 | 3.54 % |
| 69 | 31 | 33 | -2.09 | -7.41 | -4.23 % | -2.09 | -7.41 | 1.62 % |
| 70 | 31 | 32 | -2.08 | -7.01 | -3.74 % | -2.08 | -6.61 | 1.18 % |
| 71 | 31 | 31 | -2.08 | -5.90 | -9.74 % | -2.10 | -5.99 | -0.79 % |
| 72 | 31 | 30 | -2.10 | -5.73 | -4.02 % | -2.09 | -5.73 | -0.86 % |
| 73 | 31 | 29 | -2.08 | -5.51 | -7.20 % | -2.10 | -4.97 | -4.17 % |
| 74 | 31 | 28 | -2.10 | -3.72 | -4.67 % | -2.10 | -3.72 | -5.28 % |
| 75 | 31 | 27 | -2.08 | -3.41 | -9.40 % | -2.10 | -3.33 | -7.60 % |
| 76 | 31 | 26 | -2.08 | -3.21 | -5.53 % | -2.10 | -2.62 | -8.33 % |
| 77 | 31 | 25 | -2.10 | -2.52 | -6.53 % | -2.08 | -1.41 | -9.63 % |
| 78 | 30 | 35 | -1.94 | -8.79 | -2.92 % | -1.91 | -8.79 | 3.60 % |
| 79 | 30 | 34 | -1.89 | -7.53 | -2.71 % | -1.85 | -7.88 | 2.93 % |
| 80 | 30 | 33 | -1.91 | -7.41 | -4.13 % | -2.03 | -7.50 | 1.57 % |
| 81 | 30 | 32 | -1.93 | -6.61 | -6.67 % | -1.93 | -6.61 | -0.65 % |
| 82 | 30 | 31 | -1.89 | -5.88 | -2.70 % | -2.04 | -5.74 | -0.96 % |
| 83 | 30 | 30 | -2.07 | -5.73 | -4.17 % | -2.07 | -5.72 | -0.93 % |
| 84 | 30 | 29 | -1.85 | -5.00 | -4.36 % | -1.85 | -4.97 | -4.93 % |
| 85 | 30 | 28 | -1.97 | -4.76 | -6.58 % | -2.00 | -3.72 | -5.87 % |
| 86 | 30 | 27 | -2.04 | -3.34 | -4.65 % | -2.03 | -3.34 | -6.54 % |
| 87 | 30 | 26 | -2.02 | -3.32 | -4.77 % | -2.07 | -2.67 | -8.70 % |
| 88 | 30 | 25 | -1.99 | -1.89 | -5.47 % | -2.04 | -1.23 | -10.11 % |
| 89 | 29 | 35 | -1.84 | -8.34 | -4.10 % | -1.84 | -8.30 | 1.95 % |
| 90 | 29 | 34 | -1.55 | -7.59 | -3.70 % | -1.84 | -7.65 | 2.05 % |
| 91 | 29 | 33 | -1.55 | -7.48 | -7.81 % | -1.55 | -7.48 | -1.52 % |
| 92 | 29 | 32 | -1.55 | -6.89 | -5.58 % | -1.77 | -6.60 | -1.06 % |
| 93 | 29 | 31 | -1.55 | -6.17 | -3.70 % | -1.55 | -6.18 | -2.36 % |
| 94 | 29 | 30 | -1.84 | -5.72 | -2.85 % | -1.60 | -5.73 | -2.87 % |
| 95 | 29 | 29 | -1.76 | -4.78 | -7.19 % | -1.76 | -4.78 | -6.94 % |
| 96 | 29 | 28 | -1.55 | -4.33 | -5.90 % | -1.55 | -4.09 | -7.44 % |
| 97 | 29 | 27 | -1.68 | -3.34 | -9.55 % | -1.62 | -3.67 | -8.87 % |
| 98 | 29 | 26 | -1.55 | -3.20 | -5.25 % | -1.84 | -2.69 | -10.76 % |
| 99 | 29 | 25 | -1.84 | -2.02 | -7.13 % | -1.59* | -1.23* | -11.52 %* |

# REFERENCES


[1] *IHS Jane's all the world's aircraft. Development & production.* [Coulsdon, England] : IHS Global Limited, 2012.

[2] Airbus, "Global Market Forecast: Future Journeys 2013 2032," tech. rep., Airbus, Blagnac Cedex, France, 2013.

[3] Alexandrov, N. M., Lewis, R. M., Gumbert, C. R., Green, L. L., and Newman, P. A., "Optimization with variable-fidelity models applied to wing design," tech. rep., DTIC Document, 1999.

[4] Allen, D. H. and Haisler, W. E., *Introduction to aerospace structural analysis*. Wiley, 1985.

[5] American Institute of Aeronautics and Astronautics, "Space Systems - Structures, Structural Components, and Structural Assemblies," *S-100-2005*, 2005.

[6] Andersen, G. and Venkayya, V., "The roll of conceptual and preliminary design in airframe MDO," *AIAA Paper*, 1996.

[7] Anderson, J. D., *Aircraft Performance and Design*. McGraw-Hill, 1999.

[8] Anderson, J. D. and Wendt, J., *Computational fluid dynamics*, vol. 206. Springer, 1995.

[9] Ardema, M. D., Chambers, M. C., Patron, A. P., Hahn, A. S., Miura, H., and Moore, M. D., "Analytical fuselage and wing weight estimation of transport aircraft," *NASA Technical Memorandum*, vol. 110392, 1996.

[10] Arnold, S. M., Cebon, D., and Ashby, M., "Materials Selection for Aerospace Systems," tech. rep., NASA Glenn Research Center; Cleveland, OH, United States, 2012.

[11] Ashby, M. F. and Cebon, D., "Materials selection in mechanical design," *Le Journal de Physique IV*, vol. 3, no. C7, pp. C7–1, 1993.

[12] Asiedu, Y. and Gu, P., "Product life cycle cost analysis: state of the art review," *International journal of production research*, vol. 36, no. 4, pp. 883–908, 1998.

[13] Babikian, R., Lukachko, S. P., and Waitz, I. A., "The historical fuel efficiency characteristics of regional aircraft from technological, operational, and cost perspectives," *Journal of Air Transport Management*, vol. 8, no. 6, pp. 389 – 400, 2002.

[14] Bailey-Noval, N., Llamas-Sandin, R., and Moreno-Herranz, A., "Automatic generation of the structural layout of aircraft rear fuselage and tail surfaces including global finite elements and cad model.," *Civil-Comp Proceedings*, vol. 100, no. Proceedings of the 8th International Conference on Engineering Computational Technology, ECT 2012, 2012.

[15] Balling, R. J. and Sobieszczanski-Sobieski, J., "Optimization of coupled systems-A critical overview of approaches," *AIAA journal*, vol. 34, no. 1, pp. 6–17, 1996.

[16] BASF, "BASF Aerospace Materials: lightweight Composite Load Panel," tech. rep., BASF, 2013.

[17] Bauchau, O. A. and Craig, J. I., *Structural analysis: with applications to aerospace structures*, vol. 163. Springer, 2009.

[18] Berchtold, S., Böhm, C., and Kriegal, H.-P., "The pyramid-technique: towards breaking the curse of dimensionality," in *ACM SIGMOD Record*, vol. 27, pp. 142–153, ACM, 1998.

[19] Bergmann, A., "The Aeroacoustic Wind Tunnel DNW-NWB," in *18th AIAA/CEAS Aeroacoustics Conference*, pp. 4–6, 2012.

[20] Bezos-O'Connor, G. M., Mangelsdorf, M. F., Maliska, H. A., Washburn, A. E., and Wahls, R. A., "Fuel efficiencies through airframe improvements," in *3rd AIAA Atmospheric Space Environments Conference, 27 - 30 June 2011, Honolulu, Hawaii*, 2011.

[21] Bindolino, G., Ghiringhelli, G., Ricci, S., and Terraneo, M., "Multilevel structural optimization for preliminary wing-box weight estimation," *Journal of Aircraft*, vol. 47, no. 2, pp. 475–489, 2010.

[22] Black, A., "Influence of design on cost of operating airplanes.," *Mechanical Engineering*, vol. 44, p. 821, 1922.

[23] Blair, M., Hill, S., Weisshaar, T. A., and Taylor, R., "Rapid modeling with innovative structural concepts," *AIAA paper*, pp. 98–1755, 1998.

[24] Blockley, D. I., *The Nature of Structural Design and Safety*. Ellis Horwood Chichester, 1980.

[25] Bloom, F. and Coffin, D., *Handbook of thin plate buckling and postbuckling*. CRC Press, 2000.

[26] Boeing, "Current Market Outlook 2013-2032," tech. rep., Boeing, Seattle. WA, 2013.

[27] Bolkcom, C., "F-35 Joint Strike Fighter (JSF) Program: Background, Status, and Issues," tech. rep., DTIC Document, 2005.

[28] Bonanni, D. L., Johnson, E. R., and Starnes Jr, J. H., "Local buckling and crippling of composite stiffener sections," 1988.

[29] Bonanni, D. L., OHNSON, E. R., and TARNES, J. H., "Local crippling of thin-walled graphite-epoxy stiffeners," *AIAA journal*, vol. 29, no. 11, pp. 1951–1959, 1991.

[30] Boothroyd, G., "Product design for manufacture and assembly," *Computer-Aided Design*, vol. 26, no. 7, pp. 505–520, 1994.

[31] Borenstein, S., "Why Can't US Airlines Make Money?," *The American Economic Review*, vol. 101, no. 3, pp. 233–237, 2011.

[32] Bradley, K. R., "A sizing methodology for the conceptual design of blended-wing-body transports," *NASA CR*, vol. 213016, p. 2004, 2004.

[33] Brueckner, J. K., Lee, D., and Singer, E. S., "Airline competition and domestic US airfares: A comprehensive reappraisal," *Economics of Transportation*, vol. 2, no. 1, pp. 1–17, 2013.

[34] Bruhn, E. F., Bollard, R., and others, *Analysis and design of flight vehicle structures*. Jacobs, 1973.

[35] Bungartz, H.-J., Zimmer, S., Buchholz, M., Pflger, D., Le Borne, S., and Le Borne, R., *Modeling and simulation : an application-oriented introduction / Hans-Joachim Bungartz, Stefan Zimmer, Martin Buchholz, Dirk Pflger ; translated by Sabine Le Borne, Richard Le Borne.* Springer undergraduate texts in mathematics and technology, Berlin : Springer, 2013., 2013.

[36] Burr, A. H. and Cheatham, J. B., *Mechanical analysis and design*. Prentice Hall NJ, 1995.

[37] Callister, W. D., "Materials Science and Engineering: An Introduction, 94-95," 1997.

[38] Cantor, B., Assender, H., and Grant, P., *Aerospace materials*. CRC Press, 2010.

[39] Carter, D. E. and Baker, B. S., *CE, concurrent engineering: the product development environment for the 1990s*. Addison-Wesley Reading, MA, 1992.

[40] Cassidy, P. F., Gatzke, T. D., and Vaporean, C. N., "Integrating Synthesis and Simulation for Conceptual Design," *AIAA Paper*, vol. 1443, 2008.

[41] CATIA, *V6*. Vlizy-Villacoublay, France: Dassault Systmes, 2013.

[42] Cazenave, T., "Nested Monte-Carlo Search.," in *IJCAI*, vol. 9, pp. 456–461, 2009.

[43] Center, L. B. J. S., "Structural Design Requirements and Factors of Safety for Spaceflight Hardware," 2011.

[44] Chaput, A., "Airframe Weight Control - An F-35/JSF Approach," in *Society of Allied Weight Engineers - 64th Annual International Conference on Mass Properties Engineering 2005*, no. Society of Allied Weight Engineers - 64th Annual International Conference on Mass Properties Engineering 2005, p. 664p., 2005.

[45] Collier, C., Yarrington, P., Pickenheim, M., and Bednarcyk, B., "An Approach to Preliminary Design and Analysis," *AIAA Paper*, vol. 2176, 2007.

[46] Cook, R. D., *Concepts and applications of finite element analysis*. New York, NY : Wiley, c2001., 2001.

[47] Costin, D. and Wang, B., "Optimum design of a composite structure with manufacturing constraints," *Thin-walled structures*, vol. 17, no. 3, pp. 185–202, 1993.

[48] Covert, E. and others, "Aeronautical Technologies for the Twenty-first Century. Aeronautics and Space Engineering Board, National Research Council," 1992.

[49] Cramer, E. J., Dennis, Jr, J., Frank, P. D., Lewis, R. M., and Shubin, G. R., "Problem formulation for multidisciplinary optimization," *SIAM Journal on Optimization*, vol. 4, no. 4, pp. 754–776, 1994.

[50] Curran, R., Kundu, A., Raghunathan, S., and Eakin, D., "Costing tools for decision making within integrated aerospace design," *Concurrent Engineering*, vol. 9, no. 4, pp. 327–338, 2001.

[51] Curran, R., Price, M., Raghunathan, S., Benard, E., Crosby, S., Castagne, S., and Mawhinney, P., "Integrating aircraft cost modeling into conceptual design," *Concurrent Engineering*, vol. 13, no. 4, pp. 321–330, 2005.

[52] Curran, R., Raghunathan, S., and Price, M., "Review of aerospace engineering cost modelling: The genetic causal approach," *Progress in Aerospace Sciences*, vol. 40, no. 8, pp. 487–534, 2004.

[53] Davies, C., Stelmack, M., Zink, S., De La Garza, A., and Flick, P., "High Fidelity MDO Process Development and Application to Fighter Strike Conceptual Design," in *12th AIAA Aviation Technology, Integration, and Operations (ATIO) Conference and 14th AIAA/ISSMO Multidisciplinary Analysis and Optimization Conference*, 2012.

[54] Davis, L., "Genetic algorithms and simulated annealing," 1987.

[55] De Wit, A. and van Keulen, F., "Numerical comparison of multi-level optimization techniques," in *Proceedings of the 3rd AIAA multidisciplinary design optimization specialist conference, Honolulu, HI*, 2007.

[56] De Wit, A. and van Keulen, F., "Overview of methods for multi-level and/or multi-disciplinary optimization," in *Proceedings of the 51st AIAA/ASME/ASCE/AHS/ASC structures, structural dynamics, and materials conference, Orlando, Florida*, 2010.

[57] Deb, K., "Multi-objective optimization," in *Search methodologies*, pp. 403–449, Springer, 2014.

[58] Deng, D. and Murakawa, H., "FEM prediction of buckling distortion induced by welding in thin plate panel structures," *Computational Materials Science*, vol. 43, no. 4, pp. 591–607, 2008.

[59] Deng, Y.-M. and Edwards, K., "The role of materials identification and selection in engineering design," *Materials & design*, vol. 28, no. 1, pp. 131–139, 2007.

[60] Dieter, G. E., *Engineering design*. McGraw-Hill, 1991.

[61] Drela, M., "AVL overview." http://web.mit.edu/drela/Public/web/avl/, Nov 2013.

[62] Dussauge, P. and Garrette, B., "Determinants of success in international strategic alliances: Evidence from the global aerospace industry," *Journal of International Business Studies*, pp. 505–530, 1995.

[63] Eldred, L. B., Padula, S. L., and Li, W., "Enabling Rapid and Robust Structural Analysis During Conceptual Design," 2015.

[64] Elham, A., La Rocca, G., and van Tooren, M., "Development and implementation of an advanced, design-sensitive method for wing weight estimation," *Aerospace Science and Technology*, vol. 29, no. 1, pp. 100–113, 2013.

[65] Elham, A. and van Tooren, M. J., "Weight Indexing for Wing-Shape Multi-Objective Optimization," *AIAA journal*, vol. 52, no. 2, pp. 320–337, 2014.

[66] Elrod, R. and Burbage, T., "F-35 Year End Review 2004: Rising to the Challenge," tech. rep., Lokheed Martin, Bethesda, Maryland, 2004.

[67] Ender, T., Leurck, R. F., Weaver, B., Miceli, P., Blair, W. D., West, P., and Mavris, D., "Systems-of-systems analysis of ballistic missile defense architecture effectiveness through surrogate modeling and simulation," *Systems Journal, IEEE*, vol. 4, no. 2, pp. 156–166, 2010.

[68] Eriksson, S., "Globalisation and changes of aircraft manufacturing production/supply-chains: the case of China.," *International Journal of Logistics Economics and Globalisation*, vol. 3, no. 1, pp. 70 – 83, 2011.

[69] Ertas, A. and Jones, J. C., *The engineering design process*, vol. 2. John Wiley & Sons, 1996.

[70] Esbensen, H. and Kuh, E. S., "Design space exploration using the genetic algorithm," in *Circuits and Systems, 1996. ISCAS'96., Connecting the World., 1996 IEEE International Symposium on*, vol. 4, pp. 500–503, IEEE, 1996.

[71] Farag, M. M., *Materials and process selection for engineering design*. CRC Press, 2008.

[72] Federal Aviation Administration, "Airworthiness Standards: General Rotorcraft," *14 CFR 27.303*, 1990.

[73] Federal Aviation Administration, "Airworthiness Standards: Normal, Utility, Acrobatic, and Commuter Category Airplanes," *14 CFR 23.303*, 1993.

[74] Federal Aviation Administration, "Aviation & Emissions A Primer," tech. rep., FAA, Washington, DC, January, 2005.

[75] Federal Aviation Administration, "Performance measure profile NAS energy efficiency: FY 2013 methodology report," tech. rep., FAA, Washington, DC, September, 2013.

[76] Francis, L., "New Faces : Asian carriers creating new airlines in an effort to achieve a lower cost base," *Aviation Week & Space Technology*, vol. 173, no. 33, pp. 58 – 59, 2011.

[77] Galloway, T. and Mavris, D., "Aircraft Life Cycle Cost Analysis (ALCCA) Program," *NASA Ames Research Center*, 1993.

[78] Galorath, "SEER-MFG." http://gts.sourceforge.net/.

[79] Gano, S. E., Renaud, J. E., and Sanders, B., "Hybrid variable fidelity optimization by using a kriging-based scaling function," *Aiaa Journal*, vol. 43, no. 11, pp. 2422–2433, 2005.

[80] Gantois, K. and Morris, A., "The multi-disciplinary design of a large-scale civil aircraft wing taking account of manufacturing costs," *Structural and Multidisciplinary Optimization*, vol. 28, no. 1, pp. 31–46, 2004.

[81] Gauthier, B., Dewhurst, P., and Japikse, D., "Application of design for manufacture and assembly methodologies to complex aerospace products," *American Institute of Aeronautics and Astronautics*, 2000.

[82] Gertler, J., "F-35 joint strike fighter (JSF) program: Background and issues for congress," DTIC Document, 2009.

[83] Giles, G. L., "Equivalent plate analysis of aircraft wing box structures with general planform geometry," *Journal of Aircraft*, vol. 23, no. 11, pp. 859–864, 1986.

[84] Glover, F. and Laguna, M., *Tabu search*. Springer, 1999.

[85] Gutowski, T., Henderson, R., and Shipp, C., "Manufacturing costs for advanced composites aerospace parts," *SAMPE JOURNAL*, vol. 27, no. 3, pp. 37–43, 1991.

[86] Haftka, R. T. and Gürdal, Z., *Elements of structural optimization*, vol. 11. Springer Science & Business Media, 2012.

[87] Hagan, M., *Process for Evaluating Options for Materials Management Outsourcing*. PhD thesis, Massachusetts institute of Technology, 2004.

[88] Hahn, A. S., "Vehicle sketch pad: a parametric geometry modeler for conceptual aircraft design," in *48th AIAA Aerospace Sciences Meeting*, pp. 2010–657, 2010.

[89] Hahn, G. and Rosenfield, A., "Metallurgical factors affecting fracture toughness of aluminum alloys," *Metallurgical Transactions A*, vol. 6, no. 4, pp. 653–668, 1975.

[90] Hannon, C., Agyepong, L., Querin, O., and Toropov, V., "An alternative view on weight estimation for the aircraft industry: Problems and MDO solutions.," in *12th AIAA/ISSMO Multidisciplinary Analysis and Optimization Conference, MAO*, no. 12th AIAA/ISSMO Multidisciplinary Analysis and Optimization Conference, MAO, 2008.

[91] Hansen, L., Heinze, W., and Horst, P., "Blended wing body structures in multidisciplinary pre-design," *Structural and Multidisciplinary Optimization*, vol. 36, no. 1, pp. 93–106, 2008.

[92] Hodges, D. H. and Pierce, G. A., *Introduction to structural dynamics and aeroelasticity*, vol. 15. cambridge university press, 2011.

[93] Howe, D., *Aircraft Loading and Structural Layout*. Professional Engineering Publishing, 2004.

[94] Huang, C. K. and Lin, K. Y., "A method for reliability assessment of aircraft structures subject to accidental damage," *AIAA Paper*, vol. 1830, p. 2005, 2005.

[95] Huber, M., Petersson, Ö., and Baier, H., "Knowledge-based modeling of manufacturing aspects in structural optimization problems," *Advanced Materials Research*, vol. 43, pp. 111–122, 2008.

[96] HyperSizer. Newport News, VA: Collier Research Corporation.

[97] Indyk, P. and Motwani, R., "Approximate nearest neighbors: towards removing the curse of dimensionality," in *Proceedings of the thirtieth annual ACM symposium on Theory of computing*, pp. 604–613, ACM, 1998.

[98] International Civil Aviation Organization, "Resolution A37-19: Consolidated statement of continuing ICAO policies and practices related to environmental protection  climate change," in *International Civil Aviation Organization (ICAO) Assembly - 37th Session*, Montreal, October 2010.

[99] Jameson, A. and Vassberg, J. C., "Computational fluid dynamics for aerodynamic design: Its current and future impact," *AIAA paper*, vol. 538, p. 2001, 2001.

[100] Jiminez, H., Pfaender, H., and Mavris, D., "Fuel burn and CO2 system-wide assessment of environmentally responsible aviation technologies," *Journal of Aircraft*, vol. 49, no. 6, pp. 1913–1930, 2012.

[101] JMP, *11.0*. Cary, North Carolina: SAS institute, 2013.

[102] Kang, E., Jackson, E., and Schulte, W., "An approach for effective design space exploration," in *Foundations of Computer Software. Modeling, Development, and Verification of Adaptive Systems*, pp. 33–54, Springer, 2011.

[103] Kapania, R. K. and Liu, Y., "Static and vibration analyses of general wing structures using equivalent-plate models," *AIAA journal*, vol. 38, no. 7, pp. 1269–1277, 2000.

[104] Kaufmann, M., Zenkert, D., and Åkermo, M., "Cost/weight optimization of composite prepreg structures for best draping strategy," *Composites Part A: Applied Science and Manufacturing*, vol. 41, no. 4, pp. 464–472, 2010.

[105] Kaufmann, M., Zenkert, D., and Wennhage, P., "Integrated cost/weight optimization of aircraft structures," *Structural and Multidisciplinary Optimization*, vol. 41, no. 2, pp. 325–334, 2010.

[106] Kennedy, G. . . . and Martins, J. . . ., "A parallel finite-element framework for large-scale gradient-based design optimization of high-performance structures.," *Finite Elements in Analysis and Design*, vol. 87, pp. 56–73, 2014.

[107] Kennedy, J., "Particle swarm optimization," in *Encyclopedia of Machine Learning*, pp. 760–766, Springer, 2010.

[108] Kirsch, U., *Structural optimization*. Springer, 1993.

[109] Klarbring, A., *An introduction to structural optimization*, vol. 153. Springer, 2008.

[110] Korte, B. H. and Vygen, J., *Combinatorial optimization [electronic resource] : theory and algorithms / Bernhard Korte, Jens Vygen.* Algorithms and combinatorics: v. 21, Heidelberg ; New York : Springer-Verlag Berlin Heidelberg, c2012., 2012.

[111] Koziel, S. and Yang, X.-S., *Computational optimization, methods and algorithms*, vol. 356. Springer, 2011.

[112] Kundu, A., Raghunathan, S., and Cooper, R., "Effect of aircraft surface smoothness requirements on cost," *Aeronautical Journal*, vol. 104, no. 1039, pp. 415–420, 2000.

[113] La Rocca, G. and Van Tooren, M., "Enabling distributed multi-disciplinary design of complex products: a knowledge based engineering approach," *Journal of Design Research*, vol. 5, no. 3, pp. 333–352, 2007.

[114] Laughlin, T. W., Corman, J., and Mavris, D., *A parametric and physics-based approach to structural weight estimation of the hybrid wing body aircraft*. PhD thesis, Georgia Institute of Technology, 2013.

[115] Law, A. M., Kelton, W. D., and Kelton, W. D., *Simulation modeling and analysis*, vol. 2. McGraw-Hill New York, 1991.

[116] Lee, D. S., Fahey, D. W., Forster, P. M., Newton, P. J., Wit, R. C., Lim, L. L., Owen, B., and Sausen, R., "Aviation and global climate change in the 21st century," *Atmospheric Environment*, vol. 43, pp. 3520 – 3537, 2009.

[117] Lee, J. J., *Historical and future trends in aircraft performance, cost, and emissions*. PhD thesis, Massachusetts Institute of Technology, 2000.

[118] Lee, K. Y. and El-Sharkawi, M. A., *Modern heuristic optimization techniques: theory and applications to power systems*, vol. 39. John Wiley & Sons, 2008.

[119] Lee, M., Ceisel, J., Liu, Z., and Mavris, D., "A Parametric, Preliminary Structural Analysis and Optimization Approach with Manufacturing Cost Considerations," in *53rd Structures, Structural Dynamics, and Materials and Co-located Conferences, Honolulu, Hawaii*, 2012.

[120] Leifsson, L. and Koziel, S., "Multi-fidelity design optimization of transonic airfoils using physics-based surrogate modeling and shape-preserving response prediction," *Journal of Computational Science*, vol. 1, no. 2, pp. 98–106, 2010.

[121] Librescu, L. and Song, O., "On the static aeroelastic tailoring of composite aircraft swept wings modelled as thin-walled beam structures," *Composites Engineering*, vol. 2, no. 5, pp. 497–512, 1992.

[122] Liebeck, R. H., "Design of the blended wing body subsonic transport," *Journal of Aircraft*, vol. 41, no. 1, pp. 10–25, 2004.

[123] Livne, E. and Navarro, I., "Nonlinear equivalent plate modeling of wing-box structures," *Journal of Aircraft*, vol. 36, no. 5, pp. 851–865, 1999.

[124] Lomax, T. L., *Structural loads analysis for commercial transport aircraft: theory and practice*. Aiaa, 1996.

[125] Lorell, M. A., Lowell, J., Moore, R. M., Greenfield, V. A., and Vlachos-Dengler, K., *Going global? : U.S. government policy and the defense aerospace industry*. Santa Monica, CA : RAND, 2002., 2002.

[126] Marler, R. T. and Arora, J. S., "Survey of multi-objective optimization methods for engineering," *Structural and multidisciplinary optimization*, vol. 26, no. 6, pp. 369–395, 2004.

[127] Marler, R. T. and Arora, J. S., "The weighted sum method for multi-objective optimization: new insights," *Structural and multidisciplinary optimization*, vol. 41, no. 6, pp. 853–862, 2010.

[128] Martins, J. R. and Lambe, A. B., "Multidisciplinary design optimization: a survey of architectures," *AIAA journal*, vol. 51, no. 9, pp. 2049–2075, 2013.

[129] Martins, R., Joaquim, R., Alonso, J. J., and Reuther, J. J., "High-fidelity aerostructural design optimization of a supersonic business jet," *Journal of Aircraft*, vol. 41, no. 3, pp. 523–530, 2004.

[130] Marx, W. J., Mavris, D. N., and Schrage, D. P., "A knowledge-based system integrated with numerical analysis tools for aircraft life-cycle design," *AI EDAM*, vol. 12, no. 3, pp. 211–229, 1998.

[131] Maskew, B., "Prediction of subsonic aerodynamic characteristics: a case for low-order panel methods," *Journal of Aircraft*, vol. 19, no. 2, pp. 157–163, 1982.

[132] Mason, K. J., "Airframe manufacturers: Which has the better view of the future?," *Journal of Air Transport Management*, vol. 13, no. 1, pp. 9–15, 2007.

[133] MATLAB, *version 8.0.0 (R2012b)*. Natick, Massachusetts: The MathWorks Inc., 2012.

[134] Mavris, D. N., Baker, A. P., and Schrage, D. P., "IPPD through robust design simulation for an affordable short haul civil tiltrotor," 1997.

[135] Mavris, D. N., DeLaurentis, D. A., Bandte, O., and Hale, M. A., "A stochastic approach to multi-disciplinary aircraft analysis and design," in *36th Aerospace Sciences Meeting & Exhibit, Reno, NV*, 1998.

[136] Mazur, V., "A physical model of lightning initiation on aircraft in thunderstorms," *Journal of Geophysical Research: Atmospheres (1984–2012)*, vol. 94, no. D3, pp. 3326–3340, 1989.

[137] McCombs, W. F., *Engineering Column Analysis: the Analysis of Compression Members*. Datatec, Dallas, TX, 2004.

[138] McCullers, L., "Flight Optimization System," *NASA Langley Research Center, Hampton, VA*, 2009.

[139] McCullers, L., "Flight Optimization System, Release 8.11, User's Guide," 2009.

[140] McKay, M., Beckman, R., and Conover, W., "A comparison of three methods for selecting values of input variables in the analysis of output from a computer code," *Technometrics*, vol. 42, no. 1, pp. 55–61, 2000.

[141] Meixell, M. J. and Gargeya, V. B., "Global supply chain design: A literature review and critique," *Transportation Research Part E: Logistics and Transportation Review*, vol. 41, no. 6, pp. 531–550, 2005.

[142] Moffitt, B., Bradley, T. H., Mavris, D., and Parekh, D. E., "Design space exploration of small-scale PEM fuel cell long endurance aircraft," in *Proceedings of the 6th AIAA Aviation Technology, Integration, and Operations Conference, September*, pp. 25–27, 2006.

[143] Mohaghegh, M., "Evolution of structures design philosophy and criteria," *Journal of aircraft*, vol. 42, no. 4, pp. 814–831, 2005.

[144] Montgomery, D. C., *Design and analysis of experiments*, vol. 7. Wiley New York, 1984.

[145] Mooney, C. Z., *Monte Carlo Simulation*, vol. 116. Sage Publications, 1997.

[146] MSC.NASTRAN, *2013.1.* Newport Beach, California: The MacNeal-Schwendler Corporation, 2013.

[147] MSC.PATRAN. Newport Beach, California: The MacNeal-Schwendler Corporation, 2013.

[148] Mullins, J. and Kim, H., "Fidelity Forward multidisciplinary analysis and optimization: Harnessing the power of high fidelity CAD and CAE tools in conceptual design.," in *12th AIAA/ISSMO Multidisciplinary Analysis and Optimization Conference, MAO*, no. 12th AIAA/ISSMO Multidisciplinary Analysis and Optimization Conference, MAO, 2008.

[149] Murphy, G., *Similitude in engineering.* New York, Ronald Press Co. [1950], 1950.

[150] National Materials Advisory Board, *Computer-aided materials selection during structural design [computer file] / Committee on Application of Expert Systems to Materials Selection During Structural Design, National Materials Advisory Board, Commission on Engineering and Technical Systems, National Research Council.* Washington, D.C. : National Academy Press, c1995., 1995.

[151] NEi NASTRAN, *V10.2.* Westminster, California: NEi Software, 2013.

[152] Nelder, J. A. and Mead, R., "A simplex method for function minimization," *The computer journal*, vol. 7, no. 4, pp. 308–313, 1965.

[153] Niu, C., *Airframe structural design: practical design information and data on aircraft structures*. Conmilit Press Limited, 1999.

[154] NuSil Silicone Technology, "Aircraft Materials Selection guide," tech. rep., NuSil Silicone Technology, 2009.

[155] Olson, E. and Mavris, D. N., "Aircraft Conceptual Design and Risk Analysis Using Physics-Based Noise Prediction," in *12th AIAA/CEAS Aeroacoustics Conference (27th AIAA Aeroacoustics Conference)*, 2006.

[156] Olvander, J. and Krus, P., "Optimizing the Optimization–A Method for Comparison of Optimization Algorithms," *AIAA Paper*, vol. 1915, 2006.

[157] Pai, S., "Some aeroelastic properties of swept wings," *Journal of the Aeronautical Sciences (Institute of the Aeronautical Sciences)*, vol. 16, no. 2, 2012.

[158] Palermo, G., Silvano, C., and Zaccaria, V., "Multi-objective design space exploration of embedded systems," *Journal of Embedded Computing*, vol. 1, no. 3, pp. 305–316, 2005.

[159] Papalambros, P. Y. and Wilde, D. J., *Principles of optimal design: modeling and computation*. Cambridge university press, 2000.

[160] Paredis, C. J., Diaz-Calderon, A., Sinha, R., and Khosla, P. K., "Composable models for simulation-based design," *Engineering with Computers*, vol. 17, no. 2, pp. 112–128, 2001.

[161] Peery, D. J. and Azar, J., *Aircraft structures*. McGraw Hill (New York), 1982.

[162] Penner, J. E., *Aviation and the global atmosphere: a special report of IPCC Working Groups I and III in collaboration with the Scientific Assessment Panel to the Montreal Protocol on Substances that Deplete the Ozone Layer*. Cambridge University Press, 1999.

[163] Petermeier, J., Radtke, G., Stohr, M., Woodland, A., Takahashi, T., Donovan, S., and Shubert, M., "Enhanced Conceptual Wing Weight Estimation Through Structural Optimization and Simulation," 2010.

[164] Pfeifer, M., *Materials enabled designs: the materials engineering perspective to product design and manufacturing*. Amsterdam ; Boston : Elsevier/Butterworth Heinemann, c2009., 2009.

[165] Polmear, I. J. and Polmear, I., *Light alloys: metallurgy of the light metals*. Edward Arnold London, 1989.

[166] Pope, G., *On the Flexure of Thin Built-Up Wings*. Citeseer, 1962.

[167] Potter, C., Russell, S. G., Kim, V., Witte, P., Liu, Z., and Mavris, D., "A Preliminary Study of Wing Substructure Layouts Using a Parametric Structures Evaluation Tool," in *54th AIAA/ASME/ASCE/AHS/ASC Structures, Structural Dynamics and Materials Conference*, Boston, MA, April 8-11, 2013.

[168] PR Newswire, "Airline Industry to Face Rapidly Expanding Competition, According to PwC US.," *PR Newswire US*, 2014.

[169] Prasad, S. and Babbar, S., "International operations management research," *Journal of operations management*, vol. 18, no. 2, pp. 209–247, 2000.

[170] Price, M., Curran, R., Murphy, A., Raghunathan, S., Early, J., Castagne, S., Benard, E., and Crawford, B., "Integrating design, manufacturing and cost for trade-offs on aircraft configurations," in *AIAAs 6th annual aviation technology, integration, & operations (ATIO) forum, Paper No. AIAA-2006-7739, Witchita, KS*, 2006.

[171] Rais-Rohani, M. and Dean, E., "Toward manufacturing and cost considerations in multidisciplinary aircraft design," *American Institute of Aeronautics AIAA-96-1620-CP*, 1996.

[172] Rajeev, S. and Krishnamoorthy, C., "Discrete optimization of structures using genetic algorithms," *Journal of Structural Engineering*, vol. 118, no. 5, pp. 1233–1250, 1992.

[173] Rao, R. V., "A decision making methodology for material selection using an improved compromise ranking method," *Materials & Design*, vol. 29, no. 10, pp. 1949–1954, 2008.

[174] Raymer, D. P., *Aircraft design: a conceptual approach*, vol. 3. American Institute of Aeronautics and Astronautics, 1999.

[175] Rebba, R. and Mahadevan, S., "Computational methods for model reliability assessment," *Reliability Engineering & System Safety*, vol. 93, no. 8, pp. 1197–1207, 2008.

[176] Reeves, J., DePasquale, D., and Lim, E., "Affordability Engineering: Bridging the Gap between Design and Cost," *AIAA SPACE 2010 Conference & Exposition*, 2010.

[177] Rogers, C. W., "Advanced-composite material application to aircraft structures.," *Journal of Aircraft*, vol. 5, no. 3, pp. 311–316, 1968.

[178] Roskam, J., *Airplane design*. DARcorporation, 1985.

[179] Russell, E., "US airline profits start to take root.," *Airline Business*, vol. 29, no. 3, pp. 44–45, 2013.

[180] Russell, S. G., Potter, C., Kim, V., Witte, P., Liu, Z., and Mavris, D., "Development of an Integrated Structural Analysis Capability for Airframe Preliminary Design," in *54th AIAA/ASME/ASCE/AHS/ASC Structures, Structural Dynamics and Materials Conference*, Boston, MA, April 8-11, 2013.

[181] Schmit, L. A., "Structural design by systematic synthesis," in *Proc. of the Second ASCE Conference on Electronic Computation*, pp. 105–122, 1960.

[182] Schrage, D. P., "Technology for rotorcraft affordability through integrated product/process development (IPPD)," 1999.

[183] Schumann, B., Ferraro, M., Surendra, A., Scanlan, J. P., and Fangohr, H., "Better Design Decisions Through Operational Modeling During the Early Design Phases," *Journal of Aerospace Information Systems*, vol. 11, no. 4, pp. 195–210, 2014.

[184] Schutte, J., Kestner, B., Tai, J., and Mavris, D., "Updates and modeling enhancements to the assessment of NASA Environmentally Responsible Aviation technologies and vehicle concepts," in *Proceedings of the 50th AIAA Aerospace Sciences Meeting*, pp. 9–12, 2012.

[185] Schutte, J. S., Jimenez, H., and Mavris, D. N., "Technology assessment of NASA Environmentally Responsible Aviation advanced vehicle concepts," *AIAA Paper*, vol. 6, p. 2011, 2011.

[186] Shah, J. and Hazelrigg, H., "Research opportunities in engineering design," in *NSF Strategic Planning Workshop, Final Report*, 1996.

[187] Shephard, M. S., Beall, M. W., O'bara, R. M., and Webster, B. E., "Toward simulation-based design," *Finite Elements in Analysis and Design*, vol. 40, no. 12, pp. 1575–1598, 2004.

[188] Simitses, G. J. and Hodges, D. H., *Fundamentals of structural stability*. Butterworth-Heinemann, 2006.

[189] Simpson, T. W., Mauery, T. M., Korte, J. J., and Mistree, F., "Kriging models for global approximation in simulation-based multidisciplinary design optimization," *AIAA journal*, vol. 39, no. 12, pp. 2233–2241, 2001.

[190] Sinha, R., Paredis, C. J., Liang, V.-C., and Khosla, P. K., "Modeling and simulation methods for design of engineering systems," *Journal of Computing and Information Science in Engineering*, vol. 1, no. 1, pp. 84–91, 2001.

[191] Sirisalee, P., Ashby, M. F., Parks, G. T., and Clarkson, P. J., "Multi-Criteria Material Selection in Engineering Design," *Advanced Engineering Materials*, vol. 6, no. 1-2, pp. 84–92, 2004.

[192] Sobieszczanski-Sobieski, J. and Haftka, R. T., "Multidisciplinary aerospace design optimization: survey of recent developments," *Structural optimization*, vol. 14, no. 1, pp. 1–23, 1997.

[193] Sobieszczanski-Sobieski, J., James, B. B., and Dovi, A. R., "Structural optimization by multilevel decomposition," *AIAA journal*, vol. 23, no. 11, pp. 1775–1782, 1985.

[194] Sobieszczanski-Sobieski, J., James, B. B., and Riley, M. F., "Structural sizing by generalized, multilevel optimization," *AIAA Journal*, vol. 25, no. 1, pp. 139–145, 1987.

[195] Soutis, C., "Fibre reinforced composites in aircraft construction," *Progress in Aerospace Sciences*, vol. 41, no. 2, pp. 143–151, 2005.

[196] Spier, E., "Crippling/column buckling analysis and test of graphite/epoxy stiffened panels," in *Proceedings of the AIAA/ASME/SAE 16th Structures, Structural Dynamics, and Materials Conference, Denver, CO*, 1975.

[197] Stevens, B. L. and Lewis, F. L., *Aircraft control and simulation*. John Wiley & Sons, 2003.

[198] Stohr, M., Petermeier, J., Willardson, R., Nardiello, J., and Donovan, S., "Weight Estimation for Composite Wings Based on Optimized Structure with Laminate Selection," in *12th AIAA Aviation Technology, Integration, and Operations (ATIO) Conference and 14th AIAA/ISSMO Multidisciplinary Analysis and Optimization Conference*, 2012.

[199] Tam, W., "Improvement opportunities for aerospace design process," *Space*, pp. 28–30, 2004.

[200] Tang, C. S. and Zimmerman, J. D., "Managing New Product Development and Supply Chain Risks: The Boeing 787 Case.," *Supply Chain Forum: International Journal*, vol. 10, no. 2, pp. 74 – 86, 2009.

[201] Tedford, N. P. and Martins, J. R., "Benchmarking multidisciplinary design optimization algorithms," *Optimization and Engineering*, vol. 11, no. 1, pp. 159–183, 2010.

[202] Torenbeek, E., "Development and application of a comprehensive, design-sensitive weight prediction method for wing structures of transport category aircraft," tech. rep., Delft University of Technology, 1992.

[203] United States General Accounting Office, "Aviation and the Environment: Aviation's Effects on the Global Atmosphere Are Potentially Significant and Expected to Grow.," 2000.

[204] Vanderplaats, G. N., *Multidiscipline Design Optimization*. Vanderplaats Research & Development, Inc., 2007.

[205] Vasudevan, A. K. and Doherty, R. D., *Aluminum Alloys–Contemporary Research and Applications: Contemporary Research and Applications*. Elsevier, 2012.

[206] Venkataraman, S. and Haftka, R., "Structural optimization complexity: what has Moores law done for us?," *Structural and Multidisciplinary Optimization*, vol. 28, no. 6, pp. 375–387, 2004.

[207] Vos, R., Geuskens, F., and Hoogreef, M., "A new structural design concept for blended wing body cabins," in *53rd AIAA/ASME/ASCE/AHS/ASC Structures, Structural Dynamics and Materials Conference 20th AIAA/ASME/AHS Adaptive Structures Conference 14th AIAA*, p. 1998, 2012.

[208] Waggoner, E. G., "Status update on NASAs Integrated Systems Research Program," in *49th AIAA Aerospace Science Meeting, Orlando, FL*, 2011.

[209] Wegst, U. and Ashby, M., "The mechanical efficiency of natural materials," *Philosophical Magazine*, vol. 84, no. 21, pp. 2167–2186, 2004.

[210] Whitney, D. E., *Mechanical assemblies: their design, manufacture, and role in product development*, vol. 1. Oxford university press, 2004.

[211] Yegnanarayana, B., *Artificial neural networks*. PHI Learning Pvt. Ltd., 2009.

[212] Zhou, M., Fleury, R., Shyy, Y.-K., Thomas, H., and Brennan, J., "Progress in topology optimization with manufacturing constraints," in *Proceedings of the 9th AIAA MDO conference AIAA-2002-4901*, 2002.

[213] Zipfel, P. H., *Modeling and simulation of aerospace vehicle dynamics*. Aiaa, 2000.

[214] Zuo, K.-T., Chen, L.-P., Zhang, Y.-Q., and Yang, J., "Manufacturing-and machining-based topology optimization," *The International Journal of Advanced Manufacturing Technology*, vol. 27, no. 5-6, pp. 531–536, 2006.

# VITA

Charles Potter is a PhD candidate at the Georgia Institute of Technology. During his time at Georgia Tech he earned both a Bachelor's and Master's degree in Aerospace Engineering and will complete his PhD in 2015. Under the direction of professor Dimitri Mavris, Charles has spent the past six years conducting research at the Aerospace Systems Design Laboratory (ASDL). His research has focused on modeling & simulation of multivariate design problems with emphasis on using physics-based analysis to increase designer knowledge in early phases of aircraft design. This research includes multi-objective multidisciplinary design optimization as well as using statistical methods to identify key drivers of cost and performance. During his time at ASDL he has worked on several unique projects: working with the United States Air Force, he identified scenarios and measures of effectiveness for directed energy weapons, he created a parametric 3D airplane model for weight estimation using AMRaven, and he helped create SPANDSET, a preliminary wingbox substructure layout tool utilizing Excel and VBA for Triumph Aerostructures which led to three conference papers.